



University
of Glasgow

Fülöp, Réka-Hajnalka (2012) *Quantifying the magnitude and timing of Holocene soil erosion events on parent materials of known age using in-situ cosmogenic C-14 and Be-10 depth-profiles*. PhD thesis.

<http://theses.gla.ac.uk/3358/>

Copyright and moral rights for this thesis are retained by the author

A copy can be downloaded for personal non-commercial research or study

This thesis cannot be reproduced or quoted extensively from without first obtaining permission in writing from the Author

The content must not be changed in any way or sold commercially in any format or medium without the formal permission of the Author

When referring to this work, full bibliographic details including the author, title, awarding institution and date of the thesis must be given

Quantifying the magnitude and timing of Holocene
soil erosion events on parent materials of known
age using in-situ cosmogenic ^{14}C and ^{10}Be
depth-profiles

by

Réka-Hajnalka Fülöp

A thesis submitted to the
School of Geographical and Earth Sciences
at the University of Glasgow
for the degree of

Doctor of Philosophy

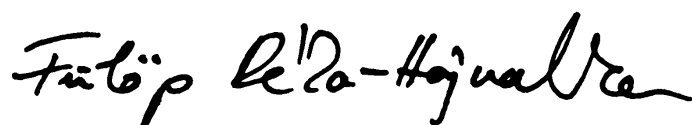
February 2012



To my grandmother, Szántó Anna, who has dedicated her life to ensuring that everybody
in her family receives a good education.

Declaration of Originality

I hereby declare that the work presented in this thesis has been carried out by myself, except where due acknowledgement is made, and has not been submitted for any other degree.

A handwritten signature in black ink, reading 'Fülöp Réka-Hajnalka' in a cursive script.

Réka-Hajnalka Fülöp

Abstract of Thesis

Conventional methods for the determination of past soil erosion provide only average rates of erosion of the sediment's source areas and are unable to determine the rate of at-a-site soil loss. This study addresses this issue by exploring the extent to which in situ cosmogenic ^{10}Be and ^{14}C depth-profiles can be used to quantify the magnitude and timing of site-specific soil erosion events on soils of known age. The study focuses on two sites located on end moraines of the Loch Lomond Readvance (LLR) in Scotland: Wester Cameron and Inchie Farm, both near Glasgow. The LLR is well documented and several LLR moraine radiocarbon ages exist in the literature allowing for the placement of a first order age constraint on soil/till emplacement. In addition, the site at Wester Cameron is in the proximity of Croftamie, a well-studied LLR type-locality. The site near Wester Cameron does not show any visible signs of soil disturbance and so this has been selected in order to test (1) whether a cosmogenic nuclide depth profile in a sediment body of Holocene age can be reconstructed, and (2) whether in situ ^{10}Be , ^{26}Al and ^{14}C yield concordant results. Field evidence suggests that the site at Inchie Farm has undergone soil erosion and so this was selected so as to explore whether the technique can also be applied to determine the broad timing of soil loss.

The results of the cosmogenic ^{10}Be , ^{14}C , and ^{26}Al analyses in the Wester Cameron site samples confirm that the cosmogenic nuclide depth-profile to be expected from a sediment body of Holocene age can be reconstructed. Moreover, the agreement between the total cosmogenic ^{10}Be inventories in the erratics and the Wester Cameron soil/till samples indicate that there has been no erosion at the sample site since the deposition of the till/moraine. Further, the Wester Cameron depth profiles show minimal signs of homogenisation, as a result of bioturbation, and minimal cosmogenic nuclide inheritance from previous exposure periods. The results of the cosmogenic ^{10}Be and ^{14}C analyses in the Inchie Farm site samples show a clear departure from the zero-erosion cosmogenic nuclide depth profiles suggesting that the soil/till at this site has undergone erosion since its stabilisation. The LLR moraine at the Inchie Farm site is characterised by the presence of a sharp break in slope, suggesting that the missing soil material was removed instantaneously by an erosion event rather than slowly by continuous erosion. The results of a Monte-Carlo type analysis carried out to constrain the magnitude and timing of this erosion event suggest that the event was relatively recent and relatively shallow, resulting in the removal of $\sim 20 - 50$ cm of soil less than 1500 years BP.

The results of sensitivity analyses show that the predicted magnitude and timing of the Inchie Farm erosion event are highly sensitive to the assumptions that are made about the background rate of continuous soil erosion at the site and also about the stabilisation age of the till. The results further indicate that the density of the sedimentary deposit will also affect the magnitude and timing of the predicted erosion event. All three parameters can be independently determined a priori and so despite the method presented in this study being sensitive to variations in these parameters, they do not impede future applications of the method to other localities. The results of the sensitivity analyses further show that the predicted erosion event magnitude and timing is very sensitive to the in situ cosmogenic ^{14}C production rate used and to the assumptions that are made about the contribution of muons to the total production of this cosmogenic nuclide. Thus, advances in this regard need to be made for the method presented in this thesis to be applicable with confidence to scenarios similar to the one presented here.

Acknowledgments

I would like to offer special thanks to David Sanderson, who is a great person and a brilliant mind, for trusting me and for giving me high hopes.

I would also like to express my gratitude to my supervisors: Paul Bishop (Glasgow), Derek Fabel (Glasgow), Gordon T Cook (SUERC), and Jeremy Everest (BGS). Paul provided excellent guidance throughout my studies at the University of Glasgow. I would particularly like to thank him for his never-ending enthusiasm for my research and for keeping me on the right track all the time. I could not have asked for a better supervisor. I would like to thank Derek for his guidance in the field and laboratory, throughout sampling and cosmogenic ^{10}Be work. I would like to thank Gordon for his very practical advice and for sharing with me his views on life that helped me keep mine in balance, and Jeremy for providing me with GIS data and maps.

Many thanks are due to Philip Naysmith (SUERC) for teaching me the *in situ* ^{14}C extraction procedures and telling me about all the problems related to this. Many thanks are also due to Fin Stuart (SUERC) for all the informal chats and free rides to SUERC. Fin has helped me understand the essence of a PhD and that of managing one's life. Christoph Schnabel, Cassandra Fenton, Leticia M-Rodriguez, Allan Davidson, Maria M-Rodriguez, and Sheng Xu all from SUERC, are thanked for help with the ^{10}Be and ^{26}Al analyses and AMS measurement respectively.

SUERC was a great place to work at. It would be very difficult to list all the people who shaped my every-days there - chocolate suppliers, screwdriver lenders, or people who just happened to smile on a grey day - but special thanks are due to my closest colleagues, Graham Muir, Elaine Dunbar, William McCormack, Robert McLeod, Willie Degnan, and Kerry Sayle, for providing me with my daily dose of fun and support. Also, they refrained from blaming me for breaking dewars or using far too much liquid nitrogen.

Mr and Mrs Wyllie and Mr Erskine are thanked for allowing us to dig pits on their farms. Kenny Roberts, Anne Dunlop, Miguel Castillo, and Delia Gheorghiu, from the University of Glasgow, are thanked for assistance during fieldwork.

Enormous thanks are due to my partner, Tibi, who was always there for me and who provided constructive (and sometimes painful) criticism of my work throughout the last four years. He has also helped me pull through all the stressful periods and survived the constant babble about my PhD. [∞ + +]

I would like to thank my friends, Réka, Jutka, Emi, Klári, and Szilvi, and especially my sister, Kinga, for all the fun and for understanding that the long working hours in the lab and in front of the computer were not a sign of neglecting them. I would also like to thank the twins, Gergő and Bence, whom I used as relaxation 'devices'. Thanks are also due to my hard-working parents for their sacrifices and for providing emotional support throughout.

The completion of this thesis would not have been possible without financial support from a University of Glasgow Postgraduate Scholarship and a British Geological Survey University Funding Initiative (BUFI) Scholarship. Additional funding was also gratefully received from the Scottish Alliance for Geoscience, Environment and Society (SAGES), the American Geophysical Union, the SUERC AMS Consortium, and the School of Geographical and Earth Sciences of the University of Glasgow.

Table of Contents

Declaration of Originality	ii
Abstract	iii
Acknowledgements	iv
Table of Contents	v
List of Figures	ix
List of Tables	xii
1 Introduction	2
1.1 Aim of thesis	2
1.2 The importance of quantifying soil erosion	2
1.3 Methods for quantifying soil erosion	3
1.3.1 Methods based on direct observation	4
1.3.2 Methods based on sediment transportation and storage	6
1.3.3 Methods based on radionuclides	8
1.3.4 Methods based on modelling	11
1.3.5 Methods based on age dating	14
1.3.6 Summary	17
1.4 <i>In situ</i> produced terrestrial cosmogenic nuclides	18
1.4.1 Theory and applications	19
1.4.2 Quantifying soil erosion using cosmogenic nuclide depth-profiles . . .	20
1.5 Objectives and organisation of thesis	22
2 <i>In situ</i> cosmogenic ^{14}C systematics and extraction system at SUERC	27
2.1 Introduction	27
2.2 <i>In situ</i> ^{14}C production and extraction methods	28
2.3 <i>In situ</i> ^{14}C extraction at SUERC	30

2.4	Results and discussion	35
2.4.1	Icelandic doublespar	36
2.4.2	Extraction blanks and shielded quartz	37
2.4.3	Reproducibility measurements	40
2.5	Summary	43
3	Study Area	45
3.1	Introduction	45
3.2	Context	47
3.3	Study site 1: Wester Cameron Farm	48
3.4	Study site 2: Inchie Farm	52
3.5	Summary	54
4	Results of the cosmogenic nuclide analyses	56
4.1	Introduction	56
4.2	Methods	56
4.3	Results and discussion	58
4.3.1	Wester Cameron	58
4.3.1.1	Depth-profile characteristics and grain-size differences . . .	59
4.3.1.2	Cosmogenic nuclide inheritance	62
4.3.2	Inchie Farm	64
4.3.3	Implications of the timing of erosion at Inchie Farm	66
4.4	Summary	67
5	The magnitude and timing of soil erosion at Inchie Farm and sensitivity analyses	70
5.1	Introduction	70
5.2	Theoretical background	70
5.3	The magnitude and timing of soil erosion at Inchie Farm	73
5.4	Sensitivity analysis	76
5.4.1	‘Non-zero’ continuous erosion rate	76
5.4.2	Measurement uncertainty and sample size	78
5.4.3	Model parameters	83
5.4.3.1	Age of the sediment body	83

5.4.3.2	Density of the sediment	85
5.4.3.3	Nuclide production pathways	85
5.4.3.4	Sea Level High Latitude production rates	88
5.5	Summary	90
6	Conclusions, Limitations, and Future Research	95
6.1	Conclusions	95
6.2	Limitations	97
6.3	Future research	99
6.3.1	Extraction and purification of <i>in situ</i> ^{14}C	99
6.3.2	<i>In situ</i> ^{14}C production systematics.	101
	References	103
	Appendices	144
A	<i>In situ</i> ^{14}C data reduction and details of the SUERC ^{14}C extraction system	145
A.1	Calculation	146
B	Sample site details	152
B.1	Peat monolith sample composition and radiocarbon analyses	153
B.1.1	Peat composition analyses	154
B.1.2	Peat radiocarbon analyses	155
B.2	Density measurement	165
B.3	Erratic samples, Inchie Farm	168
C	Cosmogenic ^{10}Be, ^{26}Al, and ^{14}C Analyses	171
C.1	Sample preparation	172
C.1.1	The preparation of ultrapure quartz separates	173
C.1.2	Purification and Be extraction, Wester Cameron Farm samples . . .	178
C.1.2.1	Sample purity check	178
C.1.2.2	Be and Al extraction	180
C.1.3	Purification and Be extraction, Inchie Farm samples	183
C.1.3.1	Sample purity check	183
C.1.3.2	Be extraction	183

C.2	AMS measurements	187
C.2.1	^{10}Be AMS measurements	187
C.2.2	^{26}Al AMS measurements	188
C.2.3	Summary of the cosmogenic ^{10}Be , ^{26}Al and ^{14}C data	190
D	R Source Code	195
D.1	Explanation of source code	196
D.1.1	Code dependencies	196
D.1.2	Model constants	196
D.1.3	Input/Output routines	197
D.1.4	Monte Carlo-type simulation	197
D.1.5	Goodness of fit statistic calculations	199
E	Publications	200

List of Figures

1.1	Summary of soil erosion methods based on radionuclides.	8
1.2	Summary of the different types of soil erosion models.	12
1.3	Number of publications on applications of cosmogenic nuclides to the study of surface processes and citations thereof.	19
1.4	Schematic illustration of post-depositional accumulation of cosmogenic nu- clides at various depths.	23
1.5	Hypothetical depth-profiles of concentrations of cosmogenic ^{10}Be , ^{26}Al and ^{14}C in a 10.5 kyr-old sedimentary deposit with various timings of surface erosion.	23
2.1	Schematic of extraction, purification, and graphitization of <i>in situ</i> ^{14}C line.	33
2.2	Results of AMS measurements on the Icelandic doublespar aliquots.	36
2.3	Results of the system blank and shielded quartz measurements.	39
2.4	Results of the reproducibility measurements (PP4).	41
3.1	Map showing the location of the study sites.	46
3.2	Photograph showing the moraine ridge at Wester Cameron Farm.	49
3.3	Description of Wester Cameron Farm sampling depth-profile.	51
3.4	Photograph showing the moraine ridge at Inchie Farm.	52
3.5	Description of Inchie Farm sampling depth-profile.	53
4.1	Depth-profiles of measured ^{10}Be concentrations at Wester Cameron Farm. .	60
4.2	Depth-profiles of measured ^{26}Al concentrations at Wester Cameron Farm. .	61
4.3	Depth-profiles of measured ^{14}C concentrations at Wester Cameron Farm. .	61
4.4	Inventories of cosmogenic ^{10}Be at Wester Cameron Farm.	62
4.5	Depth-profiles of measured ^{10}Be concentrations at Inchie Farm.	65

4.6	Depth-profiles of measured ^{14}C concentrations at Inchie Farm.	66
5.1	χ^2_{red} contour plots obtained for the ^{10}Be and ^{14}C depth-profiles assuming no continuous erosion.	74
5.2	χ^2_{red} contour plot obtained for the combined ^{10}Be and ^{14}C depth-profiles assuming no continuous erosion.	75
5.3	χ^2_{red} contour plots obtained for the combined ^{10}Be and ^{14}C depth-profiles for continuous erosion rates between 5 - 100 mm.kyr $^{-1}$	77
5.4	χ^2_{red} values of ^{10}Be and ^{14}C depth-profiles for continuous erosion rates as- suming no erosional events.	78
5.5	χ^2_{red} contour plot obtained for synthetic combined ^{10}Be and ^{14}C depth- profiles assuming no continuous erosion and varying level of uncertainty. . .	80
5.6	χ^2_{red} contour plot obtained for synthetic combined ^{10}Be and ^{14}C depth- profiles assuming no continuous erosion and varying sample number.	81
5.7	χ^2_{red} contour plots obtained for the combined ^{10}Be and ^{14}C depth-profiles at Inchie Farm with varying sample points.	82
5.8	χ^2_{red} contour plots obtained for the combined ^{10}Be and ^{14}C depth-profiles at Inchie Farm assuming no continuous erosion and varying the age of till stabilization.	84
5.9	χ^2_{red} contour plots obtained for the combined ^{10}Be and ^{14}C depth-profiles at Inchie Farm assuming no continuous erosion and varying the density of the sedimentary deposit.	86
5.10	Plot showing erosional event timing vs. density of the sedimentary deposit at Inchie Farm.	87
5.11	Plot showing erosional event magnitude vs. density of the sedimentary deposit at Inchie Farm.	87
5.12	χ^2_{red} contour plots obtained for the combined ^{10}Be and ^{14}C depth-profiles at Inchie Farm assuming no continuous erosion and varying the relative contribution of muons to the total production of ^{10}Be and ^{14}C	89
5.13	χ^2_{red} contour plots obtained for the combined ^{10}Be and ^{14}C depth-profiles at Inchie Farm assuming no continuous erosion and varying the <i>in situ</i> cosmogenic ^{10}Be SLHL production.	91

5.14	χ^2_{red} contour plots obtained for the combined ^{10}Be and ^{14}C depth-profiles at Inchie Farm assuming no continuous erosion and varying the <i>in situ</i> cosmogenic ^{14}C SLHL production.	92
A.1	Photograph showing the graphitization software.	149
A.2	Photograph showing the broken mullite tube.	149
A.3	Photograph showing the alumina boat.	150
A.4	Photograph showing the <i>in situ</i> cosmogenic ^{14}C extraction line at SUERC.	150
A.5	Photograph showing the quartz tube flaming setup.	151
B.1	Photograph showing the sampled peat monolith, Wester Cameron Farm.	153
B.2	Photograph showing the peat monolith with samples removed for density, water content, organic matter content and grain size analyses.	154
B.3	Grain size distribution plots for the peat samples, Wester Cameron Farm.	157
B.4	Grain size distribution plots for the peat samples, Wester Cameron Farm (cont1).	158
B.5	Grain size distribution plots for the peat samples, Wester Cameron Farm (cont2).	159
B.6	Grain size distribution plots for the peat samples, Wester Cameron Farm (cont3).	160
B.7	Results of the radiocarbon determinations, Wester Cameron peat.	163
B.8	Photograph showing the TLS setup, Wester Cameron Farm.	166
B.9	Photograph showing the sampled pebbles, Inchie Farm.	168
B.10	Photograph showing the relative location of sample LM09-03 collected for surface exposure dating, Inchie Farm	169
C.1	Photograph showing the pit opened for cosmogenic nuclide depth-profile sampling, Wester Cameron Farm.	172
C.2	Photograph showing the pit opened for cosmogenic nuclide depth-profile sampling, InchieFarm.	173
C.3	Photograph showing a selection of the cosmogenic nuclide depth-profile samples.	175

List of Tables

1.1	Summary of soil erosion methods based on direct observation.	5
2.1	Summary of published ^{14}C extraction methods.	31
2.2	Summary of published <i>in situ</i> ^{14}C extraction methods (continued).	32
2.3	Summary of <i>in situ</i> ^{14}C system blank measurement results.	38
2.4	Summary of <i>in situ</i> ^{14}C shielded quartz measurement results.	39
2.5	Results of the reproducibility measurements (PP-4).	42
2.6	Results of the reproducibility measurements (CRONUS-EARTH-A).	42
2.7	Results of the reproducibility measurements (Glen Roy).	43
3.1	Summary of the ^{10}Be analyses in the Wester Cameron Farm erratic boulders.	50
B.1	Peat sample density measurement results, Wester Cameron Farm.	155
B.2	Peat sample grain size distribution analyses results, Wester Cameron Farm.	156
B.3	Details of the radiocarbon determinations, Wester Cameron peat.	164
B.4	Density calculation results, Wester Cameron Farm.	167
B.5	Density calculation results, Inchie Farm.	167
B.6	Summary of the ^{10}Be analyses in the Inchie Farm ‘erratic’ pebbles.	170
C.1	Sample labels and weights.	174
C.2	Sample weights in grams after each cleaning step, Wester Cameron Farm.	176
C.3	Sample weights in grams after each cleaning step, Inchie Farm.	177
C.4	Results of the ICP/AES measurements, Wester Cameron.	179
C.5	Sample and carrier masses, WesterCameron.	180
C.6	Results of the AAS measurements, Inchie Farm.	184
C.7	Sample and carrier masses, Inchie Farm.	185
C.8	Results of the ^{10}Be AMS measurements, Wester Cameron.	188

C.9	Results of the ^{10}Be AMS measurements, Inchie Farm.	189
C.10	Results of the ^{26}Al AMS measurements, Wester Cameron.	190
C.11	<i>In situ</i> cosmogenic ^{10}Be and ^{26}Al data for the pit samples, Wester Cameron.	191
C.12	<i>In situ</i> cosmogenic ^{10}Be data for the pit samples, Inchie Farm.	192
C.13	<i>In situ</i> cosmogenic ^{14}C data for the pit samples, Wester Cameron.	193
C.14	<i>In situ</i> cosmogenic ^{14}C data for the pit samples, Inchie Farm.	194

THE WIND THAT BLOWS IS ALL THAT ANYBODY KNOWS...

[Henry D. Thoreau]

Chapter 1

Introduction

1.1 Aim of thesis

The overall aim of this thesis is to assess the extent to which the amount and timing of site-specific Holocene soil erosional events can be quantified using depth-profiles of in-situ produced cosmogenic ^{10}Be and ^{14}C .

1.2 The importance of quantifying soil erosion

Deciphering the processes that control soil erosion and quantifying its magnitude over different temporal and spatial scales have been of interest for almost a century (Bennett 1928, Campbell 1981, Loughran 1989, Stroosnijder 2005, Vrieling 2006, Le Roux et al. 2007). Initial research into soil erosion was motivated by problems related to agricultural productivity, scientists being mainly interested in developing crop-specific conservation practices (Loughran 1989, and references therein). The economic costs of soil erosion are clear (cf. Pimentel et al. 1995), but despite the substantial agro-economic research in this area many questions of a broader scientific importance have remained unanswered. It is not actually known, for example, whether human activity accelerates soil erosion (e.g., Trimble and Crosson 2000, Fuchs 2007, and references therein), but it is nonetheless widely assumed that it does so by an order of magnitude (Hewawasam et al. 2003, Wilkinson and McElroy 2007). Similarly, it is unknown whether erosional studies apparently indicating that human activity does accelerate soil erosion are simply a reflection of the variability of background (natural) erosion rates (e.g., Daniels et al. 1987).

Further, despite soils and soil erosion playing a key role in the evolution of the Earth's surface, current numerical models of long-term landscape evolution treat the former in a very simplistic way (Bishop 2007, Tucker and Hancock 2010). A better understanding of the controls on rates and depths of soil production and erosion (Bishop 2007, and references therein) is needed for the improvement of these numerical models. Numerical models have played and play an important role in our understanding of the links and feedbacks between tectonics, climate, and surface processes, and so improved models will enable us to go some way towards solving the so called 'chicken and egg' question posed by Molnar and England (1990).

Thirdly, soil is an important component of the global carbon cycle (Lal 2004). The removal of soil organic carbon by accelerated erosion could be contributing to the 740 gigatonnes of carbon in the global mass of atmospheric CO₂, with emissions of 1 gigatonne of carbon/year (Lal 2005) not just affecting the carbon stock but also carbon mineralization. Quantifying both soil erosion and soil age contributes to the understanding of the complex nature of soil carbon storage and release dynamics (Harden et al. 1992). Soil organic matter is an indicator of soil quality and plays a major role in soil structure stability (Roose and Barthés 2001): soils reduced in organic carbon becoming looser and more prone to erosion (Six et al. 2000).

1.3 Methods for quantifying soil erosion

The almost century-long research into soils and soil erosion has resulted in the development of a number of different methods for quantifying soil erosion. It is beyond the scope of this project, to provide an exhaustive review of all these methods. Rather, I attempt below to provide only a summary, highlighting the advantages and limitations of different methods. Comprehensive reviews of the methods based on field observations have been provided by Loughran (1989), Boix-Fayos et al. (2006), Stroosnijder (2005), and Le Roux et al. (2007). The use of sediment budgets and sediment yield to quantify soil erosion has been reviewed by Dearing (1991), de Araújo and Knight (2005), Brown et al. (2009). Aksoy and Kavvas (2005) and de Vente and Poesen (2005) have reviewed modelling based approaches and Walling and He (1999), and Zapata (2003) provide comprehensive reviews on the use of fallout nuclides and tracers for quantifying soil erosion.

1.3.1 Methods based on direct observation

Methods based on direct observation include erosion plots, erosion pins, profilometers, and different levelling-surveying techniques, and are based on direct field observations, enabling the investigation of site-specific processes occurring in-situ, under natural conditions (Table 1.1). Of these methods, erosion plots are by far the most commonly used, having in some instances been adapted to allow for controlling boundary conditions and modifying factors such as rainfall intensity (e.g., Fister et al. 2010). With the exception of erosion plots, all methods based on direct observation make use of a benchmark (a reference point or surface) against which they compare, using digital or analogue measurement techniques, any surface changes (Haigh 1977, McCool et al. 1981, Shakesby 1993, Metternicht and Zinck 1998, Prosser et al. 2000, Couper et al. 2002, Bewket and Sterk 2003, Perroy et al. 2010). These methods are generally simple, easy to set up, and cheap to maintain. The period of observation can span hours to decades and measurements are either made at regular time intervals or are event-based. Methods making use of photogrammetric and remote sensing techniques represent a special sub-category. With these methods, the observations are made either before or after an event, and they usually involve higher initial costs, consisting of special training, purchasing of photographs or satellite imagery and of specialised software.

Data derived using methods based on direct observation have been extensively used for calibrating soil erosion models (Govers et al. 2007, King et al. 2005). However, as noted by Boardman (2006), this extensive use is predominantly due to the low cost and ease of application of these methods. For example, erosion plots have been used by Prosser and Rustomji (2000) to parameterise sediment transport capacity, by Zhang et al. (2008) to estimate the USLE K factor, by Arvidsson (2001) to parameterise hydraulic conductivity, and by Calvo-Cases et al. (2003) to parameterise runoff generation. Further, remote sensing techniques have been employed by Schmugge et al. (2002) to determine soil moisture and surface roughness, and by Baghdadi et al. (2008) to estimate surface roughness.

Methods based on direct observation have several important limitations. First, the locations where the observation sites are set up are carefully selected so as to avoid difficult terrain. Sites are often located where soil erosion rates are high, in which case the data they yield will usually be an overestimate of erosion rates across the landscape (Brazier 2004, Van Oost et al. 2009). As well, the observation methods are not standardised,

Table 1.1: Summary of methods based on direct observation.

Name	Principle behind method	Sample studies
Erosion plot	Surface runoff and sediment leaving a parcel of land is measured using various techniques. Size of parcel varies from 1m^2 to over 500m^2 . Erosion plot can be natural (<i>in situ</i>) or artificial (in a laboratory). Natural erosion plots can have artificial boundaries (made of concrete, wood, asbestos, etc.) or have no marked boundaries. Measurements are made at specific time intervals or are event based.	Le Bissonnais et al. (1998), Bewket and Sterk (2003), Boix-Fayos et al. (2006)
Erosion pins	Rods are inserted into the ground on a parcel of land (a few m^2 in area) and used as a reference mesh for monitoring erosion and deposition. Digital rods, known as Photo-Electric Erosion Pins (PEEP) allow for automated monitoring. Erosion pins have been used for estimating sheet wash, gully erosion, channel bank retreat, and for verifying erosion plot measurements.	Haigh (1977), Thorne (1981), Lawler (1991, 1993), Oostwoud Wijdenes and Bryan (2001), Couper et al. (2002)
Profilometer/Erosion bridge	Device consisting of a frame and rods, designed to monitor soil erosion without disturbing the soil. Profilometers can be analogue or digital, the latter allowing for automated monitoring.	McCool et al. (1981), Campbell (1981), Shakesby (1993), Prosser et al. (2000)
Linear erosion measuring instrument (LEMI)	A hybrid between erosion pins and profilometers enabling the estimation of soil erosion without disturbing the soil.	Toy (1983)
Levelling/Surveying	Non-disturbing surveying techniques focusing on estimating gully and rill erosion. Have been applied to areas between few m^2 to over 100 km^2 . Early studies used levels, measuring tape, poles, and cameras. Recent studies employ theodolites, GPS, LIDAR, air photographs, and satellite imagery.	Owens (1969), Pain (1968), Boardman and Robinson (1985), Whiting et al. (1987), Rice et al. (1988), de Jong et al. (1999), Pickup and Marks (2000), Van Lynden and Mantel (2001), Gomez et al. (2003), Collins and Walling (2004), Martinez-Casanovas (2003), Bierman et al. (2005a), Le Roux et al. (2007), Ledermann et al. (2008), Perroy et al. (2010)
The exposure of tree roots	The exposed upper-root-surface height for a number of tree roots is used to estimate sediment movement and soil erosion rate across a parcel of land. The technique has been applied to estimating soil erosion integrated over a period of up to 400 years.	Carrara and Carroll (1979), Vandekerckhove et al. (2001), Bodoque et al. (2005), Paroissien et al. (2010)

there being many variations as to how the sites are set up (e.g., erosion plots with or without boundaries; Stroosnijder 2005). There is also variability in the size of study sites (Le Bissonnais et al. 1998, Cerdan et al. 2004), the number of sites per study (Boix-Fayos et al. 2006), and the duration of observations (Nearing et al. 1999), these problems prompting Zapata (2003) to question the validity of extrapolating data obtained with these methods, both in space and time. Further, in the case of levelling techniques, measurement errors can be introduced by the operator, or by phenomena such as soil creep, soil swelling, animal disturbance, frost, cyclical changes of the ground surface, disturbance by cultivation, and by the presence of a deep litter layer (Loughran 1989, Shakesby 1993, Couper et al. 2002). Common problems associated with surveying techniques include: distortion within photographs, lack of continuous photography for a given location, cloud cover, surface moisture, and interpretation differences due to the use of different algorithms (Grieve et al. 1995, Collins and Walling 2004). Moreover, the different methods are each more suited to detecting distinct erosion processes. Erosion plots, for example are useful for estimating sheet and rill erosion, whereas erosion pins, levelling, and remote sensing are better suited for detecting gully erosion (Loughran 1989).

1.3.2 Methods based on sediment transportation and storage

Methods based on the transport and storage of sediment have been used in parallel with those based on direct observations to estimate catchment-averaged erosion rates as the volumes of transported and deposited sediment are indicative of the intensity of erosion in the sediments source areas (Walling and Webb 1987 and references therein, de Vente et al. 2007 and references therein). The different metrics employed include the sediment yield and its derivatives (i.e., specific sediment yield, sediment flux, and the sediment delivery ratio) and the sediment budget.

Sediment yield (i.e., outflow of sediment per unit time) has mainly been estimated from the dissolved-, suspended- and/ or bed-load leaving a catchment or an experimental plot (e.g., Daniels et al. 1987, Wilkinson et al. 2009), but also by employing remote sensing techniques (e.g., Sekhar and Rao 2002). Gauging stations are usually used for sediment yield measurements (e.g., Judson and Ritter 1964) but reservoirs (e.g., Owens and Slaymaker 1993), and small ponds (e.g., Verstraeten and Poesen 2002) have also been used. Sediment yield data provide erosion rate estimates that can average over years to

tens of years, but when used in combination with surveying and dating techniques such as various fallout radionuclides and cosmogenic nuclides the averaging time can be increased to hundreds to tens of thousands of years (de Araújo and Knight 2005).

Sediment yield and all other methods based on transport of sediment have several limitations. First, they yield a single estimate of erosion that aggregates over different processes and may obscure information on sediment sources (Aksoy and Kavvas 2005, de Araújo and Knight 2005, Boardman 2006). Further, erosion rates obtained this way represent minimum estimates (Brown et al. 2009) as storage of sediment is common in catchments. An increase in sediment yield does not necessarily mean an increase in erosion rate, as the former could be the result of remobilisation of old sediment (Dearing 1991). Moreover, high-magnitude low frequency events such as jökulhaups, for example will increase sediment yield and therefore bias the erosion rate estimate (Starkel 1976, Morgan 1985, Bork 1989, Claessens et al. 2006, Brazier 2004, Rommens et al. 2005). Sediment yield estimates can also be influenced by rainfall (e.g., Oguchi et al. 2001), sudden tectonic processes (e.g., Korupa et al. 2004), lithology and vegetation (e.g., de Vente and Poesen 2005, Molina et al. 2008), and human activity such as land use changes and damming (e.g., Jennings et al. 2003, Merritts and Walter 2003, Vanacker et al. 2005). There can also be natural cyclic variations in sediment yield (Walling and Webb 1987). Further variability can also be introduced by changes in the sampling strategy at a given site since the beginning of monitoring (e.g., Bierman et al. 2005b).

In the case of estimating sediment budgets, the sedimentary archive acts as a proxy for sediment production (Dietrich and Dunne 1978, Fuchs 2007). The main advantage of using sediment archives is that these allow for the analysis of sediment flux over the Holocene, which is necessary to evaluate the cumulative impact of human activities (Brown et al. 2009, Förster and Wunderlich 2009). However, the accuracy of these evaluations is conditional on the method used for the calculation of sediment volumes and the dating techniques applied (Rommens et al. 2005). Further, the older the sediment archive, the more prone it is to hiatuses and the more uncertain the interpretation becomes (cf. Wilenbring and von Blanckenburg 2010a).

A further limitation with using any sediment archive, be it alluvial (e.g., Houben et al. 2006, de Moor and Verstraeten 2008), colluvial (e.g., Bertran 2004), lacustrine (e.g., Dearing 1991, Edwards and Whittington 1993, de Vente and Poesen 2005), or deltaic

(e.g., Erkens et al. 2006), is that it summarises factors such as for example sediment supply, transport efficiency, basin morphology, water circulation, shoreline stability etc., in one single value, and so the results are prone to influence by the choice of sampling strategy (Edwards and Whittington 2001). In response to this, there are now attempts to develop spatially distributed sediment budget determination strategies, these having more value since they try to link erosion, transport, and deposition over larger scales and in more detail (Wilkinson et al. 2009, Ali 2009).

1.3.3 Methods based on radionuclides

The use of fallout radionuclides in soil erosion studies has increased in recent years (Hacıyakupoglu et al. 2005). In addition to providing erosion rate estimates, these methods can also enable the estimation of depositional rates, the differentiation between different sediment sources, the construction of catchment-wide sediment budgets, and the validation of catchment-scale sediment flux models (Smith and Dragovich 2008). These methods are based around artificial tracers (e.g., ^{46}Sc , ^{51}Cr , ^{59}Fe , ^{110}Ag , ^{198}Au , Cu solutions), naturally formed fallout radionuclides (e.g., ^7Be , ^{10}Be , ^{210}Pb , ^{32}Si), artificially generated fallout radionuclides (e.g., ^{137}Cs , ^{239}Pu , ^{240}Pu), and naturally occurring radionuclides (e.g., ^{86}Sr , ^{13}C) (Zapata 2003) (Figure 1.1).

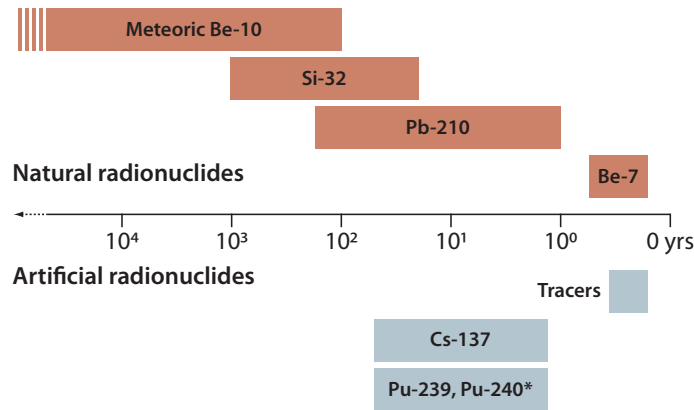


Figure 1.1: Summary of methods based on radionuclides showing the timescales over which these can be applied. *Note that as an artificially generated fallout nuclide, despite its relatively long half-life (6560 years), the timescale over which ^{240}Pu can be applied to study soil erosion is the same as for ^{137}Cs and ^{239}Pu .

The main characteristic of artificial tracers is that they bond strongly to the silt, clay and organic fractions in soils. The use of artificial tracers is limited to small areas and short timescales (from days to months) (Coutts et al. 1968, Loughran 1989), and the choice

of tracer depends on the characteristics of the study area (Krause et al. 2003). The use of artificial tracers is decreasing as these can be harmful to living organisms.

The naturally occurring fallout radionuclides, ^7Be (half-life of 53.3 days), ^{10}Be (half-life of 1.39 million years), and ^{32}Si (half-life of 144 years), are formed in the upper atmosphere by the bombardment of N, O, and Ar nuclei, respectively, by high-energy secondary cosmic particles. ^{210}Pb , with a half-life of 22.26 years, is a member of the ^{238}U decay series, being the decay product of ^{222}Rn . After being produced in the atmosphere, all of these radionuclides find their way quickly into the soil mainly by precipitation, but also through dust deposition (Appleby and Oldfield 1983, Wallbrink and Murray 1994, McHargue and Damon 1991, Barg et al. 1997, Willenbring and von Blanckenburg 2010b).

Fallout radionuclides, such as ^{10}Be are usually concentrated in the upper part of the soil profile, except for older or more slowly eroding soils, in which case the profile features a hump, the maximum concentration being located at some depth below the surface (Wallbrink and Murray 1996, Kaste et al. 2002, You et al. 1989, Graly 2011). In the case of ^7Be and ^{10}Be , the depth distribution of concentrations is also controlled by soil acidity - in soils with low pH values beryllium tends to adsorb onto aluminosilicate minerals, organic compounds, and/or to precipitate as hydroxyoxides. These fallout radionuclides have been used as a tracer for discriminating topsoil and deepsoil sources (Walling and Quine 1995, Owens et al. 1999), for providing spatially distributed information on the erosion and re-deposition of soils (Jungers et al. 2009, Schuller et al. 2010), for detecting movement of hillslope material (McKean et al. 1993), for estimating residence time of eroded sediment (Kato et al. 2010), for estimating sediment accumulation (Battarbee et al. 1985, Miguel et al. 2003), and for detecting the magnitude of erosion during major storm events (Blake et al. 1999, Matisoff et al. 2002, Sepulveda et al. 2008).

There are several important assumptions behind the use of fallout radionuclides such as ^{10}Be and ^7Be . First, it is assumed that the fallout rate is spatially uniform, and that any pre-existing nuclide inventory is also uniformly distributed in space. Further, it is also assumed that these nuclides find their way into the soil quickly and that they are only remobilised by soil movement (Walling et al. 1999). ^{32}Si has the potential to bridge the time range between 30-1000 years, currently not covered by any other fallout radionuclide, but, due to its low production rate, the detection of ^{32}Si is difficult (Fifield and Morgenstern 2009, Gale 2009), and so there remains a need for soil erosion dating techniques that cover

longer time scales, such as the Holocene. In the case of ^{210}Pb , studies do not usually take into account the post-depositional mixing of sediment (Petit 1974, Robbins et al. 1977, Kato et al. 2010) and fail to assess any of the factors controlling ^{210}Pb accumulation (Gale 2009). There are also exceptions like for example the study of Bishop et al. (2010) who explicitly use the depth distribution of ^{210}Pb to confirm that mixing of sediment has taken place.

The artificially generated fallout nuclides, such as ^{137}Cs (half life of 30.2 years), ^{239}Pu (half life of 24.1 years), and ^{240}Pu (half life of 6560 years), are the product of the thermonuclear weapons tests that started in the mid-twentieth century. The concentration of these nuclides peaked as the tests peaked in 1963 and then declined below detection levels in the atmosphere after the mid 1980's (Smith and Dragovich 2008). Nuclear tests, such as the ones carried out by France and China between 1966 and 1980, and accidents, such as at Chernobyl in 1986 and at Fukushima in 2011, caused perturbations in the fallout pattern (Campbell et al. 1988, Loughran 1989, Ritchie and McHenry 1990, Wicherek and Bernard 1995, Wallbrink and Murray 1996, Hacıyakupoglu et al. 2005, Bisinger et al. 2010, Kato et al. 2010, Yasunaria et al. 2011) introducing uncertainties in the usage of these nuclides (Stroosnijder 2005).

As for the beryllium isotopes, the fallout of artificial radionuclides varies within latitudinal zones as a function of precipitation, but can also be influenced by slope angle and orientation, exposure to precipitation, and by wind direction and velocity. Due to this variability in fallout rates, studies employing these radionuclides require base level concentration determinations at undisturbed sites, the latter often being quite difficult to find (Wicherek and Bernard 1995, Stroosnijder 2005). Again, as for the natural fallout isotopes, caesium and plutonium adsorb rapidly to the finer soil particles - with plutonium being less mobile and therefore more reliable (Everett 2009) - and accumulate in the upper few cm of the soil profile, their concentration decaying exponentially with depth (Smith and Dragovich 2008). A uniform concentration depth-profile is indicative of mixing (Ritchie and McHenry 1990), reduced concentrations suggest erosion whereas increased nuclide inventories are indicative of deposition (Hacıyakupoglu et al. 2005).

Fallout ^{137}Cs has been successfully used for investigating water-induced soil erosion on both cultivated and undisturbed soils in a wide range of environments (Kato et al. 2010) and on various spatial scales: from experimental plots to entire watersheds (Smith

and Dragovich 2008). A single visit to the field allows for the estimation of soil erosion integrated over a period of 30-40 years. ^{137}Cs determinations can provide information on soil erosion and deposition, can be used to discriminate between different processes (e.g., tillage versus sheet erosion), and when used as a fingerprinting technique, ^{137}Cs can discriminate between sources of sediment (Zapata 2003). Further, ^{137}Cs can be used to study the dynamics of soil erosion, as there is a strong correlation between soil organic carbon, nitrogen, and ^{137}Cs (Xiaojun et al. 2010).

The main limitations of artificial fallout nuclides are the uncertainties surrounding the fallout pattern and nuclear testing. Furthermore, all fallout nuclides, with the exception of ^{10}Be , are only applicable to study of contemporaneous erosion events and so are not suitable for assessing soil erosion over Holocene timescales.

Other soil erosion detection methods based on isotopes include the use of the $^{87}\text{Sr}/^{86}\text{Sr}$ ratio, and of the stable carbon and nitrogen isotope ratios. If strontium is contributed to the soil from different sources with distinct isotopic signatures, the $^{87}\text{Sr}/^{86}\text{Sr}$ ratio can provide clues as to the timing and magnitude of ancient soil erosion (Rabenhorst and Wilding 1986, Cooke et al. 2003). However this ratio may also be modified as a function of depth within the soil profile, soil age, and precipitation amount (Miller et al. 1993, Borg and Banner 1996, Kennedy et al. 1998, Stewart et al. 2001). In similar fashion, Alewell et al. (2008) use the variation of $\delta^{13}\text{C}$ and $\delta^{15}\text{N}$ in soil profiles taken at different locations along a slope was used to qualitatively assess soil degradation. Although this is promising, the $\delta^{13}\text{C}$ and $\delta^{15}\text{N}$ of soil profiles cannot provide quantitative constraints on soil erosion since these isotopes are suitable only for detecting soil movement by measuring the isotopic signal of the replaced surface organic material.

1.3.4 Methods based on modelling

Although providing detailed understanding of the erosion processes, field studies for assessment of soil erosion are time-consuming and need to be conducted for extended periods of time (Saha 2004). Models on the other hand are relatively inexpensive and can be used to simulate erosion over large spatial and temporal scales. More importantly, models are capable of simulating the complex interactions of the processes of soil erosion. The use of models for studying soil erosion started in the 1930s and to date a large number of models have been developed. It is beyond the scope of this thesis to provide a comprehensive

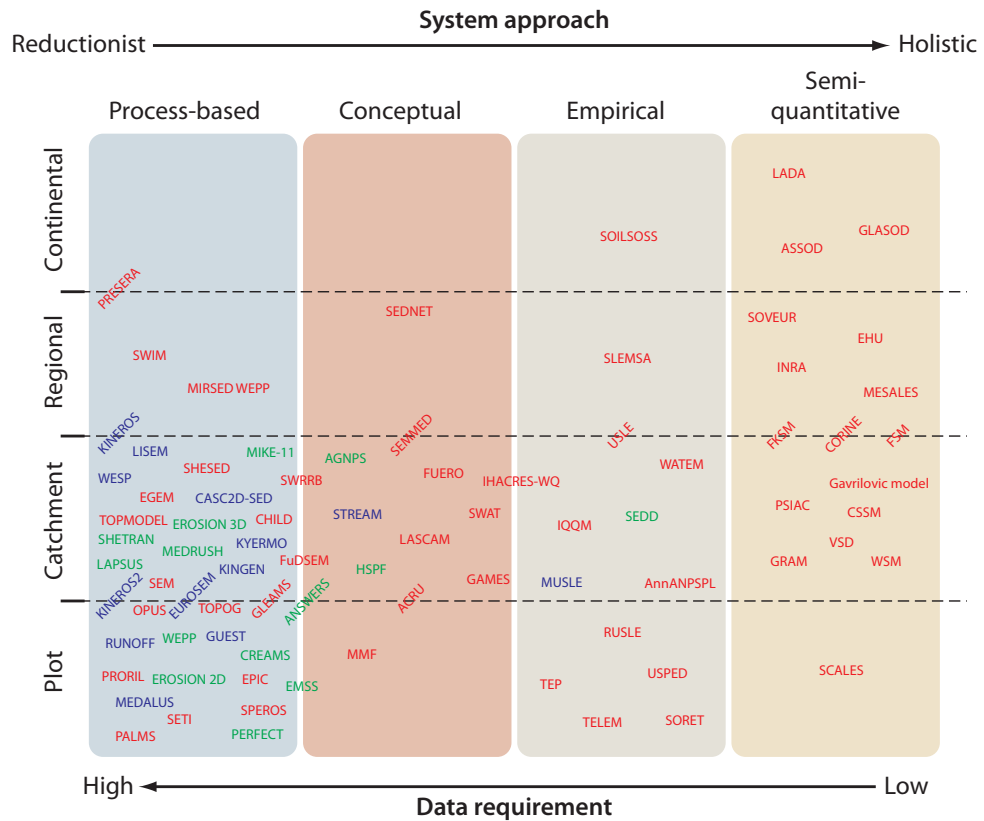


Figure 1.2: Summary of the different types of soil erosion models. Colours used for model names have the following meaning: red - continuous, blue - event based, green - models that deal with both continuous and event based soil erosion.

review of all current models. Instead, I provide a brief summary focusing on how the models are constructed and on how they treat the modelled domain. All existing models are deterministic in that the erosion and sediment transport processes are formulated using deterministic differential equations. Thus, none of the models is capable of considering fully the stochasticity of the erosion and sediment transport processes (Aksoy and Kavvas 2005).

In terms of their construction, soil erosion models can be classed as semi-quantitative, empirical, conceptual, and process-based, although most models do not fall strictly into only one category (Figure 1.2).

Semi-quantitative models use a combination of descriptive, scoring and quantitative procedures to assess soil erosion and sediment yield mainly at the catchment scale. These models offer a holistic approach towards erosion and sediment yield modelling (de Vente and Poesen 2005), but concerns have been raised with respect to the objectivity of scoring

(Le Roux et al. 2007).

Empirical (or regression) models, such as USLE and its variants, are based on field observations, are relatively simple, and have only modest data and computational requirements. The empirical nature of these models, however, means that they are limited to the areas where they have been developed. Nonetheless, the simplicity of empirical soil erosion models has made these the choice of models for decision makers (Beach 1987, Bhattarai and Dutta 2007, Le Roux et al. 2007, Zhang et al. 2009), also meaning that they are often misused (Trimble and Crosson 2000).

Conceptual models are based on a conceptual framework of erosion, hence the name. These models represent reality better than empirical models by incorporating into their structure the underlying mechanisms of sediment transfer and those of runoff generation, representing flow paths in a catchment as a series of storages (de Vente and Poesen 2005). Conceptual models are characterised by simplicity and are potentially applicable to large spatial and temporal scales.

Process-based models (also known as physically-based models) are the most sophisticated of the soil erosion models, making use of fundamental physical equations to describe erosion processes effectively. Despite this complexity, however, process-based models have many disadvantages. First, most of our knowledge on erosion processes is derived from plot-scale studies (Kirkby 1999). Further, the mathematical representation of natural processes can only be approximate and there are difficulties with parameter selection (Zhang et al. 1996, Saha 2004, Bhattarai and Dutta 2007, Le Roux et al. 2007). Many scientists advocate process-based models because (1) the models simulate real processes, and (2) since they are built on physical laws, these models do not suffer from extrapolation problems such as the empirical soil erosion models, and so can, at least in theory, be transferred to different environmental conditions (de Vente and Poesen 2005). The drawback to many such models, however, is that they require large amounts of data and computational time (Merritt et al. 2003, Beach 1987) and the combination of processes is oversimplified and ignores many complex process feedbacks (Zhang et al. 1996).

In terms of how they treat the modelled domain, soil erosion models can be classed as either lumped models or distributed models. As opposed to lumped models, distributed models incorporate spatially distributed parameters and treat the spatial variability of erosion and of the factors that control erosion, explicitly (Van Rompaey et al. 2001).

Distributed models need more input data than lumped models, and as a consequence model validation is also more troublesome for the former (Takken et al. 1999, Jetten et al. 2003). The advantage of distributed models over lumped models is that the former can be extended to entire landscapes, such as for example, is the case with whole landscape evolution models (Willgoose 2005, Codilean et al. 2006, Tucker and Hancock 2010). Most soil erosion models in use today are spatially distributed, part of the reason behind this being the developments that occurred in the fields of Geographic Information Systems (GIS) and Remote Sensing (Burrough and McDonnell 1998). GIS and Remote Sensing have been instrumental in obtaining the spatially and temporally distributed data that soil erosion models use as input. Further, GIS has provided the framework and software on which many of the currently used spatially distributed soil erosion models are based (Burrough and McDonnell 1998).

Despite both the large number of existing soil erosion models (Figure 1.2) and their diversity, the modelling of soil erosion suffers from a range of problems. First, relatively few efforts have been made to test the underlying concepts and assumptions, and complex interactions between erosion processes (de Vente and Poesen 2005, Govers et al. 2007). Further, a major gap exists between the ways soil erosion rates are measured and our understanding of the actual processes behind these rates (Wainwright et al. 2003, Parsons et al. 2004, 2006), and this flaws our understanding of the relevance of current erosion rates. For example, Govers et al. (2007) showed that the basic assumptions used to model rill erosion are to some extent flawed. Oversimplification is a further example of a problem where tillage or gully erosion is neglected (Van Rompaey et al. 2003, Van Oost et al. 2009) causing under- or over-estimation of erosion. The second problem is that of data availability. Data are needed as input to these models and are also needed to validate the results (Bennett 1974, de Vente et al. 2006, Bonilla et al. 2008, Van Oost et al. 2009). The issue of data availability is especially important as model complexity increases, as more complex models have higher data requirements (Merritt et al. 2003, Aksoy and Kavvas 2005, Le Roux et al. 2007).

1.3.5 Methods based on age dating

In addition to the methods described in the previous sections, a few others, largely based on assessing the completeness of a soil profile (or other stratigraphic records, such as lake

sediments), have also been employed for estimating soil erosion. Reconstructing soil profiles allows the assessment of total erosion over longer periods of time, placing the modern erosion in a historical context (Loughran 1989, Jankauskas and Fullen 2002, Boardman 2006). The principle behind these methods is that at adjacent sites the stratigraphic records, such as the soil profiles, for example, will have the same horization, and any differences should be indicative of erosion (Kelly et al. 1988, Huggett 1998, Brown et al. 2009). Although these methods can be applied on their own, determining the timing of any soil erosion requires them to be used in conjunction with an absolute dating technique. Moreover, their applicability is also limited by natural variability (Lewis and Lepele 1982). Thus reconstructing soil profiles works best in places where soil profiles are specific to pedogenesis like luvisols in loess, glacial till, glaciofluvial deposits or siltrich eolian sands (Rommens et al. 2005, Brown et al. 2009).

Similar benefits can also be achieved at depositional sites when combining soil profile characterization or sedimentary archives with tephrochronology or palyno-ecological studies. In volcanic regions, tephra deposits provide a unique stratigraphic record as tephras associated with different volcanic eruptions have specific and distinct physical or chemical characteristics. Layers between sites can be correlated and the age of these can be determined by linking each tephra layer with the eruption that produced it. Tephrochronology has been applied to determining accelerated soil erosion by Page and Trustrum (1997) and Dugmore et al. (2009) in New Zealand and Iceland respectively. The principle behind palyno-ecological studies is similar, in that land use and vegetation changes through time produce distinct pollen signatures in the various stratigraphic layers and so the approximate age of these layers can be determined using the pollen record (e.g., Noel et al. 2001).

The mineral-magnetic properties of lake or reservoir sediment assemblages have also been used to estimate soil erosion in the sediments source areas as high or increasing concentrations of magnetic minerals in sediments can reflect changes in the magnitude and intensity of erosion in catchments (Wang et al. 2008). However, applications of this approach may be limited by problems related to sediment transport and storage in stream channels or catchments, the distribution of sediment sources, and the depositional pattern in lakes or reservoirs (Dearing and Foster 1993). Furthermore, influences of dissolution, diagenesis, authigenesis and dilution on mineral-magnetic characteristics of sediments should be accounted for when sedimentary magnetic records are used to assess catchment-wide

soil erosion (Wang et al. 2008).

As for the absolute dating techniques that have been employed in conjunction with soil profile and other stratigraphic reconstructions, the most important are radiocarbon dating and optically stimulated luminescence (OSL). There is a vast amount of literature regarding radiocarbon measurements (Hajdas 2009, and references therein). Organic material and carbonates found in sedimentary deposits can be used to date the deposition of sediment and hence to infer average amounts of erosion of a source area that are needed to produce that volume of sediment. However, due to a plateau in the radiocarbon calibration curve between AD 1650 and AD 1950 (or 50 and 350 years BP), the method is imprecise when applied to the last 400 yrs because multiple calendar ages can be attributed to one single radiocarbon determination. Moreover, using uncalibrated ages one could interpret erosion rates to be faster than they are (Brown et al. 2009, Cornu et al. 2009, Gale 2009). Further uncertainties also arise from the ^{14}C reservoir correction required in the case of material of marine origin such as shells (Fifield and Morgenstern 2009). Additional problems associated with radiocarbon dating include the variation of ^{14}C content in the atmosphere, the hard-water effect, possible hiatuses in the sediment, the incorporation of old organic carbon matter or the incorporation of young root matter in the dated sediment, and in the case of carbonate dating, the dissolved carbon dead parent material (Lowe 1991).

OSL is often employed (Aitken 1998) in areas where there is no organic material and thus radiocarbon dating cannot be used (Lang 2003, Alexanderson and Murray 2010). Despite recent efforts to improve the OSL technique (Bailey et al. 2001, King et al. 2011), there are still problems related to incomplete bleaching of the inherited luminescence signal prior to burial, resulting in an age overestimation, in particular in young (~ 1 kyr) samples (Olley et al. 1998, Stokes et al. 2001, Jain et al. 2004, Fuchs et al. 2007). The low radiation doses which some samples receive may also limit the applicability of the technique in few hundred year old samples. In addition, temporal variations in the moisture content, depth of burial and bulk density of sediments may be difficult to reconstruct. Yet changes in these properties may have a dramatic impact on dose rates and thus on age estimates (Woodborne and Vogel 1997, Madsen et al. 2005, Gell et al. 2007, Hoare et al. 2009).

A new technique for quantifying soil age and processes has recently emerged, via the dating supergene minerals such as Fe-oxides (Short et al. 1989, Pidgeon et al. 2004, Shuster et al. 2005, Bernal et al. 2006), and as Mn-oxides (e.g., Vasconcelos 1999) with U-series

(from few kyr to 500 kyr) or (U-Th)/He (for 500 years) combined with $^4\text{He}/^3\text{He}$ and $^{40}\text{Ar}/^{39}\text{Ar}$ method (for 2 kyr). The related dating issues are discussed by Cornu et al. (2009).

1.3.6 Summary

Studies dealing with soil erosion can be divided into two groups: those interested in its agro-economic implications and those interested in its geomorphological implications. All agro-economic applications require results quickly and easily so that decision-making can be facilitated. Therefore, agro-economic studies differ substantially from those of a geomorphic nature, the latter trying to address broader scientific questions, including the magnitude, speed, and acceleration of soil erosion, how to identify the controls on soil erosion over different spatial and temporal scales, and how to couple sediment transfer with sediment yield and sediment sources. These two different approaches to the study of soil erosion mean that there are inconsistencies in the literature with respect to terminology. For example, the meaning of the terms long-term and short-term mean 100 years (most of the ^{137}Cs studies and some plot studies) and days/months, respectively, for the agro-economic soil erosion community (Schuller et al. 2006) whereas, for the geomorphological community, the two terms generally mean several hundred years as short term (Kaste et al. 2007) and the geological time frame for long term (Montgomery 2007). Soil erosion occurs over a wide variety of temporal and spatial scales and different processes and interactions likely dominate at these different scales. A large number of approaches for observing and/or measuring soil loss have been developed, leading to a lot of variability and inconsistencies in erosion studies. Most of the short timescale field measurements are limited by the fact that they do not account for erosion processes such as sediment transport and redistribution (Brazier 2004), and, in cases where they do, these different processes are dealt with in isolation (de Ploey 1990). Field and lab measurements play an important role in the study of soil erosion processes; however, results obtained with different techniques often do not match (Brazier 2004) and are limited in usage to short term (maximum few hundred years) and local processes (Boix-Fayos et al. 2006). It has been hoped that the limitations of field measurements would be overcome by the use of models (Figure 1.2). Despite the large number of models developed over that last century, this is yet to be achieved, partly because these models are themselves dependent on field

data for parameter calibration and model validation (Bennett 1974, Lal 2001, Walling et al. 2003, Hancock 2004, Stroosnijder 2005, Peeters et al. 2006). It has proven difficult to quantify rates of erosion and deposition and their spatial distribution (Brown et al. 2009, and references therein) and it is unreasonable to envisage that one single method will ever be applicable to all settings and scales (Le Roux et al. 2007). Recently, dating techniques have begun to play an important role in understanding soil processes (Hallet and Putkonen 1994), especially in the dating of ancient soils (Rommens et al. 2005, Gale 2009) as the latter can provide estimates on natural, background soil erosion rates.

Although age-controlled process rates data related to soils are still sparse (Schaller et al. 2004), different dating techniques, such as ^{14}C (Wells et al. 1987, Trumbore 1993, Anselmetti et al. 2007), U-Th series radionuclides (Cornu et al. 2009, Ma et al. 2010), OSL (Fuchs and Lang 2001), meteoric and *in situ* produced cosmogenic nuclides (Barg et al. 1997, Small et al. 1999, Heimsath et al. 1997, 1999, 2000, McKean et al. 1993, Riebe et al. 2003, Wilkinson and Humphreys 2005, Schaller et al. 2009, 2010), have been employed successfully. Of the aforementioned novel techniques, cosmogenic nuclide analysis is perhaps the most promising in terms of quantifying soil erosion, as it enables the quantification of both catchment-wide and at-a-site erosion rates, and is sensitive over the millennial timescales relevant to soil production and soil erosion. In the following section of this chapter I provide a brief introduction to cosmogenic nuclides describing the ways in which the technique can be applied to quantifying the magnitude and timing of at-a-site Holocene soil erosion events.

1.4 *In situ* produced terrestrial cosmogenic nuclides

Cosmogenic nuclide determinations are now made routinely (Figure 1.3), and the technique has been summarised in a number of review articles and more recently in a book (Dunai 2010). Given these recent publications, providing a thorough review of the technique here would be redundant. Instead the remainder of this section will summarise the principles behind the technique and its main applications to geomorphology.

The first comprehensive review of the technique has been provided by Gosse and Phillips (2001), and this has now been superseded by the work of Dunai (2010). The technical aspects of the method have also been reviewed by Cerling and Craig (1994)

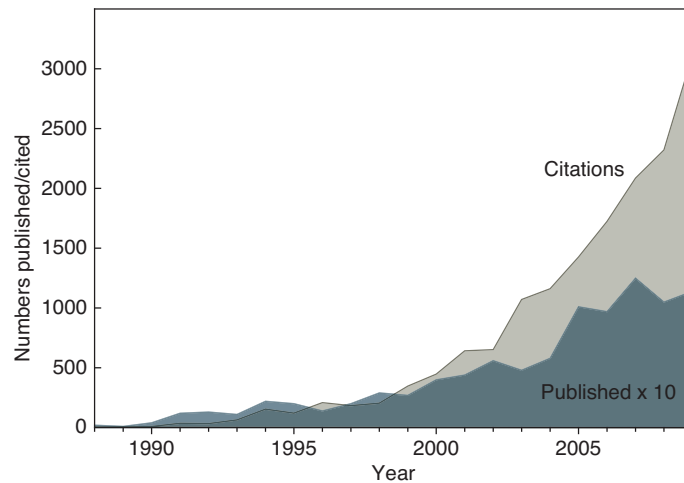


Figure 1.3: Number of publications on applications of cosmogenic nuclides to the study of surface processes and citations thereof. The number of publications is multiplied by ten to allow use of a common scale. Figure adapted from Dunai (2010).

and Niedermann (2002), and Bierman (1994), Bierman and Nichols (2004), Cockburn and Summerfield (2004) and von Blanckenburg (2005) have provided reviews of the geomorphological applications of cosmogenic nuclides. More recently Akçar et al. (2008) have reviewed the archaeological applications of cosmogenic nuclide analyses.

1.4.1 Theory and applications

Cosmogenic nuclides are produced by the interaction of high-energy secondary cosmic particles with target nuclei, such as ^{16}O , ^{27}Al , ^{28}Si , and ^{56}Fe (Dunai 2010, and references therein), in the upper few metres of the Earth's crust. Several of these nuclides, including ^3He , ^{10}Be , ^{21}Ne , and ^{26}Al , ^{36}Cl are now measured routinely, whereas the analysis of others, such as ^{14}C is still in an experimental phase. Given the very low concentration of cosmogenic nuclides in terrestrial samples, the measurement of these is only possible through accelerator mass spectrometry (AMS), in the case of radionuclides, such as ^{10}Be and ^{26}Al , and noble gas mass spectrometry, in the case of ^3He and ^{21}Ne (Elmore and Phillips 1987).

The high-energy cosmic ray flux is composed mainly of charged nucleons (mainly protons), and so the spectrum of the cosmic ray flux that penetrates Earth's atmosphere is highly dependent on the Earth's magnetic field. Thus, the production of cosmogenic nuclides at the Earth's surface varies with geomagnetic latitude - increasing between the

equator and 60° N and S latitude and remaining invariant for latitudes $> 60^\circ$ (Dunai 2010). The secondary cosmic rays are attenuated by the Earth's atmosphere, and so production rates also decrease with an increase in the thickness of penetrated atmosphere (Lal 1991, Dunai 2000, Stone 2000, Lifton et al. 2005). Other factors that influence the production rates of cosmogenic nuclides include the geometry of the surrounding topography and the geometry of the surface itself, which may shield a proportion of the incoming cosmic radiation (Dunne et al. 1999, Codilean 2006).

The concentration of cosmogenic nuclides in a sample is proportional to the amount of time that the sample has been exposed to cosmic radiation. Thus, if a surface has not experienced substantial erosion, the cosmogenic nuclide concentration in a sample from that surface will provide the exposure age of the surface (Lal 1991). However, if after exposure, the surface is buried by material of sufficient thickness to stop the further accumulation of cosmogenic nuclides, the differential decay rates of cosmogenic radionuclides (such as ^{10}Be and ^{26}Al) in a sample from that surface can be used to estimate the time elapsed since burial (Granger and Smith 2000, Granger and Muzikar 2001). In cases where a surface is experiencing ongoing denudation, the cosmogenic nuclide concentration in a sample from that surface can be used to estimate a rate of denudation. Denudation rates can be determined from either bedrock or sediment samples. Bedrock samples yield at-a-site erosion rates that only apply to the bedrock surface from where the sample was collected. On the other hand, sediment samples yield average rates that apply to the sediment's source area. A more advanced technique uses the frequency distribution of cosmogenic nuclide concentrations in a large number of grains leaving a catchment to obtain a spatially distributed erosion history of the whole catchment (Codilean et al. 2008).

1.4.2 Quantifying soil erosion using cosmogenic nuclide depth-profiles

Different cosmogenic nuclides have different production pathways, and the production rates for these different production pathways attenuate differently with depth (Strack et al. 1994, Brown et al. 1995, Heisinger et al. 1997, 2002a,b). Thus, at least in theory, the depth-profiles of cosmogenic nuclides can provide more information on the processes that operate at the Earth's surface than a single nuclide concentration obtained from a surface sample (cf. Braucher et al. 2003, Kim and Englert 2004, Schoenbohm et al. 2004). Within a surface that is eroding, a cosmogenic nuclide will reach steady state much faster at the

surface than at depth as a result of the greater depth penetration of muons as compared to neutrons. Thus, the muon component is less sensitive to short-term fluctuation of the erosion rate and may be used to quantify a mean erosion rate with a longer averaging timescale than that recorded by neutrons (Braucher et al. 2003).

The production of cosmogenic nuclides decreases exponentially with depth, and can be described by the following (Granger and Smith 2000, Granger and Muzikar 2001):

$$N(z, t) = \frac{1 - e^{-\lambda t}}{\lambda} \sum_{i=4}^4 P(0)_i e^{-\rho z / \Lambda_i} \quad (1.1)$$

where $N(z, t)$ is the cosmogenic nuclide concentration (atoms.g^{-1}) acquired by a sample as a function of time and depth below the surface, λ is the radioactive decay constant, calculated as $\ln(2)/T_{1/2}$, with $T_{1/2}$ being the radioactive half-life of the cosmogenic nuclide (yrs), t is the amount of time (yrs) since nuclide production began, $P(0)_i$ is the surface production rate ($\text{atoms.g}^{-1}.\text{yr}^{-1}$) of a given cosmogenic nuclide by a given production pathway (i.e., high energy neutrons, and slow and fast muons), ρ is the density of the target material (g.cm^{-3}), and Λ_i is the absorption mean free path for nuclear interacting particles in the target mineral for a given production pathway (g.cm^{-2}).

This exponential decrease is an especially useful property in landscapes that exhibit high erosion rates or those that have been subjected to burial (Balco and Rovey II 2008). Furthermore, the exponential decrease in nuclide production with depth has also been exploited to understand how ice has shaped the landscape (Goodfellow 2008, Morgan et al. 2010), to study long-term structural deformation rates (Siame et al. 2004), to quantify slip rates (Vassallo et al. 2005), to trace sediment sources (Phillips et al. 1998), and to estimate the depositional age of alluvial material (Anderson et al. 1996, Repka et al. 1997, Briner and Swanson 1998, Hancock et al. 1999, Schaller et al. 2010, Hein et al. 2009, Goehring et al. 2010).

Given the ‘vertical’ nature of soil processes, most studies involving soils and employing cosmogenic nuclides have used cosmogenic nuclide depth-profiles. For example, Brown et al. (1994) and Braucher et al. (1998) have used *in situ* ^{10}Be depth-profiles in lateritic tropical soils to explain the formation of certain soil deposits. Phillips et al. (1998), using a model of soil burial by colluvium and bioturbation in combination with ^{21}Ne measurements in depth-profiles, were able to estimate inheritance-corrected exposure ages

in stream terraces and an alluvial fan. Further, Schaller et al. (2003) combined ^{10}Be measurements in cover bed depth-profiles and river sediment in order to determine the effect of cover beds on catchment-wide erosion rate determinations.

The examples presented in the previous paragraph are all based on the work of Anderson et al. (1996), who showed that a cosmogenic nuclide depth-profile in an alluvial deposit can be used to calculate the depositional age of that deposit by explicitly accounting for the inherited nuclide component. In short, Anderson et al.'s (1996) method works by reconstructing the cosmogenic nuclide depth-profile of the alluvial deposit and using the shift in this profile to estimate the amount of time elapsed since emplacement of that deposit (Figure 1.4). This principle, if inverted, can at least in theory be applied to quantifying at-a-site soil erosion events in soils formed on deposits of known age. For example, if the depositional age of the deposit on which the soil is formed is known, a 'zero-erosion' theoretical cosmogenic nuclide depth-profile can be constructed and compared to the cosmogenic nuclide depth-profile measured in the soil/deposit. Any discrepancies between the two cosmogenic nuclide depth-profiles (measured and theoretical ['zero-erosion']) will be a quantitative indication of erosion.

Given that the aim of this study is to quantify both the amount and timing of at-a-site Holocene soil erosion events, two cosmogenic nuclides must be used, as there are two unknowns. Results from a modelling study by Phillips (2000) suggest that only *in situ* ^{14}C , with its relatively short half-life of 5.7 kyr, is fully capable of discriminating between different soil accumulation and soil erosion scenarios, this nuclide's depth-profile permitting both bioturbated deposits and anomalous nuclide inheritance to be identified. A similar message is also conveyed by the results of the sensitivity analyses presented in Figure 1.5 - the different scenarios are resolvable only when ^{10}Be is used in conjunction with ^{14}C .

1.5 Objectives and organisation of thesis

As noted earlier, the aim of this study is to assess the extent to which the amount and timing of site-specific Holocene soil erosional events can be quantified using depth-profiles of *in situ*-produced cosmogenic ^{10}Be and ^{14}C . Most of Scotland's soils are formed on glacial till and so this work focuses on two Loch Lomond Readvance (LLR) glacial moraines as its study sites. Unlike in the case of soils that form by the in-situ weathering of the underlying

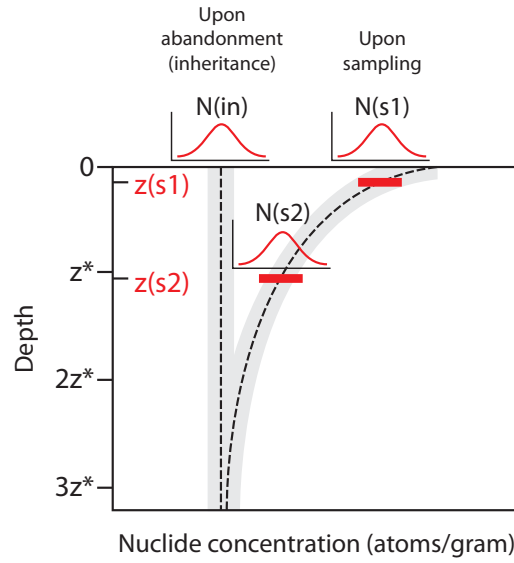


Figure 1.4: Schematic illustration of post-depositional accumulation of *in situ* cosmogenic nuclides at various depths. Upon deposition, alluvial clasts have varying cosmogenic nuclide inheritance (grey envelope around vertical dashed line) but are assumed to have been emplaced with uniform nuclide inheritance with depth characterised by mean nuclide concentration $N(in)$. Subsequent accumulation of cosmogenic nuclides results in an exponential nuclide decay depth-profile. The mean concentrations derived from two samples - (s1) collected close to the surface and (s2) collected from a certain depth - will differ from one another only by the post-depositional component. Thus both $N(in)$ and elapsed time since deposition of clasts can be calculated from measured nuclide concentrations of amalgamated samples. Modified from Anderson et al. (1996).

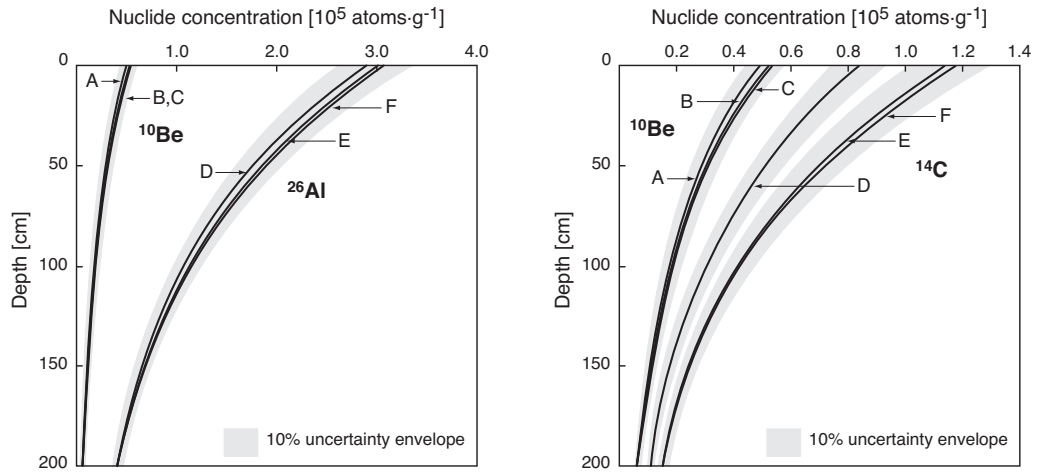


Figure 1.5: Hypothetical depth-profiles of concentrations of cosmogenic ^{10}Be , ^{26}Al and ^{14}C in a 10.5 kyr-old sedimentary deposit with various timings of surface erosion: A and D: 0 kyr (last few centuries); B and E: 4 kyr; and C and F: 6 kyr. *in situ* ^{14}C discriminates better between the different scenarios because of its shorter half-life, enabling the distinguishing of Middle Holocene erosion events from modern. 10% uncertainty envelopes (covering production rate and analytical uncertainties) are conservative.

bedrock, the age of soils formed on glacial till is quantifiable, as it is coeval with the age of till stabilization. The latter is particularly important for this study, as the cosmogenic ^{10}Be and ^{14}C -based method presented here is based on the assumption that the age of soil formation is known. The two study sites are located near Glasgow in Scotland at Wester Cameron (near Loch Lomond) and Inchie Farm (near Lake of Menteith). To achieve the aim, the thesis has the following objectives:

- (1) To constrain the depositional age of the LLR moraines, and thus the age of soil/till emplacement, using *in situ* cosmogenic ^{10}Be surface exposure dating of erratic boulders at the Wester Cameron site;
- (2) To use the soil/till emplacement age obtained at (1) to construct ‘zero erosion’ cosmogenic ^{10}Be and ^{14}C depth-profiles for the Wester Cameron site and to compare these to ^{10}Be and ^{14}C depth-profiles measured at the site. As is shown below, the soil/till at the Wester Cameron site has not undergone any visible erosion since emplacement and so the results obtained for this site serve as a benchmark for the Inchie Farm site where the soil exhibits signs of soil loss;
- (3) To reconstruct the ^{10}Be and ^{14}C depth-profiles in the soil/till at the Inchie Farm site and to use these in conjunction with a Monte-Carlo type approach to constrain the timing and magnitude of soil erosion at the site; and
- (4) To assess the sensitivity of the results obtained in (3) to the various model parameters used in the Monte-Carlo type approach.

Given that the measurement of *in situ* ^{14}C is still in infancy, the thesis continues in Chapter 2 with a comprehensive description of the analytical methods used to analyse this cosmogenic nuclide. Chapter 3 provides a description of the study area, outlining the rationale behind selecting the two sites. Chapter 4 presents the results of the ^{10}Be , ^{14}C and ^{26}Al analyses at the two sites, and Chapter 5 presents the sensitivity analyses, respectively. The final chapter, Chapter 6, includes a list of major conclusions of the thesis along with limitations and areas of future research.

Additional information relating to the *in situ* ^{14}C extraction system at Scottish Universities Environmental Research Centre (SUERC) are presented in Appendix A. All information relating to sampling sites, including peat age radiocarbon determinations, and till

density calculations are presented in Appendix B. Sample preparation, beryllium chemistry procedures, and results of the AMS measurements are detailed in Appendix C. An explanation of the source code used for the Monte-Carlo analyses in Chapter 5 is given in Appendix D. Publications to date on work contained within and/or related to the thesis are included in Appendix E.

THE TITANIC DIDNT SINK BECAUSE IT HIT AN ICEBERG; IT SANK BECAUSE THE STEEL
WAS BRITTLE AND IT CRACKED.

[S. J. Pennycook]

Chapter 2

In situ cosmogenic ^{14}C systematics and extraction system at SUERC

2.1 Introduction

Although cosmogenic nuclide analysis is now an established technique for studying the processes that shape the Earth's surface, *in situ* ^{14}C has only recently been added to the list of nuclides in the 'cosmogenic toolset'. The reason is mainly due to the difficulties in quantitatively extracting the small amounts of ^{14}C produced in terrestrial samples, and in separating the *in situ*-produced ^{14}C from the substantially more abundant ^{14}C produced in the atmosphere (from hereon referred to as 'meteoric') (Lal and Jull 1994). *In situ* cosmogenic ^{14}C (*in situ* ^{14}C) has the potential to be a very versatile tool to geoscientists. First, it has a relatively short half-life (5730 yr) (Lederer et al. 1978), meaning that when compared to the other cosmogenic nuclides, namely, ^3He , ^{10}Be , ^{21}Ne , ^{26}Al , and ^{36}Cl , ^{14}C is particularly useful for dating recent (Holocene) events and identifying rapid changes in erosion rates, but currently this is prohibited by the large analytical uncertainties involving different extraction techniques. Furthermore, *in situ* ^{14}C is produced in quartz, a mineral that is both highly resistant to weathering and common in nature, and so it can be used alongside the routinely measured longer-lived cosmogenic ^{10}Be to resolve complex exposure histories involving burial and/or erosion occurring over the past 25 kyr.

In situ ^{14}C measurements have been made in extra-terrestrial samples since the 1960s, and have been successfully used, among others, to establish the terrestrial age or the

weathering state of meteorites (Suess and Wänke 1962, Jull 2004). These measurements have been enabled mainly by the orders of magnitude larger ^{14}C abundances in extra-terrestrial samples compared to terrestrial ones (Jull et al. 1992, Pigati et al. 2010b). As already noted above, in terrestrial samples the measurement of *in situ* ^{14}C is made difficult by contamination of meteoric ^{14}C . For analyses of quartz, the contamination is further aggravated during ^{14}C extraction by the release of the gases trapped in fluid inclusions. Because it is tightly bound in the silicate matrix, the extraction of *in situ* ^{14}C is seldom possible without the fusion of the silicate minerals (Des Marais 1983, Brown et al. 1984).

The *in situ* ^{14}C extraction system of the Scottish Universities Environmental Research Centre (SUERC) was built in 2001 (Naysmith et al. 2004, Fülöp et al. 2010) and is based on the design of the extraction system at the University of Arizona (Lifton 1997, Lifton et al. 2001, Pigati 2004). The system works by step heating purified quartz in a resistance furnace in the presence of lithium metaborate (LiBO_2) and ultra-high purity oxygen. During this heating step any released carbon is oxidised and the resulting CO_2 is cryogenically separated from other gas mixtures. The extremely low carbon content of quartz requires that the gas is diluted with ^{14}C -free CO_2 , and converted to graphite. The latter is pressed into targets and analysed at the SUERC Accelerator Mass Spectrometer (AMS) (Freeman et al. 2007).

This chapter provides a brief summary of ^{14}C systematics and describes the design and performance of the *in situ* ^{14}C extraction system at SUERC. The chapter summarises the *in situ* ^{14}C measurements of system blanks, shielded quartz, and surface samples used as standards by other laboratories.

2.2 *In situ* ^{14}C production and extraction methods

The cosmogenic radionuclide ^{14}C is produced mainly in the atmosphere by the thermal neutrons of the cosmic-ray cascade, via $[\text{n,p}]$ reactions on ^{14}N (Montgomery and Montgomery 1935). Other less significant reactions include those ^{15}N $[\text{n},^2\text{H}]^{14}\text{C}$, ^{16}O $[\text{n},^3\text{He}]^{14}\text{C}$, $^{16}\text{O}[\text{n}, \alpha]^{14}\text{C}$, and ^{13}C $[\text{n},\gamma]^{14}\text{C}$. High-energy neutron spallation of $^{20,21,22}\text{Ne}$ can also result in the production of ^{14}C (Libby 1946, Lingenfelter 1963).

This atmospheric ^{14}C equilibrates with the CO_2 in the atmosphere and is incorporated into biological material, its decay forming the basis of the well-established radiocarbon

dating technique (Libby 1946, Libby et al. 1949). Meteoric ^{14}C is delivered to the Earth's surface by precipitation in the form of carbonic acid and so can potentially contaminate terrestrial samples intended for *in situ* ^{14}C analyses. This contamination, however, is quantitatively removed by leaching with oxidising acids (during the sample cleaning process) and by combusting the samples at 500°C prior to analysis (Lifton 1997, Lifton et al. 2001).

In terrestrial rocks, ^{14}C is produced mainly by high-energy secondary neutron spallation reactions on O with only about 3% being produced from reactions on Si, Mg, Al, and Fe (Jull et al. 1998). In quartz, spallation reactions by high-energy secondary neutrons on ^{16}O ($^{16}\text{O}[n, ^2\text{p}n]^{14}\text{C}$) and ^{28}Si ($^{28}\text{Si}[n, X]^{14}\text{C}$, where X is any nucleon) accounts for 83% of the total ^{14}C production, whereas the capture of negative muons by ^{16}O nuclei ($^{16}\text{O}[\mu^-, pn]^{14}\text{C}$) accounts for 15%, and fast muon induced reactions via bremsstrahlung for only 2% of the ^{14}C production (Heisinger et al. 2002b). A small fraction of ^{14}C is also produced by thermal neutrons via $[n, \alpha]$ reactions on ^{17}O and via $[n, p]$ reactions on ^{14}N if the latter is abundant in fluid inclusions (Reedy and Arnold 1972, Gosse and Phillips 2001, Dunai 2010).

In situ ^{14}C is released from the host mineral at temperatures in excess of 1000°C by diffusion of carbon through the crystal lattice (Cresswell et al. 1993), and the diffusion of CO_2 in silicate melts is found to be largely independent of composition (Watson et al. 1982). ^{14}C analyses in meteorites suggest that the temperature at which carbon is lost from the crystal lattice depends on grain-size, with carbon being released from powdered samples at lower temperatures, namely $700 - 800^\circ\text{C}$ (Jull et al. 1989a, Pineau and Javoy 1994, Des Marais and Moore 1984). The dependence of carbon extraction temperature on the grain-size of silicate minerals ceases at their melting point ($> 1600^\circ\text{C}$) as above this temperature all carbon is quantitatively removed (Fireman 1978).

Bauer (1947) was the first to contemplate the use of *in situ* ^{14}C for studying meteorites and since then the extraction and measurement of this nuclide has gone through substantial advancement. The first combustion apparatus for producing CO_2 from graphite was proposed by Craig (1953) and many subsequent studies have followed his design. Table 2.1 provides a summary of the different carbon extraction procedures employed to date. Carbon is extracted by step heating purified quartz in a resistance furnace in the presence of lithium metaborate (LiBO_2) and ultra-high purity oxygen. The main advantage of

this procedure is the use of a fluxing agent, namely LiBO_2 , which enables (1) extraction of carbon from quartz at a temperature of 1100°C and thus avoiding contamination by nitrogen, the latter being released at temperatures above 1300°C (Des Marais 1983), and (2) using other mineral phases for *in situ* ^{14}C analysis such as olivine and sanidine (cf. Pigati et al. 2010a, Dunai 2010). The following section describes in detail the extraction procedure employed as part of this study.

2.3 *In situ* ^{14}C extraction at SUERC

Prior to analysis, ultra-pure quartz separates were prepared for all samples at the University of Glasgow, following a modified version of the protocol of Kohl and Nishiizumi (1992). All samples were crushed and sieved to different size fractions. The 250-500 μm size fraction was selected for all ^{14}C analyses in order to minimize the possibility of contamination by $^{14}\text{CO}_2$ adsorbed from the atmosphere (Barker and Torkelson 1975).

The procedure used in this study is largely based on that described by Naysmith et al. (2004) with the following notable exceptions: (1) the quartz sleeve is cleaned more rigorously and handled with utmost care; (2) a quartz rod is used to push in and pull out the alumina (Al_2O_3) boat from the furnace (3) the gas is collected for an additional 1 hour after the 1100°C heating step; and (4) the temperature in all cryogenic traps is constantly monitored with a thermocouple and controlled by adding additional liquid nitrogen to the slush; (5) after the initial set of measurements, bracketed blanks were used in calculations instead of average blanks.

The extraction procedure is started by cleaning a 65 cm long and 41 mm diameter quartz sleeve that holds an alumina sample boat (135 mm length \times 13 mm width \times 17 mm depth). The quartz sleeve is placed on a surveying tripod fitted with a pre-combusted quartz rod and heated to $> 800^\circ\text{C}$ using a glass blowers torch for at least 15 minutes to oxidise any surface contamination (Figure A.5). After cleaning, the quartz sleeve is inserted into a mullite tube (60% Al_2O_3 , 40% SiO_2 alumino-silicate ceramic) that runs through the furnace (Figure 2.1). In order to avoid any post-cleaning contamination, the quartz sleeve is carefully handled using gloves and stainless steel tongs.

The Al_2O_3 boat (Figure A.3) that will hold the sample is cleaned using a jet of compressed air and placed in a separate small furnace for 8 hours at 850°C in air, and cooled.

Table 2.1: Summary of published ¹⁴C extraction methods.

Study	Sampled material	Extraction method	Sample amount [g]	Sample holder	Comb. tube	Gas	Carrier	Flux/Catalyst	Heating steps or reagents used	Contamination removal	Gas cleaning	Dilution	Gas conversion
Craig (1963)	graphite	combustion	-	Al ₂ O ₃ boat	Q [†]	200 mbar O ₂	-	-	700°C, 900-950°C	-	CuO; dry ice in a 1:1 mixture of CHCl ₃ and CCl ₄	yes	none
Suess and Wänke (1962)	meteorites	-	100	Q boat	-	1 ml Ar, 2 l STP H ₂ , 10 l STP O ₂	2.5-3 g lamp back	-	1200°C for 2 hrs, heating cont. overnight	-	CuO; dry (CH ₃) ₂ CO traps, NH ₄ OH solution (for SO ₂ removal), precipitated to SiCO ₃ (to remove SO ₂)	no	converted to C ₂ H ₂
Boeckl (1971)	meteorites	digestion	10-50	teflon still	-	N ₂	0.2 l STP (from burning anthracite)	-	1:3 HF/HNO ₃	-	CuO; ice cooled traps filled with acidified H ₂ O, passed through 1M SiCl ₄ in 39% NH ₄ OH, precipitated to SiCO ₃ , re-dissolved with 20% HCl, purified over charcoal	up to 0.2 l STP (from burning anthracite)	converted to C ₂ H ₂
Boeckl (1972)	meteorites	combustion	10	porcelain crucible	SS	270 mbar O ₂	-	60g V ₂ O ₅	800°C for 3.5 hrs	evacuated for few hrs at 100°C	CuO; dry ice-(CH ₃) ₂ CO traps, CO ₂ converted to CO with Zn at 300°C to remove Rn, re-frozen with LN ₂ , re-converted to CO ₂ over CuO	up to 0.2 l STP	converted to C ₂ H ₂
Born and Begeman (1975); based on Geel and Kohman (1962)	meteorites	fusion	10-20/200-400	Al ₂ O ₃ crucible	-	600-900 mbar O ₂	~1 g lamp back (from burning inactive benzene)	100 g 10:1 PbCrO ₄ and K ₂ CrO ₄	1100°C	the cromates has been degassed at 800°C	CuO; Pt-asbestos at 800°C (to remove SO ₂ to SO ₃) and Ag-wool at 400°C (removal of SO ₃ and halogens), CuO; -78°C H ₂ O trap	no	converted to C ₂ H ₂
Finkel et al. (1971), Fireman (1978)	meteorites	pyrolysis	1 - 10	Mo crucible	-	-	-	-	400°C, 600°C, 800°C, 1000°C, 1600°C	-	-	no	-
Brown et al. (1984); based on Fireman (1978)	meteorites	pyrolysis	-	Mo crucible (acts as a S getter)	-	-	-	-	500°C and 1000°C by resistance heating for 4 hrs, induction heating to 1600°C for 4 hrs	evacuated overnight at 150°C	CuO	yes	graphitisation using Mg at 900°C.
Des Marais and Moore (1986), Des Marais (1983)	mid-oceanic basaltic glasses	combustion	0.2 - 0.7	-	-	70 mbar O ₂	-	Pt at 1000°C	420 - 500°C; 965 - 740°C, and 1190 - 1270°C.	evacuated overnight at 100°C	variable temperature trap from which the CO ₂ and SO ₂ are released at -155°C and -95°C	no	-
Mathey et al. (1989)	basalt glass	combustion/pyrolysis	-	-	Q	670 mbar O ₂	-	-	400°C, 600°C (combustion), 800°C, 1000°C and 1200°C (pyrolysis)	ultrasonic agitation with analytical grade CH ₂ Cl ₂	CuO; variable temperature trap and n-pentane slush bath (-135°C)	no	none
Jull et al. (1989a,b)	meteorites/quartz	combustion/fusion	0.1-1	ceramic crucible	-	O ₂	-	Fe accelerator chip	800°C	preheated separately between 250°C and 800°C	fine dust filter, then through MnO ₂ at 25°C (SO removal), and through Pt/CuO at 500°C and -78°C H ₂ O trap	yes	CO ₂ , reduces to CO over Zn at 450°C and reacts further with Fe at 625°C to produce graphite.
Inamura et al. (1990)	SiO ₂ target	-	-	Pt boat	Q	-	CO ₂ carrier gas (from 30 - 60 mg CaCO ₃ crystal)	Mg metal flakes in a Q vial	900°C for 1 hrs, Mg heated for 5 hrs in 700°C	boat, Mg, and CaCO ₃ preheated to 900°C for few hrs	amorphous C and Mg cleaned with HCl, separated on a Teflon Millipore filter, and mixed with Ag	no	graphitisation
Lal et al. (1990)	ice	melting	4000-6000	pyrex flask	-	-	1.2 cm ³ ¹⁴ C-free CO and CO ₂ gases	1M HNO ₃ to lower ice pH	-	-	-	-	-

† quartz

‡ natural air with trace gases removed

Table 2.2: Summary of published *in situ* ¹⁴C extraction methods (continued).

Study	Sampled material	Extraction method	Sample amount [g]	Sample holder	Comb. tube	Gas	Carrier	Flux/Catalyst	Heating steps or reagents used	Contamination removal	Gas cleaning	Dilution	Gas conversion
Cresswell et al. (1993, 1994)	meteorites/ quartz	combustion/ pyrolysis	0.3 - 0.5	Mo crucible	Q	1 l He at 670 mbar	-	-	500°C and 900°C by induction heating for 1 hrs, 7 hrs at 1600°C	crucible preheated to 1100°C in zirconia boat for 1 hrs; then heated to white hot using an induction furnace for 3 hrs	CuO; variable temperature trap	to 3 ml	graphitisation
Krauer et al. (1994) Jull et al. (1994b)	meteorites whole rock	pyrolysis combustion	1.5 10 - 60	Al ₂ O ₃ crucible 0.0039 - 0.0050 [†] Mo foil	-	-	-	-	1000°C and 1700°C 500°C and 1000°C	-	MnO and Pt/CuO	yes -	graphitisation -
Lal and Jull (1994)	meteorites/ quartz	wet digestion	10 - 20	Cu/brass vessel/Kel-F [‡]	-	-	¹⁴ C-free CO and CO ₂ gases	-	25% HF at 60-80°C	-	CuO; 5 Å molecular sieve; 75°C H ₂ O trap (dry ke/alcohol mixture).	to 1 ml	graphite with Zn at 450°C, Fe at 625°C.
Lifton (1997)	quartz	combustion	5	ceramic crucible	Q	O ₂	-	LiBO ₂	500°C and 1000°C by resistance heating for 1 and 3 hrs 100% H ₃ PO ₄	-	-	yes	graphite with Zn at 450°C and Fe at 625°C.
Hardwenger et al. (1999)	carbonate	wet digestion	10	-	-	-	¹⁴ C-free CO	-	-	H ₃ PO ₄ degassed prior to reaction at 100°C under vacuum.	cryogenic separation; molecular sieve	-	-
Smith et al. (2000)	ice	dry grating	1000	SS grating flask	-	zero air [†]	-	-	-	-	cryogenic separation	-	graphitisation
Van Der Kemp et al. (2000) Van de Wal et al. (2007)	ice	dry digestion	3000 2500	pyrex flask	-	-	¹⁴ C-free CO (>70 mtorr STP)	Pt wire at 300°C	milled and separated to CO and CO ₂	sublimation of the outer layer of the core, for one day, under dynamic vacuum at temperatures below -15°C	Pt at 300°C	-	-
Yokoyama et al. (2004) Naysmith et al. (2004), Naysmith (2007)	quartz quartz	combustion combustion	1 - 6 5	Al ₂ O ₃ boat ceramic crucible	- Q	- O ₂	mixture of He, O ₂ , CO, and CO ₂	He, Pt at 500°C LiBO ₂	500°C to 1550°C in 100°C increments 500°C and 1000°C by resistance heating for 1 and 3 hrs	boat heated to 450°C overnight -	-	yes yes	graphitisation graphite with Zn at 450°C, and Fe at 550°C.
Lal et al. (2000, 2005)	ice	melting	2000	cooled flask	-	-	1 - 1.5 cm ³ ¹⁴ C-free CO and CO ₂ gases	H ₃ PO ₄ to lower ice pH	heated until ice melts	outer layers of the ice are removed by scraping with a serrated SS saw in a cold room	CuO; LN ₂ cooled molecular sieve (Linde 5A)	-	-
Hippe et al. (2000)	quartz	pyrolysis	5	Pt crucible	sapphire	O ₂	-	-	160°C, 500°C, 1550°C	-	CuO; variable temperature trap (-78°C, -130°C, and -145°C)	-	gas measurement

[‡] quartz[†] natural air with trace gases removed

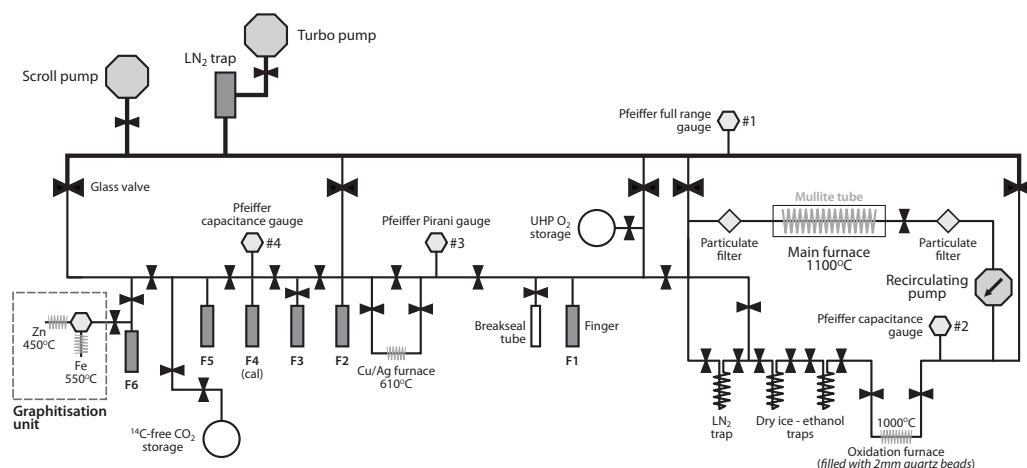


Figure 2.1: Schematic of the extraction, purification, and graphitization of *in situ* ^{14}C line.

LiBO_2 is used as the flux agent; having a melting temperature of 845°C it lowers the melting temperature of quartz. The fluxing agent is also dried in a separate oven at 500°C and 20 g are added to the Al_2O_3 boat, which is then placed inside the clean quartz sleeve. The quartz sleeve protects the main Mullite tube from the corrosive LiBO_2 vapours. The furnace and re-circulating section of the extraction line (Figures 2.1 and A.4) are pumped until the pressure drops to 10^{-5} mbar, and then the LiBO_2 is degassed in an ultra-high-purity oxygen (UHP O₂) atmosphere at a pressure of 30 - 40 mbar for 2 hours at 1100°C . The furnace is allowed to cool to below 800°C to allow the LiBO_2 to re-solidify before evacuating the extraction system. After the furnace has cooled to 180 - 250°C , it is opened and the quartz sleeve and boat removed. Five grams of quartz is placed in the boat. This has previously undergone sonic cleaning the previous day for 30 minutes in 50% HNO_3 solution to remove any absorbed carbon during sample storage, and rinsed with MilliQ water and dried in a separate furnace at 75°C . The boat is then returned to the quartz sleeve and placed back in the furnace. When performing system blank measurements the procedure outlined above is followed except that no quartz is added.

The sample undergoes a 2-stage heating process. The furnace and re-circulating section are pumped until pressure drops to 10^{-5} mbar before heating the furnace to 500°C in a re-circulating UHP O₂ atmosphere of 30 - 40 mbar for 1 hour. The recirculating pump is a 2-stage stainless steel bellows pump (Senior Flexonics Corporation, Metal Bellows Division) running at approximately 3100 RPM, with Teflon gaskets and Viton seals, ensuring that the O₂ carrier gas is continuously recirculated through the closed loop and all ^{14}C atoms are

oxidized. Pyrex glass frits installed at each end of the furnace tube protect the rest of the extraction line from particulates, while also slowing the recirculating gas flow. Any CO_2 that is produced at this heating step is considered to be from atmospheric contamination, adsorbed or incorporated during sample handling (Des Marais 1983, Jull and Donahue 1988, Jull et al. 1989b, Cresswell et al. 1994), and thus pumped away.

The extraction line is pumped to 10^{-5} mbar, and the furnace is reheated to 1100°C for 3 hours in a UHP O_2 atmosphere of 30 - 40 mbar. The resulting CO_2 , which is considered to be from *in situ* production (Lifton et al. 2001), is cryogenically trapped using liquid N_2 for an additional 1 hour. To ensure complete CO-to- CO_2 conversion, the gas evolved during extraction is circulated through an additional small furnace held at 970°C and filled with 3 mm diameter quartz beads that increase the surface area and the tortuosity of the gas flow path. Most of the water released is frozen with an ethanol/dry-ice slush at a temperature between -77 and -80°C . The remaining water vapour and contaminant gases, originating mainly from fluid inclusions (including SO_x and NO_x species), are removed by passing the resulting gas mixture through an n-pentane/liquid N_2 trap at -130°C and re-heating to 610°C in a quartz combustion tube containing Cu granules and a Ag wool molecular sieve adsorption system, for 20 minutes. This procedure re-adsorbs oxygen and guarantees complete oxidation of any residual carbon species (Pineau and Javoy 1994). In addition, the Cu granules also eliminate any halogens and convert SO_x to CuSO_4 , the latter generally reducing the conversion efficiency of CO_2 to graphite (Yokoyama et al. 2004). The Cu granules also convert NO_x to NO_2 , the latter condensing more easily than CO_2 , and so is more easily separable cryogenically (Buchanan and Corcoran 1959, Dutta and Patil 1995, Vandeputte et al. 1996).

The CO_2 gas is re-trapped in liquid nitrogen (LN_2) and cleaned with an iso-pentane/ LN_2 slush at -150°C for 15 minutes (Des Marais 1983) to ensure that only CO_2 is trapped. The cleaned CO_2 is transferred to a calibrated finger where it is measured using a highly sensitive capacitance manometer (CMR 272, Pfeiffer) and diluted to approximately 1 ml (0.5 mg C) using ^{14}C -free CO_2 derived from an infinite age Icelandic doublespar. The dilution minimizes the uncertainty in the volume measurement. The clean CO_2 is converted into an amorphous carbon deposit on the same extraction line. The CO_2 is first reduced to CO over 3 - 4 mg Zn at 450°C and after reacting further with 1 - 1.5 mg Fe at 550°C , graphite is produced (Slota et al. 1987). For all samples prepared and measured during this study, the graphite conversion efficiency monitored using a software, called SUERC Graphite

Program (made in-house), was better than 90% A.1. The graphite is removed from the vacuum extraction line and pressed into an aluminium cathode (at 180 psi) immediately prior to AMS measurement.

All AMS measurements were carried out at SUERC (Freeman et al. 2004). Some of the targets were analysed using a 5MV NEC Pelletron accelerator mass spectrometer and the remainder using a NEC 250 kV single stage accelerator mass spectrometer. The measurements are described in detail in Xu et al. (2004) and Maden et al. (2007). The $^{14}\text{C}/^{13}\text{C}$ ratios were measured using oxalic acid standards (OxII) with a consensus value of 134.07 percent modern carbon (pMC). $^{14}\text{C}/^{13}\text{C}$ ratios were corrected using a combination of extraction blanks and full procedural blanks (shielded quartz), and graphitization blanks, as set out by Donahue et al. (1990). Uncertainty of individual sample measurement was derived from the χ^2 -statistics test using statistical uncertainty of counting ^{14}C atoms and the scatter of $^{14}\text{C}/^{13}\text{C}$ ratios. Systematic uncertainties were assessed by secondary standards prepared from bulk barley mash (TIRI A) and individual Belfast cellulose (FIRI I) samples on a separate vacuum line, and from Icelandic doublespar (TIRI F) on the same vacuum line, with consensus values of 116.35 ± 0.0084 pMC, 57.10 ± 0.23 , and 0.180 ± 0.006 pMC, respectively (Gulliksen and Scott 1995, Scott 2003). Thus, final analytical errors are derived from a quadrature sum of uncertainties of individual sample $^{14}\text{C}/^{13}\text{C}$ ratios and systematic uncertainties. Precision is limited by the statistical accuracy of counting, namely, 2% in $^{14}\text{C}/^{13}\text{C}$ ratios and is dependent on the carbon content and concentration of ^{14}C in the samples (Brown et al. 1984, Pigati et al. 2010b). AMS results were reduced according to the procedures set out by Lifton (1997) and Lifton et al. (2001).

2.4 Results and discussion

Results are summarised in Tables 2.3, 2.4, 2.5, 2.6, and 2.7, and Figures 2.2, 2.3, and 2.4. Prior to November 2008, all *in situ* ^{14}C measurements at SUERC were performed without monitoring and adjusting the temperature of the cryogenic traps i.e., the temperature of the n-pentane/liquid N_2 and iso-pentane/liquid N_2 traps was not measured to ensure that they were at the appropriate temperatures of -130°C and -150°C , respectively. Since November 2008 this has changed and now the temperature of the cryogenic traps is monitored using a thermocouple and the slushes are kept at -130°C and -150°C , respectively, by slowly adding LN_2 . In Figures, 2.2 and 2.3 the switch to temperature controlled cryogenic

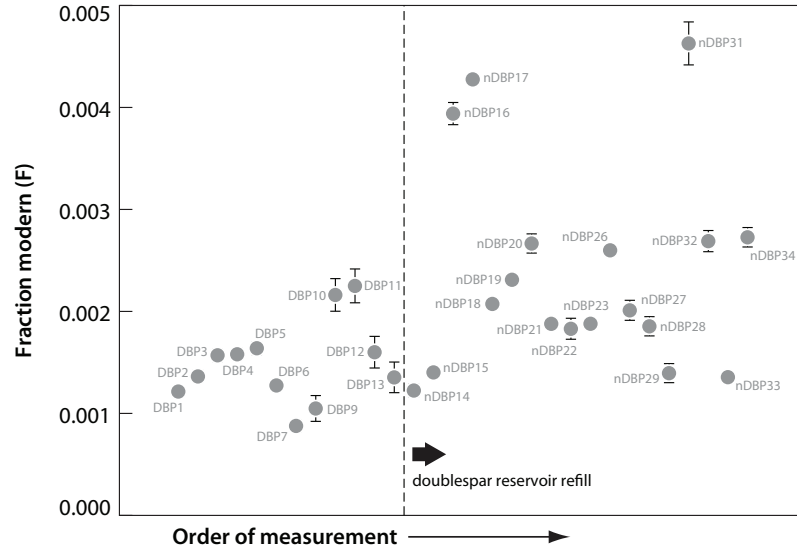


Figure 2.2: Results of AMS measurements on the Icelandic doublespar aliquots. See text for more details.

cleaning is indicated.

2.4.1 Icelandic doublespar

In addition to system blank and shielded quartz measurements, the performance of the extraction system was also monitored by AMS measurements on aliquots of the Icelandic doublespar used as the dilution gas prior to graphitization. These measurements served three purposes: (1) to assess whether the dilution gas tank connected to the extraction system is contaminated with air throughout its use, (2) to test for AMS measurement fluctuations that can result in fluctuations in the *in situ* ^{14}C data, and (3) to quantify the graphitization blank. The graphitization (gas conversion to solid targets) contributes $40.000\ ^{14}\text{C}$ atoms to the blanks. Contamination of the storage tank with air increases $\delta^{13}\text{C}$ of the gas and the obtained measured fraction modern of a background sample (F) values. The doublespar measurement results fluctuate; however, they do not exhibit a clear trend, suggesting no contamination by air (Figure 2.2). The fluctuations in the results, however, indicate fluctuations in the performance of the AMS, and the anomalously large values obtained for samples nDBP16 and nDBP17 (Figure 2.2) might explain the higher values obtained for system blank samples BLK20, BLK21, and BLK23.

2.4.2 Extraction blanks and shielded quartz

As part of the *in situ* ^{14}C extraction, blanks cannot be measured simultaneously with the samples. Thus, one must either interpolate bracketed blank values or use a long-term average blank. Given the sensitivity of the *in situ* ^{14}C extraction process to contamination by environmental ^{14}C , it is better practice to bracket each unknown sample measurement between two blank measurements and, where it was available, a full procedural blank (shielded quartz added). This bracketing approach was followed throughout this study except where stated otherwise. In order to determine the extraction blanks (BLK), the complete procedure described above was followed without placing any quartz in the alumina boat. In case of the full procedural blank, 5g of shielded quartz (SHQ) has been placed in the alumina boat. In this way, the obtained blank values represent the number of ^{14}C atoms introduced into the system from sources other than the sample (Tables 2.3 and 2.4).

To test the level of the system blanks when sample is added to the alumina boat, shielded quartz samples were also analysed. The quartz for all measurement except SHQ8, was separated from a granite taken from a depth of 1.5 km from Rosemanowes Quarry, SW England (Chen et al. 1996), and so at least theoretically it should be free of any *in situ* ^{14}C . The quartz used for SHQ8 was obtained from Bill Philips (at that time, Geography, University of Edinburgh) and yielded an anomalously large value for reasons that have not been established.

The system blanks exhibited substantial fluctuations at the beginning of the study, suggesting that the continuous running of the extraction system was slowly cleaning contaminant carbon from the line. These fluctuations in the blanks were also reduced with longer cleaning of the quartz sleeves and close monitoring of gas collecting time and of the temperature of the cryogenic traps used in the gas cleaning steps (Figure 2.3). After the replacement of the mullite tube (Figures 2.3 and A.2), system blanks exhibited the same level of fluctuation as at the beginning of the study, suggesting that the line absorbs carbon if not heated and pumped continuously.

The system blanks measured as part of this study prior to the replacement of the mullite tube yielded an average of $2.75 \pm 2.78 \times 10^5$ ^{14}C atoms ($\pm 1\sigma$). The average of system blanks that were measured prior the mullite tube replacement and with controlling the temperature of the cryogenic traps was lower, namely, $2.02 \pm 0.64 \times 10^5$ ^{14}C atoms

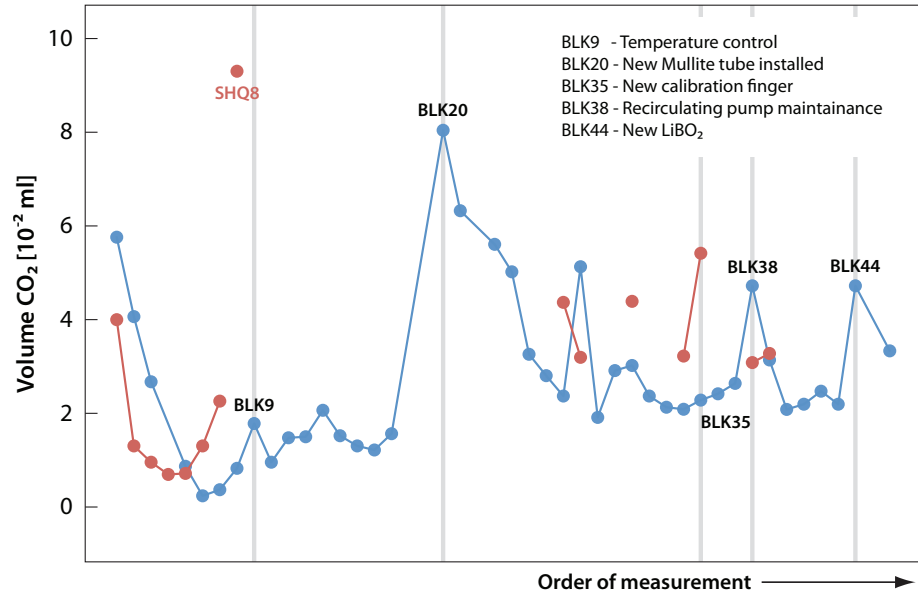
Table 2.3: Summary of system blank measurement results (Dec/2007 - Mai/2010).

AMS ID	Date and AMS	Sample ID	Extraction date	F value	$\pm 1\sigma$	CO_2 (10^{-2} ml)	Diluted CO_2 (ml)	^{14}C (10^5 atoms)	$\pm 1\sigma$
G18611	25.04.2008/5MV	BLK1	13.12.2007	0.0399	0.0004	5.748	0.996	11.51	0.10
G18616	25.04.2008/5MV	BLK2	24.01.2008	0.0183	0.0003	4.056	1.015	5.39	0.08
G18618	25.04.2008/5MV	BLK3	12.02.2008	0.0063	0.0002	2.668	0.994	1.83	0.05
G20684	08.10.2008/SSAMS	BLK5	28.05.2008	0.0029	0.0002	0.868	1.012	0.84	0.04
G20688	08.10.2008/SSAMS	BLK8	04.06.2008	0.0026	0.0002	0.824	0.990	0.74	0.05
Temperature control									
G21809	22.12.2008/5MV	BLK9	23.10.2008	0.0070	0.0003	1.779	1.002	2.04	0.09
G22985	09.04.2009/SSAMS	BLK10	26.01.2009	0.0037	0.0004	0.954	1.001	1.08	0.12
G22986	09.04.2009/SSAMS	BLK11	02.02.2009	0.0062	0.0005	1.475	1.001	1.79	0.14
G22987	09.04.2009/SSAMS	BLK12	09.02.2009	0.0056	0.0004	1.497	1.001	1.62	0.12
G22989	09.04.2009/SSAMS	BLK13	17.02.2009	0.0114	0.0005	2.061	0.998	3.28	0.16
G22990	09.04.2009/SSAMS	BLK14	05.03.2009	0.0070	0.0004	1.518	1.000	2.03	0.13
G22991	09.04.2009/SSAMS	BLK15	09.03.2009	0.0063	0.0005	1.302	1.000	1.82	0.13
G22995	09.04.2009/SSAMS	BLK16	11.03.2009	0.0060	0.0005	1.215	1.000	1.74	0.15
G22996	09.04.2009/SSAMS	BLK17	18.03.2009	0.0094	0.0006	1.562	1.002	2.74	0.17
Temperature control and new furnace									
G25684	06.10.2009/SSAMS	BLK20	03.09.2009	0.0575	0.0004	8.026	0.994	16.57	0.13
G25685	06.10.2009/SSAMS	BLK21	15.09.2009	0.0409	0.0004	6.312	0.998	11.83	0.12
G25686	06.10.2009/SSAMS	BLK23	18.09.2009	0.0301	0.0004	5.597	1.000	8.72	0.10
G26215	30.10.2009/SSAMS	BLK24	06.10.2009	0.0225	0.0003	5.011	0.999	6.51	0.10
G26216	30.10.2009/SSAMS	BLK25	08.10.2009	0.0136	0.0003	3.254	0.994	3.93	0.10
G26217	30.10.2009/SSAMS	BLK26	12.10.2009	0.0137	0.0003	2.798	0.994	3.93	0.08
G26218	30.10.2009/SSAMS	BLK27	15.10.2009	0.0149	0.0003	2.364	1.000	4.31	0.09
G27095	05.01.2010/5MV	BLK28	19.10.2009	0.0431	0.0004	5.119	1.000	12.49	0.13
G27096	05.01.2010/5MV	BLK29	21.10.2009	0.0124	0.0003	1.909	1.001	3.59	0.08
G27097	05.01.2010/5MV	BLK30	30.10.2009	0.0218	0.0003	2.907	0.999	6.30	0.10
G27105	05.01.2010/5MV	BLK31	04.11.2009	0.0218	0.0003	3.015	1.000	6.33	0.10
G27106	05.01.2010/5MV	BLK32	19.11.2009	0.0183	0.0003	2.364	1.001	5.31	0.09
G27107	05.01.2010/5MV	BLK33	26.11.2009	0.0181	0.0003	2.126	1.000	5.23	0.09
G27108	05.01.2010/5MV	BLK34	29.11.2009	0.0164	0.0003	2.082	1.000	4.75	0.09
G27115	05.01.2010/5MV	BLK35	14.12.2009	0.0147	0.0003	2.278	1.122	4.79	0.09
G27960	02.03.2010/5MV	BLK36	05.01.2010	0.0180	0.0005	2.417	1.006	5.24	0.15
G27961	02.03.2010/5MV	BLK37	11.01.2010	0.0213	0.0004	2.639	1.000	6.16	0.12
G27962	02.03.2010/5MV	BLK38	07.01.2010	0.0329	0.0005	4.722	0.999	9.51	0.15
G29551	07.06.2010/5MV	BLK39	01.03.2010	0.0191	0.0004	3.139	1.000	5.55	0.12
G29552	07.06.2010/5MV	BLK40	18.03.2010	0.0121	0.0003	2.083	1.001	3.51	0.10
G29553	07.06.2010/5MV	BLK41	23.03.2010	0.0143	0.0004	2.194	1.001	4.14	0.11
G29554	07.06.2010/5MV	BLK42	16.04.2010	0.0161	0.0004	2.472	1.001	4.67	0.11
G29555	07.06.2010/5MV	BLK43	28.04.2010	0.0135	0.0003	2.194	0.999	3.91	0.10
G29556	07.06.2010/5MV	BLK44	05.05.2010	0.0395	0.0005	4.722	0.998	11.43	0.15
G29562	07.06.2010/5MV	BLK46	13.05.2010	0.0244	0.0004	3.333	0.998	7.07	0.13
G29563	07.06.2010/5MV	BLK47	17.05.2010	0.0110	0.0004	-	0.997	3.17	0.11
Mean value - all:								5.18	3.60

Table 2.4: Summary of shielded quartz measurement results (Dec/2007 - Apr/2010).

AMS ID	Date and AMS	Sample ID	Extraction date	F value	$\pm 1\sigma$	CO_2 (10^{-2} ml)	Diluted CO_2 (ml)	^{14}C (10^4 atoms.g $^{-1}$) *	$\pm 1\sigma$
G18615	25.04.2008/5MV	SHQ1	17.12.2007	0.0244	0.0003	3.991	1.006	14.2	0.18
G18619	25.04.2008/5MV	SHQ3	27.02.2007	0.0051	0.0002	0.954	1.001	2.97	0.11
G20677	08.10.2008/SSAMS	SHQ4	05.06.2008	0.0017	0.0001	0.694	1.009	1.01	0.08
G20678	08.10.2008/SSAMS	SHQ5	09.06.2008	0.002	0.0002	0.716	1.006	1.17	0.09
G20679	08.10.2008/SSAMS	SHQ6	11.06.2008	0.0061	0.0002	1.302	0.995	3.52	0.10
Temperature control									
G22965	09.04.2009/SSAMS	SHQ7	19.01.2009	0.0074	0.0005	2.256	0.999	4.31	0.28
G22966	09.04.2009/SSAMS	SHQ8	23.01.2009	0.0065	0.0005	9.284	1.002	3.76	0.28
G27098	05.01.2010/5MV	SHQ9	16.11.2009	0.0324	0.0004	4.360	0.999	18.76	0.23
G27099	05.01.2010/5MV	SHQ10	24.11.2009	0.0226	0.0005	3.189	1.000	13.10	0.27
G27100	05.01.2010/5MV	SHQ11	08.12.2009	0.0335	0.0004	4.382	1.000	19.41	0.23
G27963	02.03.2010/5MV	SHQ12	21.01.2010	0.0176	0.0004	3.222	1.146	11.71	0.27
G27964	02.03.2010/5MV	SHQ13	02.02.2010	0.0428	0.0006	5.417	1.001	24.81	0.33
G29564	07.06.2010/5MV	SHQ14	12.04.2010	0.0163	0.0004	3.083	0.996	9.39	0.23
G29565	07.06.2010/5MV	SHQ15	22.04.2010	0.0185	0.0004	3.278	0.999	10.72	0.23
Mean value - all:								9.92	7.53

* Not corrected for extraction blanks

**Figure 2.3:** Results of the system blank (blue) and shielded quartz (red) measurements between Dec/2007 - Mai/2010. Vertical lines indicate changes in the extraction procedure. For sample SHQ8 see explanation in text.

($\pm 1\sigma$). After the mullite tube was replaced, the average system blank value increased to $5.18 \pm 3.60 \times 10^5$ ^{14}C atoms ($\pm 1\sigma$). The reason for this increase is not clear but could be linked to a problem that developed with the recirculating pump (Figure 2.1) resulting in overturning of the boats and breaking of the quartz sleeves. It is possible that the turning of the boats and breaking of the quartz sleeves resulted in molten sample being deposited on the inner walls of the mullite tube. Another possibility, of course, could be that the new mullite tube itself had an inherently higher ^{14}C content or was more porous than the previous one.

The average system blank obtained after replacing the mullite tube ($5.18 \pm 3.60 \times 10^5$ ^{14}C atoms $\pm 1\sigma$) is comparable to that reported by Hippe et al. (2009) at ETH, however, roughly twice as high as the average system blanks obtained at the University of Arizona by Miller et al. (2006): $2.40 \pm 0.12 \times 10^5$ ^{14}C atoms using the extraction procedures modified from Lifton et al. (2001), and $1.50 \pm 0.10 \times 10^5$ ^{14}C atoms using the extraction procedures modified from Pigati (2004) (Figure 2.3). The shielded quartz results exhibit the same pattern as the system blanks. Their initial variability in the ^{14}C concentrations decreases with time.

2.4.3 Reproducibility measurements

To assess the efficiency of the system I have also measured *in situ* ^{14}C in a Lake Bonneville shoreline surface quartz sample (PP4), which has been used as an internal standard at the University of Arizona (Lifton et al. 2001). The PP4 material was collected from Pleistocene Lake Bonneville wave-cut quartzite shorelines. The age of the surface was previously constrained using radiocarbon and cosmogenic nuclide measurements (Oviatt et al. 1992). Figure 2.4 shows a comparison of the PP4 results obtained as part of this study with the latest PP4 results from the University of Arizona (Miller et al. 2006, Dugan 2008).

Measurements of *in situ* ^{14}C concentrations in sample PP4 yielded an average of $3.91 \pm 0.50 \times 10^5$ ^{14}C atoms.g $^{-1}$ quartz ($\pm 1\sigma$) (Table 2.5). This value is slightly greater with that obtained by Miller et al. (2006), namely, $3.56 \pm 0.16 \times 10^5$ ^{14}C atoms.g $^{-1}$ and by Dugan (2008), namely, $3.61 \pm 0.09 \times 10^5$ ^{14}C atoms.g $^{-1}$. Nonetheless, our measurements show a considerably larger spread than those of Miller et al. (2006) and Dugan (2008). Although we do not yet know what the cause of the variability in our PP4 results is,

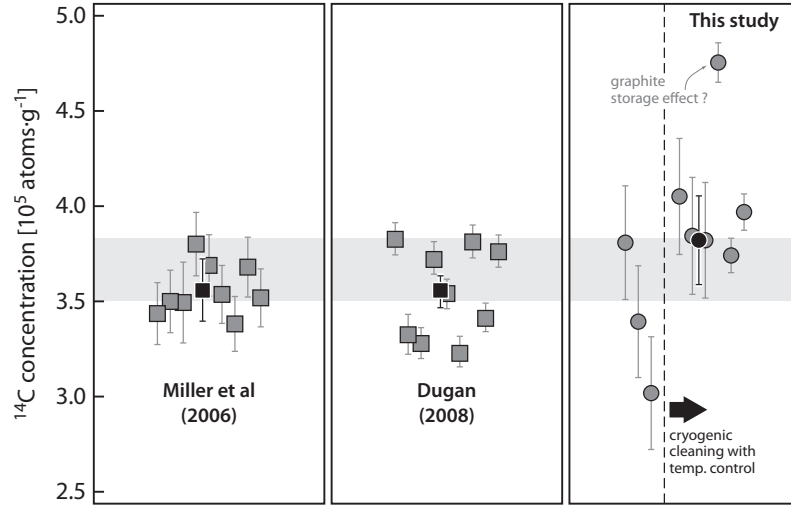


Figure 2.4: Results of the reproducibility measurements (PP4). The grey symbols are the individual data points and the black symbols are the mean values obtained for each study. The horizontal grey band represents Miller et al.’s (2006) average PP4 concentration at $\pm 2\sigma$ level. Data points plotted to the right of the dashed line were obtained by controlling the temperature of the cryogenic traps using a thermocouple and keeping the slushes previously described at -130 and -150°C .

we suspect two factors. First, some of the PP4 measurements were carried out prior to monitoring the temperature of the cryogenic traps (Figure 2.4), and although we do not have an estimate of how much the temperature of the slushes may have fluctuated during these measurements, this fluctuation might have contributed to the observed variability by trapping other gases to the calibration finger. Second, the graphite obtained from the seventh PP4 sample was stored for more than four months prior to the AMS measurement, and so there is a possibility that this sample has been contaminated by absorption of meteoric ^{14}C . Excluding the seventh PP4 sample and the ones that were measured prior to controlling the temperature of the cryogenic traps, yields an average that is slightly higher ($4.03 \pm 0.40 \times 10^5$ ^{14}C atoms.g $^{-1}$) and still indistinguishable within $\pm 2\sigma$ uncertainty from those obtained by Miller et al. (2006) and Dugan (2008).

In addition to sample PP4, the performance of the extraction system has also been tested by measurements of aliquots of two other samples: CRONUS-Earth-A from Antarctica proposed as the new *in situ* ^{14}C standard to be used for inter-laboratory comparisons (<http://www.physics.purdue.edu/primelab/CronusProject>), and a sample from the 325 m shoreline of the Parallel Roads of Glen Roy, Scotland.

Measurements of *in situ* ^{14}C in sample CRONUS-Earth-A at the University of Arizona yielded a concentration of $6.88 \pm 0.39 \times 10^5$ ^{14}C atoms.g $^{-1}$ ($n=3$) (*N. Lifton*, personal

Table 2.5: Results of the reproducibility measurements (PP-4).

AMS ID	Date and AMS	Sample ID	Extraction date	F value	$\pm 1\sigma$	CO_2 (10^{-2} ml)	Diluted CO_2 (ml)	^{14}C (10^5 atoms.g $^{-1}$) *	$\pm 1\sigma$	blank % *
No temperature control										
G20699	08.10.2008/SSAMS	PP4-1	13.06.2008	0.0717	0.0004	8.633	0.998	3.81 [†]	0.82	18
G20704	08.10.2008/SSAMS	PP4-4	21.08.2008	0.0647	0.0004	6.551	1.005	3.40 [‡]	0.82	20
G20705	08.10.2008/SSAMS	PP4-5	01.09.2008	0.0589	0.0004	6.182	1.001	3.02 [‡]	0.82	23
Temperature control										
G21793	22.12.2008/5MV	PP4-6	02.12.2008	0.0753	0.0005	7.592	1.000	4.30 [‡]	0.18	14
G21797	22.12.2008/5MV	PP4-7	05.12.2008	0.0724	0.0006	6.941	0.995	4.09 [‡]	0.18	10
G21798	22.12.2008/5MV	PP4-8	11.12.2008	0.0718	0.0006	7.072	0.999	4.07 [‡]	0.18	11
G22975	09.04.2009/SSAMS	PP4-9	15.12.2008	0.0828	0.001	7.896	0.997	4.75 [‡]	0.20	11
G22976	09.04.2009/SSAMS	PP4-10	20.01.2009	0.0665	0.001	6.573	0.999	3.74 [‡]	0.09	14
G22977	09.04.2009/SSAMS	PP4-11	19.02.2009	0.0722	0.001	7.245	1.000	3.97 [§]	0.09	14
Mean value - all:								3.91	0.50	15

* Scaled based on Lifton (1997)
[†] Corrected for system blanks (extraction blanks and shielded quartz) using a mean value of $3.18 \pm 3.67 \cdot 10^5$ atoms
[‡] Corrected for system blanks (extraction blanks and shielded quartz) using a mean value of $2.02 \pm 0.64 \cdot 10^5$ atoms
[‡] Corrected for system blanks using the mean of bracketed shielded quartz samples SHQ7 and SHQ8
[§] Corrected for system blanks using the mean of bracketed extraction blanks BLK13 and BLK14
* Ratio of system blank ^{14}C to amount of ^{14}C measured in the sample

Table 2.6: Results of the reproducibility measurements (CRONUS-EARTH-A).

AMS ID	Date and AMS	Sample ID	Extraction date	F value	$\pm 1\sigma$	CO_2 (10^{-2} ml)	Diluted CO_2 (ml)	^{14}C (10^5 atoms.g $^{-1}$) *	$\pm 1\sigma$	blank % *
G27109	05.01.2010/5MV	CRA-1	30.11.2009	0.1428	0.0007	7.766	1.001	7.29 [‡]	0.06	14
G27116	05.01.2010/5MV	CRA-3	15.12.2009	0.1475	0.0007	8.091	1	7.09 [‡]	0.07	20
Mean value:								7.19	0.14	17

[‡] Corrected for system blanks using the mean of bracketed extraction blanks BLK33 and BLK34
[‡] Corrected for system blanks using the mean of bracketed extraction blank BLK35 and shielded quartz sample SHQ11
* Ratio of system blank ^{14}C to amount of ^{14}C measured in the sample

communication, *March 2010*). Measurements as part of this study yielded a concentration of $7.19 \pm 0.14 \times 10^5$ ^{14}C atoms.g $^{-1} \pm 2\sigma$ (n=2), agreeing within uncertainty with those made at Arizona (Table 2.6).

No prior *in situ* ^{14}C measurements have been performed on the Glen Roy samples. However, Fabel et al. (2010) have done *in situ* ^{10}Be measurements on samples collected from the 325 m shoreline yielding a mean exposure age of 11.9 ± 1.6 kyrs (n=4, age calculated using scaling scheme of Desilets et al. (2006) and 4.88 ± 0.56 atoms.g $^{-1}$ SLHL production rate). Three aliquots from one of Fabel et al.'s (2010) samples has been analysed as part of this study yielding an average *in situ* ^{14}C exposure age of 12.8 ± 1.1 kyrs (n=3, calculated using the same scaling scheme as above). The two exposure ages overlap within uncertainty (Table 2.7).

Table 2.7: Results of the reproducibility measurements (Glen Roy).

AMS ID	Date and AMS	Sample ID	Extraction date	F value	$\pm 1\sigma$	CO ₂ (10^{-2} ml)	Diluted CO ₂ (ml)	^{14}C (10^5 atoms.g $^{-1}$) *	$\pm 1\sigma$	blank % *
G21801	22.12.2008/5MV	GR1-2	17.11.2008	0.0337	0.0004	3.319	1.002	1.48†	0.14	26
G21802	22.12.2008/5MV	GR1-3	24.11.2008	0.035	0.0004	3.254	1.001	1.55†	0.14	25
G21803	22.12.2008/5MV	GR1-4	28.11.2008	0.0358	0.0004	3.579	1.002	1.60†	0.14	24
Mean value - all:								1.54	0.06	25

* Corrected using a combined thickness and topographic shielding scaling factor of 0.9517

† Corrected for system blanks (extraction blanks and shielded quartz) using a mean value of $2.02 \pm 0.64 \cdot 10^5$ atoms• Ratio of system blank ^{14}C to amount of ^{14}C measured in the sample

2.5 Summary

The results of the reproducibility measurements are satisfactory. The PP4 measurements are indistinguishable within uncertainty from the latest PP4 results published by the University of Arizona ^{14}C lab Miller et al. (2006), Dugan (2008), but they are somewhat higher and exhibit more spread. Measurements in both the CRONUS-EARTH-A and Glen Roy samples agree within uncertainty with the *in situ* ^{14}C and *in situ* ^{10}Be results of the University of Arizona and Fabel et al. (2010), respectively.

The results of the extraction blank and shielded quartz measurements suggest that the continuous running of the extraction system and the monitoring of gas collecting time are key to maintaining low and stable system blanks. The results also suggest that maintaining the temperature of the cryogenic traps constant could also play a role in maintaining system blank stability. The variability in the system blank data, however, means that a blank bracketing approach should be followed instead of calculating a long-term average blank and applying this to all sample measurements.

‘SCOTIA’S HILLS OF HOARY HUE,
HEAVEN WRAPS IN WREATHES OF BLUE,
WATERING WITH ITS DEAREST DEW
THE HEALTHY LOCKS OF SCOTIA.’

[Henry Scott Riddell]

Chapter 3

Study Area

3.1 Introduction

As noted in Chapter 1, the aim of this thesis is to assess the extent to which the amount and timing of site-specific Holocene soil erosional events can be quantified using depth-profiles of *in situ* produced cosmogenic ^{10}Be and ^{14}C . A reliable control on the age of the sediment on which the soil is formed is a prerequisite. The age of the sediment body is required so that the initial (zero-erosion) cosmogenic nuclide depth-profile, to which the measured cosmogenic nuclide depth-profile is compared against, can be reconstructed. In this study, the age of the sediment body (till) on which the soil has formed is established by cosmogenic ^{10}Be exposure dating of erratic boulders at one of the two study sites (below). The two sites were selected at localities where the age of till stabilisation has been dated independently using radiocarbon so that the ^{10}Be exposure ages can be checked for consistency.

The study was conducted at two study sites: Wester Cameron Farm, near Glasgow, and Inchie Farm, near Lake of Menteith (Figure 3.1). The Wester Cameron Farm site is located on the flat crest of the Loch Lomond Readvance (LLR) moraine and shows no signs of soil erosion. This site was selected to test (1) whether cosmogenic nuclide depth profiles of *in situ* ^{10}Be and *in situ* ^{14}C can be reconstructed in a sediment body of Holocene age, and (2) whether *in situ* ^{10}Be and *in situ* ^{14}C yield results that (a) are concordant, and (b) confirm the erosional stability of the site. The Lake of Menteith site is the steep inner flank of the LLR moraine and shows clear evidence of soil erosion, including a marked erosional break of slope below the moraine crest on its inner flank, and on-going rabbit burrowing

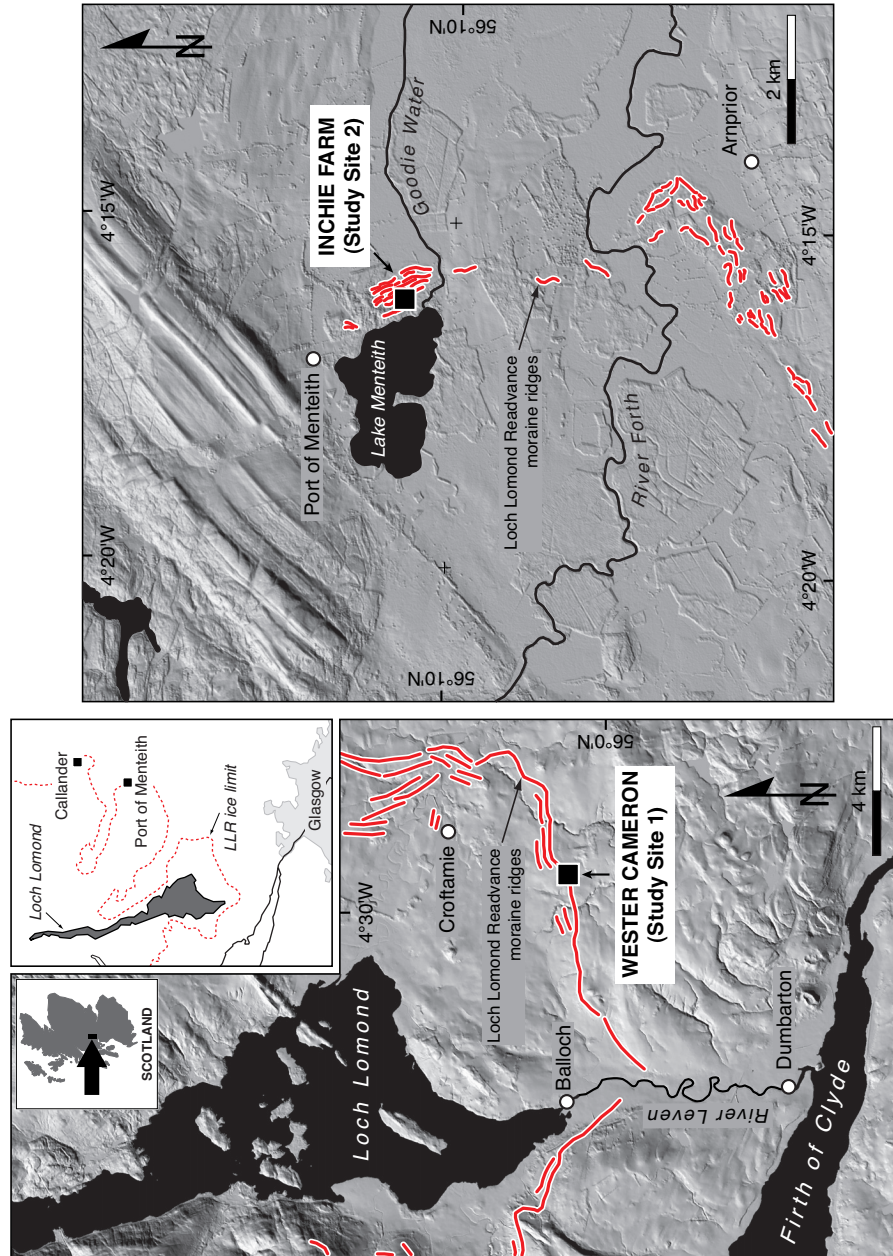


Figure 3.1: Map showing the location of the study sites. The locations of the Younger Dryas Loch Lomond Readvance (LLR) moraine ridges (in red) and LLR ice limit (inset) are based on data from Evans and Rose (2003), Evans et al. (2003) and Evans and Wilson (2006). DEM data courtesy of the British Geological Survey.

and associated soil erosion. This site was selected to assess whether the technique can also be applied to determining the timing and amount of soil loss.

Both sites are on Younger Dryas Loch Lomond Readvance end-moraines. The Younger Dryas glacial readvance is well documented in Scotland (e.g., Sissons 1967, Thorp 1991, Golledge 2010). Several published LLR moraine radiocarbon ages place a first order age constraint on the age of till deposition. In addition, the site at Wester Cameron is close to Croftamie, the well-studied LLR type-locality (Coope and Rose 2008).

3.2 Context

Scotland provides an excellent natural laboratory for undertaking the research proposed here, as its landscape is dominated by glacial landforms that have been mostly preserved from the Last Glacial Maximum, which had maximum extent between $\sim 17 - 18$ cal kyr (Stone et al. 1998).

The LLR perturbation of this landscape started at around 13 kyr (Stone and Ballantyne 2006) and peaked at the middle of the Younger Dryas, with a maximum mean annual temperature at sea level of 2°C (Ballantyne 1984). The LLR was a short-lived (~ 1.3 kyr) glacial incursion, with low erosive power and a still-debated ice thickness (Jack 1877, Sissons 1979, McIntyre and Howe 2010). Radiocarbon dating indicates that LLR glaciers achieved their maximum extent after c. 12.8 kyr (Golledge et al. 2007) and the youngest set of end moraines have been dated to around 11.6 kyr (Dugan 2008) with *in situ* ^{14}C .

The LLR was followed by rapid deglaciation (Howe et al. 2002) mainly due to Scotland's climatic position (Lowell 2000), with evidence for climatic amelioration before 10.5 kyr BP (Walker 1995). The rapid recession has been demonstrated also in glaciotectionic structural evidence (Phillips et al. 2002). Localized ice stagnation might have occurred due to the glaciers' isolation related to their accumulation areas (Benn 1992). This was the last time that the Scottish highlands have been occupied by glaciers (Golledge and Hubbard 2005, Bradwell et al. 2008).

Prominent end moraines mark the limit of the LLR at several localities north of Glasgow, including Inchie Farm near Lake of Menteith and Wester Cameron Farm, our study sites here (Evans et al. 2003) (Figure 3.1). The Lake of Menteith moraine has been interpreted as a proglacially folded and thrust moraine, with the suggestion that the LLR

moraine at Wester Cameron may have the same origin (Evans and Wilson 2006). The type section for the LLR, at Croftamie (Figure 3.1), demonstrates that the Loch Lomond glacier reached its maximum extent after 10.560 ± 160 ^{14}C yrs BP (12 - 12.7 cal kyr BP [1σ] - OxCal v.4.1, 2010) (Rose et al. 1989). There is evidence for continuous glaciomarine sedimentation after 10.350 ± 125 ^{14}C yrs BP (11.7 - 12.6 cal kyr BP [1σ] - OxCal v.4.1, 2010) (Browne and Graham 1981) suggesting a somewhat later deglaciation age (Gordon 1982), in agreement with the recent findings of (Palmer et al. 2010), placing the deglaciation closer to the Holocene. A radiocarbon age of 11.800 ± 170 ^{14}C yrs BP from a shell at the Lake of Menteith moraine (13.8 - 13.4 cal kyr BP [1σ] - OxCal v.4.1, 2011) records a Lateglacial Interstadial high sea level, suggesting that the LLR glacier advance occurred after this date (Sissons 1967). However, most of the radiocarbon age determinations on shells (which in themselves are problematic due to the marine reservoir effect) were undertaken during the 1960s and 1970s and so have large uncertainties. To date, the uncertainties related to the LLR glaciers central and eastern extensions remain unresolved (Golledge et al. 2008, Golledge 2010).

3.3 Study site 1: Wester Cameron Farm

Study site 1, on Wester Cameron Farm, is located approximately 20 km northwest of Glasgow in the vicinity of Croftamie (Figure 3.1). The sampled end moraine is at an elevation of ~ 168 m and is evidently undisturbed. The study site is away from farm tracks, is unforested (i.e., undisturbed by forestry activities) and has a flat crest where the pit for the depth profile was excavated by mechanical backhoe.

The age of moraine emplacement was established by ^{10}Be exposure dating of two erratic boulders found on the moraine (Figure 3.2). The results of the ^{10}Be analyses are summarised in Table 3.1 * and yielded an average age of 10.5 ± 0.9 kyr, slightly younger than the published radiocarbon ages for the LLR maximum ice extent (Gordon 1982).

In order to collect samples for cosmogenic nuclide depth-profile measurements, two ~ 2.5 m deep pits were opened: pit A, on the top of the moraine, on the stable crest, and pit B on the flanking side. Approximately 2 kg of amalgamated sediment was collected in contiguous 15 cm depth increments from both pits, but only the depth profile samples collected from pit A were analysed. The results of the cosmogenic nuclide analyses in these

*Full details of the analytical procedures are provided in Appendix C.



Figure 3.2: Photograph showing the moraine ridge running left to right across the centre of the of the photograph, with arrows indicating the two erratic boulders that were sampled for ^{10}Be exposure dating.

samples are presented in Chapter 4.

The Wester Cameron soil is a peaty podzol soil with a clear B horizon (Figure 3.3), and is capped by a $\sim 15 - 30$ cm thick, well-drained and ungullied peat layer. The presence of the capping peat layer suggests prolonged soil stability and lack of erosion (cf. Edwards and Whittington 2001) and confirms our initial observations about the lack of recent soil disturbance at this site. Radiocarbon determinations on eight samples collected from a $21 \times 27 \times 15$ cm peat monolith taken from the top of the moraine yield a maximum basal age for the peat of ~ 2 kyr. Complete details of the radiocarbon analyses are provided in Appendix B.

Given that (1) the intensity of secondary cosmic ray neutrons, and therefore, the production of cosmogenic nuclides decreases exponentially with depth as a function of density, and (2) tills are unsorted and therefore have highly variable densities, a terrestrial laser scanning-based approach was used to calculate the average density of each 15 cm depth increment sample in the depth profile from pit A. The results of the density calculations are summarised in Figure 3.3 with complete details being provided in Appendix B.

Table 3.1: Summary of the *in situ* ^{10}Be analyses in the Wester Cameron Farm erratic boulders.

Sample ID	Lat (deg)	Long (deg)	Elevation (m)	Thickness (cm)	Production Rate		Shielding Factor*	^{10}Be (at.g $^{-1}$)	$\pm 1\sigma$	Age (years)	$\pm 1\sigma$
					Neutrons	Muons					
Cameron A	56.0094	-4.4741	155	2	5.28	0.191	0.9987	61677	1968	10559	954
Cameron B	56.0094	-4.4741	165	3	5.28	0.192	0.9985	60499	2178	10337	950

Latitude and longitude use WGS84 datum.

Calculated with the CRONUS-Earth online calculator (Balco et al. 2008) version 2.2 (<http://hess.ess.washington.edu/>), using the time dependent Lal/Stone scaling scheme.

*Calculated according to Dunne et al. (1999).

Corrected for a full chemistry procedural blank that yielded < 3% of the number of ^{10}Be atoms in the samples.

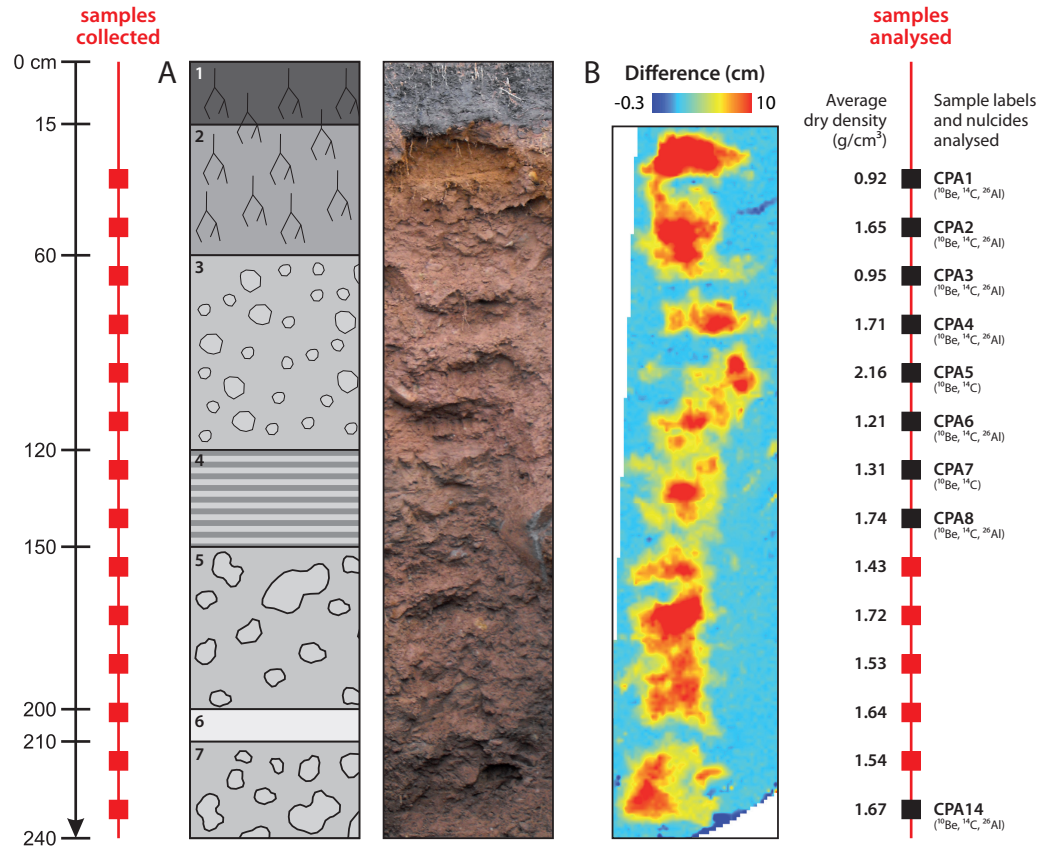


Figure 3.3: Description of Wester Cameron Farm sampling depth-profile. (A) Diagram and photograph describing the till/soil: (1) Up to 30 cm thick peat; (2) Yellowish brown peaty podzol soil with common 2 - 3 cm gravels. The layer contains abundant roots, is well drained and has a slightly bleached appearance; (3) Gradual transition from the turf line situated a 60 cm depth to a structureless till consisting of reddish-chocolate brown clay matrix enclosing sub-angular to rounded pebbles (0.5 - 11.5 cm) of mixed lithologies indicating a wide source area; (4) Sandy/gritty light clay with up to six thin red clay layers dipping slightly towards the southwest; (5) 15 - 20 cm clasts in clay-rich matrix; (6) Olive-grey-brownish sand; (7) Dull greyish-brown clay to medium sand matrix-supported diamicton with occasional gravels ranging in size from 0.2 - 0.3 cm to 1 - 30 cm, clearly bedded to laminated suggesting fluvial deposition. Similar in composition to layer (3) but with clasts up to 30 cm. (B) Terrestrial laser scanner-derived plot of the thickness of material removed during sampling, and used for determining the average dry density values shown on the right. Vertical scale is the same as in (A). Red squares indicate samples collected and black squares those that were used for cosmogenic nuclide analyses, with analysed nuclides listed in brackets.

3.4 Study site 2: Inchie Farm

Study site 2, on Inchie Farm, is located approximately 23 km west-northwest of Stirling on the shore of Lake of Menteith (Figure 3.1). The pit for a cosmogenic nuclide depth profile was excavated on the steep inner flank of the moraine (~ 50 m high), below a marked erosional break in slope. The objective was to analyse a depth profile in an obviously disturbed and eroded site.

No erratic boulders could be found on the moraine (Figure 3.4) and so to establish the age of moraine emplacement, small pebbles (Figure B.9) were collected from the top of the moraine and one bigger rock was collected from the pit wall (Figure B.10) and analysed for *in situ* cosmogenic ^{10}Be . These analyses (summarised in Table B.6) did not yield meaningful results. Given that both the Loch Lomond and Lake of Menteith lobes are mapped as part of the LLR, we assume that the ^{10}Be exposure age of 10.5 ± 0.9 kyr from Site 1, is representative for Site 2. Uncertainties that may arise as a result of using this age at Site 2 are discussed in Chapter 5.



Figure 3.4: Photograph showing the the moraine ridge at Inchie Farm near Lake of Menteith. White rectangles indicates location of pit opened for cosmogenic nuclide analyses, immediately below a marked erosional break in slope.

As at Site 2, a ~ 2.5 m deep pit was opened and samples for cosmogenic nuclide analyses were collected at contiguous 15 cm depth intervals. The average density of the

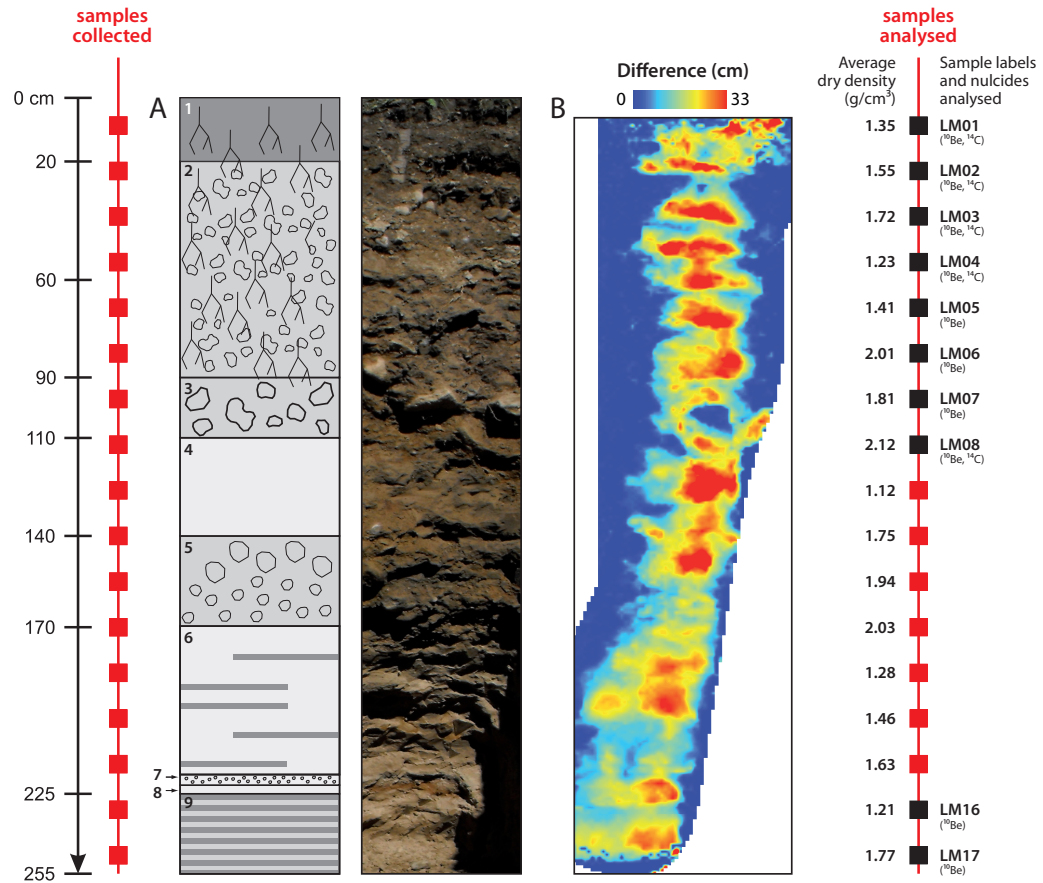


Figure 3.5: Description of Inchie Farm sampling depth-profile. (A) Diagram and photograph describing the till/soil: (1) Dark-brown gritty to clay loam; (2) Diamicton with sandy-loam matrix, with a clear boundary to (3) Diamicton with sandy-loam matrix and coarse clasts. This layer includes large angular to well-rounded cobbles; (4) Massive yellow brownish-grey fine sand, gently dipping towards the southeast; (5) Dark brown-grey sandy gravel of mixed lithology coarsening upwards and with a lower boundary dipping towards the southeast; (6) Yellow-grey fine, locally cross-bedded sand, dipping at 16 degrees to south. This unit contains an oxidised layer suggesting interaction with ground water; (7) Thin bed of yellow-grey sand and gravel; (8) Thin layer of red-brown sandy silt; (9) Fine sand layer with thinly interbedded reddish clay. (B) Terrestrial laser scanner derived surface indicating the thickness of material removed during sampling, and used for determining the average dry density values shown on the right. Vertical scale is the same as in (A). Red squares indicate samples collected and black squares those that have been analysed for cosmogenic nuclides, with analysed nuclides listed in brackets.

soil/till was also determined at 15 cm intervals using the terrestrial laser scanning-based approach. Results of the cosmogenic nuclide analyses in the samples from Site 2 are discussed in Chapter 4. The results of the density calculations are summarised in Figure 3.5 with complete details being provided in Appendix B.

3.5 Summary

On both study sites the stratigraphy described above indicates complex glacio-fluvial processes associated with ice margins (Gerrard 1992). There are uncertainties associated with the form of deposition and exact timing of the LLR. However the similarity in stratigraphy and soil development (Douglass and Bockheim 2006) and the close physical proximity between the two sites indicate that the cosmogenic ^{10}Be exposure age determined at the Western Cameron Farm is likely to be also representative of the moraine at Inchie Farm. In all further calculations the exposure age of 10.5 kyr is used as the age of till stabilization at both study sites. Neither the type of till formation nor lithology affect the cosmogenic ^{10}Be and ^{14}C depth-profiles. The attenuation with depth of cosmic rays, and therefore the shape of the depth-profiles, is mainly a function of the density of the penetrated material. The latter has been thoroughly characterised at both sample sites.

THE UNIVERSE IS MADE OF STORIES, NOT OF ATOMS.

[Muriel Rukeyser]

Chapter 4

Results of the cosmogenic nuclide analyses

4.1 Introduction

This chapter evaluates whether the full original thickness of the sediment at the two study sites is still intact. Zero-erosion cosmogenic nuclide depth-profiles are calculated for both sites using the ^{10}Be exposure age obtained from the erratic boulders from Wester Cameron (Chapter 3). These zero-erosion cosmogenic nuclide depth-profiles are compared with those obtained from ^{10}Be , ^{14}C , and ^{26}Al measurements in samples collected from the two pits described in Chapter 3. This chapter also assesses whether the depth-profile samples contain any cosmogenic nuclides inherited from previous periods of exposure, and whether any grain-size effects are discernible in the measured concentrations. The chapter opens in Section 4.2 with a brief description of the methods that are used for calculating the ‘zero-erosion’ depth-profiles. The results of the cosmogenic nuclide measurements are presented and discussed in Section 4.3.

4.2 Methods

Ultrapure quartz separates were prepared following the modified protocol of (Kohl and Nishiizumi 1992). Cosmogenic ^{10}Be and ^{26}Al was separated from the ultrapure quartz samples at the two cosmogenic isotope laboratories at the Scottish Universities Environ-

mental Research Centre (SUERC): samples from Wester Cameron were prepared at the NERC Cosmogenic Isotope Analysis Facility and samples from Inchie Farm were prepared at the Centre for Geosciences - Cosmogenic Nuclide Laboratory. The cosmogenic ^{14}C analyses were undertaken at SUERC Radiocarbon Dating Laboratory. Cosmogenic isotope ratios were determined at the SUERC AMS laboratory (Freeman et al. 2007). Appendix C give full details of the sample preparation and measurement procedures.

The zero-erosion cosmogenic nuclide depth-profiles are calculated following Granger and Smith (2000) and Granger and Muzikar (2001):

$$N(z, t) = \frac{1 - e^{-\lambda t}}{\lambda} \sum_{i=1}^4 P(0)_i e^{-\rho z / \Lambda_i} \quad (4.1)$$

where $N(z, t)$ is the cosmogenic nuclide concentration (atoms.g^{-1}) acquired by a sample as a function of time and depth below the surface, λ is the radioactive decay constant, calculated as $\ln(2)/T_{1/2}$, with $T_{1/2}$ being the radioactive half-life of the cosmogenic nuclide (yrs), t is the amount of time (yrs) since nuclide production began, $P(0)_i$ is the surface production rate ($\text{atoms.g}^{-1}.\text{yr}^{-1}$) of a given cosmogenic nuclide by a given production pathway (i.e., high energy neutrons, and slow and fast muons), ρ is the density of the target material (g.cm^{-3}), and Λ_i is the absorption mean free path for nuclear interacting particles in the target mineral for a given production pathway (g.cm^{-2}).

This study uses a ^{10}Be half-life of 1.51 Myrs (Yiou and Raisbeck 1972, Hofmann et al. 1987, Inn et al. 1987) to be consistent with the ^{10}Be standardization used at the SUERC AMS. Although recent studies have found the ^{10}Be half-life to be shorter, namely, 1.38 Myrs (Nishiizumi et al. 2007, Korschinek et al. 2010, Chmeleff et al. 2010), the choice of half-life will not affect our results, as our samples are substantially younger than the ^{10}Be half-life. For all ‘zero-erosion’ cosmogenic nuclide depth-profile calculations, we take t in equation 4.1 to be equal to 10.5 kyr, and use the measured density values presented in Chapter 3.

The formulation in equation 4.1 allows for explicitly accounting for production of cosmogenic nuclides by muons. The calculations presented here account for production of cosmogenic nuclides through high-energy neutron spallation, negative muon capture, and fast muon induced bremsstrahlung, using the exponentials given by Granger and Smith

(2000) and Granger and Muzikar (2001):

$$\begin{aligned}
 P_n(z) &= P_n(0) \exp[-\rho z/\Lambda_n] \\
 P_\mu(z) &= P_{\mu 1}(0) \exp[-\rho z/\Lambda_{\mu 1}] + P_{\mu 2}(0) \exp[-\rho z/\Lambda_{\mu 2}] \\
 P_f(z) &= P_{\mu 3}(0) \exp[-\rho z/\Lambda_{\mu 3}]
 \end{aligned}
 \tag{4.2}$$

where $P_n(0)$, $P_{\mu 1}(0)$, $P_{\mu 2}(0)$, and $P_{\mu 3}(0)$ are the surface cosmogenic nuclide production rates for neutrons (n) and slow ($\mu_{1,2}$) and fast muons (μ_3), respectively. The sea-level, high latitude muogenic production rates for ^{10}Be , ^{14}C , and ^{26}Al are taken from Heisinger et al. (2002a,b). Following Granger and Smith (2000), $\Lambda_n = 160$, $\Lambda_{\mu 1} = 738.6$, $\Lambda_{\mu 2} = 2688$, and $\Lambda_{\mu 3} = 4360 \text{ g.cm}^{-2}$, respectively.

4.3 Results and discussion

A total of 33 samples were analysed as part of this work. *In situ* cosmogenic ^{10}Be measurements were done in all 33 samples, whereas *in situ* ^{14}C measurements were restricted to 16 of these samples (see below). Cosmogenic ^{26}Al measurements were also done in nine of the Wester Cameron samples.

4.3.1 Wester Cameron

A total of 14 bulk till samples ($\sim 2 \text{ kg}$ each) were collected from the $\sim 2.50 \text{ m}$ deep pit on the flat stable moraine crest on Western Cameron farm. The till samples were wet sieved, dried, and separated into a total of 42 samples of three grain size fractions: $250 - 500 \mu\text{m}$ (labels starting with CPA-F), $500\mu\text{m} - 2\text{mm}$ (labels starting with CPA-M), and $> 2 \text{ mm}$ (labels starting with CPA-P). Of the 42 samples only 18 were processed for cosmogenic nuclide analyses after crushing and sieving to $250 - 500 \mu\text{m}$. All processed CPA-P samples mainly consisted of sandstone clasts, whereas CPA-F and CPA-M consisted of mixed lithologies. *In situ* cosmogenic ^{10}Be was analysed in all 18 of the samples, whereas due to the time-consuming nature of the *in situ* ^{14}C extraction procedure, this nuclide was only analysed in 9 of the samples. As already mentioned above, ^{26}Al was also analysed in nine of the 18 samples. Results of the cosmogenic nuclide measurements are summarized in Figures 4.1 - 4.3. Detailed descriptions and photographs of selected samples are given in Appendix C. Complete data tables with the cosmogenic nuclide measurement results are

given in Appendix C.2.

4.3.1.1 Depth-profile characteristics and grain-size differences

The cosmogenic nuclide depth-profiles show declining ^{10}Be , ^{26}Al , and ^{14}C concentrations with depth (Figures 4.1 - 4.3). There is an indication of homogenisation of the upper 70 cm, which exhibit similar concentrations. The process has mixed both the coarsest and finest grain sizes and has either acted throughout the last ~ 10.5 kyrs or be sufficiently recent to homogenise ~ 10.5 kyr of cosmogenic nuclide in-growth at the two depths. A range of mechanisms could be responsible for such mixing, including bioturbation by large soil fauna and/or large flora (e.g., by tree fall and root throw), and perhaps cryoturbation, all restricted to the top 50 - 70 cm of the till and presumably pre-dating the growth of the peat that caps the moraine. Cryoturbation is unlikely for at least two reasons: (1) no structures were evident in the till sediments indicative of cryoturbation at any depth in the moraine; and (2) if cryoturbation did occur, it would have been most likely immediately after the LLR and is unlikely in later Holocene climates at the moraines elevation. If the shallowest two samples had been cryoturbated in the early Holocene, subsequent (middle and late Holocene) acquisition of cosmogenic nuclides would have restored the exponential depth-profile.

On soils that have not been disturbed by vertical movement and homogenisation of material, erosion removes the high cosmogenic nuclide concentration surface material, reducing the total cosmogenic nuclide inventory while not affecting the exponential shape of the depth-profile. Homogenisation of the upper part of a cosmogenic nuclide depth-profile, either by bioturbation or cryoturbation, will result in migration of low nuclide concentration sediment upward. Erosion of a homogenised soil layer, therefore, creates a mismatch between the integral of the concentration in the homogenised layer and the integral of the exponential zero-erosion cosmogenic nuclide depth-profile (cf. Perg et al. 2001). To test whether the surface of the soil was eroded prior to the formation of the peat cover, the total cosmogenic ^{10}Be inventory in the Wester Cameron pit was calculated by integrating the curve obtained by joining the ^{10}Be concentrations measured in the 0.25 - 0.5 mm size fraction (cf. Hidy et al. 2010) and the one obtained by integrating the curve defined by the zero-erosion cosmogenic ^{10}Be depth-profile (Figure 4.4). The difference between the two inventories is 10% (Figure 4.4). This difference is similar to

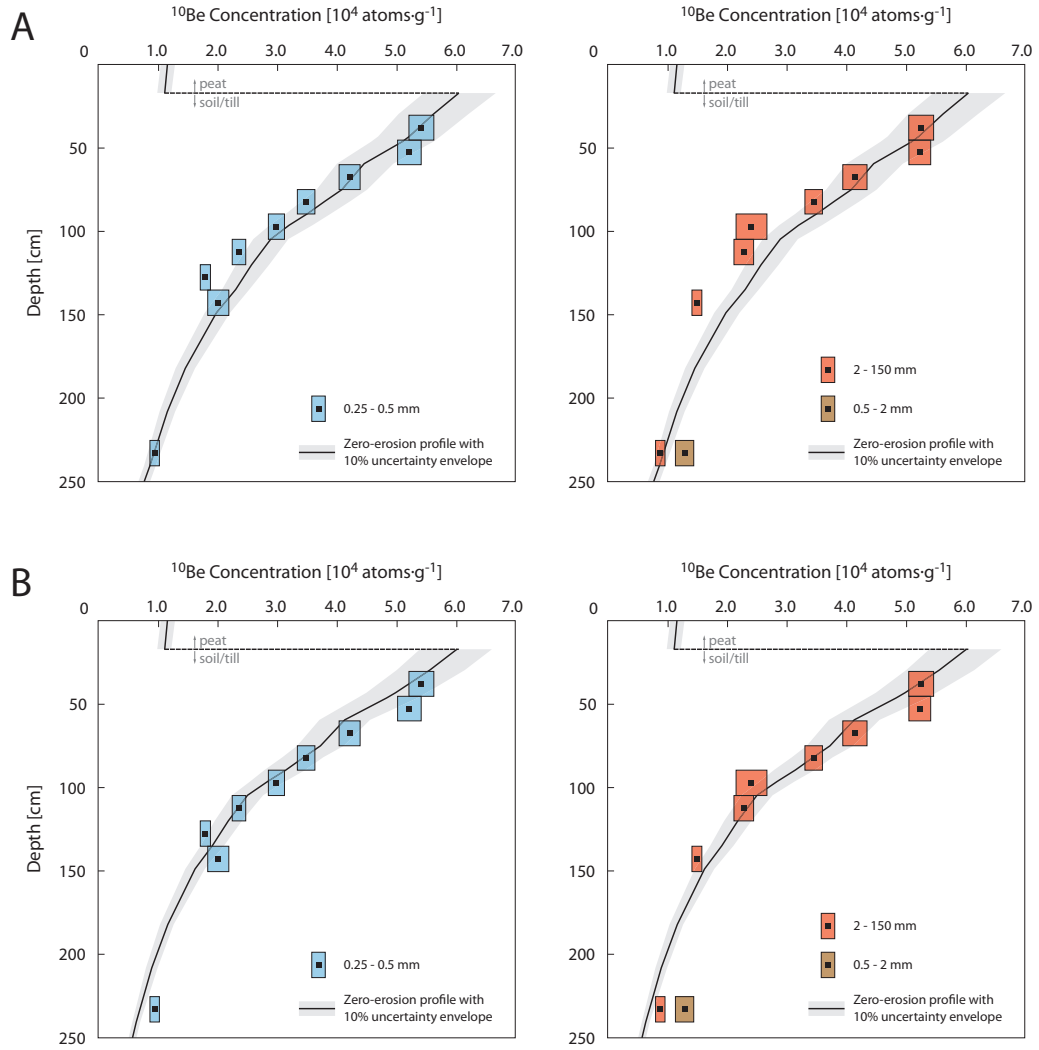


Figure 4.1: Depth-profiles of measured ^{10}Be concentrations in clasts in the pit on the LLR moraine crest, Wester Cameron. Different colours indicate different grain sizes. Black squares represent measured values. The length of each rectangle represents measurement uncertainty at the 1σ level, and height of rectangles represents the sampling depth interval (15 cm). ^{10}Be concentration was not determined for the pebble sample at 120 - 135 cm depth below the peat, and the medium grain size (gravel and coarse sand) of only the deepest sample was analysed for ^{10}Be . The continuous line with 10% uncertainty envelope (covering production rate and analytical uncertainties) gives the theoretical ('zero-erosion') depth-profile for a sedimentary body with the bulk densities determined for the sampled profile (calculations using dry density shown in Figure 4.1A and those using wet density are shown in Figure 4.1B), and which has been exposed for $\sim 10.5\text{kyr}$ and capped by a peat with the measured density (including water content) of the Wester Cameron peat ($\sim 0.8\text{ g}\cdot\text{cm}^{-3}$) developing at a constant rate from 2 kyr.

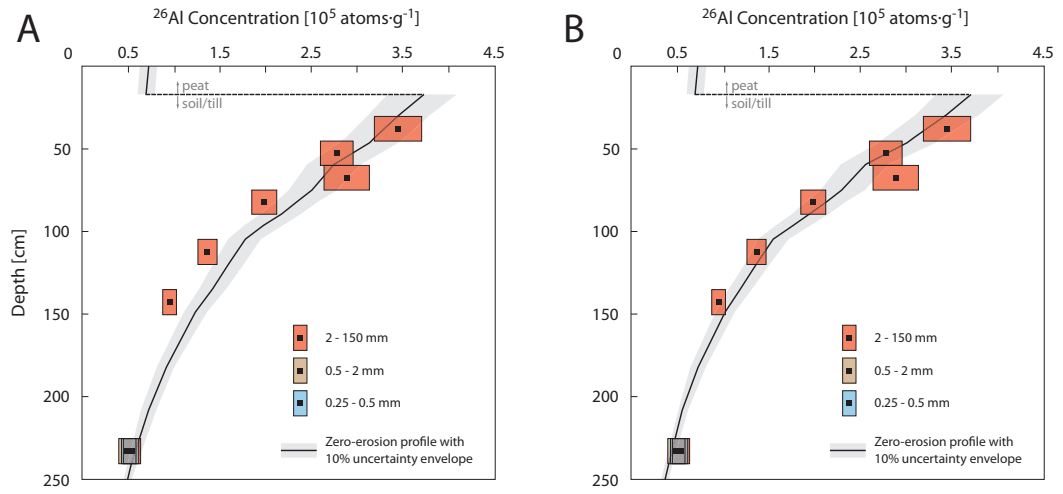


Figure 4.2: Depth-profiles of measured ^{26}Al concentrations in clasts in the LLR moraine crest, Wester Cameron. For details see caption of Figure 4.1.

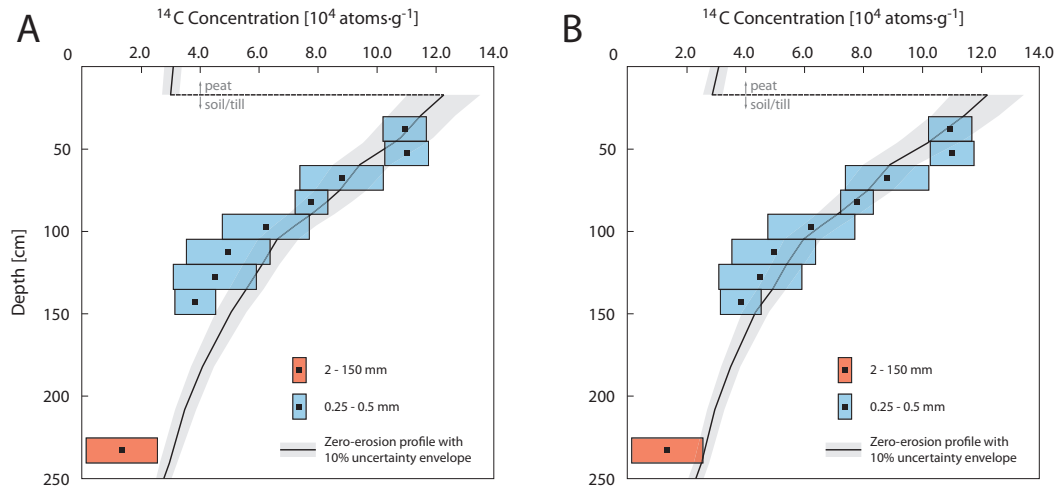


Figure 4.3: Depth-profiles of measured ^{14}C concentrations in clasts in the LLR moraine crest, Wester Cameron. For details see caption of Figure 4.1.

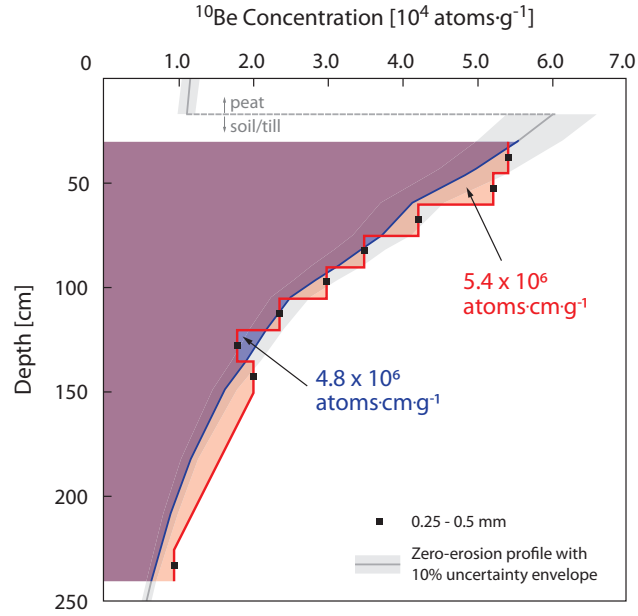


Figure 4.4: Inventories of cosmogenic ^{10}Be in the Wester Cameron pit calculated using ‘zero erosion’ depth-profile (blue) and measured ^{10}Be concentrations (red). See text for more details.

the uncertainty of the zero-erosion depth-profile, suggesting that the two inventories are essentially identical, suggesting in turn that the sediment at the Western Cameron site has not been eroded since its stabilization.

There is generally little differentiation in ^{10}Be concentration by grain-size, and in the two cases where this is observed (at 97 cm and 142 cm sample depths) the coarser fraction has the lower concentration. This difference in ^{10}Be concentration between the different grain-sizes could simply be due to the fact that the coarser fraction amalgamates substantially fewer individual clasts than the finer fraction (i.e., ~ 10 individual clasts in the coarser fraction vs. $\sim 10^5$ sand grains in the finer fraction), and so may easily under- or over-estimate the true mean ^{10}Be concentration (cf. Hidy et al. 2010).

4.3.1.2 Cosmogenic nuclide inheritance

A depth-profile of terrestrial cosmogenic nuclide concentrations through a sedimentary body can be used to determine the nuclide inheritance in the sediments and hence the depositional age of the sediments upper surface (Phillips et al. 1990, Chadwick et al. 1994, Trull et al. 1995, Anderson et al. 1996, Repka et al. 1997, Phillips et al. 1998, Perg et al. 2001, Hidy et al. 2010). The nuclide concentration at ~ 2.5 m depth in the

sedimentary deposit provides an estimate of the nuclide inheritance, on the assumption that cosmogenic nuclide production at that depth is negligible (Anderson et al. 1996, Burbank and Anderson 2001, Phillips et al. 1998). The depth-profile of cosmogenic nuclide concentrations, and hence the inherited component at ~ 2.5 m depth, can be inferred by fitting an exponential depth-profile of nuclide concentrations to a surface sample and a sample at depth (e.g., Anderson et al. 1996), if it is assumed that the profile has not been perturbed by post-depositional burial (or erosion), by vertical movement of clasts (by, for example, cryoturbation or bioturbation), and/or by bulk density changes (Anderson et al. 1996, Phillips et al. 1998, Hancock et al. 1999).

Glacial settings are susceptible to the issue of inheritance in exposure dating (Briner and Swanson 1998, Fabel et al. 2002, Bierman 2007). Such inheritance may arise, for example, from clasts dropping onto the ice surface from the exposed valley side above the ice, or, probably more likely, in situations where an ice mass erodes and deposits material that has been exposed to cosmic radiation prior to that glacial episode, which does not erode sufficient depth of material (~ 2 m) to be then eroding cosmogenic nuclide-free material (Stroeven et al. 2002, Bierman and Nichols 2004). This situation commonly arises when cold-based ice achieves minimal erosion because it is frozen to the bed (Staiger et al. 2005). There is little evidence in the Wester Cameron LLR moraine depth-profile of nuclide inheritance, with all but one of the measured ^{10}Be concentrations (i.e., apart from the top bioturbated sample at 70 cm depth) lying either side of, and overlapping with, the calculated ‘zero-erosion’ depth-profiles, within the uncertainties of that calculated profile and the measured concentrations. The only possible exception is the medium-sized fraction of the deepest sample (225-240 cm), which returned a ^{10}Be nuclide concentrations slightly greater than that predicted by the calculated depth-profile for a ~ 10.5 kyr-old moraine with the densities of the Wester Cameron till (Figure 4.1). The ^{10}Be concentrations of the coarse- and fine-grained fractions of that deepest sample lie squarely within the uncertainties of the calculated depth-profile and the nuclide concentration measured in the medium-sized fraction is indistinguishable at 1σ from the nuclide concentrations measured in those other two size fractions. It is therefore reasonable to conclude that the clasts record minimal inherited nuclide concentration. It is important to remember that even though the deepest clasts have ^{10}Be concentrations of the order of $10^3 - 10^4 \text{ atoms.g}^{-1}$ (corresponding to <2 kyr of exposure for a production rate of $\sim 5 \text{ atoms.g}^{-1}.\text{yr}^{-1}$ at the ground surface), the calculated depth-profile shows that that concentration will accumulate over 10.5 kyr

at that depth in clasts with a minimal amount of inheritance (equivalent to a maximum of ~ 800 years of exposure) in a sedimentary body with the measured densities of the Wester Cameron moraine.

The low nuclide inheritance in clasts in the Wester Cameron LLR moraine is likely to reflect several factors. Firstly, the Younger Dryas Loch Lomond valley glacier was not cold-based and hence was able to erode its bed and remove much of the upper ~ 2 m of ground surface that was exposed during the preceding ice-free Windermere Interstadial. Secondly, the Windermere Interstadial was of relatively short duration, meaning that the clasts in the LLR moraine sampled here had relatively short duration of exposure to cosmic radiation, hence minimising the in-growth of cosmogenic ^{10}Be prior to the LLR. Thirdly, and conversely, the LLR was itself of relatively short duration, making it more likely that boulders with nuclide inheritance would have been retained within the system and be available for sampling. Departures of the measured LLR till ^{10}Be depth-profile from the ‘zero-erosion’ cosmogenic nuclide depth-profiles for a ~ 10.5 kyr-old Wester Cameron-type till are minor, pointing to a relatively simple post-depositional history of acquisition of ^{10}Be . The simple exposure history of the soil/till at the Wester Cameron site is also confirmed by the insignificant departures of the ^{26}Al and ^{14}C results from the ‘zero-erosion’ cosmogenic nuclide depth-profiles (Figures 4.2 and 4.3).

4.3.2 Inchie Farm

A total of 17 bulk till samples ($\sim 2\text{--}5$ kg each) were collected from the ~ 2.55 m pit at the inner edge of the moraine crest on Inchie Farm. The till samples were wet sieved, dried, and separated into a total of 51 samples of three grain sizes fractions: $250 - 500\ \mu\text{m}$ (labels starting with CPA-F), $500\ \mu\text{m} - 2\ \text{mm}$ (labels starting with CPA-M), and $> 2\ \text{mm}$ (labels starting with CPA-P). Of the 51 samples only 15 were processed for cosmogenic nuclide analyses after crushing and sieving to $250 - 500\ \mu\text{m}$, except for LM-17F, for which only the $125 - 250\ \mu\text{m}$ size fraction was available. All processed LM-P samples consisted of sandstone clasts, whereas LM-F and LM-M consisted of material of mixed lithologies. *In situ* cosmogenic ^{10}Be was analysed in all 15 of the samples. Due to the time consuming nature of the *in situ* ^{14}C extraction procedure (cf. Chapter 2), *in situ* ^{14}C was only analysed in 7 of the samples. The results of the cosmogenic nuclide measurements are summarized in Figures 4.5 and 4.6. Detailed descriptions and photographs of selected

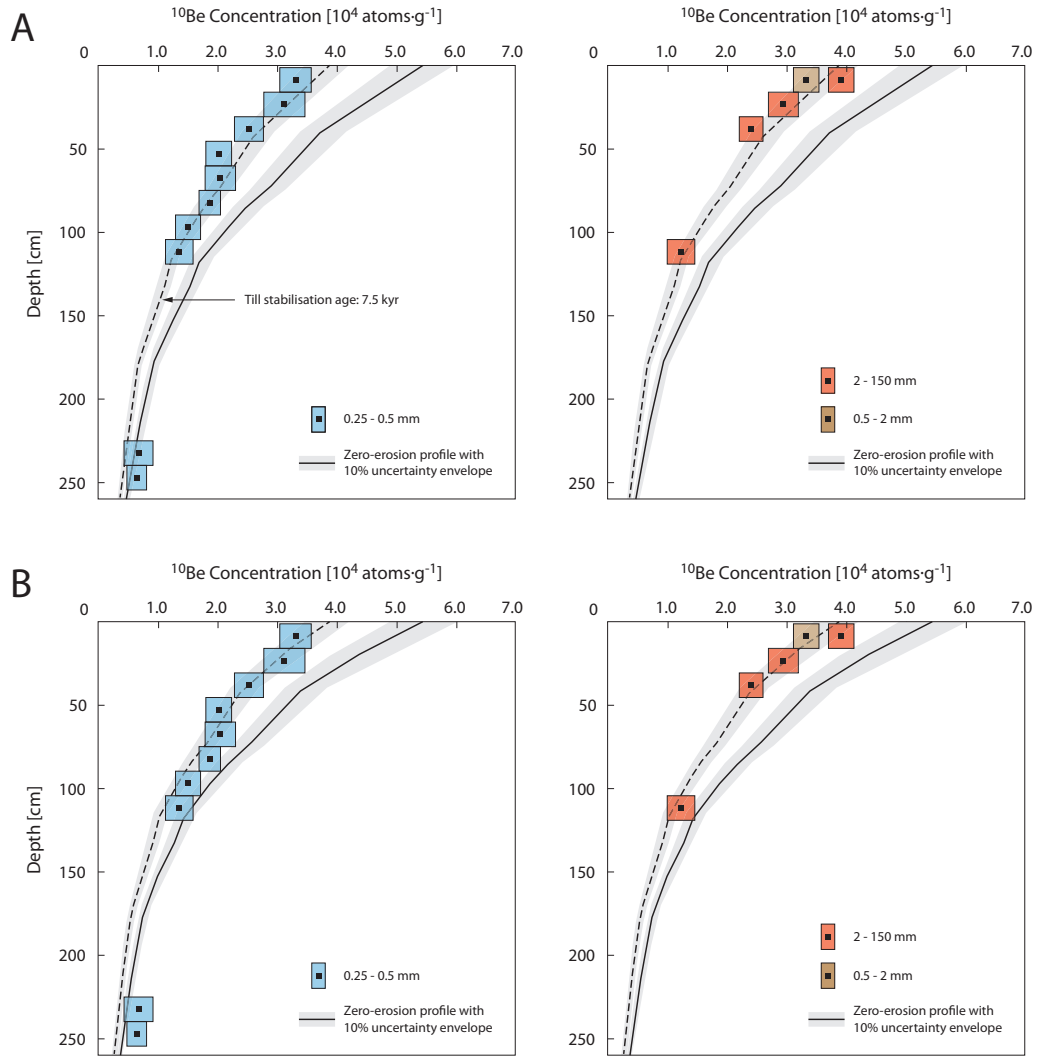


Figure 4.5: Depth-profiles of measured ^{10}Be concentrations in clasts in the LLR moraine crest, Inchie Farm. For details see caption of Figure 4.1.

samples are given in Appendix C. Complete data tables with the cosmogenic nuclide measurement results are given in Appendix C.2.3.

Unlike the results for the Wester Cameron site, the ^{10}Be and ^{14}C concentrations at the Inchie Farm site show a clear departure from the ‘zero-erosion’ cosmogenic nuclide depth-profiles obtained for an exposure duration of 10.5 kyr (Figures 4.5 and 4.6). The measured profiles lie to the left of the ‘zero-erosion’ depth-profiles, indicating that either (1) the soil/till at this site has undergone erosion sufficiently recently since its emplacement that has not permitted the full ‘uneroded’ depth-profile to be re-established; or (2) the soil/till was shielded by a layer of peat that has been subsequently removed; or (3) there was no erosion but the age of soil/till stabilisation is younger than 10.5 kyr. The possibility

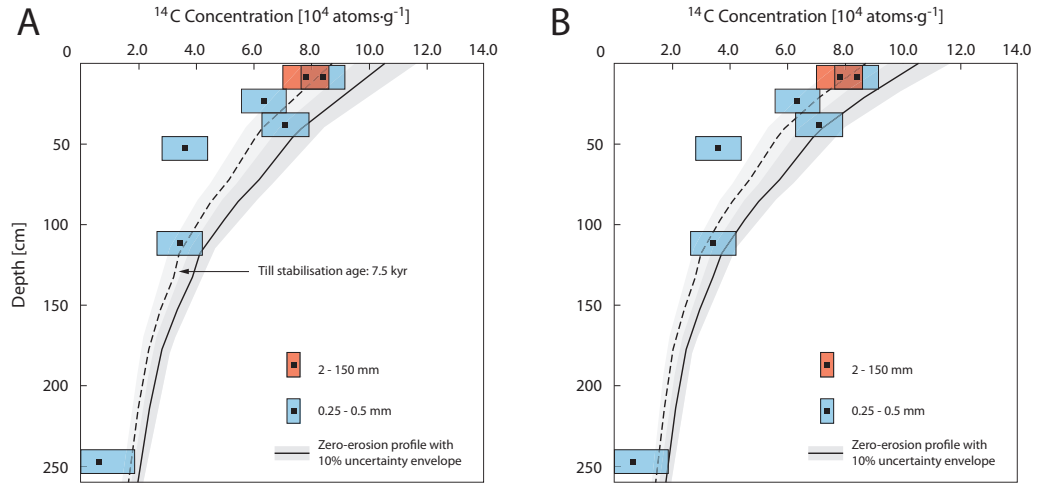


Figure 4.6: Depth-profiles of measured ^{14}C concentrations in clasts in the LLR moraine crest, Inchie Farm. For details see caption of Figure 4.1.

of a peat cover can be easily excluded. The relatively low density of peat means that a peat cover of at least 60 cm is needed for an exposure duration of at least 10.5 kyr, to explain the departure from the ‘zero-erosion’ cosmogenic nuclide depth-profiles observed at Inchie Farm. Moreover, the presence of a cover that has been subsequently removed is tantamount to (1). In the absence of erosion, an exposure duration of 7.5 kyr is necessary to reproduce the ^{10}Be and ^{14}C concentrations obtained at Inchie Farm (dashed lines in Figures 4.5 and 4.6). This age is substantially younger than the deglaciation ages recorded in Scotland (Benn and Lukas 2006). Moreover, the similarity in stratigraphy and soil development (Douglass and Bockheim 2006) and close physical proximity between Inchie Farm and Wester Cameron indicate that the cosmogenic ^{10}Be exposure age determined at the Western Cameron Farm is likely to be also representative of the moraine at Inchie Farm. Therefore, the most likely explanation for the obtained ^{10}Be and ^{14}C concentrations is that the soil/till at this site has undergone erosion sufficiently recently since its emplacement. The amount and timing of this erosion are quantified in the following chapter.

4.3.3 Implications of the timing of erosion at Inchie Farm

The main aim of this study was the testing on a new cosmogenic nuclide-based approach to determining the amount and timing of an erosion event, and so the sample strategy was designed accordingly. We have selected two sites: one, at Wester Cameron, where we could ascertain that no soil erosion occurred, and the surface of the moraine was intact;

and one, at Inchie Farm, where there were visible signs of soil loss. The results of our Monte Carlo analyses suggest that the erosion event at Inchie Farm occurred in the last 1.5 kyr, with a best fit at 300 years B.P. Given that we only have one site, and therefore have only one estimate of the timing of the erosion event that removed the soil from this site, we can only speculate as to what the geomorphological meaning of this erosion event timing estimate is, if at all there is one.

Studies employing a range of tools, including pollen, potassium, magnetic susceptibility, and radiocarbon analyses, have observed throughout Scotlands lakes, increases in sedimentation attributed to agricultural activity during the mid Holocene at 5, 4, 3, 1.5, and in some cases also at 0.3 kyr B.P. (Edwards and Whittington 2001). In the 18th century, grain production in Scotland has increased following the independence war and the Union of Scotland and England 1707 Agriculture Progress Regulation Act. This century has also seen increases in deforestation as sheep grazing pressure increased with wool production becoming an important part of the economy (Smout and Fenton 1965). This intensification of agriculture coupled with deforestation in 18th century Scotland could potentially be one explanation for the 300 years B.P. timing of the erosion event obtained at Inchie Farm. Taking into account the uncertainty associated with our erosion event timing estimate, however, the loss of soil at Inchie Farm could also be linked to the advent of iron tools at around 500 B.C. (Barrett 1981).

4.4 Summary

Cosmogenic ^{10}Be , ^{14}C , and ^{26}Al determinations in samples collected from depth-profiles at two sites on the crests of the LLR moraine were compared with theoretical ‘zero-erosion’ cosmogenic nuclide depth-profiles obtained for a soil/till emplacement age of 10.5 kyr, in order to evaluate whether the full original thickness of the soil/till at the two study sites is still intact. The results of the cosmogenic ^{10}Be , ^{14}C , and ^{26}Al analyses in the Wester Cameron site samples confirm that the cosmogenic nuclide depth-profile to be expected from a sediment body of Holocene age can be reconstructed. Moreover, the agreement between the total cosmogenic ^{10}Be inventories in the erratics and the Wester Cameron soil/till samples (Figure 4.4) confirm that there has been no erosion at the sample site since the deposition of the till/moraine. Further, the Wester Cameron depth-profiles show minimal signs of homogenisation, as a result of bio- or cryoturbation, and minimal

cosmogenic nuclide inheritance from previous exposure periods. The cosmogenic ^{10}Be and ^{14}C data from the Inchie Farm samples show a clear departure from the ‘zero-erosion’ cosmogenic nuclide depth-profiles suggesting that the soil/till at this site has undergone erosion since its emplacement.

OFTEN STATISTICS ARE USED AS A DRUNKEN MAN USES LAMPPOSTS: FOR SUPPORT
RATHER THAN ILLUMINATION.

[Unknown]

Chapter 5

The magnitude and timing of soil erosion at Inchie Farm and sensitivity analyses

5.1 Introduction

As shown in Chapter 4, the results of the *in situ* cosmogenic ^{10}Be and ^{14}C analyses in the Inchie Farm site samples show a clear departure from the ‘zero-erosion’ cosmogenic nuclide depth-profiles, suggesting that the till at this site has been eroded since its emplacement. A Monte-Carlo type approach is used in this chapter to model *in situ* cosmogenic ^{10}Be and ^{14}C depth-profiles for a wide range of till erosional events, thereby to constrain the magnitude and timing of till erosion at Inchie Farm. The Monte-Carlo type approach is further employed to assess the sensitivity of the results to the model parameters. The chapter opens in Section 5.2 by outlining the theoretical background of the Monte-Carlo approach used here. The magnitude and timing of till erosion at Inchie Farm are determined in Section 5.3, and Section 5.4 presents the results of the sensitivity analyses.

5.2 Theoretical background

The temporal evolution of the cosmogenic nuclide concentration (N) in a sample is described by the differential equation:

$$\frac{dN(z, t)}{dt} = P(z, t) - \lambda N(z, t) \quad (5.1)$$

where $N(z, t)$ is cosmogenic nuclide concentration as a function of depth below the surface and time, $P(z, t)$ is the production rate, again as a function of depth below the surface and time, and λ is the decay constant of a radionuclide ($\lambda = \ln(2)/T_{1/2}$, $T_{1/2}$ being the half-life) (Lal 1991, Niedermann 2002). Taking $t = 0$ as present and z_0 as the initial burial depth, the depth of a mineral grain below an eroding surface can be calculated as:

$$z(t) = z_0 - \epsilon t \quad (5.2)$$

where ϵ is the erosion rate (cm.yr^{-1}). Solving Equation 5.1 yields:

$$N(z, t) = N(z, 0)e^{-\lambda t} + \sum_{i=4}^4 \frac{P(0)_i}{\lambda + \rho\epsilon/\Lambda_i} e^{-\frac{\rho(z_0 - \epsilon t)}{\Lambda_i}} \left(1 - e^{-(\lambda + \rho\epsilon/\Lambda_i)t}\right) \quad (5.3)$$

where $P(0)_i$ and Λ_i are the surface production rate ($\text{atoms.g}^{-1}.\text{yr}^{-1}$) and mean cosmic ray attenuation length (g.cm^{-2}) for the different production pathways (i.e., high energy neutrons, slow and fast muons; see Chapter 4 for more details) (Lal 1991, Niedermann 2002, Granger and Smith 2000), and (Granger and Muzikar 2001). Given that the initial burial depth (z_0) is not known, Equation 5.3 can be modified such that the present burial depth (z_p) is used instead:

$$z_0 - \epsilon t = z_p + \epsilon t \quad (5.4)$$

Equations 5.3 and 5.4 accurately describe the accumulation of cosmogenic nuclides in a mineral grain buried beneath an eroding or non-eroding surface, and are implemented in a relatively simple numerical model used to calculate the evolution through time of the ^{10}Be and ^{14}C concentrations of the samples in the Inchie Farm depth-profile. The model works as follows. After stabilisation of the moraine, *in situ* cosmogenic ^{10}Be and ^{14}C start accumulating in the sediment body, against a continuous (steady-state) erosion rate (ϵ in Equation 5.3). At a given moment in time (between sediment stabilisation and the present), a given thickness of soil is instantaneously removed from the surface of the sediment body by an erosional event, truncating the cosmogenic ^{10}Be and ^{14}C

depth-profiles. Following this erosional event, *in situ* cosmogenic ^{10}Be and ^{14}C continue to accumulate against the same or a different steady-state erosion rate. The accumulation of ^{10}Be and ^{14}C is calculated using two versions of Equation 5.3. In the first version, t is the amount of time since moraine stabilization to time of erosion event, and in the second t is the amount of time since erosion event and present. The numerical model has four unknowns: the timing and magnitude of the erosional event, and the steady-state erosion rates that characterize the soil before and after the erosional event. A Monte-Carlo type approach using a chi-squared inversion method is employed to identify the magnitude and timing of the erosional event that best fits both measured cosmogenic ^{10}Be and ^{14}C depth-profiles. The steady-state erosion rates for before and after the erosional event cannot be quantified, and so the Monte-Carlo approach is also used to test the sensitivity of the obtained erosional event magnitude and timing pair to a range of realistic estimates of these steady-state erosion rates. Therefore, for the purposes of the chi-squared inversion, the magnitude and timing of the erosional event are the only two unknowns. For complete details on how Equation 5.3 is implemented in the numerical model, the reader is referred to Appendix D.

For any cosmogenic nuclide depth-profile corresponding to a single erosional event with a given timing and magnitude, one can minimize the difference between the measured ^{10}Be and ^{14}C depth-profiles and those predicted by the model and therefore find the solution that best fits the data. However, given that the measured ^{10}Be and ^{14}C concentrations have an associated uncertainty, more than one erosional event timing and magnitude pair will provide a reasonable fit to the data. Under these circumstances the statistically most likely model solution can be obtained by minimising the chi-square (χ^2) statistic, given by (Bevington and Robinson 2003):

$$\chi^2 = \sum \left(\frac{N_{Measured} - N_{Modelled}}{\sigma N_{Measured}} \right)^2 \quad (5.5)$$

where $N_{Measured}$ and $N_{Modelled}$ are the measured and modelled ^{10}Be and ^{14}C concentrations in each sample, respectively, and $\sigma N_{Measured}$ is the uncertainty in the measured ^{10}Be and ^{14}C concentrations. The χ^2 approach has been successfully applied to quantifying the depositional ages of eroding alluvial terraces (Siame et al. 2004, Hein et al. 2009, Braucher et al. 2009, Guralnik et al. 2010, Hidy et al. 2010) and eroding moraines (Schaller et al. 2009).

When used as a goodness-of-fit indicator, χ^2 is reduced by dividing by the degrees of freedom given as $N_s - m$, where N_s is the number of measurements and m is the number of model parameters (Bevington and Robinson 2003). If the modelled cosmogenic nuclide depth-profile is a good fit to the data, the reduced χ^2 (χ_{red}^2) should approach unity ($\chi_{red}^2 = 1$). Values that are large or < 1 indicate that the modelled cosmogenic nuclide depth-profile is not appropriate at describing the measured concentrations (Bevington and Robinson 2003).

Given that the *in situ* cosmogenic ^{10}Be and ^{14}C depth-profiles are independent of each other, separate χ_{red}^2 maps (see below) can be produced for each nuclide and the intersection of the two will constrain the erosional event timing and magnitude pair that best fits the two datasets.

The model was implemented in the R statistical language (Ihaka and Gentleman 1996, R Development Core Team 2011) and the code is provided in Appendix D. The model predicts *in situ* cosmogenic ^{10}Be and ^{14}C depth-profiles for erosional events with timings calculated at 100-year increments (from 10.5 kyr to present) and magnitudes at 10 cm increments (from 0 to 100 cm). Model results are provided as contoured maps of χ_{red}^2 values obtained for the full range of erosional event timing and magnitude pairs. The timing-magnitude pair with the lowest χ_{red}^2 (if not < 1) is considered to be the one that is most likely to explain the data. The 68% (1σ level) confidence interval around the best-fit parameter combination is given by $\chi_{red}^2 + 1$ (Bevington and Robinson 2003).

5.3 The magnitude and timing of soil erosion at Inchie Farm

The LLR moraine at the Inchie Farm site is characterized by a sharp apparently erosional break-in-slope on its inner flank (Figure C.2), suggesting that the missing soil material was removed instantaneously in a short erosional event. Had the moraine been subjected to slow continuous erosion, rather than a virtually instantaneous erosional event, the break-in-slope would very likely have been rounded off and erased.

The shape of the Inchie Farm moraine suggests some post-glacial stabilization, since fresh LLR moraines tend to be triangular in cross section (Derek Fabel, *personal communication*, June 2011), and sharp-crested moraines will tend to stabilise to being shorter, as material moves from the moraines crest to its flanks and toe (Anderson and Humphrey

1989, Hallet and Putkonen 1994, O’Neal 2006, Putkonen et al. 2007, Pelletier 2008). This stabilisation most likely occurs relatively soon after deglaciation and hence will not effect the *in situ* cosmogenic ^{10}Be and ^{14}C results. And even if the post-glacial stabilisation is not ‘instantaneous’, it will presumably slow with time as the ‘adjusted’ form is approached.

The Inchie Farm depth-profiles were sampled immediately below the observed break in slope, and given the above, it is assumed that the departure of these depth-profiles from the theoretical, ‘zero-erosion’ depth-profiles calculated for this site (Chapter 4) are the results of an erosional event. The likely magnitude and timing of this erosional event are constrained below using the Monte-Carlo approach described in the preceding section. This analysis assumes no (or negligible) continuous soil erosion but the possibility that the LLR moraine at Inchie Farm experienced continuous erosion cannot be completely ruled out. The following section therefore explores the sensitivity of the obtained erosional event magnitude and timing pair to an assumed continuous erosion rate.

The Monte-Carlo type analysis was carried out at first for each cosmogenic nuclide separately. For each nuclide, an almost infinite combination of erosional event magnitude and timing pairs produce fits with low χ^2_{red} values (Figure 5.1) suggesting that a single nuclides cannot constrain the magnitude and timing of a Holocene soil erosional event.

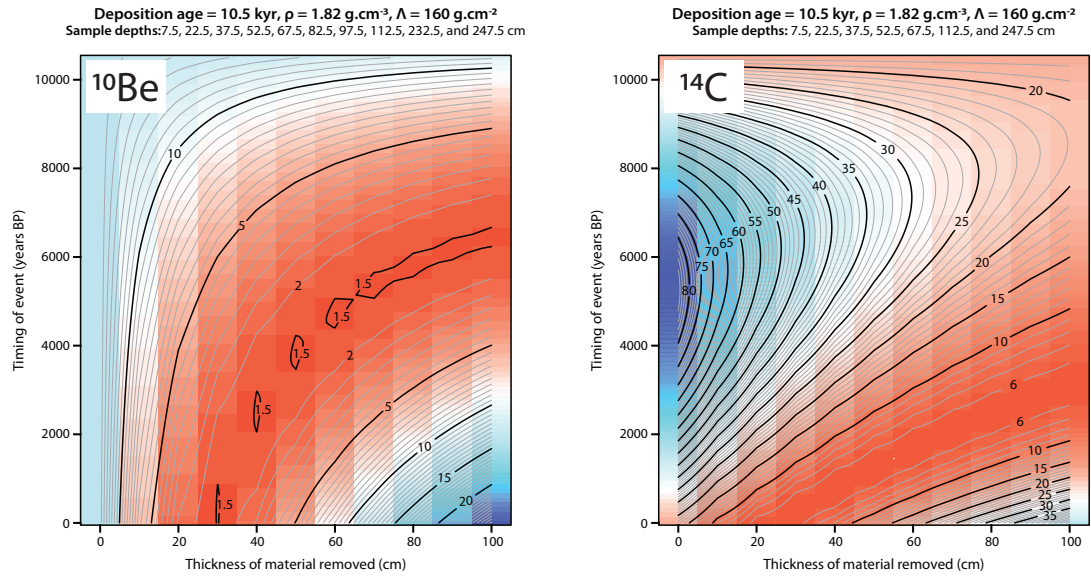


Figure 5.1: χ^2_{red} contour plots obtained for the ^{10}Be (left) and ^{14}C (right) depth-profiles assuming no continuous erosion. Dark red indicates a small χ^2_{red} and therefore a reasonable fit to the data, showing that when taken independently, both ^{10}Be and ^{14}C depth-profiles can be explained by a nearly infinite combination of erosional event magnitude and timing pairs.

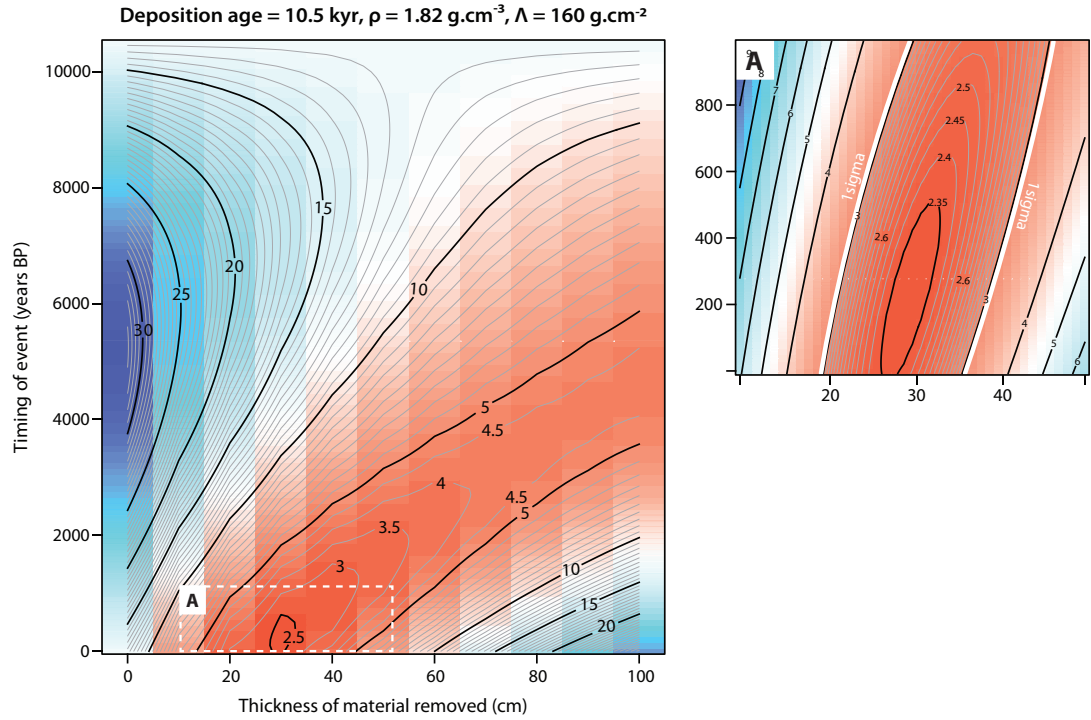


Figure 5.2: χ^2_{red} contour plot obtained for the combined ^{10}Be and ^{14}C depth-profiles assuming no continuous erosion. The inset shows an enlargement of the area of the plot with the lowest obtained χ^2_{red} values and the 68% (1σ) confidence envelope.

However, the χ^2_{red} contour plots obtained for the two nuclides are markedly different and when used together, ^{10}Be and ^{14}C will substantially narrow the range of erosional event magnitude and timing pairs that provide good fits to the data. Combining the two nuclides and performing the analysis using both ^{10}Be and ^{14}C depth-profiles together yields a narrower set of likely erosional event magnitude-timing pairs (Figure 5.2). The lowest χ^2_{red} value is 2.3 and was obtained for an erosional event that occurred 300 years ago and resulted in the instantaneous removal of 30 cm of soil. Considering the 68% confidence interval (Figure 5.2) ($\min \chi^2_{red} + 1 = 3.3$), the results of the Monte-Carlo analysis indicate that the erosional event is very likely to be relatively recent ($< \sim 1500$ years) and removed (20 - 50 cm).

5.4 Sensitivity analysis

The analyses presented in the preceding section suggest that the moraine at Inchie Farm lost material as a result of a relatively shallow (20 - 50 cm) erosional event in the last 1.5 kyr. These results, however, are based on the assumption that the background long-term erosion rate on the moraine is negligible. This section explores the sensitivity of the obtained erosional event magnitude and timing pair to an assumed continuous erosion rate. This section also explores the sensitivity of the results to sample size and measurement accuracy, and to the parameter values used.

5.4.1 ‘Non-zero’ continuous erosion rate

The Monte-Carlo type analyses were repeated for continuous erosion rates ranging between 5 and 100 mm.kyr⁻¹ (Figure 5.3). Continuous erosion rates of up to 10 mm.kyr⁻¹ yield χ_{red}^2 contour plots that are almost identical to that obtained when assuming a zero background erosion rate (Figure 5.2) suggesting that continuous erosion rates <10 mm.kyr⁻¹ will not affect the ¹⁰Be and ¹⁴C depth-profiles sufficiently to perturb the erosional event ‘signal’.

As for the < 10 mm.kyr⁻¹ case, low χ_{red}^2 values are obtained for recent and shallow erosional events when assuming a continuous erosion rate of 20 mm.kyr⁻¹. However, the ¹⁰Be and ¹⁴C depth-profiles are also equally well fitted by any erosional event older than 10 kyrs BP. For continuous erosion rates > 20 mm.kyr⁻¹, the ¹⁰Be and ¹⁴C depth-profiles are perturbed sufficiently such that no erosional event magnitude and timing pair provides a reasonable fit to the measured ¹⁰Be and ¹⁴C depth-profiles.

The fact that (1) for background erosion rates > 20 mm.kyr⁻¹ ¹⁰Be and ¹⁴C depth-profiles poorly fit the data, and (2) for background erosion rates > 20 mm.kyr⁻¹ these fits have lower χ_{red}^2 values than those obtained for the same rates but assuming no erosional events (Figure 5.4), suggest that a continuous erosion alone (i.e. without an erosional event) is not sufficient to explain the data, and that the data are best explained by a combination of a discrete erosional event superimposed on a zero or relatively low (< 20 mm.kyr⁻¹) continuous erosion rate.

The sensitivity analyses clearly show that for the magnitude and timing of an erosional event to be determined with confidence, the continuous erosion rate should first be constrained. The latter can be achieved by measuring cosmogenic nuclide depth-profiles on

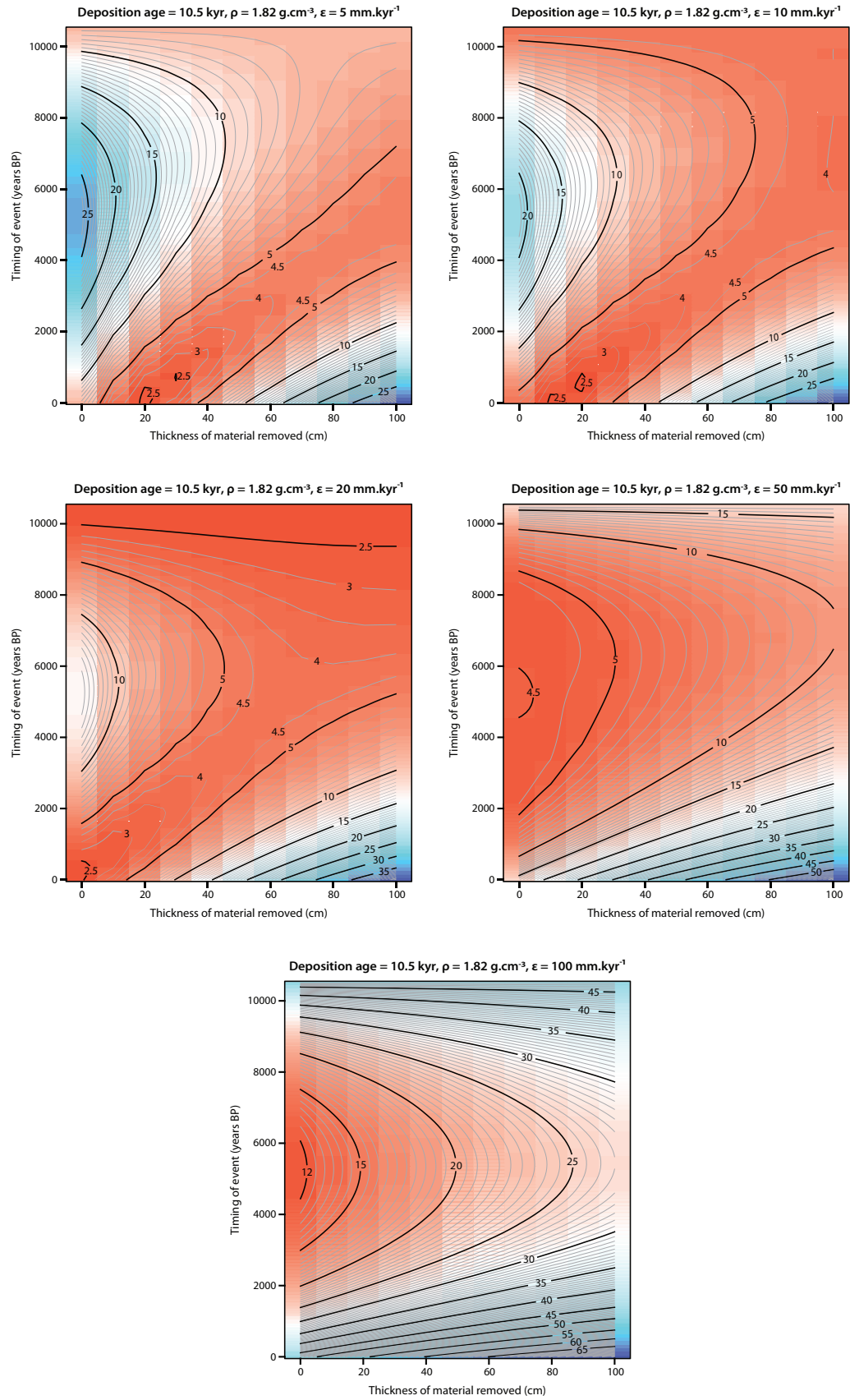


Figure 5.3: χ^2_{red} contour plots obtained for the combined ^{10}Be and ^{14}C depth-profiles for continuous erosion rates between 5 - 100 mm.kyr^{-1}

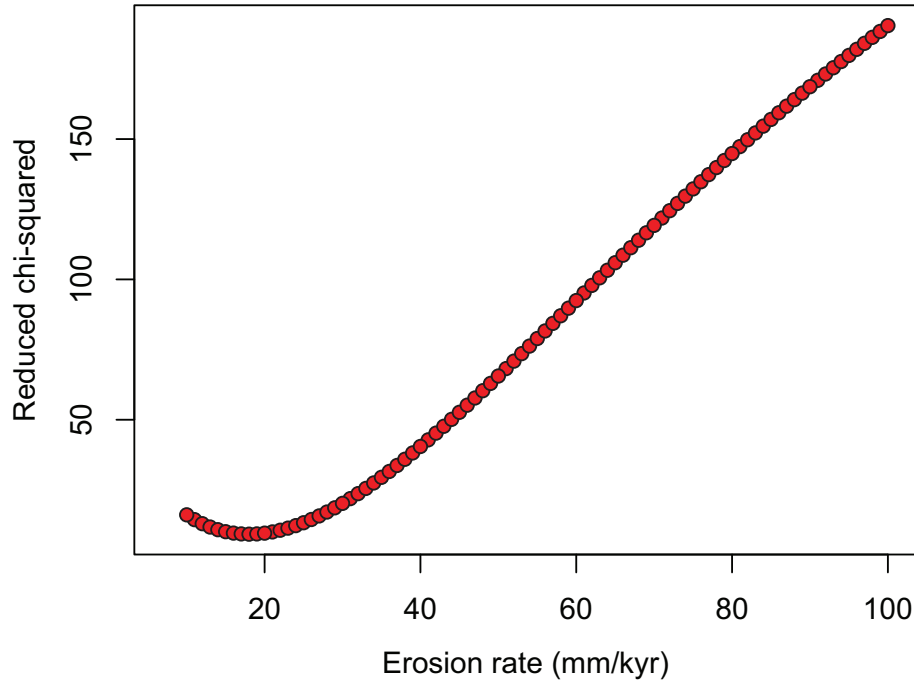


Figure 5.4: χ_{red}^2 values obtained for the combined ^{10}Be and ^{14}C depth-profiles for continuous erosion rates between 5 - 100 mm.kyr^{-1} and assuming no erosional events.

those parts of the same moraine that do not show obvious signs of erosion (e.g., the stable crest of the moraine). Alternatively, measured (empirical) erosion rates may be assumed to apply. The relatively few studies of soil erosion rates in Scotland generally report negligible or relatively low rates. For example, Kirkbride and Reeves (1993) found no erosion occurring on grasslands and Duck and McManus (1987) used reservoir sedimentation over periods of 35 - 121 years to calculate erosion rates of $2.1 - 52 \text{ t.km}^2.\text{yr}^{-1} / 1.2 - 28 \text{ mm.kyr}^{-1}$ (at two hours drive from Inchie Farm at Angus, Scotland).

5.4.2 Measurement uncertainty and sample size

χ_{red}^2 is calculated as the difference between measured and modelled values, divided by the measurement uncertainty (Equation 5.5, Bevington and Robinson 2003). Consequently meaning that high measurement uncertainties result in artificially low χ_{red}^2 values that do not necessarily represent a better fit of the model to the data.

To test the effect of measurement uncertainty on χ_{red}^2 , the Monte-Carlo type analyses were conducted using synthetic ^{10}Be and ^{14}C depth-profiles produced assuming an erosion event that occurred 200 years ago and resulted in the removal of 30 cm of soil. The

analyses were conducted for assigned uncertainties of 3%, 5%, and 10% (Figure 5.5). For synthetic data the analyses should yield $\chi_{red}^2 = 0$ for the above erosion event timing and magnitude pair (i.e., 200 years/30 cm) (cf. Bevington and Robinson 2003)

However, as inferred above, an increase in measurement uncertainty results in overall lower χ_{red}^2 values for all but the 200 years/30 cm timing and magnitude pair, for which $\chi_{red}^2 = 0$. If the two depth-profiles are not synthetic, but consist of real measurements, the observed minimum χ_{red}^2 would be different from zero and increase inversely proportionally to measurement uncertainty. The three contour plots in Figure 5.5 exhibit the same overall pattern, indicating that while measurement uncertainty has an effect on the absolute χ_{red}^2 values, it does not affect the overall structure of the results. This means that although the uncertainty on the measurements will determine the confidence that can be assigned to a certain outcome, it does not determine the likelihood of that outcome not being the best-fit scenario.

To explore the extent to which sample size affects the χ_{red}^2 values obtained, further synthetic depth-profiles were produced with different numbers of data points. As above, all depth-profiles have an associated uncertainty of 5% and are obtained for the removal of 30 cm of soil 200 years BP. Figure 5.6 shows the results for ^{10}Be and ^{14}C depth-profiles with data points at 7.5 cm ($n=35$) and 15 cm ($n=17$) depth intervals, and for depth-profiles consisting of two data points only (7.5 cm and 255 cm depth). Surprisingly all scenarios (i.e., 35, 17, and 2 data points) yield similar χ_{red}^2 distribution plots, suggesting that at least in theory two data points (topmost and bottom) per nuclide are sufficient to constrain the erosion event timing and magnitude pair (cf. Anderson et al. 1996).

In practice, however, the uncertainties associated with the measured data points will likely be larger than 5% and so have a substantial effect on the χ_{red}^2 results (Figure 5.7) meaning that two data points per nuclide will not be sufficient. The ^{14}C analyses are likely to have more variable uncertainties than the ^{10}Be analyses, and since the former require more time and effort, a better solution, as suggested by the results in Figure 5.7, is to reconstruct the full ^{10}Be profile using a large number of ^{10}Be measurements and only a few ^{14}C measurements for the ^{14}C profile ($n = 3$). Reconstructing the full profile with at least one nuclide is important as the form of the depth-profile provides information about the concentration of inherited nuclide, and/or soil mixing, and about the erosional history of the profile.

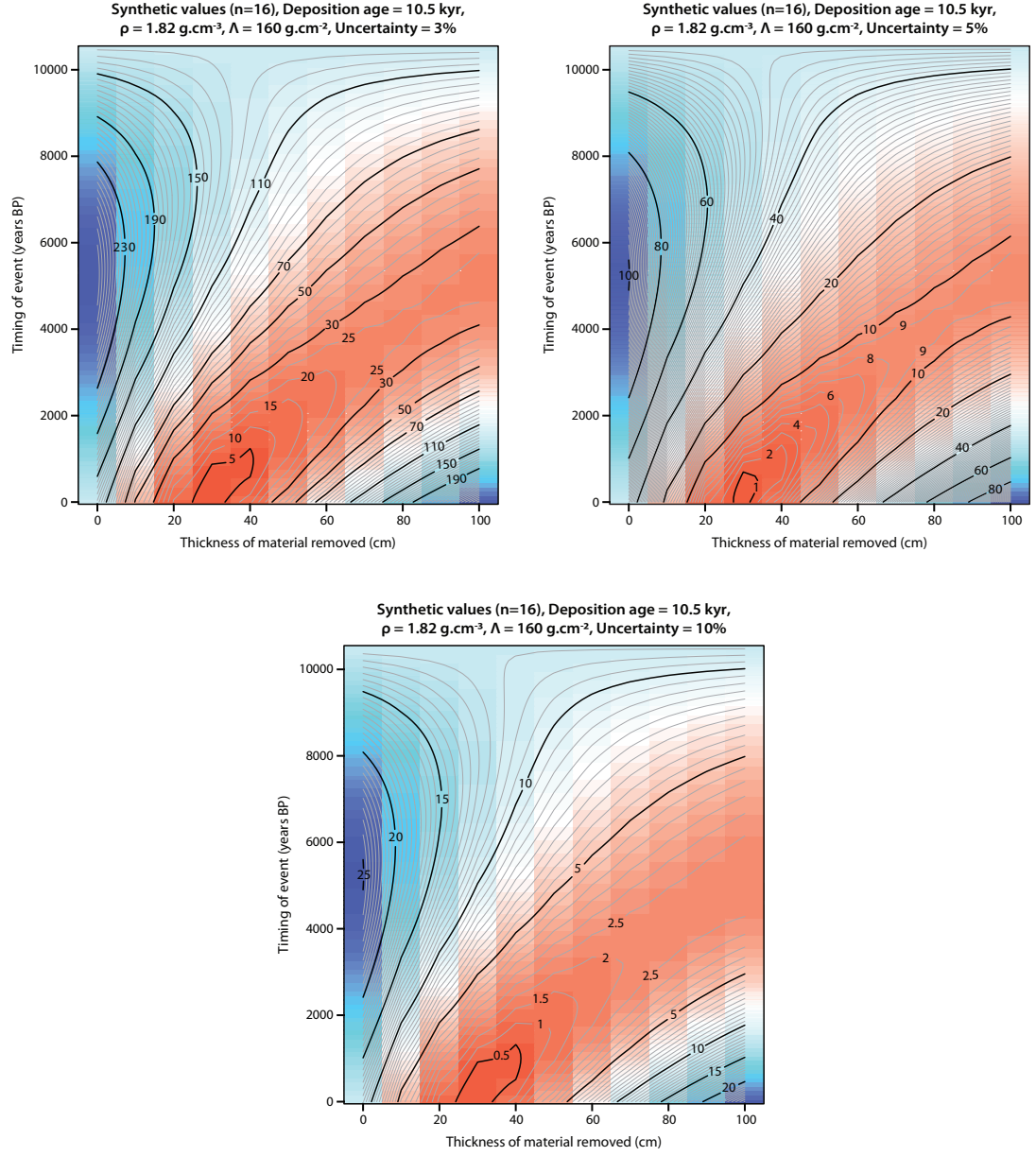


Figure 5.5: χ^2_{red} contour plots obtained for the combined ^{10}Be and ^{14}C depth-profiles assuming no continuous erosion, and varying the level of uncertainty on the ^{10}Be and ^{14}C concentrations. Synthetic ^{10}Be and ^{14}C depth-profiles were used instead of the measured ones.

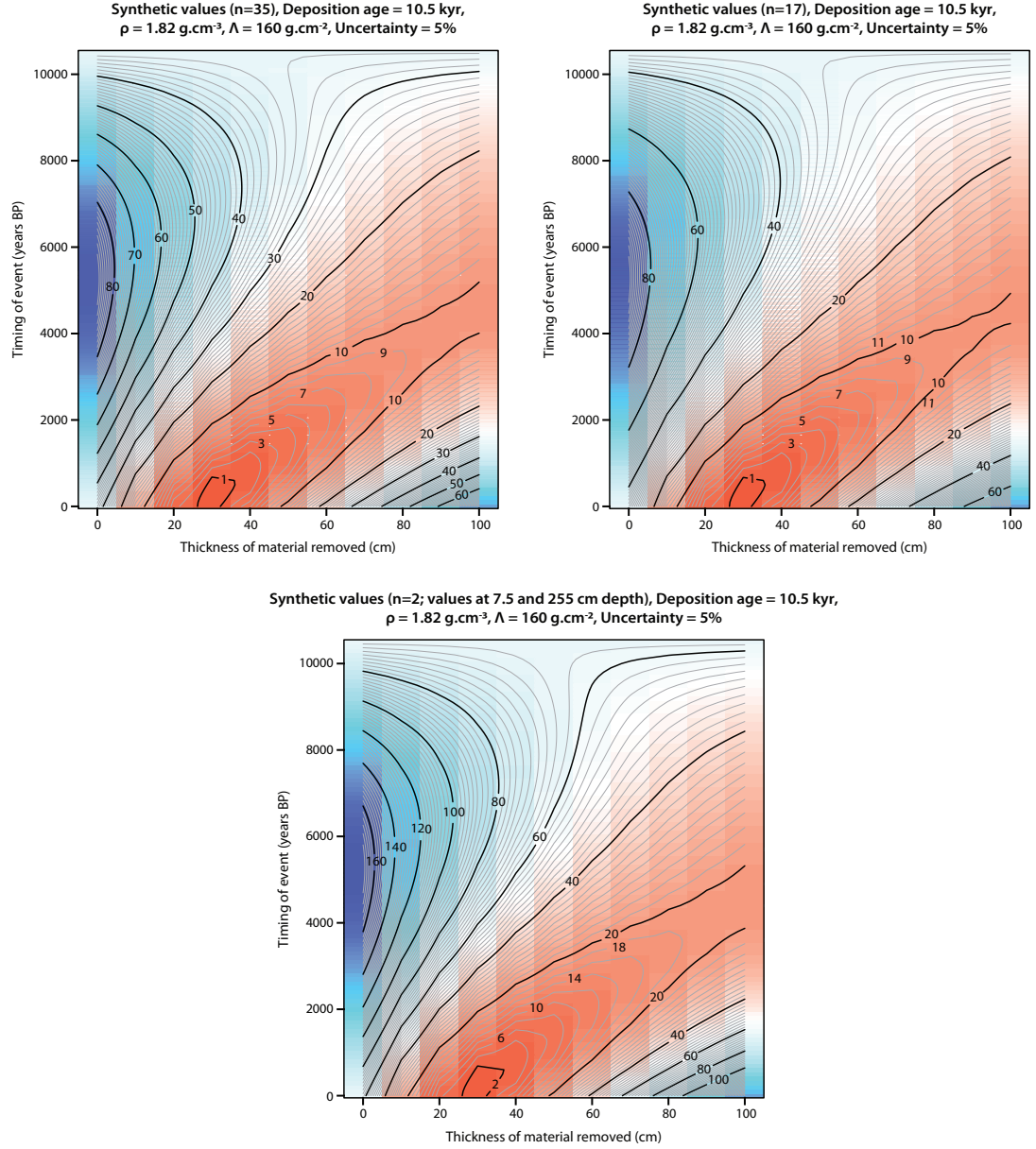


Figure 5.6: χ^2_{red} contour plots obtained for the combined synthetic ^{10}Be and ^{14}C depth-profiles assuming no continuous erosion and 5% uncertainty on the ^{10}Be and ^{14}C concentrations. (left) using 35 sample points per nuclide; (middle) using 17 sample points per nuclide; (right) using only two data points: at 7.5 and 255 cm depth respectively.

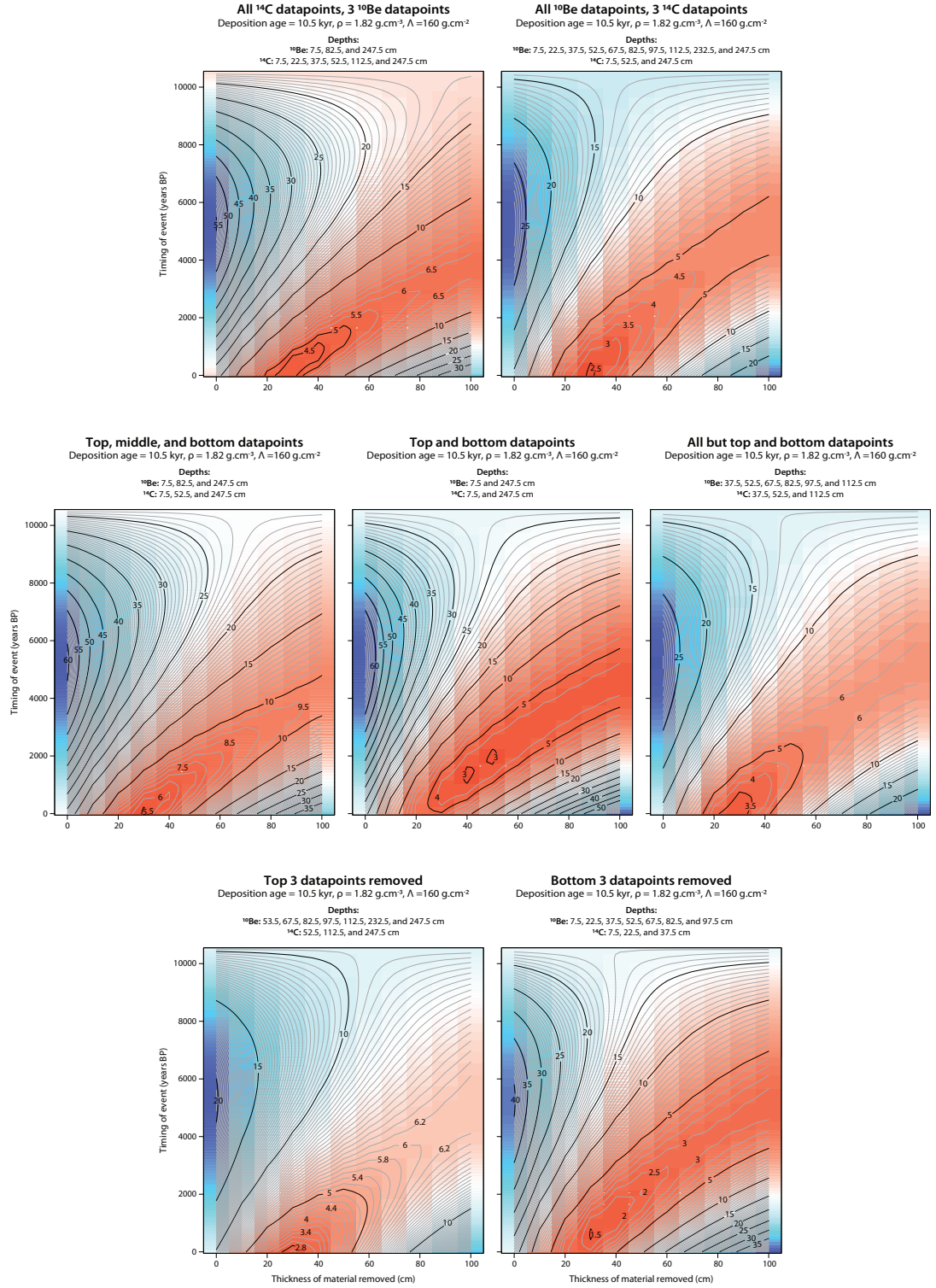


Figure 5.7: χ^2_{red} contour plots obtained for the combined ^{10}Be and ^{14}C depth-profiles at Inchie Farm assuming no continuous erosion and using subsets of the measured ^{10}Be and ^{14}C values.

5.4.3 Model parameters

The equations implemented in the numerical model used in this thesis to predict the ^{10}Be and ^{14}C depth-profiles for a given erosional event magnitude and timing pair rely on a number of parameters with known values. These parameters are: the age of till stabilisation, density of the deposit, cosmogenic nuclide production mechanisms (i.e., relative proportion of neutron spallation vs. muon interactions), and sea level and high latitude cosmogenic nuclide production rates. Although changing these parameters simultaneously will result in very different model results, for the sensitivity analysis presented here, each of the above parameters is changed in isolation while all others are held constant.

5.4.3.1 Age of the sediment body

All model results presented above were obtained taking the Wester Cameron erratic boulders mean ^{10}Be exposure age of 10.5 kyr to be the age of till stabilization at both the Wester Cameron and Inchie Farm sites. However, as mentioned in Chapter 3, the timing of the LLR has been dated using radiocarbon measurements in samples from various locations including one collected from the vicinity of the Inchie Farm sample site (see Golledge et al. 2007 for a list of LLR radiocarbon ages). This latter sample was a marine shell found below the till deposit and yielded a radiocarbon age of 11.8 ± 0.17 ^{14}C kyr (Sissons 1967) calibrated to 13.5 kyr BP using OxCal v.4.1.7. Gordon (1982) has argued that this age has, being measured in marine shells, likely been affected by the reservoir and hard-water effects (Heier Nielsen et al. 1995, Ascough et al. 2009). Moreover, of a time lag between moraine formation and the radiocarbon age, unless the age is measured on the remains of a living organism buried during moraine formation (Lowell et al. 1990). Thus it is likely that the mean ^{10}Be exposure age obtained at Wester Cameron is closer to the true age of till stabilization than the radiocarbon age of 13.5 kyr BP. Nonetheless the effect of an older till stabilization age on the predicted erosional event magnitude and timing pair is explored in Figure 5.8.

Assuming an age of 13.5 kyr BP as the age of till stabilization predicts an erosional event that is deeper and earlier (Figure 5.8). For each 1 kyr increase in the age of till stabilization, the model predicts an increase of 30% in the depth of the erosional event and a 60% increase in the timing of the event (Figure 5.8). This clearly illustrates the importance of accurately constraining the age of deposition if the magnitude and timing

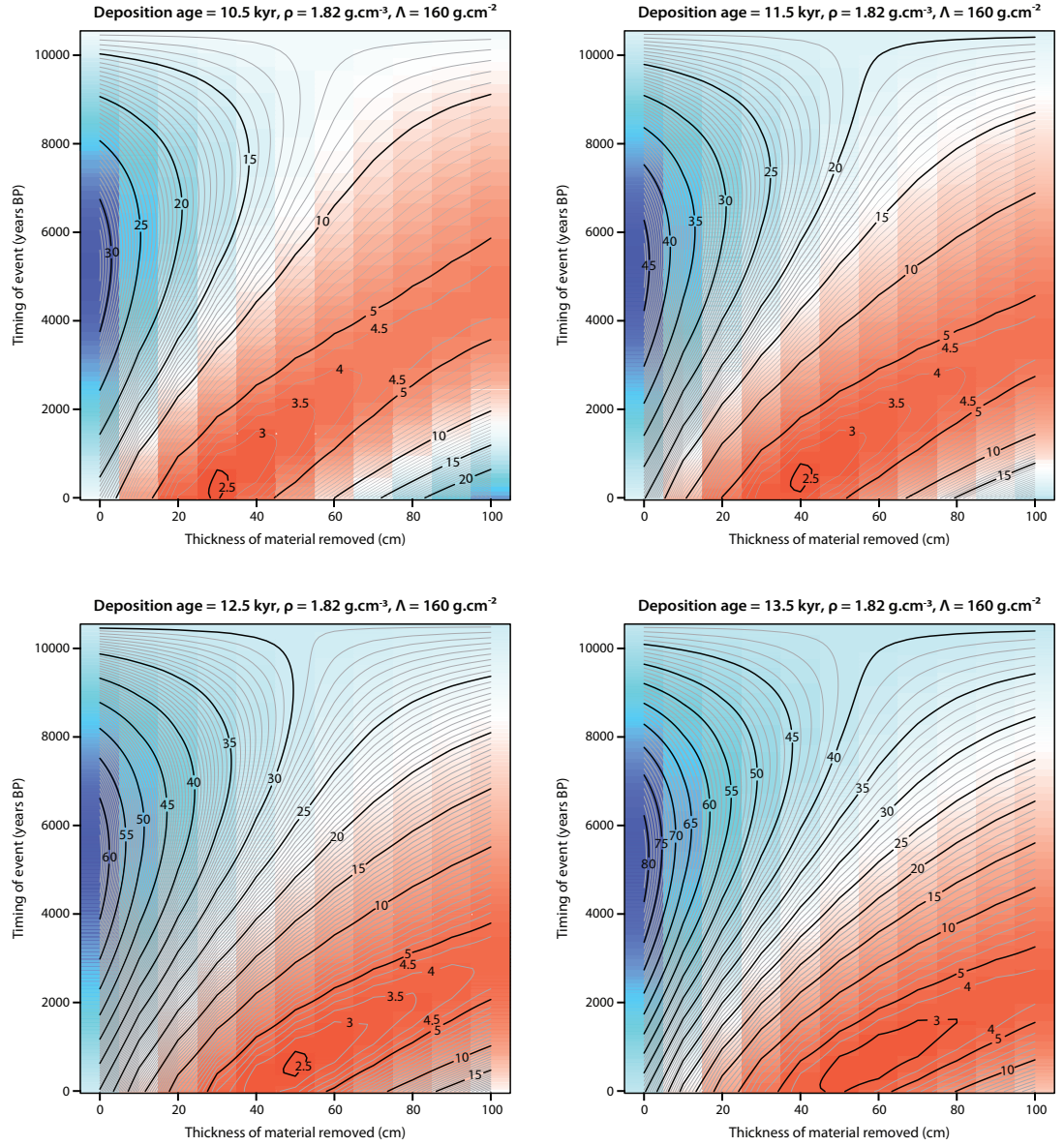


Figure 5.8: χ^2_{red} contour plots obtained for the combined ^{10}Be and ^{14}C depth-profiles at Inchie Farm assuming no continuous erosion and varying the age of till stabilization.

of the erosional event are to be reliably determined.

5.4.3.2 Density of the sediment

The density of till at both the Wester Cameron and Inchie Farm sites was determined at high resolution as described in Chapter 3. However, the density of glacial deposits is highly variable both from deposit to deposit and within an individual profile, and so a sensitivity analysis provides useful insights regarding future applications of this method to sites where such high-resolution data on till density are not available.

For the purposes of the sensitivity analysis (Figure 5.9), till/soil density was allowed to vary at 0.1 g.cm^{-3} increments between 1.5 g.cm^{-3} and 2.4 g.cm^{-3} , the range typically quoted in the literature for glacial deposits (Fausey et al. 2000, Staiger et al. 2006). Although the density of a sedimentary deposit can also vary through time (cf. Rodés et al. 2011), this temporal variation is likely to be relatively insignificant in glacial deposits when compared to the spatial variation (i.e., between deposits) or the variation within a profile, and so such temporal variation is not considered here.

The results of the sensitivity analysis are shown in Figures 5.10 - 5.11, and illustrate that while there is no relationship between the density of the sedimentary deposit and the predicted best-fit erosional event timing, the former determines the obtained best-fit erosional event magnitude in both a predictable (the higher the density the shallower the best-fit erosional event) and substantial way ($\sim 40 \text{ cm}$ depth difference for a density range of 1 g.cm^{-3}). Thus, for the method presented in this study to be applicable successfully to other sites, data on the density of the sedimentary deposit must be obtained a priori.

5.4.3.3 Nuclide production pathways

Brown et al. (1995) have argued that the production of cosmogenic nuclides in the upper 1 - 2 metres of a soil is predominantly due to neutron spallation and muogenic contributions can be ignored. This statement has however been since challenged by Brown et al. (2003) and Braucher et al. (2009) who found that considering both high energy neutron spallation and muon reactions substantially improves the determination of ages and denudation rates from cosmogenic nuclide depth-profiles.

Muon reactions are particularly important for ^{14}C ; slow and fast muons are thought

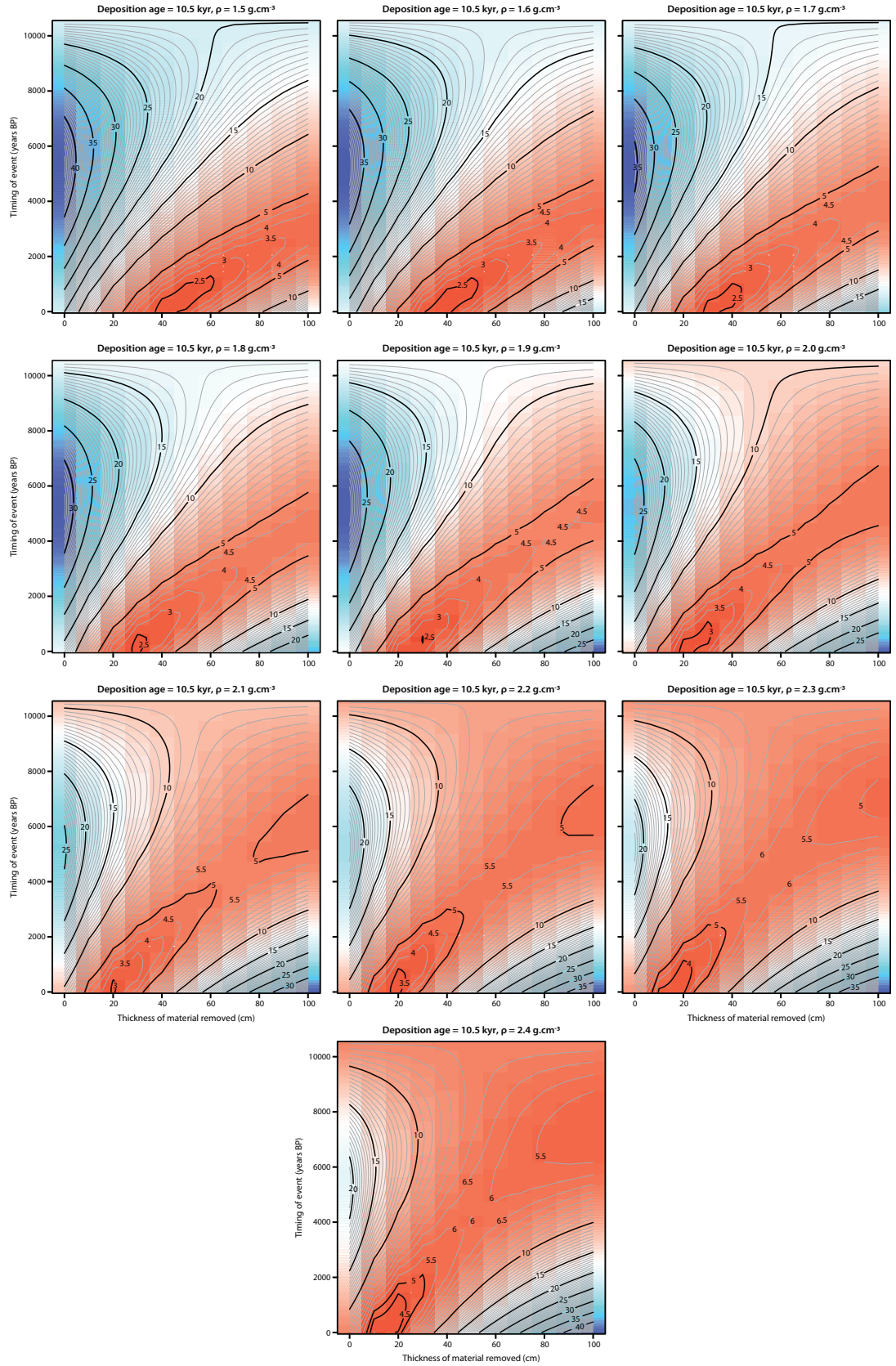


Figure 5.9: χ_{red}^2 contour plots obtained for the combined ^{10}Be and ^{14}C depth-profiles at Inchie Farm assuming no continuous erosion and varying the density of the sedimentary deposit.

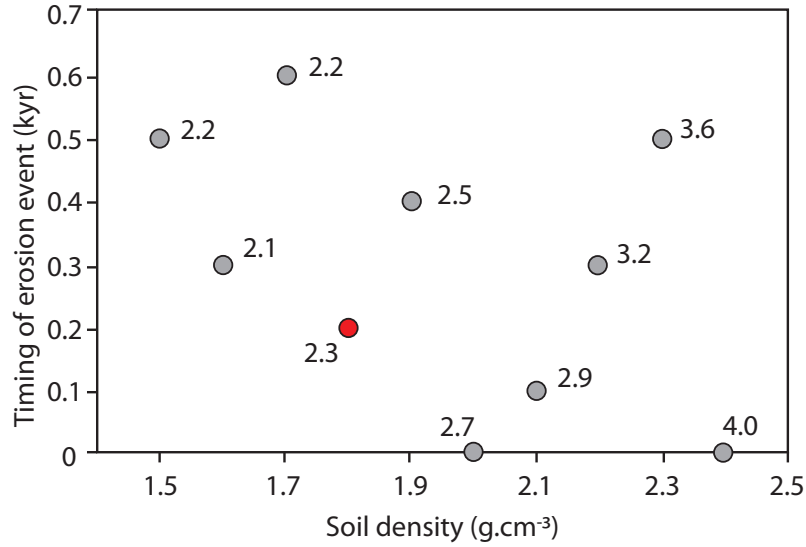


Figure 5.10: Plot showing erosional event timing vs. density of the sedimentary deposit. Grey circles represent best-fit timings ($\min \chi_{red}^2$) for erosional events with a range of soil/till densities. Red circle represents best-fit erosional event timing obtained for the mean density determined for the Inchie Farm site and used in this study.

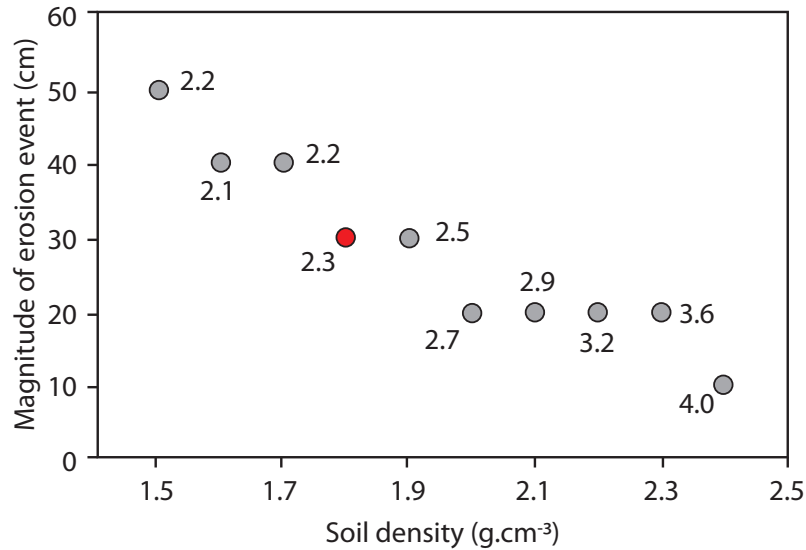


Figure 5.11: Plot showing erosional event magnitude (i.e., depth of material removed) vs. density of the sedimentary deposit. Grey circles represent best-fit ($\min \chi_{red}^2$) erosional event magnitudes obtained for a range of density values. Red circle represents best-fit erosional event magnitude obtained for the mean density determined for the Inchie Farm site and used in this study.

to account for 17% of ^{14}C production at the surface (Heisinger et al. 2002a,b) and this importance is clearly shown in Figure 5.12. While ignoring muogenic production for ^{10}Be does not result in significant changes in the structure of the χ_{red}^2 plot (Figure 5.12 - middle), ignoring muogenic production for ^{14}C yields a χ_{red}^2 plot that is substantially different in its structure to that obtained when both high energy neutron spallation and muon interactions are considered (Figure 5.2).

The systematics of *in situ* ^{14}C production are still poorly understood. The currently used production rate of this nuclide is based on a very limited number of calibration sites (cf. Lifton et al. 2005, 2008, Balco et al. 2008, Dunai 2010, White et al. 2011) and our current understanding of the role of muons in the production of cosmogenic nuclides is based on a single study (i.e., Heisinger et al. 2002a,b) that might considerably overestimate the importance of muons in the production of *in situ* ^{14}C (Nat Lifton, *personal communication*, August, 2011). Consequently successful future application of the method presented in this thesis requires an improvement of our understanding of *in situ* ^{14}C production mechanism.

5.4.3.4 Sea Level High Latitude production rates

The results of age or denudation rate calculations involving cosmogenic nuclides depend highly on the sea level high latitude (SLHL) production rates that are used. The quality (or ‘accuracy’) of these production rates depend on (1) the quality of the calibration data sets, and (2) the quality of the altitude/latitude scaling schemes used to calculate the production rates (Balco et al. 2008, Dunai 2010). Calibration data sets represent cosmogenic nuclide concentration measurements at sites that have undergone negligible denudation and have ages that have been independently determined (see Balco et al. 2008 and Lifton et al. 2005, 2008 for a list of calibration sites used for ^{10}Be and ^{14}C). As the calibration site ages have associated uncertainties, these propagate into local cosmogenic nuclide production rates. Moreover, all calibration-site-specific local cosmogenic nuclide production rates are standardized to sea level and high latitude using one of the many altitude/latitude scaling schemes (e.g., Stone 2000, Dunai 2000, Lifton et al. 2008). Each of these have an uncertainty. It is difficult to calculate the uncertainties of the currently used SLHL production rates but Balco et al. (2008) estimated that the 1σ uncertainty introduced by empirical scaling schemes may be as large as 10%. In short, although the

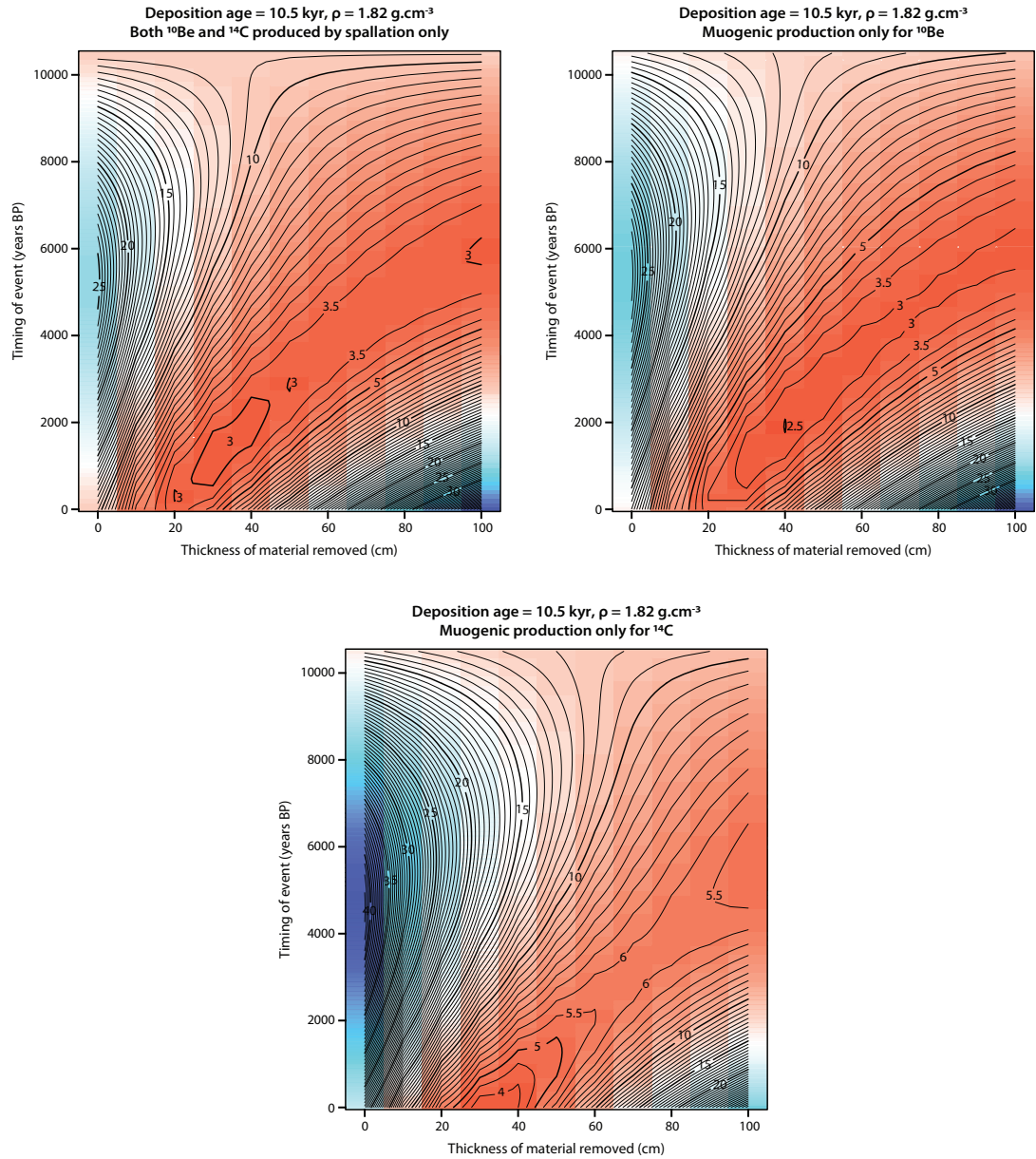


Figure 5.12: χ^2_{red} contour plots obtained for the combined ^{10}Be and ^{14}C depth-profiles at Inchie Farm assuming no continuous erosion and varying the relative contribution of muons to the total production of ^{10}Be and ^{14}C .

currently used SLHL production rates for ^{10}Be and ^{14}C have ‘quoted’ uncertainties, the true absolute uncertainties are unknown.

The production rate is important when ages rather than rates are calculated (such as in this study). To assess the effect that these production rate uncertainties have on the χ^2_{red} results, SLHL production rates of both nuclides have been varied by $\pm 15\%$ in 5% increments.

The results presented in Figures 5.13 and 5.14 indicate, as expected, a substantial affect on χ^2_{red} . Surprisingly the two nuclides affect the structure of the χ^2_{red} results in opposite ways: decreasing the ^{14}C SLHL production rate results in older and deeper erosional events whereas the same is obtained when the ^{10}Be SLHL production rate is increased.

Figures 5.13 and 5.14 also show that χ^2_{red} is more sensitive to changes in the production rate of ^{14}C than ^{10}Be . This is important as, to date, the *in situ* cosmogenic ^{14}C SLHL production rate is the least well constrained (cf. Dunai 2010). Thus, as with muon production that successful future application of the method presented in this thesis requires an improvement of our understanding of the systematics of *in situ* ^{14}C .

5.5 Summary

The LLR moraine at the Inchie Farm site is characterised by the presence of a sharp break in slope, suggesting that the missing soil material was removed instantaneously by an erosional event. The hypothesis of an erosional event is also supported by the clear departure from the zero-erosion cosmogenic nuclide depth-profiles shown by the ^{10}Be and ^{14}C measurements in the Inchie Farm samples. A Monte-Carlo type analysis suggests that the erosional event is very likely to be relatively recent and also relatively shallow, resulting in the removal of circa 20 - 50 cm of soil circa 1500 years BP. The sensitivity analyses undertaken show that the predicted magnitude and timing of the Inchie Farm erosion event are highly sensitive to assumptions about the background rate of continuous soil erosion at the site and also about the stabilisation age of the till. Further, the results also indicate that the density of the sedimentary deposit will also affect the predicted magnitude and timing of the erosional event. All of the above properties can be independently determined *a priori* and so, although critical, they do not impede future applications of the method presented in this study to other sites. The sensitivity analyses also show that the predicted

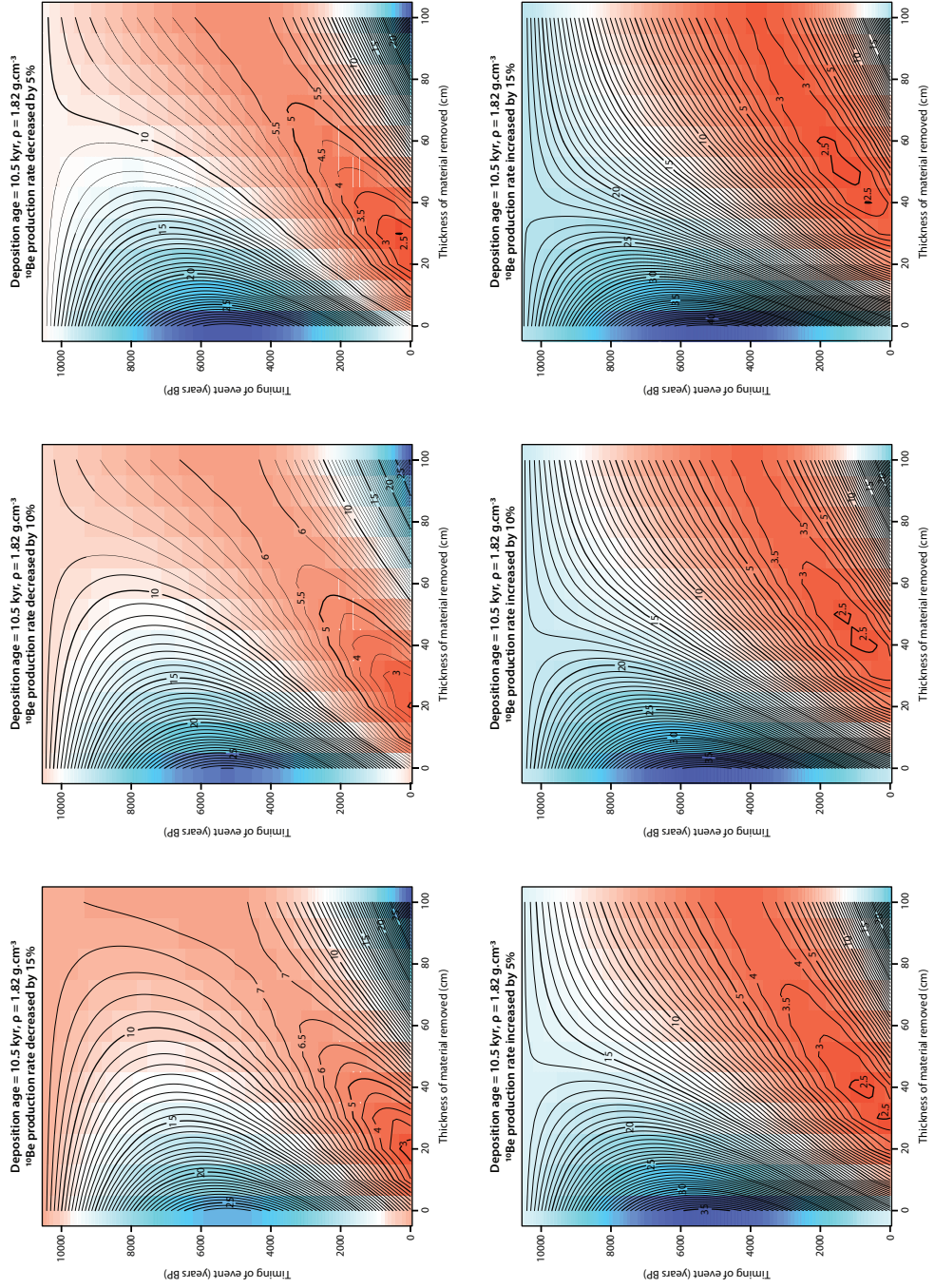


Figure 5.13: χ^2_{red} contour plots obtained for the combined ^{10}Be and ^{14}C depth-profiles at Inchie Farm assuming no continuous erosion and varying the ^{10}Be production by $\pm 15\%$ in 5% increments.

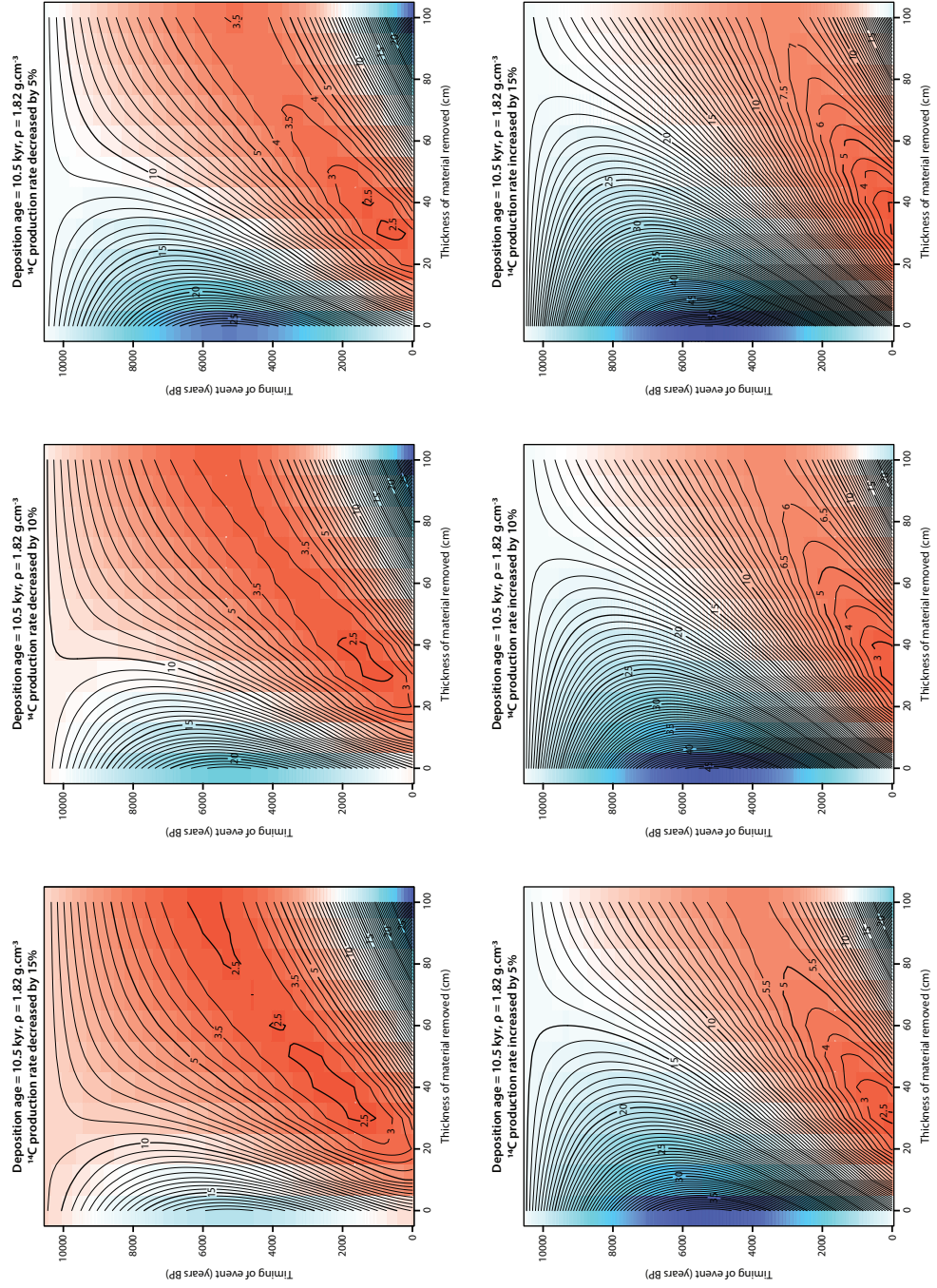


Figure 5.14: χ^2_{red} contour plots obtained for the combined ^{10}Be and ^{14}C depth-profiles at Inchie Farm assuming no continuous erosion and varying the ^{14}C SLHL production by $\pm 15\%$ in 5% increments.

erosional event magnitude and timing are very sensitive to the *in situ* cosmogenic ^{14}C SLHL production rate used and to the assumptions that are made about the contribution of muons to the total production of this cosmogenic nuclide. Given that the production systematics of *in situ* ^{14}C are less well understood than those of other more routinely used cosmogenic nuclides, advances in this regard need to be made for the method presented in this thesis to be applicable with confidence to scenarios similar to the one presented in this thesis (as well as to the wider application of *in situ* ^{14}C analysis more generally).

THERE'S NO SENSE IN BEING PRECISE WHEN YOU DON'T EVEN KNOW WHAT YOU'RE
TALKING ABOUT.

[John von Neumann]

Chapter 6

Conclusions, Limitations, and Future Research

6.1 Conclusions

The present study has explored the extent to which *in situ* cosmogenic ^{10}Be and ^{14}C depth-profiles can be used to quantify the magnitude and timing of site-specific erosional events over Holocene timescales on soils/sediments of known age. The study has focused on two sites located on end moraines of the Loch Lomond Readvance in Scotland: Wester Cameron and Inchie Farm near Glasgow. Conclusions from the data and the results of the numerical simulations can be divided into three broad categories: (1) those concerning the amount and timing of erosion at both sites, (2) those concerning the broader implications of the sensitivity analyses, and (3) those concerning the extraction and measurement of *in situ* ^{14}C .

The conclusions concerning the amount and timing of soil erosion at the Wester Cameron and Inchie Farm sites are as follows:

- (1) The results of the *in situ* cosmogenic ^{10}Be , ^{14}C and ^{26}Al analyses in the Wester Cameron site samples confirm that the cosmogenic nuclide depth-profile to be expected from a sediment body of Holocene age can be reconstructed. Moreover, the agreement between the total cosmogenic ^{10}Be inventories in the erratics and the Wester Cameron soil/till samples indicate that there has been no erosion at the sample site since the deposition of the till/moraine. Further, the Wester Cameron

depth-profiles show minimal signs of homogenisation, as a result of bioturbation, and minimal cosmogenic nuclide inheritance from previous exposure periods.

- (2) The results of the *in situ* cosmogenic ^{10}Be and ^{14}C analyses in the Inchie Farm site samples show a clear departure from the ‘zero-erosion’ cosmogenic nuclide depth-profiles suggesting that the soil/till at this site has undergone erosion since its emplacement. The LLR moraine at the Inchie Farm site is characterised by the presence of a sharp break in slope upslope of the sampled depth-profile, suggesting that the missing soil material was removed instantaneously by an erosional event rather than by slow continuous erosion. Monte-Carlo type analysis carried out to constrain the magnitude and timing of this erosion event suggests that this event was relatively recent and relatively shallow, resulting in the removal of circa 20 - 50 cm of soil at a maximum of 1500 years BP.

The conclusions concerning the broader implications of the sensitivity analyses are as follows:

- (1) The results of the sensitivity analyses show that the predicted magnitude and timing of the Inchie Farm erosion event are highly sensitive to (i) assumptions about the background rate of continuous soil erosion at the site and (ii) the stabilisation age of the till. The results further indicate that the density of the sedimentary deposit (iii) will also affect the magnitude and timing of the predicted erosional event. All three parameters can be independently determined a priori and so despite the fact that the method presented in this study is sensitive to variations in these parameters, they do not impede future applications of the method.
- (2) The results of the sensitivity analyses also show that the predicted magnitude and timing of the erosional event are very sensitive to the *in situ* cosmogenic ^{14}C SLHL production rate used and to assumptions about the contribution of muons to the total production of this nuclide. Given that the production systematics of *in situ* ^{14}C are less well understood than those of other more routinely used cosmogenic nuclides, advances in this regard need to be made for the method presented in this thesis to be applicable with confidence to scenarios similar to that presented here.

The experimental nature of *in situ* ^{14}C analysis has meant that a large part of the work in this study has been concerned with characterising and improving the performance of

the *in situ* ^{14}C vacuum extraction system at SUERC. The conclusions that can be drawn from the data obtained from this part of the work are as follows:

- (1) The results of reproducibility measurements on the SUERC *in situ* ^{14}C extraction system are satisfactory. This projects measurements of the PP4 University of Arizona internal standard are indistinguishable within uncertainty from the latest PP4 results published by the University of Arizona ^{14}C lab (Miller et al. 2006, Dugan 2008), but they are somewhat higher and more dispersed. Measurements of both the CRONUS-EARTH-A, a new *in situ* ^{14}C standard, and Glen Roy samples agree within uncertainty with the *in situ* ^{14}C and *in situ* ^{10}Be results of the University of Arizona ^{14}C lab and those of Fabel et al. (2010), respectively.
- (2) The results of the system blank and shielded quartz measurements suggest that the continuous running of the extraction system and the monitoring of gas collecting time are key to maintaining low and stable system blanks on an *in situ* ^{14}C extraction system following the design of Lifton (1997). The results also suggest that maintaining the temperature of the cryogenic traps constant can also play a role in maintaining system blank stability. The variability in the system blank data, however, means that a blank bracketing approach should be followed instead of calculating a long-term average blank and applying this to all sample measurements.

6.2 Limitations

- (1) The overall aim of this study was to assess the extent to which cosmogenic ^{10}Be and ^{14}C depth-profiles can be used to constrain the magnitude and timing of a Holocene age erosion event. To this end, the Inchie Farm study site was carefully selected as representing an apparently undisturbed (i.e., not eroding) sediment body of Holocene age that has been truncated by an erosional event. Thus all interpretations of the results were made under the assumption that the background long-term erosion rate on the Inchie Farm moraine is negligible. Although the assumption of zero background erosion is supported by both field evidence and the ^{10}Be and ^{14}C results obtained at the first study site, Wester Cameron, a non-zero background erosion rate cannot be completely ruled out. Analyses show that background erosion rates of up to 10 mm.kyr^{-1} yield χ^2_{red} contour plots that are almost identical to that

obtained when assuming a zero background erosion rate suggesting that background erosion rates $< 10 \text{ mm.kyr}^{-1}$ will not affect the *in situ* ^{10}Be and ^{14}C depth-profiles sufficiently to perturb the erosion event signal. When assuming background erosion rates $> 20 \text{ mm.kyr}^{-1}$, reasonable fits to the ^{10}Be and ^{14}C depth-profiles are obtained without the need to invoke any erosional events. However, these fits have slightly higher χ^2_{red} values than those obtained for the same background erosion rates but also assuming one erosional event. The latter suggests that a continuous background erosion rate alone (i.e. without an erosional event) is not sufficient to explain the data, and that the data are best explained by a combination of erosion evental and a zero or relatively low ($< 20 \text{ mm.kyr}^{-1}$) background erosion rate. Despite the above, the fact that the rate of continuous background soil erosion at Inchie Farm was not quantified independently is a limitation of this work.

- (2) A prior condition to using cosmogenic nuclide depth-profiles to constrain the magnitude and timing of soil erosion events is having a reliable control on the age of the sedimentary deposit (soil or till) under investigation. All model results presented in this study were obtained taking the mean ^{10}Be exposure age of 10.5 kyr obtained from the erratic boulders at Wester Cameron to be the age of till stabilisation at both the Wester Cameron and Inchie Farm sites. No erratic boulders could be found at Inchie Farm and so to establish the age of moraine stabilisation at this site, small pebbles were collected from the top of the moraine and analysed for *in situ* cosmogenic ^{10}Be . The results of these analyses, however, did not yield meaningful results (Appendix B.3). Given that the two study sites (Wester Cameron and Inchie Farm) are located on two moraines formed by two adjacent lobes of the same glacial readvance, the assumption that the Wester Cameron ^{10}Be exposure age of 10.5 kyrs is representative for Inchie Farm is probably correct. Nonetheless, the absence of an independent cosmogenic ^{10}Be based moraine stabilisation age estimate at Inchie Farm is a limitation of this work. The moraines at Wester Cameron and Inchie Farm have been dated using conventional and AMS radiocarbon, Rose et al. (1989) obtaining a maximum age of $\sim 12.5 \text{ kyr BP}$ for the Wester Cameron moraine and Sissons (1967) obtaining a maximum age of $\sim 13.5 \text{ kyr BP}$ for the Inchie Farm moraine. Both of these ages are older than the $10.5 \pm 0.9 \text{ kyr}$ ^{10}Be exposure age obtained as part of this study. However, as argued by Lowell (2000), there is often a time lag between moraine formation and the obtained radiocarbon age, unless the latter is obtained

from the remains of a living organism buried during moraine formation. Moreover, the Inchie Farm radiocarbon age was determined in a marine shell that has likely been affected by the reservoir and hard-water effects (Gordon 1982, Heier Nielsen et al. 1995, Ascough et al. 2009). Thus it is likely that the mean ^{10}Be exposure age obtained at Wester Cameron is closer to the true age of till stabilization than the radiocarbon ages. Despite these various complications related to the two radiocarbon ages, the discrepancy between these and the ^{10}Be exposure age obtained for Wester Cameron could also be explained by both the exposure dated erratic boulders and the adjacent soil in which the *in situ* ^{10}Be and ^{14}C profiles were measured being previously covered by a layer of soil or till that shielded some of the cosmic radiation. This shielding would result in lower nuclide concentrations and so younger ages as compared to the radiocarbon ones. The possibility of such shielding is not considered in this work.

6.3 Future research

Following the early work of Craig (1953), the extraction and measurement of *in situ* ^{14}C has advanced substantially. Jull et al. (1992) were the first to develop a system for extracting *in situ* produced cosmogenic ^{14}C in terrestrial rocks. Although nearly two decades have now passed, *in situ* cosmogenic ^{14}C is still not routinely used in the study of Earth surface processes (see Chapter 2). For *in situ* ^{14}C to be used routinely by geomorphologists, advances have to be made in at least two areas:

6.3.1 Extraction and purification of *in situ* ^{14}C .

- (1) Unlike pyrolysis, combustion of a sample in the presence of oxygen converts all carbon contained within the sample into CO_2 with an efficiency of 100 % (Wright et al. 2003) and so future research effort should be directed towards improving combustion based ^{14}C extraction systems. The size of the extraction system at SUERC has meant that a substantial amount of time had to be spent waiting for the required level of vacuum to be reached. Further a large extraction system means a larger surface area and a system that is more prone to contamination. Reducing the size of the *in situ* ^{14}C extraction system will no doubt increase sample throughput and this will make blank

bracketing practical, the latter allowing for better corrections and thus more reliable data.

- (2) A small fraction of ^{14}C is produced by thermal neutrons via $[n, \alpha]$ reactions on ^{17}O and via $[n, p]$ reactions on ^{14}N (Reedy and Arnold 1972, Gosse and Phillips 2001, Dunai 2010). The latter can be abundant in fluid inclusions (Duke et al. 1990). Fluid inclusions will be released during sample combustion and in those samples that are rich in these, the ^{14}C hosted in the inclusions will contribute to the measured total ^{14}C . Even if fluid inclusions contain only minimal amounts of ^{14}N and thus minimal ^{14}C , they are also likely to contain CO_2 and CH_4 (Van den Kerkhof and Hein 2001). The release of these gases during sample combustion will bias the estimation of the volume of ^{14}C -containing- CO_2 derived from the combustion of the sample - and this volume is required for calculating the concentration of ^{14}C in the sample (see Calculation A). To date no research has investigated the effect of fluid inclusions on *in situ* ^{14}C extraction. Methods based on laser Raman spectroscopy (Rosso and Bodnar 1995, Karim and Hong 2010) could be used to efficiently and non-destructively assess the composition of fluid inclusions. Further, samples can be crushed under vacuum thereby releasing all gases trapped in fluid inclusions as in case of ^{21}Ne extraction.
- (3) Irrespective of the vacuum extraction system design, during sample loading the interior of the furnace is exposed to air (and possibly dust) that will result in contamination with not only atmospheric ^{14}C but also moisture, resulting in more time required for reaching a high vacuum. The problem of moisture and atmospheric ^{14}C adsorption could be alleviated by flushing the furnace with He or Ar gas during sample loading such that the flow of gas is from inside outwards. Flushing might not be practical with the current furnace of the SUERC extraction system, given its large size. However, flushing with He or Ar would work with smaller furnaces. Further, flushing the entire extraction system with He gas between samples could also keep blanks low and limit any memory effects in the long term (Paul and Skrzypek 2006).
- (4) In the current design, slushes (mixtures of LN_2 and n-pentane and iso-pentane; see Chapter 2) are employed for cleaning the released CO_2 from contaminants such as CH_4 , SO_x , and NO_x . The use of slushes has been one of the obstacles in automating the extraction of ^{14}C . Molecular sieves have been used to separate CH_4 and other compounds from CO_2 (Morishige 2011) and so they could potentially replace slushes

enabling automation and therefore higher sample throughput (see also (1) above).

- (5) Lasers have now become a versatile tool in the geosciences, being used for heating samples or as ablation tools often directly coupled to a mass spectrometer (Kelley 2002, Stuart et al. 1999, Sylvester 2001). Recently Balco and Shuster (2009) have used a 75 W diode laser to extract and analyse Ne from quartz samples by heating the samples packed in Ta foil. A similar laser based heating system could greatly benefit the extraction of *in situ* ^{14}C , although a metal-free solution would need to be developed.

6.3.2 *In situ* ^{14}C production systematics.

- (1) The production systematics of *in situ* ^{14}C are less well understood than those of the more routinely used ^{10}Be . The value of the *in situ* ^{14}C SLHL production rate is based on a very small number of calibration sites all located at relatively high latitudes (e.g., Miller et al. 2006, Dugan 2008). The network of cosmogenic nuclide production calibration sites has been improved as the results of the CRONUS Earth and CRONUS EU research efforts (<http://www.physics.purdue.edu/primelab/CronusProject/cronus/> and <http://www.cronus-eu.net/>), but the lack of calibration sites located at low latitudes remains a problem.
- (2) Heisinger et al.'s (2002a, 2002b) work suggests that 17% of the *in situ* cosmogenic ^{14}C found in quartz is produced by slow and fast muon reactions. This proportion is considerably higher than those found for the other cosmogenic nuclides that are routinely analysed in this mineral (i.e., ^{10}Be , ^{26}Al , and ^{21}Ne), namely 2 % (Heisinger et al. 2002a,b, Balco and Shuster 2009). Heisinger et al.'s (2002a, 2002b) results for ^{14}C are based on targets prepared using the *in situ* ^{14}C wet extraction procedure of Lal and Jull (1994) (see Table 2.1) and so additional experiments, using the more common *in situ* ^{14}C extraction procedures described in Chapter 2 (e.g., Lifton et al. 2001, Hippe et al. 2009, Fülöp et al. 2010) are needed in order to test for the validity of Heisinger et al.'s (2002a, 2002b) results.

The method described in this work was aimed at a very specific scenario: the quantification of the magnitude and timing of an erosional event that resulted in the instantaneous removal of material from a soil/till of known age. However, the method is readily applicable

to other scenarios that involve the instantaneous removal of a certain layer of material (soil, sediment, or bedrock) as long as the initial undisturbed cosmogenic-nuclide depth-profile can be reconstructed. As such the method could be extended to eroding soils of unknown age that are in steady state, as in the case of these the cosmogenic nuclide depth-profile is time invariant being the result of an equilibrium between soil production as a result of weathering of the parent material and soil loss as a result of continuous surface erosion. For these soils the initial un-truncated cosmogenic nuclide depth-profile can be reconstructed using samples collected from depth-profiles at sites that have not been disturbed by the erosion event.

Processes related to seismic activity (e.g., shallow landslides, movement along faults) result in displacement of material and thus in many cases will also results in truncation of the cosmogenic nuclide depth-profile. Therefore, the method developed in this work could readily be applied to quantifying the timing of such seismic events.

References

- Aitken, M.: 1998, *An Introduction to Optical Dating*, Oxford University Press, Oxford.
- Akçar, N., Ivy-Ochs, S. and Schlüchter, C.: 2008, Application of in-situ produced terrestrial cosmogenic nuclides to archaeology: A schematic review, *Quaternary Science Journal* **57**(1-2), 226–238.
- Aksoy, H. and Kavvas, L. M.: 2005, A review of hillslope and watershed scale erosion and sediment transport models, *Catena* **64**(2-3), 247–271.
- Alewell, C., Meusburger, K., Brodbeck, M. and Bänninger, M.: 2008, Methods to describe and predict soil erosion in mountain regions, *Landscape and Urban Planning* **88**, 46–53.
- Alexanderson, H. and Murray, A. S.: 2010, Problems and potential of OSL Holocene sediments in Sweden, *Quaternary Science Reviews* **Article in Press, Corrected Proof**.
- Ali, F.: 2009, *Construction of sediment budgets in large scale drainage basins: the case of the Upper Indus river*, PhD thesis, University of Saskatchewan.
- Anderson, R. S. and Humphrey, N. F.: 1989, Interaction of weathering and transport processes in the evolution of arid landscapes, in T. A. Cross (ed.), *Quantitative Dynamic Stratigraphy*, Prentice-Hall, Englewood Cliffs, pp. 349–361.
- Anderson, R. S., Repka, J. and Dick, G.: 1996, Explicit treatment of inheritance in dating depositional surfaces using in situ ^{10}Be and ^{26}Al , *Geology* **24**(1), 47–51.
- Anselmetti, F. S., Hodell, D. A., Ariztegui, D., Brenner, M. and Rosenmeier, M. F.: 2007, Quantification of soil erosion rates related to ancient Maya deforestation, *Geology* **35**, 915–918.
- Appleby, P. G. and Oldfield, F.: 1983, The assessment of ^{210}Pb data from sites with varying sediment accumulation rates, *Hydrobiologia* **103**, 29–35.

- Arvidsson, J.: 2001, Subsoil compaction caused by heavy sugarbeet harvesters in southern Sweden I. Soil physical properties and crop yield in six field experiment, *Soil & Tillage Research* **60**, 67–78.
- Ascough, P. L., Cook, G. T. and Dugmore, A. J.: 2009, North Atlantic marine ^{14}C reservoir effects: Implications for late-Holocene chronological studies, *Quaternary Geochronology* **4**, 171–180.
- Baghdadi, N., Cerdan, O., Zribi, M., Auzet, V., Darboux, F., El Hajj, M. and Kheir, R. B.: 2008, Operational performance of current synthetic aperture radar sensors in mapping soil surface characteristics in agricultural environments: application to hydrological and erosion modelling, *Hydrological Processes* **22**, 9–20.
- Bailey, S. D., Wintle, A. G., Duller, G. A. T. and Bristow, C. S.: 2001, Sand deposition during the last millennium at Aberffraw, Anglesey, North Wales as determined by OSL dating of quartz, *Quaternary Science Reviews* **20**, 701–704.
- Balco, G. and Rovey II, C. W.: 2008, An isochron method for cosmogenic-nuclide dating of buried soils and sediments, *American Journal of Science* **308**(10), 1083–1114.
- Balco, G. and Shuster, D. L.: 2009, Production rate of cosmogenic ^{21}Ne in quartz estimated from ^{10}Be , ^{26}Al and ^{21}Ne concentrations in slowly eroding Antarctic bedrock surfaces, *Earth and Planetary Science Letters* **281**, 48–58.
- Balco, G. and Stone, J. O.: 2003, Measuring the density of rock, sand, till, etc., <http://depts.washington.edu/cosmolab/chem.html> **26**. August 2011.
- Balco, G., Stone, J. O., Lifton, N. A. and Dunai, T. J.: 2008, A complete and easily accessible means of calculating surface exposure ages or erosion rates from ^{10}Be and ^{26}Al measurements, *Quaternary Geochronology* **3**, 174–195.
- Ballantyne, C. K.: 1984, The Late Devensian periglaciation of upland Scotland, *Quaternary Science Reviews* **3**, 311–343.
- Barg, E., Lal, D., Pavich, M. J., Caffee, M. W. and Southon, J. R.: 1997, Beryllium geochemistry in soils: evaluation of $^{10}\text{Be}/^{9}\text{Be}$ ratios in authigenic minerals as a basis for age models, *Chemical Geology* **140**(3-4), 237–258.
- Barker, C. and Torkelson, B. E.: 1975, Gas adsorption on crushed quartz and basalt, *Geochimica et Cosmochimica Acta* **39**, 212–218.

- Barrett, J. C.: 1981, Aspects of the Iron Age in Atlantic Scotland. A case study in the problems of aachaeological interpretation, *Proceedings of the Society of Antiquaries of Scotland* **111**(205-219).
- Battarbee, R. W., Flower, R. J., Stevenson, A. C. and Rippey, B.: 1985, Lake acidification in Galloway: a palaeoecological test of competing hypotheses, *Nature* **314**(28), 350–352.
- Bauer, C. A.: 1947, Production of helium in meteorites by cosmic radiation, *Physical Review* **72**, 354.
- Beach, T.: 1987, A review of soil erosion modeling, in D. Brown and P. Gersmehl (eds), *File Structure Design and Data Specification for Water Resources Geographic Information Systems*, Vol. 10, Water Resources Research Center Special Publication, University of Minnesota, St. Paul, MN.
- Benn, D. I.: 1992, The genesis and significance of ‘hummocky moraine’: evidence from the Isle of Skye, Scotland, *Quaternary Science Reviews* **11**, 781–799.
- Benn, D. I. and Lukas, S.: 2006, Younger Dryas glacial landsystems in North West Scotland: an assessment of modern analogues and palaeoclimatic implications, *Quaternary Science Reviews* **25**, 2390–2408.
- Bennett, H. H.: 1928, The geographical relation of soil erosion to land productivity, *Geographical Review* **18**(4), 579–605.
- Bennett, J. P.: 1974, Concepts of mathematical modeling of sediment yield, *Resources Research* **10**(3), 1–8.
- Bernal, J. P., Eggins, S. M., Mcculloch, M. T., Grun, R. and Eggleton, R. A.: 2006, Dating of chemical weathering processes by in situ measurement of U-series disequilibria in supergene Fe-oxy/hydroxides using LA-MC-ICPMS, *Chemical Geology* **235**, 76–94.
- Bertran, P.: 2004, Soil erosion in small catchments of the Quercy region (southwestern France) during the Holocene, *The Holocene* **14**(4), 597–606.
- Bevington, P. R. and Robinson, K. D.: 2003, *Data Reduction and Error Analysis for the Physical Sciences*, McGraw-Hill, Boston MA.

- Bewket, W. and Sterk, G.: 2003, Assessment of soil erosion in cultivated fields using a survey methodology for rills in the Chemoga watershed, Ethiopia, *Agriculture, Ecosystems and Environment* **97**, 81–93.
- Bhattacharai, R. and Dutta, D.: 2007, Estimation of soil erosion and sediment yield using GIS at catchment scale, *Water Resources Management* **21**, 1635–1647.
- Bierman, P. R.: 1994, Using in situ produced cosmogenic isotopes to estimate rates of landscape evolution: A review from the geomorphic perspective, *Journal of Geophysical Research* **99**, 13885–13896.
- Bierman, P. R.: 2007, Cosmogenic glacial dating, 20 years and counting, *Geology* **35**, 575–576.
- Bierman, P. R., Caffee, M. W., Davis, P. T., Marsella, K., Pavich, M., Colgan, P., Mickelson, D. and Larsen, J.: 2002, Rates and timing of Earth surface processes from in-situ-produced cosmogenic ^{10}Be , in E. S. Grew (ed.), *Beryllium: Mineralogy, Petrology and Geochemistry*, Vol. 50 of *Reviews in Mineralogy and Geochemistry*, Mineralogical Society of America, pp. 147–205.
- Bierman, P. R., Howe, J., Stanley-Mann, E., Peabody, M., Hilke, J. and Massey, C. A.: 2005a, Old images record landscape change through time, *GSA Today* **15**(4), 4–10.
- Bierman, P. R. and Nichols, K. K.: 2004, Rock to sediment - slope to sea with ^{10}Be - rates of landscape change, *Annual Review of Earth and Planetary Sciences* **32**, 215–255.
- Bierman, P. R., Reuter, J. M., Pavich, M., Gellis, A. C., Caffee, M. W. and Larsen, J.: 2005b, Using cosmogenic nuclides to contrast rates of erosion and sediment yield in a semi-arid, arroyo-dominated landscape, Rio Puerco Basin, New Mexico, *Earth Surface Processes and Landforms* **30**, 935–953.
- Bishop, P.: 2007, Long-term landscape evolution: linking tectonics and surface processes, *Earth Surface Processes and Landforms* **32**, 329–365.
- Bishop, P., Muñoz-Salinas, E., MacKenzie, A. B., Pulford, I. and McKibbin, J.: 2010, The character, volume and implications of sediment impounded in mill dams in Scotland: The case of the Baldernock Mill dam in East Dunbartonshire, *Earth and Environmental Science Transactions of the Royal Society of Edinburgh* **101**, 97–110.

- Bisinger, T., Hippler, S., Michel, R., Wacker, L. and Synal, H.-A.: 2010, Determination of plutonium from different sources in environmental samples using alpha-spectrometry and AMS, *Nuclear Instruments and Methods in Physics Research B* **268**, 1269–1272.
- Blake, W. H., Walling, D. E. and He, Q.: 1999, Fallout beryllium-7 as a tracer in soil erosion investigations, *Applied Radiation and Isotopes* **51**(5), 599–605.
- Blott, S. J., Croft, D. J., Pye, K., Saye, S. E. and Wilson, H. E.: 2004, *Particle size analysis by laser diffraction*, Vol. Special Publications 232, Geological Society, London, pp. 63–73.
- Boardman, J.: 2006, Soil erosion science: reflections on the limitations of current approaches, *Catena* **68**(2-3), 73–86.
- Boardman, J. and Robinson, D. A.: 1985, Soil erosion, climatic vagary and agricultural change on the Downs around Lewes and Brighton, autumn 1982, *Applied Geography* **5**(3), 243–258.
- Bodoque, J. M., Díez-Herrero, A., Martín-Duque, J. F., Rubiales, J. M., Godfrey, A., Pedraza, J., Carrasco, R. M. and Sanz, M. A.: 2005, Sheet erosion rates determined by using dendrogeomorphological analysis of exposed tree roots: Two examples from Central Spain, *Catena* **64**, 81–102.
- Boeckl, R.: 1971, A depth profile of ^{14}C in the lunar rock 12002, *Earth and Planetary Science Letters* **16**, 269–272.
- Boeckl, R.: 1972, Terrestrial age of nineteen stony meteorites derived from their radiocarbon content, *Nature* **236**(3), 25–26.
- Boix-Fayos, C., Martínez-Mena, M., Arnau-Rosalén, E., Calvo-Cases, A., Castillo, V. and Albaladejo, J.: 2006, Measuring soil erosion by field plots: Understanding the sources of variation, *Earth Science Reviews* **78**, 267–285.
- Bonilla, C., Norman, J., Molling, C., Karthikeyan, K. and Miller, P.: 2008, Testing a grid-based soil erosion model across topographically complex landscapes, *Soil Science Society of America Journal* **72**(6), 1745–1755.
- Borg, L. E. and Banner, J. L.: 1996, Neodymium and strontium isotopic constraints on soil sources in Barbados, West Indies, *Geochimica et Cosmochimica Acta* **60**, 4193–4206.

- Bork, H.-R.: 1989, Soil erosion during the past millennium in central Europe and its significance within the geomorphodynamics of the Holocene, *in* F. Ahnert (ed.), *Landform and Landform Evolution in West Germany*, Vol. 15, Catena, pp. 121–132.
- Born, W. and Begeman, F.: 1975, ^{14}C - $^{39}\text{Ar}_{Me}$ correlations in chondrites and their pre-atmospheric size, *Earth and Planetary Science Letters (ISSN 0012-821X)* **25**(2), 159–169.
- Borren, W., Bleuten, W. and Lapshina, E. D.: 2004, Holocene peat and carbon accumulation rates in the southern taiga of western Siberia, *Quaternary Research* **61**(1), 42–51.
- Bradwell, T., Fabel, D., Stoker, M. S., Mathers, H., McHargue, L. R. and Howe, J. A.: 2008, Ice caps existed throughout the Lateglacial Interstadial in northern Scotland, *Journal of Quaternary Science* **23**, 401–407.
- Braucher, R., Brown, E. T., Bourlès, D. L. and Colin, F.: 2003, In situ produced ^{10}Be measurements at great depths: implications for production rates by fast muon, *Earth and Planetary Science Letters* **211**, 251–258.
- Braucher, R., Colin, F., Brown, E. T., Bourlès, D. L., Bamba, O., Raisbeck, G. M., Yiou, F. and Koud, J. M.: 1998, African laterite dynamics using in situ-produced ^{10}Be , *Geochimica and Cosmochimica Acta* **62**, 1501–1507.
- Braucher, R., Del Castillo, P., Siame, L., Hidy, A. J. and Bourlès, D. L.: 2009, Determination of both exposure time and denudation rate from an in situ-produced ^{10}Be depth profile: A mathematical proof of uniqueness. Model sensitivity and applications to natural cases, *Quaternary Geochronology* **4**, 56–67.
- Brazier, R.: 2004, Quantifying soil erosion by water in the UK: a review of monitoring and modelling approaches, *Progress in Physical Geography* **28**(3), 340–365.
- Briner, J. P. and Swanson, T. W.: 1998, Using inherited cosmogenic ^{36}Cl to constrain glacial erosion rates of the Cordilleran ice sheet, *Geology* **26**(1), 3–6.
- Bronk Ramsey, C.: 2009, Bayesian analysis of radiocarbon dates, *Radiocarbon* **51**(1), 337–360.
- Brown, A. G., Carey, C., Erkens, G., Fuchs, M., Hoffmann, T., Macaire, J.-J., Moldenhauer, K.-M. and Walling, D. E.: 2009, From sedimentary records to sediment budgets: Multiple approaches to catchment sediment flux, *Geomorphology* **108**, 35–47.

- Brown, E. T., Bourlès, D. L., Colin, F., Sanfo, Z., Raisbeck, G. M. and Yiou, F.: 1994, The development of iron crust lateritic systems in Burkina Faso, West Africa examined with in-situ-produced cosmogenic nuclides, *Earth and Planetary Science Letters* **124**, 19–33.
- Brown, E. T., Colin, F. and Bourlès, D. L.: 2003, Quantitative evaluation of soil processes using in situ-produced cosmogenic nuclides, *Comptes Rendus Geoscience* **335**, 1161–1171.
- Brown, E. T., Stallard, R. F., Larsen, M. C., Raisbeck, G. M. and Yiou, F.: 1995, Denudation rates determined from the accumulation of in situ-produced ^{10}Be in the Luquillo Experimental Forest, Puerto Rico, *Earth and Planetary Science Letters* **129**, 193–202.
- Brown, R. M., Andrews, H. R., Ball, G. C., Burn, N., Imahori, Y., Milton, J. C. D. and Fireman, E. L.: 1984, ^{14}C content of ten meteorites measured by tandem accelerator mass spectrometry, *Earth and Planetary Science Letters* **67**(1), 1–8.
- Browne, M. A. E. and Graham, D. K.: 1981, Glaciomarine deposits of the Loch Lomond Stade glacier in the Vale of Leven between Dumbarton and Balloch, west-central Scotland, *Quaternary Newsletter* **34**, 1–7.
- Buchanan, D. L. and Corcoran, B. J.: 1959, Sealed tube combustions for the determination of Carbon-14 and Total Carbon, *Analytical Chemistry* **31**(10), 1635–1638.
- Buckley, S. J., Howell, J. A., Enge, H. D. and Kurz, T. H.: 2008, Terrestrial laser scanning in geology: data acquisition, processing and accuracy considerations, *Journal of the Geological Society, London* **165**, 625–638.
- Burbank, D. W. and Anderson, R. S.: 2001, *Tectonic Geomorphology*, Blackwell, Malden, M A.
- Burrough, P. A. and McDonnell, R. A.: 1998, *Principles of Geographic Information Systems*, Oxford University Press, Oxford.
- Calvo-Cases, A., Boix-Fayos, C. and Imeson, A. C.: 2003, Runoff generation, sediment movement and soil water behaviour on calcareous (limestone) slopes of some Mediterranean environments in southeast Spain, *Geomorphology* **50**, 269–291.
- Campbell, B. L., Loughran, R. J. and Elliott, G. L.: 1988, A method for determining sediment budgets using caesium-137, *Sediment Budgets (Proceedings of the Porto Alegre Symposium)*, Vol. 174, IAHS, pp. 171–179.

- Campbell, I. A.: 1981, Spatial and temporal variations in erosion measurements, *Erosion and Sediment Transport Measurement (Proceedings of the Florence Symposium)*, Vol. 133, IAHS, pp. 447–456.
- Carrara, P. E. and Carroll, T. R.: 1979, The determination of erosion rates from exposed tree roots in the Piceance basin, Colorado, *Earth Surface Processes* **4**, 307–317.
- Cerdan, O., Le Bissonnais, Y., Govers, G., Lecomte, V., van Oost, K., Couturier, A., King, C. and Dubreuil, N.: 2004, Scale effect on runoff from experimental plots to catchments in agricultural areas in Normandy, *Journal of Hydrology* **299**(1-2), 4–14.
- Cerling, T. E. and Craig, H.: 1994, Geomorphology and in-situ cosmogenic isotopes, *Annual Review of Earth and Planetary Sciences* **22**, 273–317.
- Chadwick, O., Hall, R., Conel, J., Phillips, F., Zreda, M. and Gosse, J.: 1994, Glacial deposits and river terraces in Wind River Basin, in O. e. Chadwick (ed.), *Quaternary Geology of the Wind River Basin, Wyoming: Friends of the Pleistocene, Rocky Mountain Cell field guide: Pasadena*, California Institute of Technology, Jet Propulsion Laboratory, pp. 1–15.
- Chen, Y., Zentilli, M., Clark, A., Farrar, E., Grist, A. and Willis Richards, J.: 1996, Geochronological evidence for post-Variscan cooling and uplift of the Carnmenellis granite, SW England, *Journal of the Geological Society* **153**, 191–195.
- Child, D., Elliott, G., Mifsud, C., Smith, A. M. and Fink, D.: 2000, Sample processing for earth science studies at ANTARES, *Nuclear Instruments and Methods in Physics Research B* **172**, 856–860.
- Chmeleff, J., von Blanckenburg, F., Kossert, K. and Jakob, D.: 2010, Determination of the ^{10}Be half-life by multicollector ICP-MS and liquid scintillation counting, *Nuclear Instruments & Methods In Physics Research Section B-Beam Interactions With Materials And Atoms* **268**(2), 192–199.
- Claessens, L., Lowe, D. J., Hayward, B. W., Schaap, B. F., Schoorl, J. M. and Veldkamp, A.: 2006, Reconstructing high-magnitude/low-frequency landslide events based on soil redistribution modelling and a Late-Holocene sediment record from New Zealand, *Geomorphology* **74**, 29–49.

- Cockburn, H. A. P. and Summerfield, M. A.: 2004, Geomorphological applications of cosmogenic isotope analysis, *Progress in Physical Geography* **28**, 1–42.
- Codilean, A. T.: 2006, Calculation of the cosmogenic nuclide production topographic shielding scaling factor for large areas using DEMs, *Earth Surface Processes and Landforms* **31**, 785–794.
- Codilean, A. T., Bishop, P. and Hoey, T. B.: 2006, Surface process models and the links between tectonics and topography, *Progress in Physical Geography* **30**, 307–333.
- Codilean, A. T., Bishop, P., Stuart, F. M., Hoey, T. B., Fabel, D. and Freeman, S. P. H. T.: 2008, Single-grain cosmogenic ^{21}Ne concentrations in fluvial sediments reveal spatially variable erosion rates, *Geology* **36**, 159–162.
- Collins, A. L. and Walling, D. E.: 2004, Documenting catchment suspended sediment sources: problems, approaches and prospects, *Progress in Physical Geography* **28**(2), 159–196.
- Cook, G. T., Dugmore, A. J. and Shore, J. S.: 1998, The influence of pretreatment on humic acid yield and ^{14}C age of carex peat, *Radiocarbon* **40**(1), 21–27.
- Cooke, M. J., Stern, L. A., Banner, J. L., Mack, L. E., Jr. Stafford, T. W. and S., I. T. R.: 2003, Precise timing and rate of massive late Quaternary soil denudation, *Geology* **31**(10), 853–856.
- Coope, G. R. and Rose, J.: 2008, Palaeotemperatures and palaeoenvironments during the Younger Dryas: Arthropod evidence from Croftamie at the type area of the Loch Lomond Readvance, and significance for the timing of glacier expansion during the Lateglacial period in Scotland, *Scottish Journal of Geology* **44**, 43–49.
- Cornu, S., Montagne, D. and Vasconcelos, P. M.: 2009, Dating constituent formation in soils to determine rates of soil processes: A review, *Geoderma* **153**(3–4), 293–303.
- Couper, P., Stott, T. and Maddock, I.: 2002, Insights into river bank erosion processes derived from analysis of negative erosion-pin recordings: observations from three recent UK studies, *Earth Surface Processes and Landforms* **27**(1), 59–79.
- Coutts, J. R. H., Kandil, M., Nowland, J. L. and Tinsley, J.: 1968, Use of radioactive ^{59}Fe for tracing soil particle movement, *European Journal of Soil Science* **19**(2), 325–341.

- Craig, H.: 1953, The geochemistry of the stable carbon isotopes, *Geochimica et Cosmochimica Acta* **2**, 53–92.
- Craig, H.: 1957, Isotopic standards for carbon and oxygen and correction factors for mass-spectrometric analysis of carbon dioxide, *Geochimica et Cosmochimica Acta* **12**(1–2), 133–149.
- Cresswell, R. G., Beukens, R. P., Rucklidge, J. C. and Miura, Y.: 1994, Distinguishing spallogenic from non-spallogenic carbon in chondrites using gas and temperature separations, *Nuclear Instruments and Methods in Physics Research Section B* **92**, 505–509.
- Cresswell, R. G., Miura, Y., Beukens, R. P. and Rucklidge, J. C.: 1993, ^{14}C terrestrial ages of nine Antarctic meteorites using CO and CO₂ temperature extractions, *Proceedings NIPR Symposium on Antarctic Meteorites*, Vol. 6, pp. 381–390.
- Daniels, B., Gilliam, J. W., Cassel, D. K. and Nelson, L. A.: 1987, Quantifying the effects of past soil erosion on present soil productivity, *Journal of Soil and Water Conservation* **42**(3), 183–187.
- de Araújo, J. C. and Knight, D. W.: 2005, A review of the measurement of sediment yield in different scales, *Rem: Revista Escola de Minas* **58**(3), 257–265.
- de Jong, S. M., Paracchini, M. L., Bertolo, F., Folving, S., Megier, J. and de Roo, A. P. J.: 1999, Regional assessment of soil erosion using the distributed model SEMMED and remotely sensed data, *Catena* **37**, 291–308.
- de Moor, J. J. W. and Verstraeten, G.: 2008, Alluvial and colluvial sediment storage in the Geul River catchment (The Netherlands)-combining field and modelling data to construct a Late Holocene sediment budget, *Geomorphology* **95**, 487–503.
- de Ploey, J.: 1990, Modelling the erosional susceptibility of catchments in terms of energy, *Catena* **17**(2), 175–183.
- de Vente, J. and Poesen, J.: 2005, Predicting soil erosion and sediment yield at the basin scale: Scale issues and semi-quantitative models, *Earth Science Reviews* **71**, 95–125.
- de Vente, J., Poesen, J., Arabkhedri, M. and Verstraeten, G.: 2007, The sediment delivery problem revisited, *Progress in Physical Geography* **31**(2), 155–178.

- de Vente, J., Poesen, J. and Verstraeten, G.: 2006, Predicting catchment sediment yield in Mediterranean environments: the importance of sediment sources and connectivity in Italian drainage basins, *Earth Surface Processes and Landforms* **31**(8), 1017–1034.
- Dearing, J. A.: 1991, Lake sediment records of erosional processes, *Hydrobiologia* **214**(1), 99–106.
- Dearing, J. A. and Foster, I. D. L.: 1993, Lake sediments and geomorphological processes: some thoughts, in J. McManus and R. W. Duck (eds), *Geomorphology and sedimentology of lakes and reservoirs*, John Wiley & Sons, Chichester, pp. 5–14.
- Des Marais, D. J.: 1983, Light element geochemistry and spallogeneis in lunar rocks, *Geochimica et Cosmochimica Acta* **47**, 1769–1781.
- Des Marais, D. J. and Moore, G. J.: 1984, Carbon and its isotopes in mid-oceanic basaltic glasses, *Earth and Planetary Science Letters (ISSN 0012-821X)* **69**, 43–57.
- Desilets, D., Zreda, M. and Prabu, T.: 2006, Extended scaling factors for in situ cosmogenic nuclides: New measurements at low latitude, *Earth and Planetary Science Letters (ISSN 0012-821X)* **246**, 265–276.
- Dietrich, W. E. and Dunne, T.: 1978, Sediment budget for a small catchment in mountainous terrain, *Zeitschrift für Geomorphologie Supplement* **29**, 191–206.
- Donahue, D. J., Linick, T. W. and Jull, A. J. T.: 1990, Isotope-ratio and background corrections for accelerator mass spectrometry radiocarbon measurements, *Radiocarbon* **32**, 135–142.
- Douglass, D. and Bockheim, J.: 2006, Soil-forming rates and processes on Quaternary moraines near Lago Buenos Aires, Argentina, *Quaternary Research* **65**(2), 293–307.
- Duck, R. W. and McManus, J.: 1987, Soil erosion near Barry, Angus, *Scottish Geographical Magazine* **103**, 44–46.
- Dugan, B.: 2008, *New production rate estimates for in situ cosmogenic ^{14}C from Lake Bonneville, Utah, and Northwestern Scotland*, Master's thesis, University of Arizona, Tucson.

- Dugmore, A. J., Gísladóttir, G., Simpson, I. A. and Newton, A.: 2009, Conceptual models of 1200 years of Icelandic soil erosion reconstructed using tephrochronology, *Journal of the North Atlantic* **2**, 1–18.
- Duke, E. F., Galbreath, K. C. and Trusty, K. J.: 1990, Fluid inclusion and carbon isotope studies of quartz-graphite veins, Black Hills, South Dakota, and Ruby Range, Montana, *Geochimica et Cosmochimica Acta* **54**, 683–698.
- Dunai, T. J.: 2000, Scaling factors for production rates of in situ produced cosmogenic nuclides: a critical reevaluation, *Earth and Planetary Science Letters* **176**, 157–169.
- Dunai, T. J.: 2010, *Cosmogenic Nuclides: Principles, Concepts and Applications in the Earth Surface Sciences*, Cambridge University Press.
- Dunne, J., Elmore, D. and Muzikar, P.: 1999, Scaling factors for the rates of production of cosmogenic nuclides for geometric shielding and attenuation at depth on sloped surfaces, *Geomorphology* **27**, 3–11.
- Dutta, N. N. and Patil, G. S.: 1995, Developments in CO separation, *Gas Separation & Purification* **9**(4), 277–283.
- Edwards, K. J. and Whittington, G.: 1993, Aspects of the environmental and depositional history of a rock basin lake in eastern Scotland, UK, in J. McManus and R. W. Duck (eds), *Geomorphology and sedimentology of lakes and reservoirs*, Wiley, Chichester, pp. 155–180.
- Edwards, K. J. and Whittington, G.: 2001, Lake sediments, erosion and landscape change during the Holocene in Britain and Ireland, *Catena* **42**(2-4), 143–173.
- Elmore, D. and Phillips, F. M.: 1987, Accelerator mass-spectrometry for measurement of long-lived radioisotopes, *Science* **236**(4801), 543–550.
- Erkens, G., Cohen, K. M., Gouw, M. J. P., Middelkoop, H. and Hoek, W. Z.: 2006, Holocene sediment budgets of the Rhine Delta (The Netherlands): a record of changing sediment delivery, *Sediment Dynamics and the Hydromorphology of Fluvial Systems (Proceedings of a symposium held in Dundee, UK, July 2006)*, Vol. 306, IAHS, pp. 406–415.

- Evans, D. J. A. and Rose, J.: 2003, Late Quaternary stratigraphy of the Western Highland Boundary, in D. J. A. Evans (ed.), *The Quaternary of the Western Highland Boundary - Field Guide*, Quaternary Research Association, pp. 21–29.
- Evans, D. J. A. and Wilson, S. B.: 2006, Scottish landform example 39: The Lake of Menteith glacetectonic hill-hole pair, *Scottish Geographical Journal* **122**(4), 352–364.
- Evans, D. J. A., Wilson, S. B. and Rose, J.: 2003, Glacial geomorphology of the western highland boundary, in D. J. A. Evans (ed.), *The Quaternary of the Western Highland Boundary - Field Guide*, Quaternary Research Association, pp. 5–20.
- Everett, S.: 2009, *Assessment of plutonium as a tracer of soil and sediment transport using accelerator mass spectrometry*, PhD thesis, Australian National University, Canberra.
- Fabel, D., Small, D., Miguens Rodriguez, M. and Freeman, S. P. H. T.: 2010, Cosmogenic nuclide exposure ages from the ‘Parallel Roads’ of Glen Roy, Scotland, *Journal of Quaternary Science* **25**(4), 597–603.
- Fabel, D., Stroeve, A. P., Harbor, J., Kleman, J., Elmore, D. and Fink, D.: 2002, Landscape preservation under fennoscandian ice sheets determined from in situ produced ^{10}Be and ^{26}Al , *Earth and Planetary Science Letters* **201**, 397–406.
- Fausey, N. R., Hall, G. F., Bigham, J. M., Allred, B. J. and Christy, A. D.: 2000, Properties of the fractured glacial till at the Madison County, Ohio, Field Workshop Pit Site, *The Ohio Journal of Science* **100**(3-4), 107–112.
- Fifield, L. K. and Morgenstern, U.: 2009, Silicon-32 as a tool for dating the recent past, *Quaternary Geochronology* **4**(5), 400–405.
- Finkel, R. C., Arnold, J., Imamura, M., Reedy, R., Fruchter, J., Loosli, H., Evans, J., Delany, A. and Shedlovsky, J.: 1971, Depth variation of cosmogenic nuclides in a lunar surface rock and lunar soil, *Lunar and Planetary Science Conference Proceedings*, Vol. 2, pp. 1773–1789.
- Fireman, E. L.: 1978, Carbon-14 in lunar soil and in meteorites, *Lunar and Planetary Science Conference Proceedings*, Vol. 9, pp. 1647–1654.
- Fister, W., Iserloh, T., Marzen, M., Ries, J. B. and Schmidt, R.-G.: 2010, Experimental measurement of wind and water erosion in Aragon and Andalusia, Spain, *Geophysical Research Abstracts*, Vol. 12 (EGU2010-12982), EGU General Assembly.

- Förster, H. and Wunderlich, J.: 2009, Holocene sediment budgets for upland catchments: The problem of soilscape model and data availability, *Catena* **77**(2), 143–149.
- Freeman, S. P. H. T., Bishop, P., Bryant, C., Cook, G., Dougans, D., Ertunc, T., Fallick, A., Ganeshram, R., Maden, C., Naysmith, P., Schnabel, C., Scott, M., Summerfield, M. A. and Xu, S.: 2007, The SUERC AMS laboratory after 3 years, *Nuclear Instruments and Methods in Physics Research B* **259**, 66–70.
- Freeman, S. P. H. T., Bishop, P., Bryant, C., Cook, G. T., Fallick, A. and Harkness, D.: 2004, A new environmental sciences AMS laboratory in Scotland, *Nuclear Instruments and Methods In Physics Research B* **223**, 31–34.
- Fuchs, M.: 2007, An assessment of human versus climatic impacts on Holocene soil erosion in NE Peloponnese, Greece, *Quaternary Research* **67**, 349–356.
- Fuchs, M. and Lang, A.: 2001, OSL dating of coarse-grain fluvial quartz using single-aliquot protocols on sediments from NE Peloponnese, Greece, *Quaternary Science Reviews* **20**, 783–787.
- Fuchs, M., Woda, C. and Bürkert, A.: 2007, Chronostratigraphy of a sediment record from the Hajar mountain range in north Oman: Implications for optical dating of insufficiently bleached sediments, *Quaternary Geochronology* **2**, 202–207.
- Fülöp, R.-H., Naysmith, P., Cook, G. T., Fabel, D., Xu, S. and Bishop, P.: 2010, Update on the performance of the SUERC in situ cosmogenic ^{14}C extraction line, *Radiocarbon* **52**(2-3), 1288–1294.
- Gale, S. J.: 2009, Dating the recent past, *Quaternary Geochronology* **4**(5), 374–377.
- Gale, S. J. and Hoare, P. G.: 1991, *Quaternary Sediments*, John Wiley & Sons, New York.
- Gell, P. A., Tibby, J. C., Little, F., Baldwin, D. and Hancock, G. J.: 2007, The impact of regulation and salinisation on floodplain lakes: the lower River Murray, Australia, *Hydrobiologia* **591**, 135–146.
- Gerrard, J.: 1992, *Soil Geomorphology, an integration of pedology and geomorphology*, Chapman and Hall, London.

- Goehring, B. M., Kelly, M. A., Schaefer, J. M., Finkel, R. C. and Lowell, T. V.: 2010, Dating of raised marine and lacustrine deposits in east Greenland using ^{10}Be depth profiles and implications for estimates of subglacial erosion, *Journal of Quaternary Science* **25**(6), 865–874.
- Goel, P. S. and Kohman, T. P.: 1962, Cosmogenic carbon-14 in meteorites and terrestrial ages of ‘finds’ and craters, *Science* **136**, 875–876.
- Golledge, N. R.: 2010, Glaciation of Scotland during the Younger Dryas stadial: a review, *Journal of Quaternary Science* **25**(4), 550–566.
- Golledge, N. R., Fabel, D., Everest, J. D., Freeman, S. and S., B.: 2007, First cosmogenic ^{10}Be age constraint on the timing of Younger Dryas glaciation and ice cap thickness, western Scottish Highlands, *Journal of Quaternary Science* **22**(8), 785–791.
- Golledge, N. R. and Hubbard, A.: 2005, Evaluating Younger Dryas glacier reconstructions in part of the western Scottish Highlands: a combined empirical and theoretical approach, *Boreas* **34**, 274–286.
- Golledge, N. R., Hubbard, A. and Sugden, D. E.: 2008, High-resolution numerical simulation of Younger Dryas glaciation in Scotland, *Quaternary Science Reviews* **27**(9–10), 888–904.
- Gomez, B., Banbury, K., Marden, M., Trustrum, N. A., Peacock, D. H. and Hoskin, P. J.: 2003, Gully erosion and sediment production: Te Weraroa Stream, New Zealand, *Water Resources Research* **39**(7), 1187–1195.
- Goodfellow, B. W.: 2008, *Relict non-glacial surfaces and autochthonous blockfields in the Northern Swedish Mountains*, PhD thesis, Department of Physical Geography and Quaternary Geology Stockholm University.
- Gordon, J. E.: 1982, Croftamie, in J. E. Gordon and D. G. Sutherland (eds), *Geological Conservation Review Series*, Vol. 6: Quaternary of Scotland, Chapman and Hall, London, chapter 13: Western Highland Boundary, p. 695.
- Gosse, J. C. and Phillips, F. M.: 2001, Terrestrial in situ cosmogenic nuclides: theory and application, *Quaternary Science Reviews* **20**, 1475–1560.

- Govers, G., Giménez, R. and Van Oost, K.: 2007, Rill erosion: Exploring the relationship between experiments, modelling and field observations, *Earth Science Reviews* **84**, 87–102.
- Graly, J.: 2011, *Interpretation of meteoric ^{10}Be in marginal ice-bound sediment of the Greenland Ice Sheet*, PhD thesis, Department of Geology and Rubenstein School of the Environment and Natural Resources University of Vermont.
- Granger, D. E. and Muzikar, P. F.: 2001, Dating sediment burial with in situ-produced cosmogenic nuclides: theory, techniques, and limitations, *Earth and Planetary Science Letters* **188**, 269–281.
- Granger, D. E. and Smith, A. L.: 2000, Dating buried sediments using radioactive decay and muogenic production of ^{26}Al and ^{10}Be , *Instruments and Methods in Physics Research B* **172**, 822–826.
- Grieve, I. C., Davidson, D. A. and Gordon, J. E.: 1995, Nature, extent and severity of soil erosion in upland Scotland, *Land Degradation & Rehabilitation* **6**, 41–55.
- Gulliksen, S. and Scott, E. M.: 1995, Report of the TIRI workshop, Saturday, 13 August 1994, *Radiocarbon* **37**, 820–821.
- Guralnik, B., Matmon, A., Avni, Y., Porat, N. and Fink, D.: 2010, Constraining the evolution of river terraces with integrated OSL and cosmogenic nuclide data, *Quaternary Geochronology* **6**(1), 22–32.
- Haciyakupoglu, S., Ertek, A., Walling, D. E., Ozturk, Z. F., Karahan, G., Erginal, A. E. and Celebi, N.: 2005, Using caesium-137 measurements to investigate soil erosion rates in western Istanbul (NW Turkey), *Catena* **64**(2-3), 222–231.
- Haigh, M. J.: 1977, The use of erosion pins in the study of slope evolution, *British Geomorphological Research Group Technical Bulletin* **18**, 31–49.
- Hajdas, I.: 2009, Radiocarbon dating and its applications in Quaternary studies, *Quaternary Science Journal* **57**(1-2), 2–24.
- Hallet, B. and Putkonen, J. K.: 1994, Surface dating of dynamic landforms: Young boulders on aging moraines, *Science* **265**, 937–940.

- Hancock, G. R.: 2004, Modelling soil erosion on the catchment and landscape scale using landscape evolution models – a probabilistic approach using digital elevation model error, *SuperSoil 2004: 3rd Australian New Zealand Soils Conference*, www.regional.org.au/au/asssi/, University of Sydney, Published on CDROM, Australia.
- Hancock, G. S., Anderson, R. S., Chadwick, O. A. and Finkel, R. C.: 1999, Dating fluvial terraces with ^{10}Be and ^{26}Al profiles: application to the Wind River, Wyoming, *Geomorphology* **27**(1-2), 41–60.
- Handwerger, D. A., Cerling, T. E. and Bruhn, R. L.: 1999, Cosmogenic ^{14}C in carbonate rocks, *Geomorphology* **27**, 13–24.
- Harden, J. W., Sundquist, E. T., Stallard, R. F. and Mark, R. K.: 1992, Dynamics of soil carbon during deglaciation of the Laurentide Ice Sheet, *Science* **258**(5090), 1921–1924.
- Heier Nielsen, S., Heinemeier, J., Nielsen, H. L. and Rud, N.: 1995, Recent reservoir ages for Danish fjords and marine waters, *Radiocarbon* **37**(3), 875–882.
- Heimsath, A. M., Chappell, J., Dietrich, W. E., Nishiizumi, K. and Finkel, R. C.: 2000, Soil production on a retreating escarpment in southeastern Australia, *Geology* **28**, 787–790.
- Heimsath, A. M., Dietrich, W. E., Nishiizumi, K. and Finkel, R. C.: 1997, The soil production function and landscape equilibrium, *Nature* **388**, 358–361.
- Heimsath, A. M., Dietrich, W. E., Nishiizumi, K. and Finkel, R. C.: 1999, Cosmogenic nuclides, topography, and the spatial variation of soil depth, *Geomorphology* **27**, 151–172.
- Hein, A. S., Hulton, N. R. J., Dunai, T. J., Schnabel, C., Kaplan, M. R., Naylor, M. and Xu, S.: 2009, Middle Pleistocene glaciation in Patagonia dated by cosmogenic-nuclide measurements on outwash gravels, *Earth and Planetary Science Letters* **286**(1-2), 184–197.
- Heisinger, B., Lal, D., Jull, A. J. T., Kubik, P., Ivy-Ochs, S., Knie, K. and Nolte, E.: 2002b, Production of selected cosmogenic radionuclides by muons. 2: Capture of negative muons, *Earth and Planetary Science Letters* **200**, 357–369.

- Heisinger, B., Lal, D., Jull, A. J. T., Kubik, P., Ivy-Ochs, S., Neumaier, S., Knie, K., Lazarev, V. and Nolte, E.: 2002a, Production of selected cosmogenic radionuclides by muons. 1: Fast muons, *Earth and Planetary Science Letters* **200**, 345–355.
- Heisinger, B., Niedermayer, M., Hartmann, F. J., Korschinek, G., Nolte, E., Morteani, G., Neumaier, S., Petitjean, C., Kubik, P., Synal, A. and Ivy-Ochs, S.: 1997, In-situ production of radionuclides at great depths, *Nuclear Instruments and Methods in Physics Research B* **123**, 341–346.
- Hewawasam, T., von Blanckenburg, F., Schaller, M. and Kubik, P.: 2003, Increase of human over natural erosion rates in tropical highlands constrained by cosmogenic nuclides, *Geology* **31**(7), 597–600.
- Hidy, A. J., Gosse, J., Pederson, J. L., Mattern, J. P. and Finkel, R. C.: 2010, A geologically constrained Monte Carlo approach to modeling exposure ages from profiles of cosmogenic nuclides: An example from Lees Ferry, Arizona, *Geochemistry Geophysics Geosystems* **11**, 1–18.
- Hippe, K., Kober, F., Baur, H., Ruff, M., Wacker, L. and Wieler, R.: 2009, The current performance of the in situ ^{14}C extraction line at ETH, *Quaternary Geochronology* **4**, 493–500.
- Hoare, P. G., Gale, S. J., Robinson, R. A. J., Connell, E. R. and Larkin, N. R.: 2009, Marine Isotope Stage 7–6 transition age for beach sediments at Morston, north Norfolk, UK: implications for Pleistocene chronology, stratigraphy and tectonics, *Journal of Quaternary Science* **24**, 311–316.
- Hofmann, H. J., Beer, J., Bonani, G., Gunten, H. R. V., Raman, S., Suter, M., Walker, R. L., Wölfli, W. and Zimmermann, D.: 1987, ^{10}Be : Half-life and AMS-standards, *Nuclear Instruments and Methods In Physics Research B* **29**, 32–36.
- Houben, P., Hoffmann, T., Zimmermann, A. and Dikau, R.: 2006, Land use and climatic impacts on the Rhine system (RheinLUCIFS): Quantifying sediment fluxes and human impact with available data, *Catena* **66**(1-2), 42–52.
- Howe, J. A., Shimmield, T., Austin, W. E. N. and Longva, O.: 2002, Post-glacial depositional environments in a mid-high latitude glacially-overdeepened sea loch, inner Loch Etive, western Scotland, *Marine Geology* **185**, 417–433.

- Huggett, R. J.: 1998, Soil chronosequences, soil development, and soil evolution: a critical review, *Catena* **32**, 155–172.
- Ihaka, R. and Gentleman, R.: 1996, R: A language for data analysis and graphics, *Journal of Computational and Graphical Statistics* **5**, 299–314.
- Imamura, M., Nagai, H., Takabatake, M., Shibata, S., Kobayashi, K., Yoshida, K., Ohashi, H., Uwamino, Y. and Nakamura, T.: 1990, Measurement of production cross sections of ^{14}C and ^{26}Al with high-energy neutrons up to $E_n=38$ MeV by accelerator mass spectrometry, *Nuclear Instruments and Methods in Physics Research Section B* **52**, 595–600.
- Inn, K. G. W., Raman, S., Coursey, B. M., Fassett, J. D. and Walker, R. L.: 1987, Development of the NBS $^{10}\text{Be}/^{9}\text{Be}$ isotopic standard reference material, *Nuclear Instruments and Methods In Physics Research B* **29**(1-2), 27–31.
- Jack, L.: 1877, Notes on a till or boulder clay with broken shells, in the lower valley of the river Endrik, near Loch Lomond, and its relation to certain other glacial deposits, *Transactions of the Geological Society of Glasgow* **V**, 1–25.
- Jain, M., Murray, A. S., Bøtter-Jensen, L. and Wintle, A. G.: 2004, A single-aliquot regenerative-dose method based on IR (1.49 eV) bleaching of the fast OSL component in quartz, *Radiation Measurements* **39**, 309–318.
- Jankauskas, B. and Fullen, M.: 2002, A pedological investigation of soil erosion severity on undulating land in Lithuania, *Canadian Journal of Soil Science* **82**(3), 311–321.
- Jennings, K. L., Bierman, P. R. and Southon, J.: 2003, Timing and style of deposition on humid-temperate fans, Vermont, United States, *Bulletin of the Geological Society of America* **115**(2), 182–199.
- Jetten, V., Govers, G. and Hessel, R.: 2003, Erosion models: quality of spatial predictions, *Hydrological Processes* **17**, 887–900.
- Judson, S. and Ritter, D. F.: 1964, Rates of regional denudation in the United States, *Journal of Geophysical Research* **69**, 3395–3401.
- Jull, A. J. T.: 2004, Meteorites and the early solar system II, in D. S. Lauretta and H. Y. McSween Jr. (eds), *Terrestrial Ages of Meteorites*, University of Arizona Press and the Lunar and Planetary Institute, pp. 1–17.

- Jull, A. J. T., Cloudt, S., Donahue, D. J., Sisterson, J. M., Reedy, R. C. and Masarik, J.: 1998, ^{14}C depth profiles in Apollo 15 and 17 cores and lunar rock 68815, *Geochimica et Cosmochimica Acta* **62**(17), 3025–3036.
- Jull, A. J. T. and Donahue, D. J.: 1988, Terrestrial age of the Antarctic shergottite EETA79001, *Geochimica et Cosmochimica Acta* **52**, 1295–1297.
- Jull, A. J. T., Donahue, D. J. and Linick, T. W.: 1989a, ^{14}C activities in recently fallen meteorites and Antarctic meteorites, *Geochimica et Cosmochimica Acta* **53**(8), 2095–2100.
- Jull, A. J. T., Donahue, D. J., Linick, T. W. and Wilson, G. C.: 1989b, Spallogenic ^{14}C in high altitude rocks in Antarctic meteorites, *Radiocarbon* **31**, 719–724.
- Jull, A. J. T., Lifton, N., Phillips, W. M. and Quade, J.: 1994a, Studies of the production rate of cosmic-ray produced ^{14}C in rock surfaces, *Nuclear Instruments and Methods in Physics Research B* **92**, 308–310.
- Jull, A. J. T., Wilson, A. E., Burr, G. S., Toolin, L. J. and Donahue, D. J.: 1992, Measurements of cosmogenic ^{14}C produced by spallation in high-altitude rocks, *Radiocarbon* **34**(3), 737–744.
- Jungers, M. C., Bierman, P. R., Matmon, A., Nichols, K. K., Larsen, J. and Finkel, R.: 2009, Tracing hillslope sediment production and transport with in situ and meteoric ^{10}Be , *Journal of Geophysical Research* **114**(F04020), 1–16.
- Karim, D. and Hong, H.: 2010, An assessment of fluid inclusions composition using the Raman Spectroscopy at Daleishan Goldfield, Dawu County, Hubei Province, P. R. China, *Journal of American Science* **6**(7), 30–37.
- Kaste, J. M., Heimsath, A. M. and Bostick, B. C.: 2007, Short-term soil mixing quantified with fallout radionuclides, *Geology* **35**(3), 243–246.
- Kaste, J. M., Norton, S. A. and Hess, C. T.: 2002, Environmental chemistry of beryllium-7, *Reviews in Mineralogy and Geochemistry* **50**, 271–289.
- Kato, H., Onda, Y. and Tanaka, Y.: 2010, Using ^{137}Cs and $^{210}\text{Pb}_{ex}$ measurements to estimate soil redistribution rates on semi-arid grassland in Mongolia, *Geomorphology* **114**(4), 508–519.

- Kelley, S.: 2002, K-Ar and Ar-Ar dating, in D. P. Porcelli, C. Ballentine and Wieler (eds), *Noble Gases in Geochemistry and Cosmochemistry, Reviews in Mineralogy and Geochemistry*, Vol. 47, Mineralogy Society of America, Washington, D. C., pp. 785–818.
- Kelly, E. F., Aguilar, R., Muhaimed, A. S., Deutsch, P. C. and Heil, R. D.: 1988, Profile reconstruction: A method to quantify changes in soil properties resulting from cultivation, *Agriculture, Ecosystems and Environment* **21**, 153–162.
- Kennedy, M. J., Chadwick, O. A., Vitousek, P. M., Derry, L. A. and Hendricks, D. M.: 1998, Replacement of weathering with atmospheric sources of base cations during ecosystem development, Hawaiian Islands, *Geology* **26**, 1015–1018.
- Kim, K. J. and Englert, P. A. J.: 2004, Profiles of in situ ^{10}Be and ^{26}Al at great depths at the Macraes Flat, East Otago, New Zealand, *Earth and Planetary Science Letters* **223**, 113–126.
- King, C., Baghdadi, N., Lecomte, V. and Cerdan, O.: 2005, The application of remote-sensing data to monitoring and modelling of soil erosion, *Catena* **62**, 79–93.
- King, G. E., Finch, A. A., Robinson, R. A. J. and Hole, D. E.: 2011, The problem of dating quartz 1: Spectroscopic ionoluminescence of dose dependence, *Radiation Measurements* **46**(1), 1–9.
- Kirkbride, M. P. and Reeves, A. D.: 1993, Soil erosion caused by low-intensity rainfall in Angus, Scotland, *Applied Geography* **13**, 299–311.
- Kirkby, M.: 1999, From plot to continent: Reconciling fine and coarse scale erosion models, in D. E. Stott, R. H. Molnar and G. C. Steinhardt (eds), *Sustaining the Global Farm Selected papers from the 10th International Soil Conservation Organization Meeting held May 24-29*, Purdue University and the USDA-ARS National Soil Erosion Research Laboratory, pp. 860–870.
- Knauer, M., Neupert, U., Michel, R., Bonani, G., Dittrich-Hannen, B., Hajdas, I., Ivy Ochs, S., Kubik, P. W. and Suter, M.: 1994, Measurement of the long-lived radionuclides ^{10}Be , ^{14}C , ^{26}Al in meteorites from hot and cold deserts by accelerator mass spectrometry (AMS), *Proceedings of a Workshop on "Meteorites in Hot and Cold Deserts"*, Vol. Nördlingen, July 20-22, 1994, LPI Techn. Rep.95-02, The Lunar and Planetary Institute, Houston, pp. 38–42.

- Kohl, C. P. and Nishiizumi, K.: 1992, Chemical isolation of quartz for measurement of in-situ-produced cosmogenic nuclides, *Geochimica et Cosmochimica Acta* **56**(9), 3583–3587.
- Korschinek, G., Bergmaier, A., Faestermann, T., Gerstmann, U. C., Knie, K., Rugel, G., Wallner, A., Dillmann, I., Dollinger, G., Lierse von Gostomski, C., Kossert, K., Maiti, M., Poutivtsev, M. and Remmert, A.: 2010, A new value for the half-life of ^{10}Be by Heavy-Ion Elastic Recoil Detection and liquid scintillation counting, *Nuclear Instruments & Methods In Physics Research Section B-Beam Interactions With Materials And Atoms* **268**(2), 187–191.
- Korupa, O., McSaveney, M. J. and Davies, T. R. H.: 2004, Sediment generation and delivery from large historic landslides in the Southern Alps, New Zealand, *Geomorphology* **61**, 189–207.
- Krause, A. K., Franks, S. W., Kalma, J. D., Loughran, R. J. and Rowan, J. S.: 2003, Multi-parameter fingerprinting of sediment deposition in a small gullied catchment in SE Australia, *Catena* **53**, 327–348.
- Lal, D.: 1991, Cosmic ray labeling of erosion surfaces - In situ nuclide production rates and erosion models, *Earth and Planetary Science Letters* **104**, 424–439.
- Lal, D. and Jull, A. J. T.: 1994, Studies of cosmogenic in-situ ^{14}CO and $^{14}\text{CO}_2$ produced in terrestrial and extraterrestrial samples: experimental procedures and applications, *Nuclear Instruments and Methods In Physics Research B* **92**, 291–296.
- Lal, D., Jull, A. J. T., Burr, G. S. and Donahue, D. J.: 2000, On the characteristics of cosmogenic in situ ^{14}C in some GISP2 Holocene and late glacial ice samples, *Nuclear Instruments and Methods in Physics Research B* **172**, 623–631.
- Lal, D., Jull, A. J. T., Donahue, D. J., Burtner, D. and Nishiizumi, K.: 1990, Polar ice ablation rates measured using in situ cosmogenic ^{14}C , *Nature* **346**(6282), 350–352.
- Lal, D., Jull, A. J. T., Pollard, D. and Vacher, L.: 2005, Evidence for large century time-scale changes in solar activity in the past 32 Kyr, based on in-situ cosmogenic ^{14}C in ice at Summit, Greenland, *Earth and Planetary Science Letters* **234**, 335–349.
- Lal, R.: 2001, Soil degradation by erosion, *Land Degradation and Development* **12**(6), 519–539.

- Lal, R.: 2004, Soil carbon sequestration impacts on global climate change and food security, *Science* **304**, 1623–1627.
- Lal, R.: 2005, Soil erosion and carbon dynamics, *Soil & Tillage Research* **81**(2), 137–142.
- Lang, A.: 2003, Phases of soil erosion-derived colluviation in the loess hills of south germany, *Catena* **51**, 209–221.
- Lawler, D. M.: 1991, A new technique for the automatic monitoring of erosion and deposition rates, *Water Resources Research* **27**(8), 2125–2128.
- Lawler, D. M.: 1993, The measurement of river bank erosion and lateral channel change: A review, *Earth Surface Processes and Landforms* **18**(9), 777–821.
- Le Bissonnais, Y., Benkhadra, H., Chaplot, V., Fox, D., King, D. and Daroussin, J.: 1998, Crusting, runoff and sheet erosion on silty loamy soils at various scales and upscaling from m² to small catchments, *Soil & Tillage Research* **46**, 69–80.
- Le Roux, J., Newby, T. and Sumner, P.: 2007, Monitoring soil erosion in South Africa at a regional scale: review and recommendations, *South African Journal of Science* **103**(7-8), 329–335.
- Lederer, C. M., Shirley, V. S., Browne, W., Diairiki, J. M., Doeblner, R. E., Shihab Eldin, A. A., Jardine, L. J., Tuli, J. K. and Buyn, A. B.: 1978, *Table of Isotopes*, John Wiley & Sons, New York, p. 690.
- Ledermann, T., Herweg, K., Liniger, H., Schneider, F., Hurni, H. and Prasuhn, V.: 2008, Erosion damage mapping: Assessing current soil erosion damage in Switzerland, *Advances in Geoecology* **39**, 263–284.
- Lewis, D. T. and Lepele, M. J.: 1982, Quantification of soil loss and sediment produced from eroded land, *Soil Science Society of America Journal* **46**, 369–372.
- Libby, W. F.: 1946, Atmospheric helium-three and radiocarbon from cosmic radiation, *Physical Review* **69**, 671–672.
- Libby, W. F., Anderson, E. C. and Arnold, J. R.: 1949, Age determination by radiocarbon content – worldwide essay of natural radiocarbon, *Science* **109**, 227–228.
- Lifton, N. A.: 1997, *A New Extraction Technique and Production Rate Estimate for In Situ Cosmogenic ¹⁴C in Quartz*, PhD thesis, University of Arizona, Tucson.

- Lifton, N. A., Bieber, J. W., Clem, J. M., Duldig, M. L., Evenson, P., Humble, J. E. and Pyle, R.: 2005, Addressing solar modulation and long-term uncertainties in scaling secondary cosmic rays for in situ cosmogenic nuclide applications, *Earth and Planetary Science Letters* **239**(1-2), 140–161.
- Lifton, N. A., Jull, A. J. T. and Quade, J.: 2001, A new extraction technique and production rate estimate for in situ cosmogenic ^{14}C in quartz, *Geochimica et Cosmochimica Acta* **65**(12), 1953–1969.
- Lifton, N. A., Smart, D. F. and Shea, M. A.: 2008, Scaling time-integrated in situ cosmogenic nuclide production rates using a continuous geomagnetic model, *Earth and Planetary Science Letters* **268**, 190–201.
- Lingenfelter, R. E.: 1963, Production of ^{14}C by cosmic-ray neutrons, *Reviews of Geophysics* **1**, 35–55.
- Loughran, R. J.: 1989, The measurement of soil erosion, *Progress in Physical Geography* **13**, 216–233.
- Lowe, J. J.: 1991, *Radiocarbon dating: recent applications and future potential*, John Wiley & Sons, pp. 1–89.
- Lowell, T. V.: 2000, As climate changes, so do glaciers, *Proceedings of the National Academy of Sciences of the United States of America* **97**, 1351–1354.
- Lowell, T. V., Savage, K. M., Brockman, S. C. and Stuckenrath, R.: 1990, Radiocarbon analyses from Cincinnati, Ohio, and their implications for glacial stratigraphic interpretations, *Quaternary Research* **34**, 1–11.
- Ma, L., Chabaux, F., Pelt, E., Blaes, E., Jin, L. and Brantley, S.: 2010, Regolith production rates calculated with uranium-series isotopes at Susquehanna/Shale Hills Critical Zone Observatory, *Earth and Planetary Science Letters* **297**(1-2), 211–225.
- Maden, C., Anastasi, P., Dougans, D., Freeman, S., Kitchen, R. and Klody, G.: 2007, SUERC AMS ion detection, *Nuclear Instruments and Methods in Physics Research B* **259**(1), 131–139.
- Madsen, A. T., Murray, A. S., Andersen, T. J., Pejrup, M. and Breuning-Madsen, H.: 2005, Optically stimulated luminescence dating of young estuarine sediments: a comparison with ^{210}Pb and ^{137}Cs dating, *Marine Geology* **214**, 251–268.

- Martinez-Casanovas, J. A.: 2003, A spatial information technology approach for the mapping and quantification of gully erosion, *Catena* **50**, 293–308.
- Matisoff, G., Bonniwell, E. C. and Whiting, P. J.: 2002, Soil erosion and sediment sources in an Ohio Watershed using beryllium-7, cesium-137, and lead-210, *Journal of Environmental Quality* **31**, 54–61.
- Mattey, D. P., Exley, R. A. and Pillinger, C. T.: 1989, Isotopic composition of CO₂ and dissolved carbon species in basalt glass, *Geochimica et Cosmochimica Acta* **53**, 2377–2386.
- McCool, D. K., Dossett, M. G. and Yecha, S. J.: 1981, A portable rill meter for field measurement of soil loss, *International Association of Hydrological Science Publication* **133**, 479–484.
- McHargue, L. R. and Damon, P. E.: 1991, The global Beryllium 10 cycle, *Reviews of Geophysics* **29**(2), 141–158.
- McIntyre, K. L. and Howe, J. A.: 2010, *Scottish west coast fjords since the last glaciation: a review*, Vol. Special Publications 344, Geological Society, London.
- McKean, J. A., Dietrich, W. E., Finkel, R. C., Southon, J. R. and Caffee, M. W.: 1993, Quantification of soil production and downslope creep rates from cosmogenic ¹⁰Be accumulations on a hillslope profile, *Geology* **21**, 343–346.
- Merritt, W., Letcher, R. and Jakeman, A.: 2003, A review of erosion and sediment transport models, *Environmental Modelling and Software* **18**(8), 761–799.
- Merritts, D. and Walter, M. R.: 2003, Colonial millponds of Lancaster County, Pennsylvania as a major source of sediment pollution to the Susquehanna River and Chesapeake Bay, in D. Merritts, M. R. Walter and A. Dewitt (eds), *Channeling Through Time: Landscape evolution, land use change, and stream restoration in the lower Susquehanna Basin, SEFOP*, Guidebook, Franklin and Marshall College, Lancaster, pp. 56–65.
- Metternicht, G. I. and Zinck, J. A.: 1998, Evaluating the information content of JERS-1 SAR and Landsat TM data for discrimination of soil erosion features, *SPRS Journal of Photogrammetry and Remote Sensing* **53**(3), 143–153.

- Middleton, R., Brown, L., Dezfouly-Arjomandy, B. and Klein, J.: 1993, On ^{10}Be standards and the half-life of ^{10}Be , *Nuclear Instruments and Methods In Physics Research B* **82**, 399–403.
- Miguel, S., Bolívar, J. and García-Tenorio, R.: 2003, Mixing, sediment accumulation and focusing using ^{210}Pb and ^{137}Cs , *Journal of Paleolimnology* **29**(1), 1–11.
- Miller, E. K., Blum, J. D. and J., F. A.: 1993, Determination of soil exchangeable-cation loss and weathering rates using Sr isotopes, *Nature* **362**, 438–441.
- Miller, G., Briner, J., Lifton, N. A. and Finkel, R.: 2006, Limited ice-sheet erosion and complex in situ cosmogenic ^{10}Be , ^{26}Al , and ^{14}C on Baffin Island, Arctic Canada, *Quaternary Geochronology* **1**(1), 74–85.
- Molina, A., Govers, G., Poesen, J., Van Hemelryck, H., De Bièvre, B. and Vanacker, V.: 2008, Environmental factors controlling spatial variation in sediment yield in a central Andean mountain area, *Geomorphology* **98**, 176–186.
- Molnar, P. and England, P.: 1990, Late Cenozoic uplift of mountain ranges and global climate change: chicken or egg?, *Nature* **346**, 29–34.
- Montgomery, C. and Montgomery, D.: 1935, The variation with altitude of the production of bursts of cosmic-ray ionization, *Physical Review* **47**(6), 429–434.
- Montgomery, D. R.: 2007, Soil erosion and agricultural sustainability, *Proceedings of the National Academy of Sciences* **104**(33), 13268–13272.
- Morgan, D., Putkonen, J., Balco, G. and Stone, J. O.: 2010, Degradation of glacial deposits quantified with cosmogenic nuclides, Quartermain Mountains, Antarctica, *Earth Surface Processes and Landforms* **article in press**.
- Morgan, R. P. C.: 1985, Soil erosion measurement and soil conservation research in cultivated areas of the UK, *The Geographical Journal* **151**(1), 11–20.
- Morishige, K.: 2011, Adsorption and separation of CO_2/CH_4 on amorphous silica molecular sieve, *The Journal of Physical Chemistry C* **115**, 9713–9718.
- Naysmith, P.: 2007, *Extraction and measurement of cosmogenic in situ ^{14}C from quartz*, Master's thesis, University of Glasgow, Glasgow.

- Naysmith, P., Cook, G. T., Phillips, W., Lifton, N. A. and Anderson, R.: 2004, Preliminary results for the extraction and measurement of cosmogenic in situ ^{14}C from quartz, *Radiocarbon* **46**(1), 201–206.
- Nearing, M. A., Govers, G. and Norton, L. D.: 1999, Variability in soil erosion data from replicated plots, *Soil Science Society of America Journal* **63**, 1829–1835.
- Niedermann, S.: 2002, Cosmic-ray-produced noble gases in terrestrial rocks: Dating tools for surface processes, in D. P. Porcelli, C. J. Ballentine and R. Wieler (eds), *Noble Gases*, Vol. 47 of *Reviews in Mineralogy and Geochemistry*, The Mineralogical Society of America, pp. 731–784.
- Nishiizumi, K., Imamura, M., Caffee, M. V., Southon, J. R., Finkel, R. C. and McAninch, J.: 2007, Absolute calibration of ^{10}Be ams standards, *Nuclear Instruments & Methods In Physics Research Section B-Beam Interactions With Materials And Atoms* **258**(2), 403–413.
- Noel, H., Garbolino, E., Brauer, A., Lallier-Verges, E., de Beaulieu, J.-L. and J.-R., D.: 2001, Human impact and soil erosion during the last 5000 yrs as recorded in lacustrine sedimentary organic matter at Lac d’Annecy, the French Alps, *Journal of Paleolimnology* **25**(2), 229–244.
- Oguchi, T., Saito, K., Kadomura, H. and Grossman, M.: 2001, Fluvial geomorphology and paleohydrology in Japan, *Geomorphology* **39**(1-2), 3–19.
- Olley, J., Caitcheon, G. and Murray, A.: 1998, The dispersion of apparent dose as determined by optical stimulated luminescence in small aliquots of fluvial quartz: implications for dating young sediments, *Quaternary Science Reviews* **17**, 1033–1040.
- O’Neal, M. A.: 2006, The effects of slope degradation on lichenometric dating of Little Ice Age moraines, *Quaternary Geochronology* **1**, 121–128.
- Oostwoud Wijdenes, D. J. and Bryan, R.: 2001, Gully-head erosion processes on a semi-arid valley floor in Kenya: a case study into temporal variation and sediment budgeting, *Earth Surface Processes and Landforms* **26**(9), 911–933.
- Oviatt, C. G., Currey, D. R. and Sack, D.: 1992, Radiocarbon chronology of Lake Bonneville flood eastern Great Basin, USA, *Palaeogeography Palaeoclimate and Palaeoecology* **99**, 225–241.

- Owens, I. F.: 1969, Causes and rates of soil creep in the Chilton Valley, *Cass. Arctic and Alpine Research* **1**, 213–220.
- Owens, P. N., Walling, D. E. and Leeks, G. J. L.: 1999, Use of floodplain sediment cores to investigate recent historical changes in overbank sedimentation rates and sediment sources in the catchment of the River Ouse, Yorkshire, UK, *Catena* **36**, 21–47.
- Owens, P. and Slaymaker, O.: 1993, Lacustrine sediment budgets in the coast mountains of British Columbia, Canada, in J. McManus and R. W. Duck (eds), *Geomorphology and Sedimentology of Lakes and Reservoirs*, Wiley, New York, pp. 105–123.
- Page, M. J. and Trustrum, N. A.: 1997, A late holocene lake sediment record of the erosion response to land use change in a steep-land catchment, New Zealand, *Zeitschrift für Geomorphologie* **41**(3).
- Pain, C. F.: 1968, Geomorphic effects of floods in the Orere River catchment, eastern Hunua Ranges, *New Zealand Journal of Hydrology* **7**, 62–74.
- Palmer, A. P., Rose, J., Lowe, J. and Macleod, A.: 2010, Annually resolved events of Younger Dryas glaciation in Lochaber (Glen Roy and Glen Spean), Western Scottish Highlands, *Journal of Quaternary Science* **25**(4), 581–596.
- Paroissien, J. B., Lagacherie, P. and Le Bissonnais, Y.: 2010, A regional-scale study of multi-decennial erosion of vineyard fields using vine-stock unearthing–burying measurements, *Catena* **82**(3), 159–168.
- Parsons, A. J., Wainwright, J., Brazier, R. E. and Powell, D. M.: 2006, Is sediment delivery a fallacy?, *Earth Surface Processes and Landforms* **31**(10), 1325–1328.
- Parsons, A. J., Wainwright, J., Powell, D. M., Kaduk, J. and Brazier, R. E.: 2004, A conceptual model for understanding and predicting erosion by water, *Earth Surface Processes and Landforms* **29**(10), 1293–1302.
- Paul, D. and Skrzypek, G.: 2006, Flushing time and storage effects on the accuracy and precision of carbon and oxygen isotope ratios of sample using the Gasbench II technique, *Rapid Communications in Mass Spectrometry* **20**, 2033–2040.
- Peeters, I., Rommens, T., Verstraeten, G., Govers, G., Rompaey, V., A. Poesen, J. and Van Oost, K.: 2006, Reconstructing ancient topography through erosion modeling, *Geomorphology* **78**, 250–264.

- Pelletier, J. D.: 2008, *Quantitative modeling of earth surface processes*, Cambridge University Press.
- Perg, L. A., Anderson, R. S. and Finkel, R. C.: 2001, Use of a new ^{10}Be and ^{26}Al inventory method to date marine terraces, Santa Cruz, California, USA, *Geology* **29**, 879–882.
- Perroy, R. L., Bookhagen, B., Asner, G. P. and Chadwick, O. A.: 2010, Comparison of gully erosion estimates using airborne and ground-based LiDAR on Sant Cruse Island, California, *Geomorphology* **118**, 288–300.
- Petit, D.: 1974, ^{210}Pb et isotopes stables du plomb dans des sediments lacustres, *Earth and Planetary Science Letters* **23**, 199–205.
- Phillips, E. R., Evans, D. J. A. and Auton, C. A.: 2002, Polyphase deformation at an oscillating ice margin following the Loch Lomond Readvance, central Scotland, UK, *Sedimentary Geology* **149**, 157–182.
- Phillips, F. M.: 2000, Muogenic nuclides: a method for dating rapidly eroding landforms, *Geochimica et Cosmochimica Acta* **66**, S1–A599.
- Phillips, F. M., Zreda, M. G., Smith, S. S., Elmore, D., Kubik, P. W. and Sharma, P.: 1990, Cosmogenic chlorine-36 chronology for glacial deposits at Bloody Canyon, eastern Sierra Nevada, *Science* **248**, 1529–1532.
- Phillips, W. M., McDonald, S. L., Reneau, S. L. and Poths, J.: 1998, Dating soils and alluvium with cosmogenic ^{21}Ne depth profiles: case studies from the Pajarito Plateau, New Mexico, USA, *Earth and Planetary Science Letters* **160**(1-2), 209–223.
- Pickup, G. and Marks, A.: 2000, Identifying large-scale erosion and deposition processes from airborne gamma radiometrics and digital elevation models in a weathered landscape, *Earth Surface Processes and Landforms* **25**, 535–557.
- Pidgeon, R. T., Brander, T. and Lippolt, H. J.: 2004, Miocene (U–Th)/He ages of ferrous nodules from lateritic duricrust, Darling Range, Western Australia, *Australian Journal of Earth Sciences* **51**, 901–909.
- Pigati, J. S.: 2004, *Experimental developments and application of ^{14}C and in situ cosmogenic nuclide dating techniques*, PhD thesis, University of Arizona, Tucson.

- Pigati, J. S., Lifton, N. A., Jull, A. J. T. and Quade, J.: 2010a, Extraction of in situ cosmogenic ^{14}C from olivine, *Radiocarbon* **52**(2-3), 1244–1260.
- Pigati, J. S., Lifton, N. A., Jull, A. J. T. and Quade, J.: 2010b, A simplified in situ cosmogenic ^{14}C extraction system, *Radiocarbon* **52**(2-3), 1236–1243.
- Pimentel, D., Harvey, C., Resosudarmo, P., Sinclair, K., Kurz, D., McNair, M., Crist, S., Shpritz, L., Fitton, L., Saffouri, R. and Blair, R.: 1995, Environmental and economic costs of soil erosion and conservation benefits, *Science* **267**(5201), 1117–1123.
- Pineau, F. and Javoy, M.: 1994, Strong degassing at ridge crests: The behaviour of dissolved carbon and water in basalt glasses at 14°N, Mid-Atlantic Ridge, *Earth and Planetary Science Letters (ISSN 0012-82)* **123**, 179–198.
- Prosser, I. P., Hughes, A. O. and Rutherford, I. D.: 2000, Bank erosion of an incised upland channel by subaerial processes: Tasmania, Australia, *Earth Surface Processes and Landforms* **25**(10), 1085–1101.
- Prosser, I. P. and Rustomji, P.: 2000, Sediment transport capacity relations for overland flow, *Progress in Physical Geography* **24**, 179–193.
- Putkonen, J. K., Connolly, J. and Orloff, T.: 2007, Landscape evolution degrades the geologic signature of past glaciations, *Geomorphology* **97**, 208–217.
- R Development Core Team: 2011, *R: A Language and Environment for Statistical Computing*, R Foundation for Statistical Computing, Vienna, Austria. ISBN 3-900051-07-0.
URL: <http://www.R-project.org>
- Rabenhorst, M. C. and Wilding, L. P.: 1986, Pedogenesis on the Edwards Plateau, Texas: I. Nature and continuity of parent material, *Soil Science Society of America Journal* **50**, 678–687.
- Reedy, R. C. and Arnold, J. R.: 1972, Interaction of solar and galactic cosmic-ray particles with the moon, *Journal of Geophysical Research* **77**, 537–555.
- Reimer, P. J., Baillie, M. G. L., Bard, E., Bayliss, A., Beck, J. W., Blackwell, P. G., Bronk Ramsey, C., Buck, C. E., Burr, G. S., Edwards, R. L., Friedrich, M., Grootes, P. M., Guilderson, T. P., Hajdas, I., Heaton, T. J., Hogg, A. G., Hughen, K. A., Kaiser, K. F., Kromer, B., McCormac, F. G., Manning, S. W., Reimer, R. W., Richards, D. A.,

- Southon, J. R., Talamo, S., Turney, C. S. M. and van der Plicht, J.: 2009, IntCal09 and Marine09 Radiocarbon Age Calibration Curves, 0–50,000 Years cal BP, *Radiocarbon* **51**(4), 1111–1150.
- Repka, J. L., Anderson, R. S. and Finkel, R. C.: 1997, Cosmogenic dating of fluvial terraces, Fremont River, Utah, *Earth and Planetary Science Letters* **152**, 59–73.
- Rice, C., Wilson, B. N. and Appleman, M.: 1988, Soil topography measurements using image processing techniques, *Computers and Electronics in Agriculture* **3**(2), 97–107.
- Riebe, C. S., Kirchner, J. W. and Finkel, R. C.: 2003, Long-term rates of chemical weathering and physical erosion from cosmogenic nuclides and geochemical mass balance, *Geochimica et Cosmochimica Acta* **67**(22), 4411–4427.
- Ritchie, C. J. and McHenry, R. J.: 1990, Application of radioactive fallout cesium-137 for measuring soil erosion and sediment accumulation rates and patterns: A review, *Journal of Environmental Quality* **19**, 215–233.
- Robbins, J. A., Krezoski, J. and Mosley, S. C.: 1977, Radioactivity in sediments of the Great Lakes: Post-depositional redistribution by deposit feeding organisms, *Earth and Planetary Science Letters* **36**, 325–333.
- Rodés, A., Pallás, R., Braucher, R., Moreno, X., Masana, E. and Bourlès, D. L.: 2011, Effect of density uncertainties in cosmogenic ^{10}Be depth-profiles: Dating a cemented Pleistocene alluvial fan (Carboneras Fault, SE Iberia), *Quaternary Geochronology* **6**, 186–194.
- Rommens, T., Verstraeten, G., Lang, A., Poesen, J., Govers, G., van Rompaey, A. and Peeters, I.: 2005, Soil erosion and sediment deposition in the Belgian loess belt during the Holocene: establishing a sediment budget for a small agricultural catchment, *The Holocene* **15**(7), 1032–1043.
- Roose, E. and Barthés, B.: 2001, Organic matter management for soil conservation and productivity restoration in Africa: a contribution from Francophone research, *Nutrient Cycling in Agroecosystems* **61**, 159–170.
- Rose, J., Lowe, J. J. and Switsur, R.: 1989, A radiocarbon date on plant detritus beneath till from the type area of the Loch Lomond Readvance, *Scottish Journal of Geology* **24**, 113–124.

- Rosso, K. M. and Bodnar, R. J.: 1995, Microthermometric and Raman spectroscopic detection limits of CO₂ in fluid inclusions and the Raman spectroscopic characterization of CO₂, *Geochimica et Cosmochimica Acta* **59**(19), 3961–3975.
- Saha, S. K.: 2004, Water and wind induced soil erosion assessment and monitoring using Remote Sensing and GIS, *in* M. V. K. Sivakumar, P. S. Roy, K. Harsen and S. K. Saha (eds), *Satellite Remote Sensing and GIS Applications in Agricultural Meteorology*, World Meteorological Organization (WMO), pp. 315–330.
- Schaller, M., Blum, J. D. and Ehlers, T. A.: 2009, Combining cosmogenic nuclides and major elements from moraine soil profiles to improve weathering rate estimates, *Geomorphology* **106**(3-4), 198–205.
- Schaller, M., Ehlers, T. A. and Blum, J. D.: 2010, Soil transport on a moraine foreslope, *Geomorphology* **115**(1-2), 117–128.
- Schaller, M., von Blanckenburg, F., Hovius, N., Veldkamp, A., van de Berg, M. W. and Kubik, P. W.: 2004, Paleoerosion rates from cosmogenic ¹⁰Be in a 1.3 Ma terrace sequence: Response of the River Muse to changes in climate and rock uplift, *The Journal of Geology* **112**, 127–144.
- Schaller, M., von Blanckenburg, F., Veit, H. and Kubik, P. W.: 2003, Influence of periglacial cover beds on in-situ produced cosmogenic ¹⁰Be in soil sections, *Geomorphology* **49**, 255–267.
- Schmugge, T. J., Kustas, W. P., Ritchie, J. C., Jackson, T. J. and Rango, A.: 2002, Remote sensing in hydrology, *Advances in Water Resources* **25**, 1367–1385.
- Schnabel, C., Reinhardt, L., Barrows, T. T., Bishop, P., Davidson, A., Fifield, L. K., Freeman, S., Kim, J. Y., Maden, C. and Xu, S.: 2007, Inter-comparison in ¹⁰Be analysis starting from pre-purified quartz, *Nuclear Instruments and Methods B* **259**, 571–575.
- Schoenbohm, L., Kurz, M., Ackert, R., Brook, E. and Brown, E. T.: 2004, Erosion history from cosmogenic ³He, ²¹Ne, ¹⁰Be and ²⁶Al depth profiles: Dry Valleys, Antarctica, *in* E. G. Assembly (ed.), *Geophysical Research Abstracts*, Vol. 6, p. EGU01062.
- Schuller, P., Iroume, A., Walling, D. E., Mancilla, H. B., Castillo, A. and Trumper, R. E.: 2006, Use of beryllium-7 to document soil redistribution following forest harvest operations, *Journal of Environmental Quality* **35**(5), 1756–1763.

- Schuller, P., Walling, D. E., Iroume, A. and Castillo, A.: 2010, Use of beryllium-7 to study the effectiveness of woody trash barriers in reducing sediment delivery to streams after forest clearcutting, *Soil & Tillage Research* **110**, 143–153.
- Scott, E. M.: 2003, The Fourth International Radiocarbon Intercomparison (FIRI), *Radiocarbon* **45**, 135–291.
- Sekhar, K. R. and Rao, B. V.: 2002, Evaluation of sediment yield by using remote sensing and GIS: a case study from the Phulling Vagu watershed, Nizamabad District (AP), India, *International Journal of Remote Sensing* **23**(20), 4499–4509.
- Sepulveda, A., Schuller, P., Walling, D. E. and Castillo, A.: 2008, Use of ^7Be to document soil erosion associated with a short period of extreme rainfall, *Journal of Environmental Radioactivity* **99**(1), 35–49.
- Shakesby, R.: 1993, The soil erosion bridge: a device for micro-profiling soil surfaces, *Earth Surface Processes and Landforms* **18**(9), 823–827.
- Short, S. A., Lowson, R. T., Ellis, J. and Price, D. M.: 1989, Thorium-uranium disequilibrium dating of the Late Quaternary ferruginous concretions and rinds, *Geochimica et Cosmochimica Acta* **53**, 1379–1389.
- Shuster, D. L., Vasconcelos, P. M., Heim, J. A. and Farley, K. A.: 2005, Weathering geochronology by (U–Th)/He dating of goethite, *Earth and Planetary Science Letters* **69**, 659–673.
- Siame, L., Bellier, O., Braucher, R., Sebrier, M., Cushing, M., Bourlès, D. L., Hamelin, B., Baroux, E., de Voogd, B., Raisbeck, G. and Yiou, F.: 2004, Local erosion rates versus active tectonics: cosmic ray exposure modelling in Provence (South-East France), *Earth and Planetary Science Letters* **220**(3–4), 345–364.
- Sissons, J. B.: 1967, Glacial stages and radiocarbon dates in Scotland, *Scottish Journal of Geology III*, Vol. 3, Geological Societies of Edinburgh and Glasgow, Oliver & Boyd LTD, pp. 375–381.
- Sissons, J. B.: 1979, The Loch Lomond Stadial in the British Isles, *Nature* **280**, 199–203.
- Six, J., Elliott, E. T. and Paustian, K.: 2000, Soil macroaggregate turnover and microaggregate formation: a mechanism for C sequestration under no-tillage agriculture, *Soil Biology & Biochemistry* **32**, 2099–2103.

- Slota, P. J. J., Jull, A. J. T., Linick, T. W. and Toolin, L. J.: 1987, Preparation of small samples for ^{14}C accelerator targets by catalytic reduction of CO, *Radiocarbon* **29**(2), 303–306.
- Small, E. E., Anderson, R. S. and Hancock, G. S.: 1999, Estimates of the rates of regolith production using ^{10}Be and ^{26}Al from an alpine hillslope, *Geomorphology* **27**(1-2), 131–150.
- Smith, A. M., Levchenko, V. A., Etheridge, D. M., Lowe, D. C., Hua, Q., Trudinger, C., Zoppi, U. and Elcheikh, A.: 2000, In search of in-situ radiocarbon in Law Dome ice and firn, *Nuclear Instruments and Methods in Physics Research B* **172**(1), 610–622.
- Smith, H. and Dragovich, D.: 2008, Improving precision in sediment source and erosion process distinction in an upland catchment, south-eastern Australia, *Catena* **72**(1), 191–203.
- Smout, T. C. and Fenton, A.: 1965, Scottish Agriculture before the improvers-an Exploration, *Agricultural History Review* **13**, 73–93.
- Staiger, J. K. W., Gosse, J. C., Johnson, J. V., Fastook, J., Gray, J. T., Stockli, D. F., Stockli, L. and Finkel, R. C.: 2005, Quaternary relief generation by polythermal glacier ice, *Earth Surface Processes and Landforms* **30**, 1145–1159.
- Staiger, J. K. W., Gosse, J., Little, E. C., Utting, D. J., Finkel, R., Johnson, J. V. and Fastook, J.: 2006, Glacial erosion and sediment dispersion from detrital cosmogenic nuclide analyses of till, *Quaternary Geochronology* **1**, 29–42.
- Starkel, L.: 1976, The role of extreme (catastrophic) meteorological events in contemporary evolution of slopes, in E. Derbyshire (ed.), *Geomorphology and Climate*, Wiley, Chichester, pp. 203–237.
- Stewart, B. W., Capo, R. C. and Chadwick, O. A.: 2001, Effects of rainfall on weathering rate, base cation provenance, and Sr isotope composition of Hawaiian soils, *Geochimica et Cosmochimica Acta* **65**, 1087–1099.
- Stokes, S., Bray, H. E. and Blum, M. D.: 2001, Optical resetting in large drainage basins: Tests of zeroing assumptions using single-aliquot procedures, *Quaternary Science Reviews* **20**, 879–886.

- Stone, C. O. and Ballantyne, J. K.: 2006, Dimensions and deglacial chronology of the Outer Hebrides Ice Cap, Northwest Scotland: implications of cosmic ray exposure dating, *Journal of Quaternary Science* **21**(1), 75–84.
- Stone, J. O.: 2000, Air pressure and cosmogenic isotope production, *Journal of Geophysical Research* **105**, 23753–23760.
- Stone, J. O., Ballantyne, C. K. and Fifield, L. K.: 1998, Exposure dating and validation of periglacial weathering limits, northwest Scotland, *Geology* **26**, 587–590.
- Strack, E., Heisinger, B., Dockhorn, B., Hartmann, F. J., Korschinek, G., Nolte, E., Morteani, G., Petitjean, C. and Neumaier, S.: 1994, Determination of erosion rates with cosmogenic ^{26}Al , *Nuclear Instruments and Methods in Physics Research Section B: Beam Interactions with Materials and Atoms* **92**, 317–320.
- Stroeven, A. P., Fabel, D., Hattestrand, C. and Harbor, J.: 2002, A relict landscape in the centre of the Fennoscandian glaciation: cosmogenic radionuclide evidence of tors preserved through multiple glacial cycles, *Geomorphology* **44**, 145–154.
- Stroosnijder, L.: 2005, Measurement of erosion: is it possible?, *Catena* **62**(2-3), 162–173.
- Stuart, F. M., Harrop, P. J., Knott, S. and Turner, G.: 1999, Laser extraction of helium isotopes from Antarctic micrometeorites: Source of He and implications for the flux of extraterrestrial ^3He to earth, *Geochimica et Cosmochimica Acta* **63**(17), 2653–2665.
- Suess, H. E. and Wänke, H.: 1962, Radiocarbon content and terrestrial age of twelve stony meteorites and one iron meteorite, *Geochimica et Cosmochimica Acta* **26**, 475–480.
- Sylvester, P. (ed.): 2001, *Laser-Ablation-ICPMS in the Earth Sciences: Principles and Applications*, Vol. 29, Mineralogy Association of Canada Short Course Series, Ottawa, Canada.
- Takken, I., Beuselinck, L., Nachtergaele, J., Govers, G., Poesen, J. and Degraer, G.: 1999, Spatial evaluation of a physically based distributed erosion model (LISEM), *Catena* **37**, 431–447.
- Thorne, C.: 1981, Field measurements of rates of bank erosion and bank material strength, *Erosion and Sediment Transport Measurement*, Vol. 133, IAHS, pp. 503–512.

- Thorp, P. W.: 1991, Surface profiles and basal shear stresses of outlet glaciers from a Late-glacial mountain ice field in western Scotland, *Journal of Glaciology* **37**(125), 77–88.
- Toy, T. J.: 1983, A linear erosion/elevation measuring instrument (LEMI), *Earth Surface Processes And Landforms* **8**, 313–322.
- Trimble, S. W. and Crosson, P.: 2000, Land use - US soil erosion rates - myth and reality, *Science* **289**(5477), 248–250.
- Trull, T. W., Brown, E. T., Marty, B., Raisbeck, G. M. and Yiou, F.: 1995, Cosmogenic ^{10}Be and ^3He accumulation in Pleistocene beach terraces in Death Valley, California, USA. Implications for cosmic-ray exposure dating of young surfaces in hot climates, *Chemical Geology* **119**, 191–207.
- Trumbore, S. E.: 1993, Comparison of carbon dynamics in tropical and temperate soils using radiocarbon measurements, *Global Biogeochemical Cycles* **7**(2), 275–290.
- Tucker, G. E. and Hancock, G. R.: 2010, Modelling landscape evolution, *Earth Surface Processes And Landforms* **35**, 28–50.
- Van de Wal, R. S. W., Meijer, H. A. J., De Rooij, M. and Van der Veen, C.: 2007, Radiocarbon analyses along the EDML ice core in Antarctica, *Tellus Series B-Chemical And Physical Meteorology* **59**(1), 157–165.
- Van den Kerkhof, A. M. and Hein, U. F.: 2001, Fluid inclusions petrography, *Lithos* **55**, 27–47.
- Van Der Kemp, W. J. M., Alderliesten, C., Van Der Borg, K., Holmlund, P., De Jong, A. F. M., Karlöf, L., Lamers, R. A. N., Oerlemans, J., Thomassen, M. and Van de Wal, R. S. W.: 2000, Very little in situ produced radiocarbon retained in accumulating Antarctic ice, *Nuclear Instruments and Methods in Physics Research B: Beam Interactions with Materials and Atoms* **172**(1-4), 632–636.
- Van Lynden, G. W. J. and Mantel, S.: 2001, The role of GIS and remote sensing in land degradation assessment and conservation mapping: some user experiences and expectations, *International Journal of Applied Earth Observation and Geoinformation* **3**(1), 61–68.

- Van Oost, K., Cerdan, O. and Quine, T. A.: 2009, Accelerated sediment fluxes by water and tillage erosion on European agricultural land, *Earth Surface Processes And Landforms* **34**, 1625–1634.
- Van Rompaey, A. J. J., Verstraeten, G., Van Oost, K., Govers, G. and Poesen, J.: 2001, Modelling mean annual sediment yield using a distributed approach, *Earth Surface Processes And Landforms* **26**(11), 1221–1236.
- Van Rompaey, A. J. J., Vieillefont, V., Jones, R. J. A., Montanarella, L., Verstraeten, G., P., B., Dostal, T., Krasa, J., de Vente, J. and Poesen, J.: 2003, Validation of soil erosion estimates at European scale, *Technical Report No.13, EUR 20827 EN*, Office for Official Publications of the European Communities 26 pp, Luxembourg.
- Vanacker, V., Molina, A., Govers, G., Poesen, J., Dercon, G. and Deckers, S.: 2005, River channel response to short-term human-induced change in landscape connectivity in Andean ecosystems, *Geomorphology* **72**, 340–353.
- Vandekerckhove, L., Muys, B., Poesen, J., de Weerd, B. and Coppe, N.: 2001, A method for dendrochronological assessment of medium-term gully erosion rates, *Catena* **45**, 123–161.
- Vandeputte, K., Moens, L. and Dams, R.: 1996, Improved sealed-tube combustion of organic samples to CO₂ for stable isotope analysis, radiocarbon dating and percent carbon determinations, *Analytical Letters* **29**(15), 2761–2773.
- Vasconcelos, P. M.: 1999, K-Ar and ⁴⁰Ar/³⁹Ar geochronology of weathering processes, *Annual Review of Earth and Planetary Sciences* **27**, 183–229.
- Vassallo, R., Ritz, J. F., Braucher, R. and Carretier, S.: 2005, Dating faulted alluvial fans with cosmogenic ¹⁰Be in the Gurvan Bogd mountain range (Gobi-Altay, Mongolia): climatic and tectonic implications, *Terra Nova* **17**(3), 278–285.
- Verstraeten, G. and Poesen, J.: 2002, Using sediment deposits in small ponds to quantify sediment yield from small catchments: possibilities and limitations, *Earth Surface Processes and Landforms, Special Issue: Linking Sediment Delivery from Hillslope to Catchment Scale* **27**(13), 1425–1439.
- von Blanckenburg, F.: 2005, The control mechanisms of erosion and weathering at basin

- scale from cosmogenic nuclides in river sediment, *Earth and Planetary Science Letters* **237**, 462–479.
- Vrieling, A.: 2006, Satellite remote sensing for water erosion assessment: A review, *Catena* **1**, 2–18.
- Wainwright, J., Parsons, A. J., Michaelides, K., Powell, D. M. and Brazier, R. E.: 2003, Linking short-and long-term soil-erosion modelling, in A. Lang (ed.), *Modelling approaches for the Rhein LUCIFS research framework*, Springer Verlag, Berlin.
- Walker, M. J. C.: 1995, Climatic changes in Europe during the Last Glacial/Interglacial transition, *Quaternary International* **28**, 63–76.
- Wallbrink, P. J. and Murray, A. S.: 1994, Fallout of ^7Be in south eastern Australia, *Journal of Environmental Radioactivity* **25**(3), 213–228.
- Wallbrink, P. J. and Murray, A. S.: 1996, Distribution and variability of ^7Be in soils under different surface cover conditions and its potential for describing soil redistribution processes, *Water Resources Research* **32**, 467–476.
- Walling, D. E., Collins, A. L. and Sickingabula, H. M.: 2003, Using unsupported lead-210 measurements to investigate soil erosion and sediment delivery in a small Zambian catchment, *Geomorphology* **52**, 193–213.
- Walling, D. E. and He, Q.: 1999, Using fallout lead-210 measurements to estimate soil erosion on cultivated land, *Soil Science Society of America Journal* **63**(5), 1404–1412.
- Walling, D. E., He, Q. and Blake, W.: 1999, Use of ^7Be and ^{137}Cs measurements to document short- and medium-term rates of water-induced soil erosion on agricultural land, *Water Resources Research* **35**, 3865–3874.
- Walling, D. E. and Quine, T. A.: 1995, The use of fallout radionuclide measurements in soil erosion investigations: Nuclear techniques in soil-plant studies for sustainable agriculture and environmental preservation, *International Atomic Energy Agency IAEA-SM-334/35*, 597–619.
- Walling, D. E. and Webb, W. B.: 1987, Material transport by the world's rivers: evolving perspectives, in J. C. Rodda and N. C. Matalas (eds), *Water for the future: Hydrology in perspective (Proceedings of the Rome Symposium)*, Vol. 164, IAHS, pp. 313–329.

- Wang, H., Huo, Y., Zeng, L., Wu, X. and Cai, Y.: 2008, 42-yr soil erosion record inferred from mineral magnetism of reservoir sediments in a small carbonate-rock catchment Guizhou Plateau, southwest China, *Journal of Paleolimnology* **40**(3), 897–921.
- Watson, E. B., Sneeringer, M. A. and Ross, A.: 1982, Diffusion of dissolved carbonate in magmas: experimental results and applications, *Earth and Planetary Science Letters* **61**(2), 346–358.
- Wells, S. G., Mcfadden, L. D. and Dohrenwend, J. C.: 1987, Influence of Late Quaternary climatic changes on geomorphic and pedogenic processes on a desert piedmont, Eastern Mojave Desert, California, *Quaternary Research* **27**, 130–146.
- White, D., Fülöp, R.-H., Bishop, P., Mackintosh, A. and Gordon, T. C.: 2011, Can in-situ cosmogenic ^{14}C be used to assess the influence of clast recycling on exposure dating of ice retreat in Antarctica?, *Quaternary Geochronology* **6**, 289–294.
- Whiting, M. L., De Gloria, S. D., Benson, A. S. and Wall, S. L.: 1987, Estimating conservation tillage residue using aerial photography, *Journal of Soil and Water Conservation* **2**, 130–132.
- Wicherek, S. P. and Bernard, C.: 1995, Assessment of soil movements in a watershed from Cs-137 data and conventional measurements (example: the Parisian Basin), *Catena* **25**, 141–151.
- Wilkinson, B. H. and McElroy, B. J.: 2007, The impact of humans on continental erosion and sedimentation, *Geological Society of America Bulletin* **119**, 140–156.
- Wilkinson, M. T. and Humphreys, G. S.: 2005, Exploring pedogenesis via nuclide-based soil production rates and OSL-based bioturbation rates, *Australian Journal of Soil Research* **43**(6), 767–779.
- Wilkinson, S. N., Prosser, I. P., Rustomjid, P. and Read, A. M.: 2009, Modelling and testing spatially distributed sediment budgets to relate erosion processes to sediment yields, *Environmental Modelling and Software* **24**, 489–501.
- Willenbring, J. K. and von Blanckenburg, F.: 2010a, Long-term stability of global erosion rates and weathering during late-Cenozoic cooling, *Nature* **465**, 211–214.

- Willenbring, J. K. and von Blanckenburg, F.: 2010b, Meteoric cosmogenic Beryllium-10 adsorbed to river sediment and soil: Applications for Earth-surface dynamics, *Earth Science Reviews* **98**(1-2), 105–122.
- Willgoose, G. R.: 2005, Mathematical modelling of whole landscape evolution, *Annual Review of Earth and Planetary Sciences* **33**, 443–459.
- Wilson, P., Bentley, M. J., Schnabel, C., Clark, R. and Xu, S.: 2008, Stone run (block stream) formation in the Falkland islands over several cold stages, deduced from cosmogenic isotope (^{10}Be and ^{26}Al) surface exposure dating, *Journal of Quaternary Science* **23**(5), 461–473.
- Woodborne, S. and Vogel, J. C.: 1997, Luminescence dating at Rose Cottage Cave: a progress report, *South African Journal of Science* **93**, 476–478.
- Wright, I. P., Sims, M. R. and Pillinger, C. T.: 2003, Scientific objectives of the Beagle 2 lander, *Acta Astronautica* **52**, 219–225.
- Xiaojun, N., Xiaodan, W., Suzhen, L., Shixian, G. and Haijun, L.: 2010, ^{137}Cs tracing dynamics of soil erosion, organic carbon and nitrogen in sloping farmland converted from original grassland in Tibetan plateau, *Applied Radiation and Isotopes* **68**, 1650–1655.
- Xu, S., Anderson, R., Bryant, C., Cook, G. T., Dougans, A., Freeman, S. P. H. T., Naysmith, P., Schnabel, C. and Scott, E. M.: 2004, Capabilities of the new SUERC 5MV AMS Facility for ^{14}C dating, *Radiocarbon* **46**, 51–58.
- Yasunaria, T. J., Stohl, A., Hayano, R. S., Burkhart, J. F., Eckhardt, S. and Yasunari, T.: 2011, Cesium-137 deposition and contamination of Japanese soils due to the Fukushima nuclear accident, *PNAS* **108**(49), 19530–19534.
- Yiou, F. and Raisbeck, G. M.: 1972, Half-life of ^{10}Be , *Physical Review Letters* **29**, 372–375.
- Yokoyama, Y., Caffee, M. W., Southon, J. R. and Nishiizumi, K.: 2004, Measurements of in situ produced ^{14}C in terrestrial rocks, *Nuclear Instruments and Methods in Physics Research B* **223-224**, 253–258.
- You, C.-F., Lee, T. and Li, Y.-H.: 1989, The partition of ^7Be between soil and water, *Chemical Geology* **77**, 105–118.

- Zapata, F.: 2003, The use of environmental radionuclides as tracers in soil erosion and sedimentation investigations: recent advances and future developments, *Soil & Tillage Research* **69**, 3–13.
- Zhang, K. L., Shu, A. P., Xu, X. L., Yang, Q. K. and Yu, B.: 2008, Soil erodibility and its estimation for agricultural soils in China, *Journal of Arid Environments* **72**, 1002–1011.
- Zhang, L., O'Neill, A. L. and Lacey, S.: 1996, Modelling approaches to the prediction of soil erosion in catchments, *Environmental Software* **11**(1-3), 123–133.
- Zhang, Y., Degroote, J., Wolter, C. and Sugumaran, R.: 2009, Integration of modified universal soil loss equation (MUSLE) into a GIS framework to assess soil erosion risk, *Land Degradation and Development* **20**, 84–91.

DUCT TAPE IS LIKE THE FORCE. IT HAS A LIGHT SIDE, AND A DARK SIDE, AND IT
HOLDS THE UNIVERSE TOGETHER

[Carl Zwanzig]

Appendix A

In situ ^{14}C data reduction and details of the SUERC ^{14}C extraction system

A.1 Calculation

All *in situ* ^{14}C AMS data were reduced following the calculations presented in Lifton (1997). These calculations are presented below. The AMS laboratory at SUERC has supplied a $^{14}\text{C}/^{13}\text{C}$ ratio for each sample in several batches between December 2007 and May 2010. The $^{14}\text{C}/^{13}\text{C}$ ratios are needed in order to correct for the graphitization background and the carbon isotope fractionation occurring during sample extraction.

A ‘fractionation factor’ is applied to correct the $^{13}\text{C}/^{12}\text{C}$ AMS ratios for isotopic fractionation. The ^{14}C activity of all the samples is normalised relative to a $^{13}\text{C}/^{12}\text{C}$ ratio of -25‰, corresponding to the theoretical ratio for 1890 wood. This is done by also measuring the $^{13}\text{C}/^{12}\text{C}$ ratio in the samples. The $^{13}\text{C}/^{12}\text{C}$ stable isotope ratio is reported in the $\delta^{13}\text{C}$ notation relative to V-PDB, where V-PDB is a Cretaceous belemnite from the Peedee formation in South Carolina and is the primary standard for $\delta^{13}\text{C}$ determinations. The ‘fractionation factor’ is calculated using the following equation:

$$FF = \frac{975}{1000 + \delta^{13}\text{C}} \quad (\text{A.1})$$

where FF is the ‘fractionation factor’ used to correct measured ratios for isotopic fractionation and $\delta^{13}\text{C}$ is the on-line $^{13}\text{C}/^{12}\text{C}$ of the sample measured in the AMS.

The uncertainty of FF is calculated using:

$$\sigma FF = FF \sqrt{\left(\frac{\sigma \delta^{13}\text{C}}{1000 + \delta^{13}\text{C}} \right)^2} \quad (\text{A.2})$$

The ‘measured fraction modern’ is calculated using the equation below, with fractionation corrections being applied to both the sample and oxalic acid standard:

$$FM = \frac{^{14}\text{C}/^{13}\text{C}_s \times FF}{0.7459 \times ^{14}\text{C}/^{13}\text{C}_{Oxi} \times FF_{Oxi}} \quad (\text{A.3})$$

where FM is the ‘measured fractionation modern’, $^{14}\text{C}/^{13}\text{C}_s$ is the measured ratio of the sample, and $^{14}\text{C}/^{13}\text{C}_{Oxi}$ is the measured ratio of the oxalic acid standard included in every AMS batch.

The uncertainty of the ‘measured fraction modern’ is calculated using the following:

$$\sigma FM = FM \sqrt{\left(\frac{\sigma^{14}\text{C}/^{13}\text{C}_s}{^{14}\text{C}/^{13}\text{C}_s}\right)^2 + \left(\frac{\sigma FF_s}{FF_s}\right)^2 + \left(\frac{\sigma^{14}\text{C}/^{13}\text{C}_{Oxii}}{^{14}\text{C}/^{13}\text{C}_{Oxii}}\right)^2 + \left(\frac{\sigma FF_{Oxii}}{FF_{Oxii}}\right)^2} \quad (\text{A.4})$$

Every batch of samples that was run on the accelerator includes a number of background samples prepared in the purification and graphitization part of the *in situ* ^{14}C extraction system (Figure 2.1). The Icelandic doublespar (DBP) sample (as background sample) is put through the same graphitization procedures as the unknown samples to try and quantify how much contamination is added to the sample during the graphitization (Donahue et al. 1990) illustrated on A.1. To calculate the ‘measured fraction modern of a background sample’ F , all the background samples are grouped together and used to calculate an apparent fraction modern of the background, by using the average of the measured $^{14}\text{C}/^{13}\text{C}$ ratios of all the DBPs in a batch, and the associated 1σ uncertainties.

F is calculated using the following:

$$F = FM_s \times (1 + FM_{DBP}) - FM_{DBP} \quad (\text{A.5})$$

and the corresponding 1σ uncertainty is calculated using the following:

$$\sigma F = \sigma FM_s + \sigma FM_{DBP} + FM_s \times FM_{DBP} \sqrt{\left(\frac{\sigma FM_s}{FM_s}\right)^2 + \left(\frac{\sigma FM_{DBP}}{FM_{DBP}}\right)^2} \quad (\text{A.6})$$

where F is the apparent fraction modern of a background sample, the DBP is the acronym of the Icelandic doublespar.

In this study the data is presented as the number of ^{14}C atoms from a single combustion for blanks and unknown samples. The calculation to determine the number of ^{14}C atoms in a blank sample is given below:

$$N[^{14}\text{C}]_{atoms} = \frac{F_s \times \lambda \times A \times V_s}{V_a} \quad (\text{A.7})$$

where $N[^{14}\text{C}]_{atoms}$ is the number of ^{14}C atoms without blank correction, F_s is the corrected fraction modern of a sample, λ is the fractional abundance of ^{14}C in modern carbon (1.177

$\times 10^{-12}$ for $^{14}\text{C}/^{12}\text{C}$), A is Avogadro's number (6.023×10^{23}), V_s is the volume of CO_2 collected in a combustion step, V_a is volume of 1mole of CO_2 at STP.

Blanks are corrected for using the following:

$$N_{BLKsub} = N_S - \frac{(N_{BLK1} + N_{BLK2})}{2} \quad (\text{A.8})$$

where N_S is the number of ^{14}C atoms in a sample, and N_{BLK} is the number of ^{14}C atoms in the blank.

In this study the extraction blank is obtained by taking an alumina boat (see Figure A.3) filled with LiBO_2 and putting it through the same procedures as an unknown sample. A system blank (or full procedural blank) is the same as an extraction blank but shielded quartz is added to the alumina boat. The variability in system blanks is caused mainly by the fragility of the *in situ* ^{14}C extraction line (see Figure A.2), and so, where possible, a blank bracketing approach was followed instead of the normal approach where corrections are made using a long-term average blank value.

Finally the concentration (atoms.g $^{-1}$) of *in situ* ^{14}C in a sample, and its corresponding uncertainty are calculated using:

$$N_{a.g^{-1}} = \frac{N_{BLKsub}}{S_g} \quad (\text{A.9})$$

$$\sigma N_{a.g^{-1}} = N_{BLKsub} \times \sqrt{\left(\frac{\sigma N_{BLK}}{N_{BLK}}\right)^2 + \left(\frac{\sigma S_g}{S_g}\right)^2} \quad (\text{A.10})$$

where S_g is sample mass in grams.

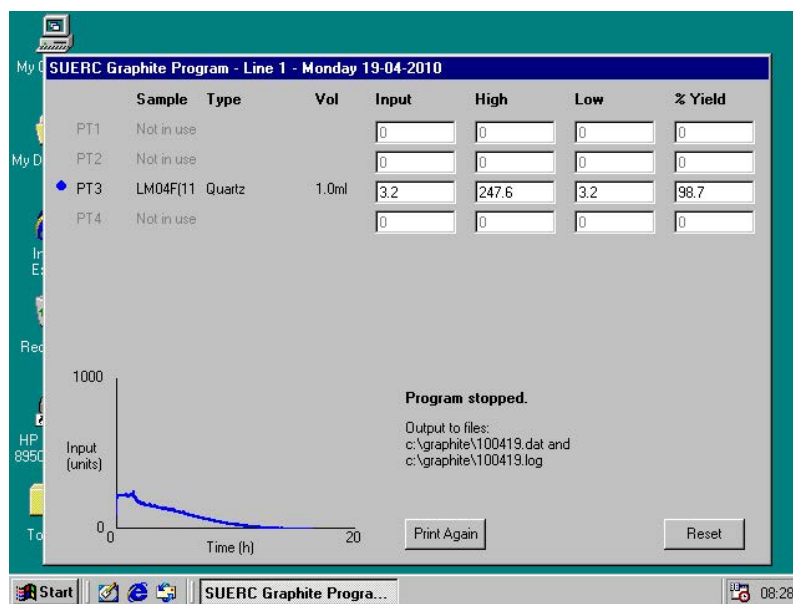


Figure A.1: Photograph showing the graphitization software.



Figure A.2: Photograph showing the broken mullite tube.



Figure A.3: Photograph showing the alumina boat.

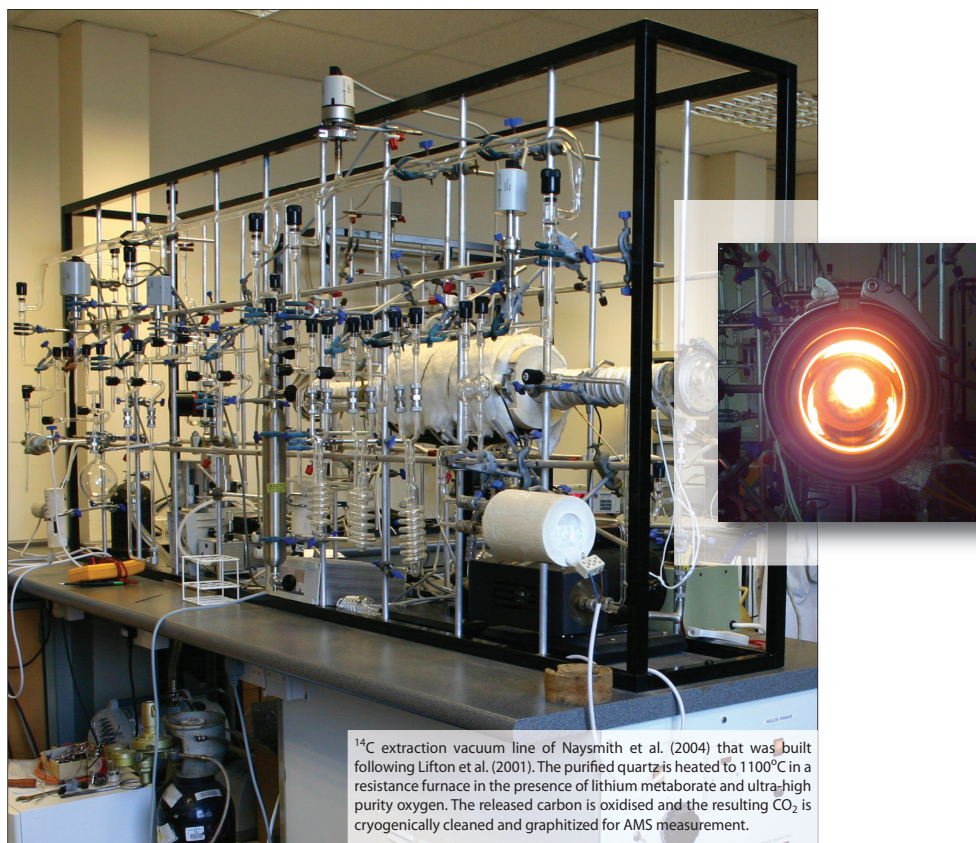


Figure A.4: Photograph showing the *in situ* cosmogenic ^{14}C extraction line at SUERC.

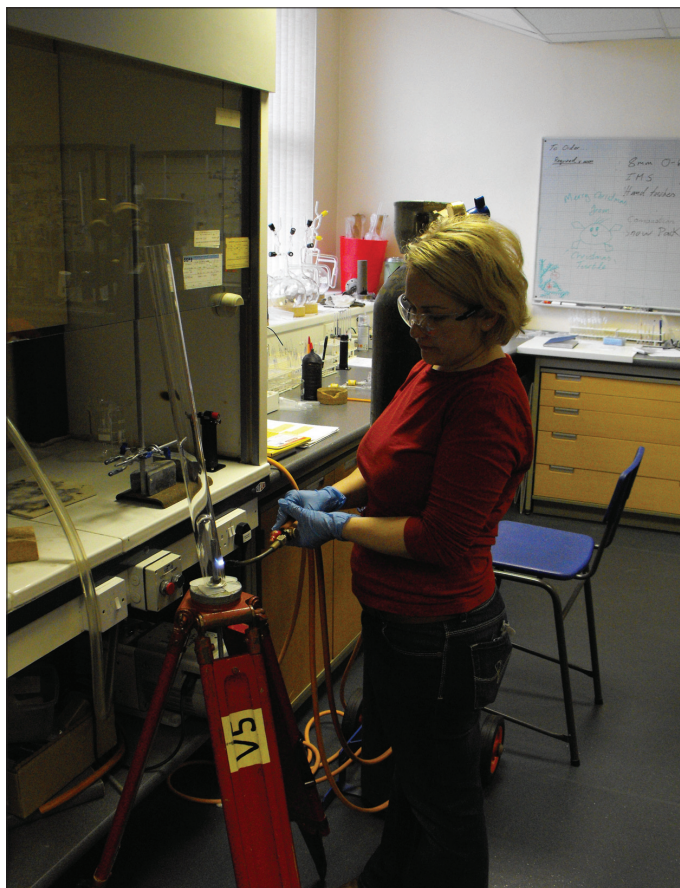


Figure A.5: Photograph showing the quartz tube flaming setup.

Appendix B

Sample site details

B.1 Peat monolith sample composition and radiocarbon analyses

Blanket peats formed throughout the Holocene (due cool and wet temperate climate) and occupy quite an extensive area of Scotland. Blanketed peat is formed as a result of slow decomposition of organic matter, mainly sphagnum moss (Borren et al. 2004). The peat cover at Wester Cameron is not gullied and is well drained. The peat cover is relatively shallow (15 - 30 cm) and has an angulated mineral rich base (Figure B.1).

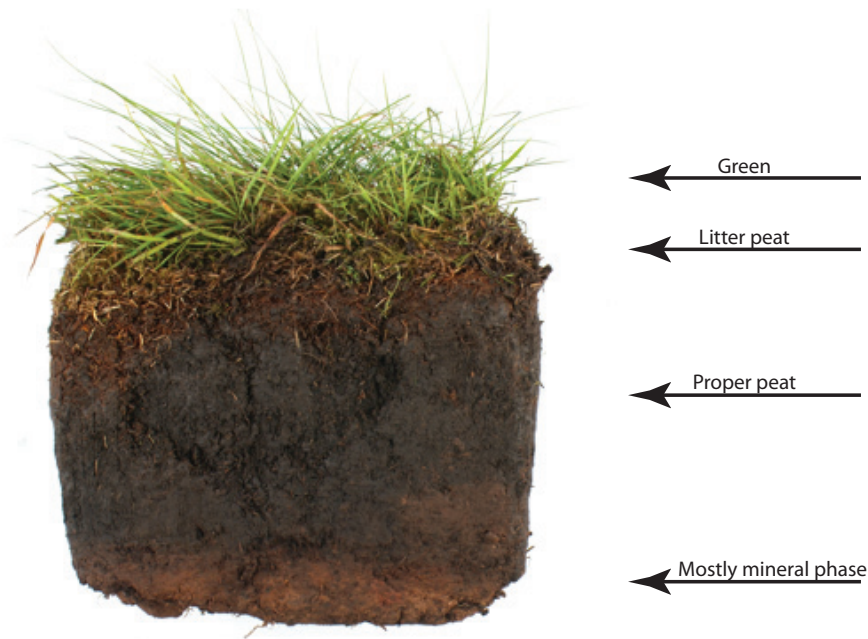


Figure B.1: Photograph showing the sampled peat monolith, Wester Cameron Farm.

A $21 \times 27 \times 15$ cm monolith peat sample was collected for radiocarbon measurements. The sample was collected from around one metre to the east of the cosmogenic depth profile sample site and was located on the top of the moraine. The monolith sample was taken with a shovel and was wrapped in aluminium foil and kept in cold storage until sampling was undertaken. Prior to sampling the monolith was split into two. One half was sampled for AMS radiocarbon analyses and the other half was sampled for particle size distribution, water content, organic matter content and density. The latter analyses were aimed at characterising the peat and at assessing whether this has incorporated any moraine material.

B.1.1 Peat composition analyses

The aliquots for bulk density, organic matter content, and particle-size analyses were collected using a metal ring with a volume of 5 cm³ at every 2 cm (Figure B.2). Dry bulk density was measured after drying at 105°C (Table B.1). Total organic matter content was estimated as loss-on-ignition at 500°C (Gale and Hoare 1991) and showed a linear decrease with depth, indicating that the growth of the peat layer was continuous. Particle size distribution was analysed on 0.3 - 0.6 g aliquots of the dried material using a Coulter LS 230 laser granulometer (see Table B.2 and Figures B.3, B.4, B.5 and B.6). The LS230 measures particle size distribution of a sample homogeneously mixed within a calgon solution, based on the principle that particles scatter and diffract light at certain angles based on their size, shape, and optical properties. This method enables the measurement of particles between 0.4 μm - 2 mm, size range typical for mud and soil samples (Blott et al. 2004).

Throughout the profile the amount of fine sand was constant ($\sim 8 - 10\%$), the uppermost samples containing substantially more silt than the deeper ones, the latter containing higher percentages of clay. The analysed material changed incrementally from silty loam to silty clay.



Figure B.2: Photograph showing the peat monolith with samples removed for density, water content, organic matter content and grain size analyses.

Table B.1: Peat sample density measurement results, Wester Cameron Farm.

First set						
Sample ID	Wet weight [g]	Dry weight [g]	Organic content %	Dry density [g/cm ⁻³]	Wet density [g/cm ⁻³]	Grain size [g]
P1	2.5	0.1	86.36	0.1	0.5	0.0762
P2	3.4	0.3	74.7	0.2	0.7	0.2788
P3	5.2	1.1	51.87	0.4	1.0	0.6084
P4	5.9	2.2	29.93	0.6	1.2	0.6126
P5	5.7	2.5	22.38	0.6	1.1	0.6417
P6	5.7	2.8	18.07	0.7	1.2	0.6118
P7	6	3.5	9.94	0.8	1.2	0.6079
Average:				0.5	1	

Replicate						
Sample ID	Wet weight [g]	Dry weight [g]	Organic content %	Dry density [g/cm ⁻³]	Wet density [g/cm ⁻³]	Grain size [g]
P9	2.4	0.1	90.35	0.1	0.5	0.0472
P10	3	0.2	80.93	0.2	0.6	0.1632
P11	3.3	0.5	60.53	0.2	0.7	0.4646
P12	5.3	1.4	44.31	0.5	1.1	0.6253
P13	4.2	1.6	29.19	0.4	0.8	0.606
P14	4.7	2.0	22.3	0.5	0.9	0.6294
P15	4.9	2.6	11.1	0.6	1.0	0.6086
Average:				0.4	0.8	

B.1.2 Peat radiocarbon analyses

Each AMS radiocarbon aliquot comprised of at least 40 g of sediment and was >1 cm thick. The aliquots were washed and all recognizable plant remains were removed. Peat is commonly used in radiocarbon dating, but complexity of biota can contribute to dating anomalies, usually there being discrepancies between the radiocarbon ages determined from the humin and humic fractions. In this study the humic acid (alkali soluble, acid insoluble) was used for dating, and this can provide younger ages as it is mobile and can incorporate rootlets (Cook et al. 1998).

All aliquots underwent an acid-alkali-acid (AAA) pre-treatment. The acid wash consisting of 0.5 M HCL for 2 hrs at 80°C is used to remove the fluvic acid. After neutralisation the material is heated to 80°C in 0.5 M NaOH for 2 hrs to extract the humic and remaining fluvic acids. The humic acid solution is filtered off. Acidification (to pH2) with 4 M HCl after the alkali treatment precipitates humic acids and removes CO₂ dissolved from air during alkali treatment. The precipitated humic fraction was washed with distilled water,

Table B.2: Peat sample grain size distribution analyses results, Wester Cameron Farm.

First set										
Sample ID	Mean (μm)	Median (μm)	D(3,2)	Mode (μm)	SD (μm)	CV %	Skewness	Kurtosis	Sand %	Silt % Clay %
P1	36.7	12.2	4.3	8.5	51.6	141	2	3.6	9.6	70.4 20.0
P2	69.5	16.1	3.8	9.4	104	149.6	2.2	5.1	12.6	56.1 31.4
P3	44.1	17.5	3.5	10.6	64.3	145.5	3	12.8	11.6	65.4 23.0
P4	65.8	25.2	3.6	109.8	93.7	142.5	2.4	7.4	11.6	56.4 31.9
P5	101	43.1	4.1	153.8	139.4	137.8	2.3	6.3	10.4	46.9 42.7
P6	85.7	43.2	4.1	153.8	104.7	122	1.9	3.9	8.3	51.1 40.7
P7	92	54.6	5.4	80.1	121.5	132	3.4	16	5.7	49.2 45.1

Replicate										
Sample ID	Mean (μm)	Median (μm)	D(3,2)	Mode (μm)	SD (μm)	CV %	Skewness	Kurtosis	Sand %	Silt % Clay %
P9	32.7	12.6	4.7	9.4	44.2	135.1	2	3.3	8.8	73.8 17.4
P10	36.5	10.3	3.3	9.1	63	171.3	2.8	8.9	12.3	70.7 17.0
P11	72.3	18.6	3.4	9.4	110.1	152.2	2.3	6.1	12.7	55.5 31.8
P12	80.9	26.1	3.8	158.8	116.4	143.9	2.3	6.3	10.8	53.4 35.7
P13	115.5	59.2	4.5	185.4	141.5	122.4	1.8	3.9	9.5	41.6 48.9
P14	95.2	44.1	3.5	168.9	123.2	129.2	2.1	5.2	9.9	47.6 42.5
P15	70.1	30	3.4	131.8	95.5	136	2.3	6.3	10.7	55 34.4

Standard deviation (SD) and coefficient of variation (CV)

Values are the average of three runs from the same samples.

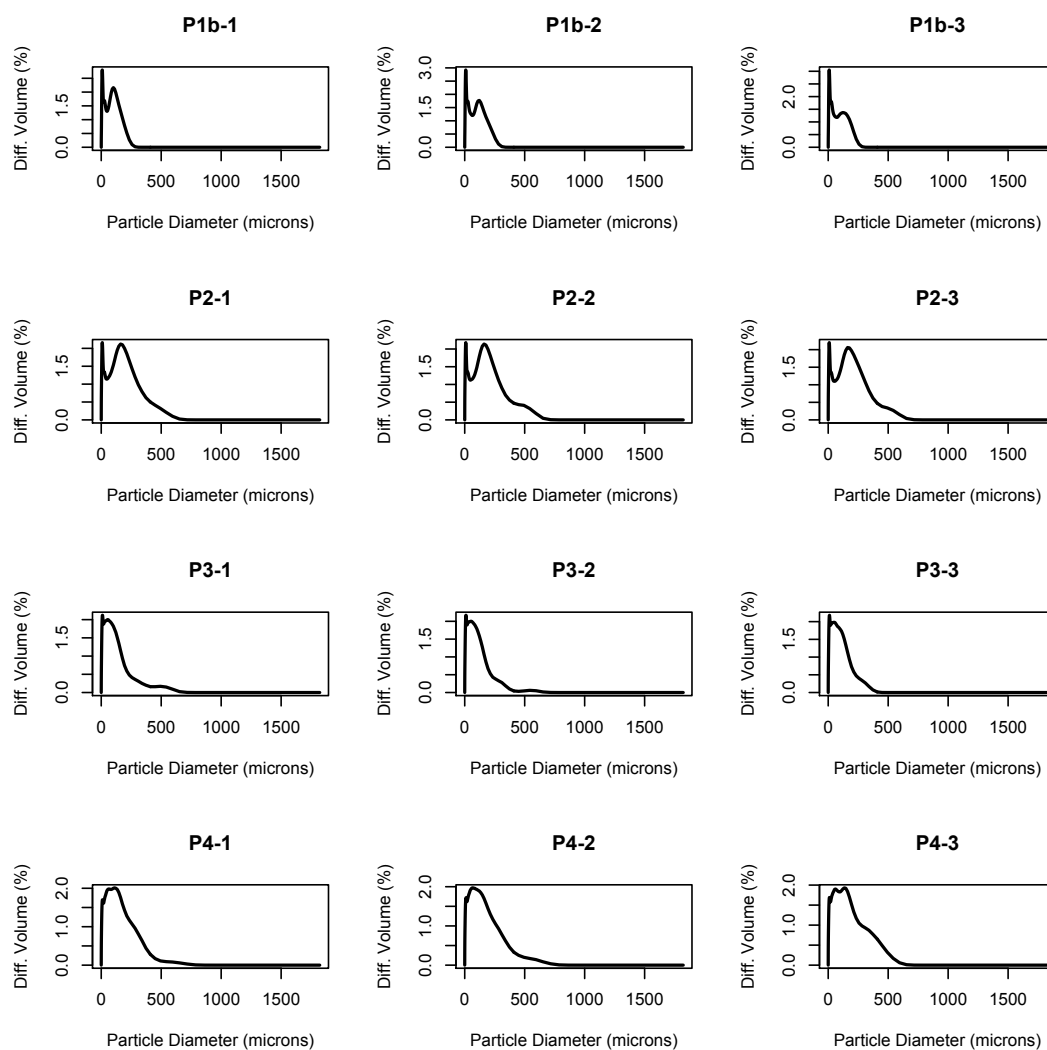


Figure B.3: Grain size distribution plots for the peat samples, Wester Cameron Farm.

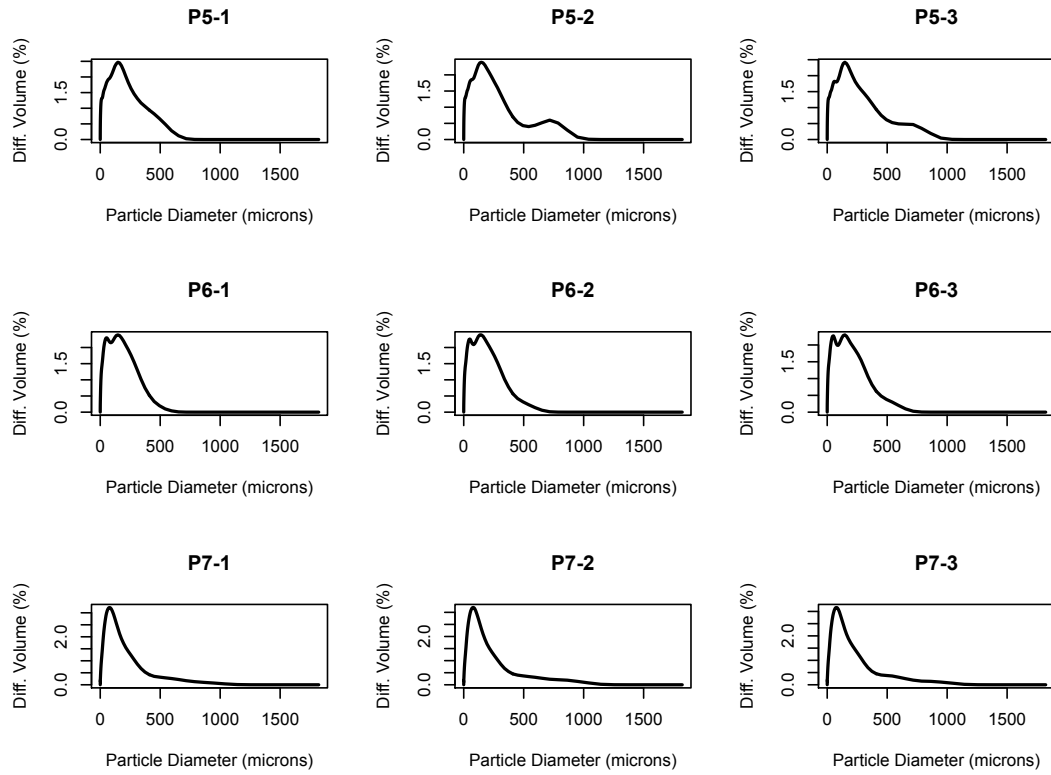


Figure B.4: Grain size distribution plots for the peat samples, Wester Cameron Farm (cont1).

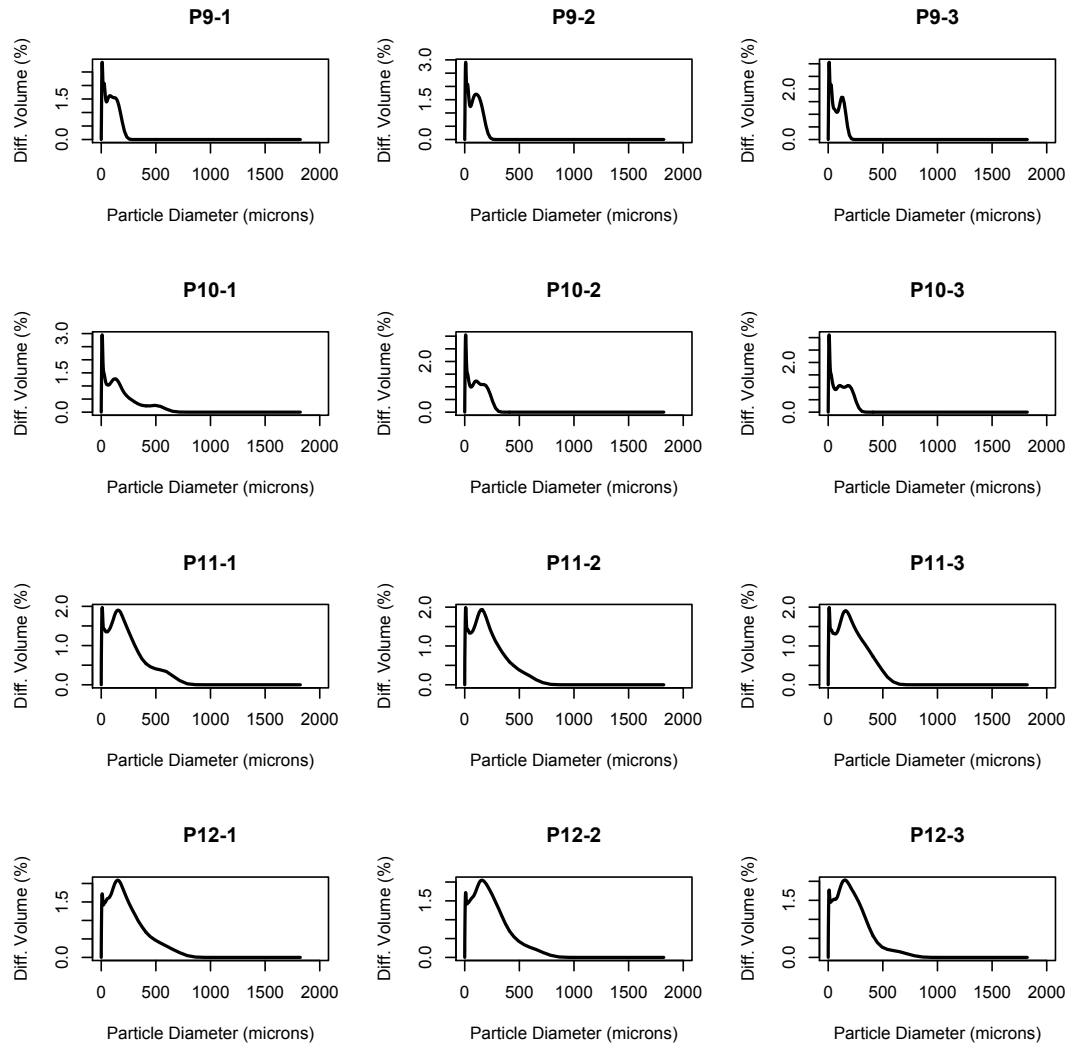


Figure B.5: Grain size distribution plots for the peat samples, Wester Cameron Farm (cont2).

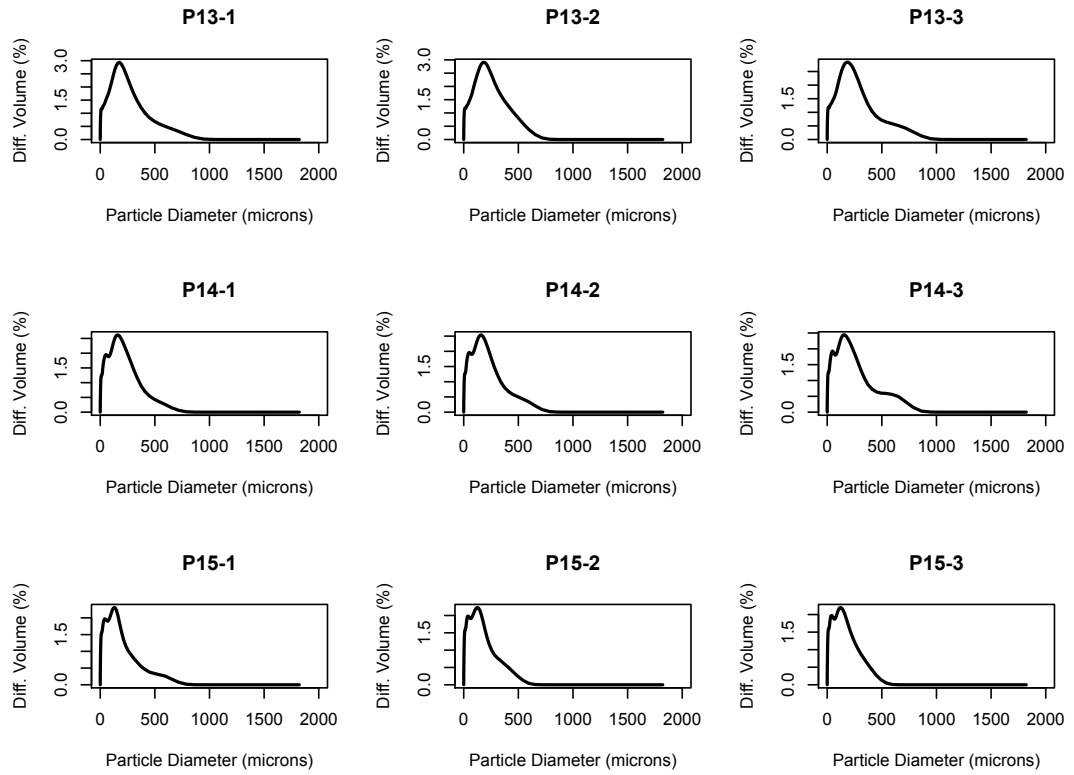


Figure B.6: Grain size distribution plots for the peat samples, Wester Cameron Farm (cont3).

centrifuged for 3 minutes at 6000 rpm and oven dried and weighed. Following, the samples were combusted and converted to CO₂ with CuO and silver wool, cryogenically purified, and then graphitized in the presence of Fe and Zn (Slota et al. 1987).

All radiocarbon analyses were done at the SUERC AMS (Xu et al. 2004). A small fraction of the CO₂ gas was used for the measurement of the $\delta^{13}\text{C}$ fraction, in a conventional mass spectrometer and was pMC (percent Modern Carbon) corrected for fractionation. During stable isotope ratio measurements the relative abundances of masses 44, 45 and 46 in the gas are compared with those of a working standard reference gas of known isotopic composition. In practice this is achieved by automatic valve switching and data collection whereby reference gas and sample gas are alternately bled into the mass spectrometer switching ten times over a period of several minutes thus obtaining a mean delta value for the sample with respect to the reference gas using the delta notation shown below:

$$\delta_{s-r} = \left(\frac{R_{\text{sample}}}{R_{\text{reference}}} - 1 \right) \times 10^3 \quad (\text{B.1})$$

where R is the 45/44 ratio (for obtaining the $\delta^{13}\text{C}$). δ is in units of ‰.

Contributions to the 45 and 46 peaks from minor isotope combinations (e.g. ¹⁷O) in the CO₂ molecules are compensated for using the Craig corrections by the software (Craig 1957). The latter procedure provides raw δ 's with respect to the internal reference gas. Adjusting the δ 's to get values with respect to the international standards (V-PDB and V-SMOW) involves the equation below:

$$\delta_{a-c} = \delta_{a-b} + \delta_{b-c} + 10^{-3} \times \delta_{a-b} \times \delta_{b-c} \quad (\text{B.2})$$

where a is the sample gas, b is the internal reference gas and c is the international standard. $\delta_{(b-c)}$ is the value (in ‰) of the internal reference gas with respect to the international standard. The internal reference gas has been pre-calibrated using carbon dioxide sample gases of known isotopic composition produced from International Reference Materials such as NBS-19 and IAEA standards.

All radiocarbon dates are reported in calendar years before present, where the present is defined as AD 1950, and were calibrated with Oxcal v.4.1 (Bronk Ramsey 2009) using the INTCAL09 atmospheric calibration curve (Reimer et al. 2009) and a bayesian framework.

Values are expressed as 95%($\pm 2\sigma$) confidence limits. The radiocarbon ages are stratigraphically coherent, except for the reversal of CPT5 and CPT6. The two samples were collected from the contact zone between the peat and the underlying mineral substrate. This reversal is thought to reflect the introduction of younger carbon by groundwater percolating along the relatively impermeable surface at the base of the peat (i.e., along the top of the mineral material) (Gordon Cook, SUERC, *personal communication*, 25 August 2008). CPT1 is modern. Accepting the radiocarbon determinations for CPT2, CPT3, CPT4, CPT7 and CPT8 as correct implies a basal age for the peat of 1400-2000 ^{14}C years depending on whether the top of the peat or the root zone is taken to be the reference point (which returned the modern age) or the present ground surface. Basal age is calculated as follows:

$$\text{Basal age} = (\text{Current year} - \text{Calibrated year}) / (\text{sampling depth} \times \text{total depth}) \quad (\text{B.3})$$

Based on the basal age determination peat formation started at between 500 - 2157 years ago. No matter whether the minimum or maximum calibrated ages are used or whether the root zone or ground surface are used as a reference point, the peat started forming at a maximum of 2000 years BP. This relatively young age combined with a bulk density of 0.5 - 0.9 g.cm^{-3} indicates that the peat cover did not shield substantially the soil from cosmic rays and so did not have a substantial effect on the accumulated cosmogenic nuclide concentrations.

The results of the AMS radiocarbon analyses are presented in Table B.3 and Figure B.7.

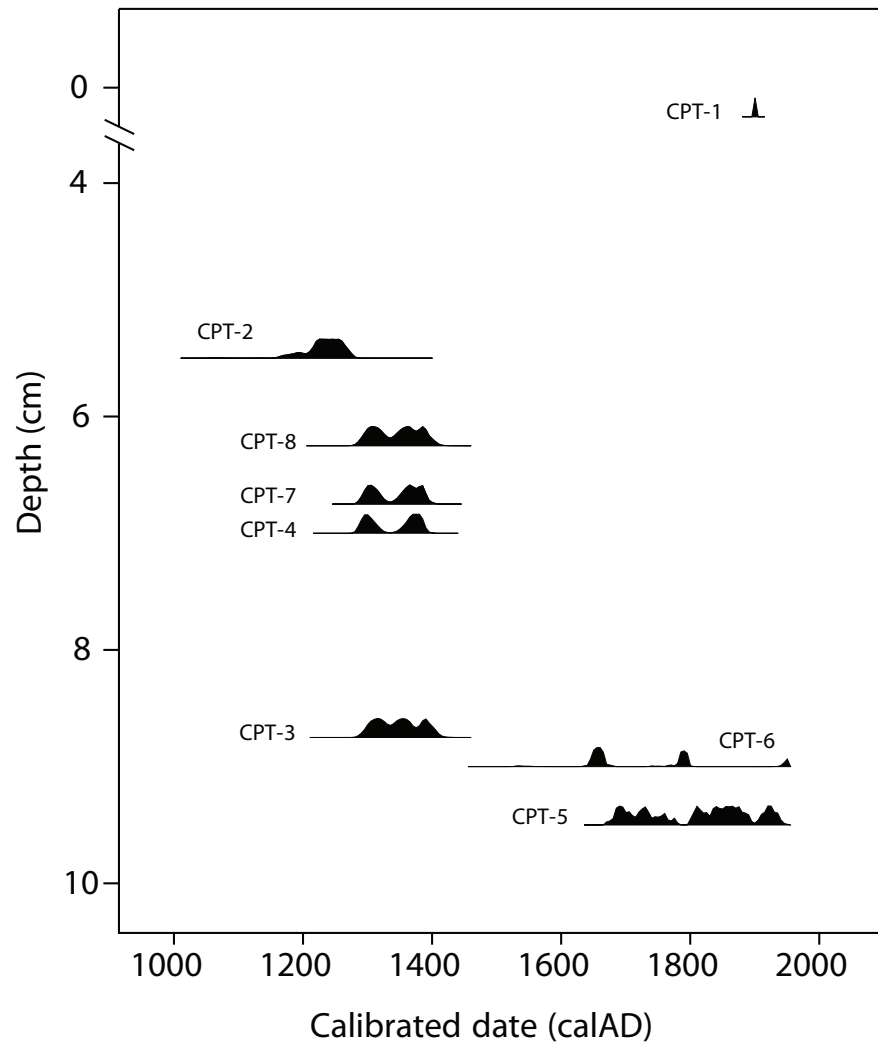


Figure B.7: Results of the radiocarbon determinations, Wester Cameron peat (OxCal v4.1.7 Bronk Ramsey 2009; Atmospheric data from Reimer et al. 2009)

Table B.3: Details of the radiocarbon determinations, Wester Cameron peat.

Sample ID	SUERC ID	GU ID	Depth (cm)	δ^{13}	Age (years)	1 σ Age	Age from	Age to Cal AD	Probability
CPT-1	SUERC-19861	17117	0.5-1.5	-29.8	1.1661	0.0045	modern	modern	-
CPT-2	SUERC-19862	17118	5.5-6.5	-28.8	800	35	1175	1277	95.4
CPT-3	SUERC-19863	17119	8.5-10	-28.9	610	35	1294	1406	95.4
CPT-4	SUERC-21596	17862	6.5-8.5	-29.2	650	35	1279	1396	95.4
CPT-5	SUERC-21600	17863	10.5	-29.1	125	35	1675	1942	95.4
CPT-6	SUERC-21601	17864	9-10	-28.7	240	35	1522	1955	95.5
CPT-7	SUERC-21602	17865	5.5-8	-29.4	640	35	1282	1398	95.4
CPT-8	SUERC-21603	17866	5-8.5	-31	625	35	1289	1400	95.4

The error, which is expressed at the 2 σ level of confidence, includes components from the counting statistics on the sample, modern reference standard and blank and the random machine error. humic acid extracted from the peat
The calibrated age ranges are determined from the University of Oxford Radiocarbon Accelerator Unit calibration program (OxCal v4.1.6 Bronk Ramsey 2009; Atmospheric data from Reimer et al. 2009)

B.2 Density measurement

Information on the density of the material making up a deposit is key in calculating the cosmogenic nuclide depth profile in that deposit. This is because the attenuation of the intensity of cosmic rays in a material depends on the density of that material (Lal 1991):

$$P(z) = P(0) \exp \left[-\frac{\rho z}{\Lambda} \right] \quad (\text{B.4})$$

where $P(z)$ is the cosmogenic nuclide production rate at depth ($\text{atoms.g}^{-1}.\text{yr}^{-1}$) within a material (e.g., rock or soil), $P(0)$ is the cosmogenic nuclide production rate at the surface, z is depth (cm), Λ is the mean cosmic ray attenuation length (g.cm^{-2}), and ρ is material density (g.cm^{-3}).

Both pits were opened on moraines characterised by unsorted sediment consisting of clasts of varying sizes, and so standard methods for calculating density (cf. Balco and Stone 2003) could not be applied here.

To calculate and map changes in the density of the till a novel method based on terrestrial laser scanning was utilised. Terrestrial laser scanning (TLS) is increasingly applied in geosciences because of relatively fast and reliable 3D point cloud data acquisition. The TLS applications in geology are mainly concerned with representing the surface of objects (for a review see Buckley et al. 2008). A close-range TLS (e.g., Leica Scanstation2 with a generator for power supply) enables the collection of high precision and high accuracy point cloud data with relative ease. However, the weight of the instrument is ~ 60 kg and so transporting to the field is not straightforward (see on Figure B.8).

The sampled pit walls were scanned using a laser scanner before and after sampling so that a high resolution DEM of the two surfaces can be constructed. During measurement the instrument was held fixed on a tripod and the scanned wall was clearly visible both horizontally and vertically from this. The time required for one scan was of 15 minutes. The instrument was positioned 2 - 3 metres from the scanned wall and this yielded a resolution of 1 mm. The vertical range was limited to 45° below horizontal and 35° above horizontal. The point clouds were reduced using Cyclone (version 6.5) so that surplus data are reduced and the scans are registered together and geo-referenced and exported into an ASCII format. The point clouds were reduced to 25% of the initial size so that they can be handled by ArcGIS.



Figure B.8: Photograph showing the TLS setup, Wester Cameron Farm..

After importing into ArcGIS the point clouds were triangulated and the resulting Triangulated Irregular Networks (TIN) converted into regular grids. Triangulating first and then converting into a regular grid was preferred to directly interpolating the point cloud due to the rather poor selection of interpolating techniques that are offered in ArcGIS. The obtained regular grids (surfaces) were filtered to remove obvious artifacts (e.g., measuring tape present in some of the scans) and then used to calculate volume of material removed by sampling per each pixel by simply subtracting the pre-sampling grid from the post-sampling grid. Given that the TLS was held fixed on a tripod, a difference between the pre- and post-sampling grids only occurs for pixels where material has been removed by sampling (i.e., for pixels where no material was sampled, the difference between the two surfaces = 0). The per pixel volume grids were then cut into 15 cm bands (as each sample was collected 15 cm intervals) and the values summed for each band so as to yield the total volume removed from that band (= the total volume of each sample). Samples were weighed before and after drying in an oven and the sample masses and sample volumes were then used to calculate both an average dry and an average wet density for each 15 cm band.

The obtained values are listed in tables B.4 and B.5

Table B.4: Density calculation results, Wester Cameron Farm.

Wester Cameron					
From top (15 cm bands)	Volume (cm ⁻³)	Dry Mass (g)	Dry Density (g.cm ⁻³)	Wet Mass (g)	Wet density (g.cm ⁻³)
1	2007	1841	0.92	2681	1.34
2	1194	1974	1.65	2373	1.99
3	1706	1621	0.95	1871	1.1
4	1141	1952	1.71	2240	1.96
5	938	2031	2.16	2367	2.52
6	1435	1731	1.21	2016	1.41
7	1226	1602	1.31	1900	1.55
8	1298	2254	1.74	2637	2.03
9	1212	1738	1.43	1995	1.65
10	1706	2927	1.72	3293	1.93
11	1545	2362	1.53	2661	1.72
12	1124	1840	1.64	2160	1.92
13	1287	1988	1.54	2287	1.78
14	1110	1856	1.67	2171	1.96
Average density:				1.51	1.77

Table B.5: Density calculation results, Inchie Farm.

Inchie Farm					
From top (15 cm bands)	Volume (cm ⁻³)	Dry Mass (g)	Dry Density (g.cm ⁻³)	Wet Mass (g)	Wet density (g.cm ⁻³)
1	1907	2569	1.35	3538	1.85
2	2230	3452	1.55	4156	1.86
3	2152	3706	1.72	4110	1.91
4	2741	3368	1.23	3699	1.35
5	2420	3404	1.41	3869	1.6
6	2283	4593	2.01	5225	2.29
7	1976	3573	1.81	4048	2.05
8	1839	3899	2.12	4337	2.36
9	2808	3134	1.12	3619	1.29
10	2215	3865	1.75	4597	2.08
11	2057	3994	1.94	4370	2.12
12	1629	3304	2.03	3522	2.16
13	2586	3303	1.28	3554	1.37
14	2857	4180	1.46	4471	1.56
15	1618	2637	1.63	2966	1.83
16	2217	2691	1.21	2915	1.32
17	2360	4247	1.8	4713	2
Average density:				1.61	1.82

B.3 Erratic samples, Inchie Farm

Figures B.9 and B.10 are showing the location of samples as well as the type of material collected for surface exposure dating at Inchie Farm.



Figure B.9: Photograph showing the sampled pebbles, Inchie Farm.

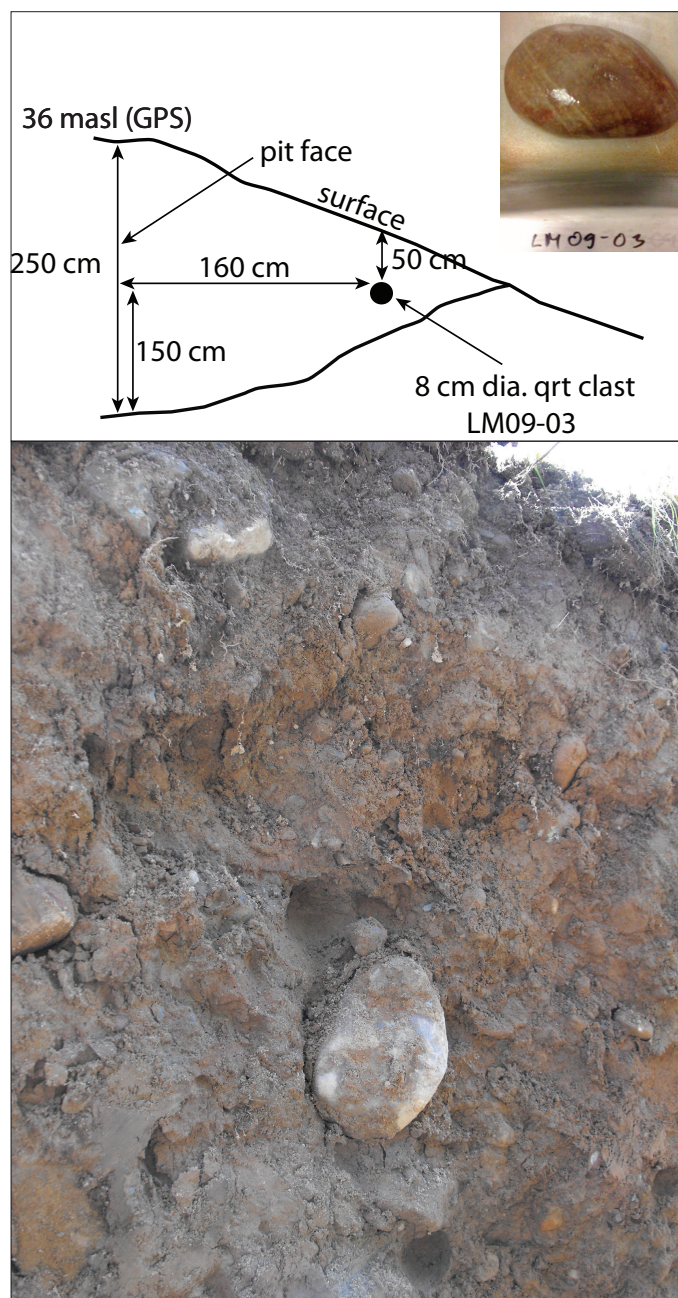


Figure B.10: Photograph showing the relative location of sample LM09-03 collected for surface exposure dating, Inchie Farm

Table B.6: Summary of the ^{10}Be analyses in the Inchie Farm ‘erratic’ pebbles.

Sample ID	Lat (deg)	Long (deg)	Elevation (m)	Thickness (cm)	Production Rate ($\text{at}\cdot\text{g}^{-1}\cdot\text{yr}^{-1}$)		Shielding Factor*	^{10}Be ($\text{at}\cdot\text{g}^{-1}$)	$\pm 1\sigma$	Age (years)	$\pm 1\sigma$
					Neutrons	Muons					
LM0901	56.17488	-4.27385	50	1	4.78	0.184	1	23009	1778	4338	497
LM0902	56.17488	-4.27385	50	1	4.78	0.184	1	20027	1919	3775	482
LM0903	56.17488	-4.27385	35	8	2.53	0.182	0.570	21147	2332	7296	1014

Latitude and longitude use WGS84 datum.

Calculated with the CRONUS-Earth online calculator (Balco et al. 2008) version 2.2 (<http://hess.ess.washington.edu/>), using the time dependent Lal/Stone scaling scheme.

*Calculated according to Dunne et al. (1999).

Corrected for a full chemistry procedural blank that yielded < 3% of the number of ^{10}Be atoms in the samples.

Appendix C

Cosmogenic ^{10}Be , ^{26}Al , and ^{14}C Analyses

C.1 Sample preparation

The procedures used to isolate and clean quartz, and to extract Be and Al for AMS analyses are based on Kohl and Nishiizumi (1992). The samples collected from Wester Cameron (Figure C.1) were prepared at the NERC Cosmogenic Isotope Analysis Facility at SUERC, and the samples collected from Inchie Farm (Figure C.2) were prepared at the Glasgow University Cosmogenic Isotope Analysis Facility also based at SUERC. The two labs follow slightly different Be and Al chemistry procedures and therefore both are provided here.



Figure C.1: Photograph showing the pit opened for cosmogenic nuclide depth-profile sampling, Wester Cameron Farm.

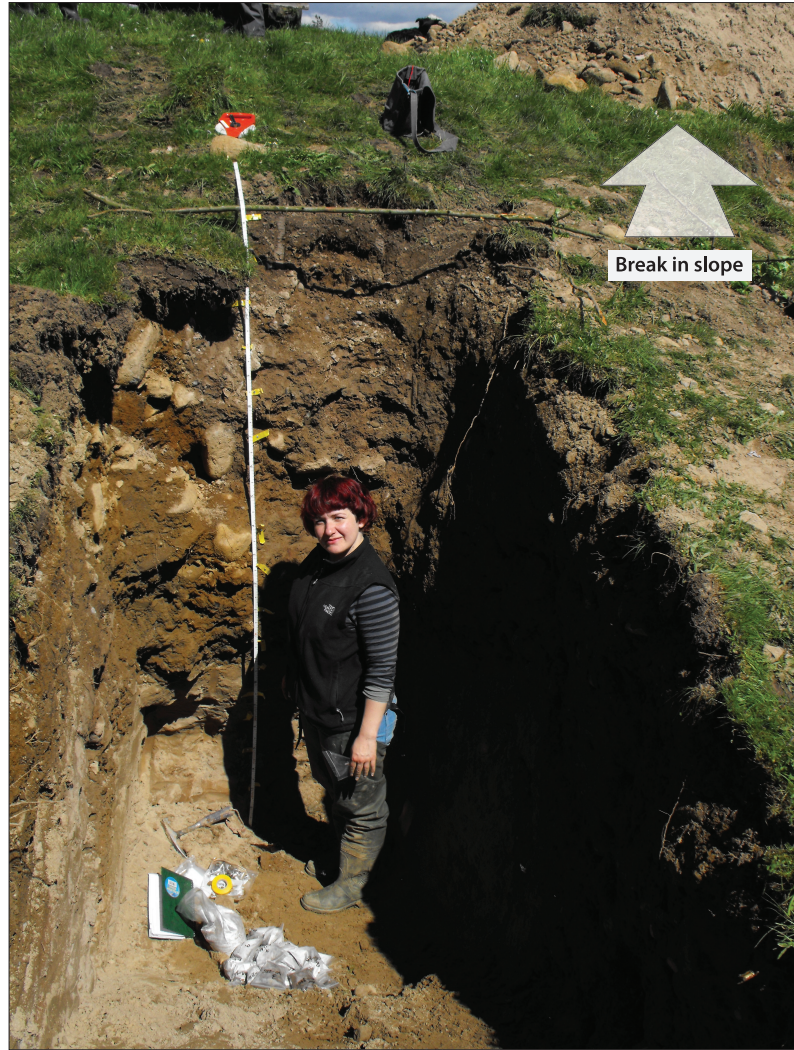


Figure C.2: Photograph showing the pit opened for cosmogenic nuclide depth-profile sampling, Inchie Farm.

C.1.1 The preparation of ultrapure quartz separates

Around 2-5 kg of samples were collected at 15 cm depth intervals from both field sites from two ~2.5 m deep pits (Table C.1).

Samples were wet sieved and the 250 - 500 μm fraction that is commonly used in cosmogenic nuclide studies (cf. Gosse and Phillips 2001, Bierman et al. 2002, Bierman and Nichols 2004, Dunai 2010) has been separated and labeled as CPA-F and LM-F, for Wester Cameron and Inchie Farm, respectively. The remaining sample material was separated in two size fractions: a coarse one ($> 2 \text{ mm}$) labeled CPA-P and LM-P, and one with grains between 0.5 mm - 2 mm labeled CPA-M and LM-M, respectively (Figure C.3). These

Table C.1: Sample labels and weights.

Western Cameron Fram		Inchie Farm	
Sample name	Bulk sampling weight (kg)*	Sample name	Bulk sampling weight (kg)*
CPA-1	2.86	LM-01F	3.54
CPA-2	2.68	LM-02F	4.16
CPA-3	2.72	LM-03F	4.11
CPA-4	2.78	LM-04F	3.7
CPA-5	2.29	LM-05F	3.87
CPA-6	2.19	LM-06F	5.23
CPA-7	1.76	LM-07F	4.05
CPA-8	2.16	LM-08F	4.34
CPA-14	1.84	LM-16F	2.9
-	-	LM-17F	4.68

*wet weight

coarse (P) and medium (M) size fraction samples were then crushed using a jaw crusher, washed and dried. The amount of material lost after each cleaning step is shown in Table C.2 and C.3. On average, around 60 - 70% of the material was lost during sample cleaning.

The separated aliquots were leached several times in 10 to 20% HCl/HNO₃ for 12 hours on a hotplate at 110°C to remove carbonates and metals. The HCl/HNO₃ solution also acts to open pathways within grains along which HF can attack solid inclusions and lithic fragments. All samples were then washed in distilled H₂O and dried overnight. After drying, all samples were passed through a Frantz isodynamic magnetic mineral separator to split each sample into a magnetic fraction (mostly lithic) and a non-magnetic fraction (mostly quartz and feldspar).

All Wester Cameron samples and sample LM-01M from Inchie Farm were further purified using 85% pyro-phosphoric acid, which rapidly dissolves aluminosilicates, but only minimally attacks quartz. Ortho-phosphoric acid heated to 220 - 250°C efficiently dissolves feldspars, but is less efficient at removing amphiboles, garnets, and oxides. Sample and acid are heated in a 600W mantle (EM1000/CE) to ~240°C. Mineral dissolution proceeds rapidly (30 - 60 minutes at ~240°C), after the water content of the acid boiled off and the acid becomes more viscous. After 1 hour of dissolution, the samples are cooled down to ~150°C and rinsed with hot (60 - 70°C) water to dissolve remaining acid and silica. The supersaturated silica solution in a form of gelatinized film adhering to the flask and quartz grains is dissolved with sodium hydroxide (50%), heated for 10 minutes. The



Figure C.3: Photograph showing a selection of the cosmogenic nuclide depth-profile samples.

Table C.2: Sample weights in grams after each cleaning step, Wester Cameron Farm.

250 - 500 μm					
Sample ID	Dry weight (250 - 500 μm)	HCl/HNO ₃	Magnetic separation	H ₃ PO ₄	HF leaching
CPA-1F	166.5 (39.1*)	99.2	95.6 (2*)	75.2	61.1
CPA-2F	155.7 (27*)	111.3	105.5 (5.3*)	79.4	67.1
CPA-3F	155.1 (34*)	106.4	96.2	73	58.8
CPA-4F	210.9 (80.1*)	116.9	108 (7.8*)	77	62.9
CPA-5F	121.5	109.6	103.4 (2.8*)	74.2	59.8
CPA-6F	168.3 (22.3*)	131.4	125.8 (24.8*)	70.1	54.7
CPA-7F	205.8 (65.9*)	124.9	114.8 (14.5*)	72	57.4
CPA-8F	138.2	118.9	107.8 (7.8*)	72.4	58.8
CPA-14F	80.7	70.8	61.2	44.5	33.9

> 2mm					
Sample ID	Dry weight after crushing (250 - 500 μm)	HCl/HNO ₃	Magnetic separation	H ₃ PO ₄	HF leaching
CPA-1P	145.7	123.9	108.6 (7.9*)	60.6	43.9
CPA-2P	140.6	121.5	100.2	60.9	43.2
CPA-3P	125.8	106.1	68.7	39.4	22
CPA-4P	224.2	178.8	141.5 (40.7*)	51.1	32.4
CPA-5P	95.8	79.8	53.4	27.4	8.5
CPA-6P	87.1	76.1	58.2	39.9	27.7
CPA-7P	17.1	13.1	9.2	5.6	2.2
CPA-8P	132.7	123.6	118.1 (17*)	79.7(6.7*)	61.4
CPA-14P	142.1	129.7	108.7	63.2	38.5

500 - 2 mm					
Sample ID	Dry weight after crushing (250 - 500 μm)	HCl/HNO ₃	Magnetic separation	H ₃ PO ₄	HF leaching
CPA-14M	74.1	65.5	49.5	32.4	19.9

*archived

Table C.3: Sample weights in grams after each cleaning step, Inchie Farm.

250 - 500 μm						
Sample ID	Dry weight (250 - 500 μm)	HCl/HNO ₃	Magnetic separation	Flotation	H ₃ PO ₄	HF leaching
LM-01F	176	113.7	74.8	60.9	-	48.2
LM-02F	179.4	132.4	81.9	68.4	-	56.4
LM-03F	125.1	105.5	69.3	53.8	-	42.2
LM-04F	185.7	145.8	79.1	61.7	-	49.8
LM-05F	148.9	118.8	73.7	55.5	-	42.4
LM-06F	175.8	151.6	100.4	81.9	-	64.7
LM-07F	103.4	86.2	56.7	45.1	-	33
LM-08F	109.6	86.7	57.6	39.5	-	28.4
LM-16F	129.6	120.1	83.8	63.6	-	50.2
LM-17F	518.6(3.8 [†])	311.4	268.9 (66.5*)	123.6	-	68.4

> 2mm						
Sample ID	Dry weight after crushing (250 - 500 μm)	HCl/HNO ₃	Magnetic separation	Flotation	H ₃ PO ₄	HF leaching
LM-1P	214.8 (14.4*)	183.2	84	54.8	-	40.4
LM-2P	272.6 (70.6*)	186.8	82	64.4	-	47.8
LM-3P	334.9 (133.2*)	191.4	113.9	71.6	-	57.1
LM-8P	361.6 (160.1*)	195.8	184.1 (25.4*)	147.1	-	130.4

500 - 2 mm						
Sample ID	Dry weight after crushing (250 - 500 μm)	HCl/HNO ₃	Magnetic separation	Flotation	H ₃ PO ₄	HF leaching
LM-1M	96.1	87.8	51.4	41	35.3	26.7

*archived

[†]after wet sieving only 3.8 g remained of the 250 - 500 μm size fraction, the 125 - 250 μm has been used instead

remaining sample is rinsed in water several times and dried. Because this process allows the processing of only three samples per day, the Lake Menteith samples were further purified using a froth-flotation process. A carbonator is used to mix CO_2 with a solution consisting of 11 l of H_2O , 1 g Lauryl Amine (n-Dodecylamine) surfactant, and 1 mL Acetic acid. This CO_2 -solution mixture is sprayed onto the sample sitting in 1% HF solution and a few drops of Eucalyptus oil, and results in most aluminosilicates floating and therefore being removed from the sample.

The remaining aluminosilicates can be removed by selective dissolution using dilute HF, leaving a very pure quartz residue behind. Thus, to remove all feldspars the samples were transferred to 500 mL high-density polyethylene bottles and were leached in a 2% HF/ HNO_3 solution for several days at 80°C under constant ultrasonic agitation. This process does not only dissolve feldspars but strips off the outer rim off individual quartz grains to ensure that all meteoric ^{10}Be is removed. To assess the purity of the quartz, the aluminum content of the clean separates is measured. The Al concentrations should preferably be in the range 10 - 100 ppm (Kohl and Nishiizumi 1992, Bierman et al. 2002). A higher concentration generally (though not always) indicates the presence of an impurity such as feldspar, muscovite or an insoluble fluoride residue from the quartz clean-up (e.g., Na_3AlF_6).

C.1.2 Purification and Be extraction, Wester Cameron Farm samples

C.1.2.1 Sample purity check

Sample aliquots of 0.4 g were dissolved in 40% HF and the reaction temperature was increased gradually during this process. After complete dissolution and evaporation of hydrofluoric acid, the fluorides were taken up in a mixture of 6M HCl and 70% HNO_3 . This mixture was evaporated at temperatures below 110°C to drive off HF but to avoid losses of Al by volatilization. The residues were re-dissolved in 3% HNO_3 and transferred to centrifuge tubes and further diluted with 3% HNO_3 . The results of the ICP/AES measurements are shown in Table C.4

Table C.4: Results of the ICP/AES measurements, Wester Cameron.

Sample ID	Reported Al Conc ($\mu\text{g/mL}$)	Mass Q (g)	Mass Sol'n (g)	Dilution factor	Estimated Al Conc (ppm)	Actual Al Conc ($\mu\text{g/mL}$)	Al (ppm)
CPA-1P	6.305	0.4088	7.9209	19.38	122.17	6.82	132
CPA-2P	6.197	0.4255	7.9974	18.8	116.47	6.71	126
CPA-3P	5.118	0.4086	8.0903	19.8	101.34	5.53	109
CPA-4P	5.802	0.4122	8.0511	19.53	113.32	6.27	123
CPA-5P	-	-	-	-	-	-	-
CPA-6P	2.633	0.4211	7.9794	18.95	49.89	2.81	53
CPA-8P	3.038	0.4239	8.0405	18.97	57.62	3.25	62
CPA-14P	4.472	0.4089	8.0097	19.59	87.6	4.82	94
CPA-14M	4.668	0.4048	7.9772	19.71	91.99	5.04	99
CPA-1F	6.428	0.403	8.0185	19.9	127.9	6.96	138
CPA-2F	7.507	0.4115	8.0147	19.48	146.21	8.14	159
CPA-3F	6.734	0.403	8.0307	19.93	134.19	7.29	145
CPA-4F	7.278	0.4076	7.9307	19.46	141.61	7.89	153
CPA-5F	6.95	0.4054	8.016	19.77	137.42	7.53	149
CPA-6F	7.24	0.4088	7.9962	19.56	141.62	7.85	153
CPA-7F	7.991	0.4036	8.0784	20.02	159.95	8.67	173
CPA-8F	6.913	0.409	7.9544	19.45	134.45	7.49	146
CPA-14F	4.962	0.4192	8.0954	19.31	95.82	5.36	103

Blank (3% Nitric) < 0.010 Drift correction 1.0931 ± 0.0673

The samples were analysed using a modification of OSHA ID121 and an Inductively Coupled Plasma/Atomic Emission Spectrometry (ICP/AES).

C.1.2.2 Be and Al extraction

The Be and Al extraction procedures described below are those described in Wilson et al. (2008) based on Cristoph Schnabel protocol (CIAF). Beryllium is a very rare element in quartz and so it is necessary to spike the sample with a known quantity of ^9Be . The aim of spiking is (1) to allow tracing the movement of the *in situ* cosmogenic ^{10}Be through the processing, and (2) to obtain sufficient *in situ* cosmogenic ^{10}Be at the end of the processing to generate an ion beam in the AMS. The aim is not to introduce any ^{10}Be to the sample, thus a Be carrier solution with known concentration of ^9Be is used. It is critical that a low-level carrier is used for samples with potentially low levels of ^9Be . The samples were dissolved with 40% HF incremental addition, and then 400 - 490 mg Be in dilute nitric acid was added to the resulting residue (Table C.5).

Table C.5: Sample and carrier masses, WesterCameron.

Sample ID	Quartz (g)	Be-carrier mass (g)	Al-carrier mass (g)	Be Spike (μg)	1σ Be Spike	Al Spike (μg)	1σ Al Spike
CPA-1P	33.009	0.4877	-	197.7	4	-	-
CPA-2P	33.014	0.4875	-	197.6	4	-	-
CPA-3P	15.013	0.4043	-	163.9	3.3	-	-
CPA-4P	25.148	0.4033	-	163.5	3.3	-	-
CPA-5P	7.033	0.3321	-	134.6	2.7	-	-
CPA-6P	19.912	0.4039	-	163.7	3.3	-	-
CPA-8P	34.553	0.404	-	163.8	3.3	-	-
CPA-14P	30.753	0.4024	-	163.1	3.3	-	-
CPA-14M	13.124	0.328	-	133	2.7	-	-
CPA-1F	33.002	0.4878	-	197.8	4	-	-
CPA-2F	33.029	0.489	-	198.2	4	-	-
CPA-3F	35.041	0.4055	-	164.4	3.3	-	-
CPA-4F	35.029	0.4051	-	164.2	3.3	-	-
CPA-5F	35.016	0.4046	-	164	3.3	-	-
CPA-6F	34.432	0.4033	-	163.5	3.3	-	-
CPA-7F	34.89	0.4034	-	163.5	3.3	-	-
CPA-8F	34.57	0.403	-	163.4	3.3	-	-
CPA-14F	26.891	0.4029	-	163.3	3.3	-	-

Be-carrier concentration: 405 ± 8.1 ppm

Once all the quartz had been dissolved the residue was then taken up in 4 mL 6M HCl and 2 mL 70% HNO_3 and repeatedly dried down at $< 110^\circ\text{C}$ with 4 mL 6M HCl. Successive evaporations and re-dissolutions of the samples eliminate fluoride (as HF) almost entirely. Fe, Ti, Al, Be, and alkalis are left as chloride salts ready for anion exchange clean-up. The sample is diluted with 4 mL 6M HCl, transferred to a centrifuge tube and centrifuged at 3700 - 3900 rpm for 7 minutes. The supernatant from the centrifugation step is transferred

to a new centrifuge tube and the residues washed in with 250 mL 6M certified HCl, centrifuged again and the whole solution is weighted. For analysis of inherent ^{27}Al using an ICP/AES a 250 mL aliquot is taken from this solution. Because ^{26}Al measurements were not part of the initial plans, these aliquots were placed in storage.

Anion exchange columns are used to separate remaining impurities such as Fe and Ti from the samples. The anion chromatography procedure utilises columns filled with AG-1 X8 200-400# anion resin. Prior to loading the samples, the columns were stripped with 10 mL 0.2M HCl, and were conditioned using 8 mL 6M HCl. Al and Be were eluted from each column by loading the 4 mL 6M HCl solution directly from the centrifuge tube. After Al and Be elution, 1 mL of 0.5M H_2SO_4 was added to each sample and the solutions were dried-down on a hotplate at $\sim 90 - 110^\circ\text{C}$. The samples were re-dissolved using 5 - 6 drops of $\sim 2\%$ H_2O_2 and 2 mL 0.04 M H_2SO_4 with traces of H_2O_2 . Where Ti (in the form of $\text{TiO}[\text{H}_2\text{O}_2]^{2+}$) was present the solution turned amber-gold. The samples were dried-down again on a hotplate at $\sim 90 - 110^\circ\text{C}$. The 2 mL 0.04M H_2SO_4 with traces of H_2O_2 was added and dried down repeatedly. At the end of this procedure the samples were either a compact white cake or small syrupy droplets of involatile H_2SO_4 . The final dried cake was re-dissolved in 2 mL 0.04M H_2SO_4 with traces of H_2O_2 and let it stay overnight. The sample is transferred to a cleaned centrifuge tube with 1 mL 0.5M H_2SO_4 and centrifuge for 5 min at 3500 rpm.

Sulphate-based cation chromatography (2 mL 50 WX8 column) was used to remove Ti and elute to Al and Be, separately. The cation chromatography procedure utilises columns filled with AG-50W X8 200-400# cation resin. Prior to loading the samples, the columns were stripped with 9 mL 6M HCl followed by 8 mL 1.2M HCl, then 9 mL 0.2 M H_2SO_4 with traces of 2% H_2O_2 . The sample is loaded from previous centrifuge tube stored as 3 mL H_2SO_4 solution. Ti formed a narrow red-brown band at the top of each column resin bed. The band of Ti was slowly moved down the column by the slow addition of 2 + 6 mL of 0.5M H_2SO_4 containing a trace of $\sim 2\%$ H_2O_2 . For Ti-rich samples (CPA-10F, CPA-10P, CPA-12F and CPA-13F), it was necessary to add a further 1 - 4 mL of 0.5 M H_2SO_4 . The total amount of 12 mL 0.5 M H_2SO_4 should not be exceeded to avoid elution of Be. After the removal of Ti, Be was eluted by draining through 10 mL 1.2M HCl. Al was eluted from the columns by draining through 6 mL of 4.5M HCl and stored in test tubes. If the Be fraction is yellowish-greenish Ti has still to be separated completely. In such a case $\text{TiO}(\text{OH})_2 \times \text{H}_2\text{O}$ is precipitated at $\text{pH} = 4$ after the following procedure. The

Be and Al fraction (10 mL) is reduced on a hotplate to less than 1 mL and transferred to a 15 mL centrifuge tube. 25% aqueous NH_3 (PRIMAR) carefully added until about pH 2 - 2.5 is reached, continued with dropwise addition of 1.5% aq. NH_3 (PRIMAR). The pH should be at least 3.9, but less than 4.2. The precipitate is centrifuged for 6 min at 3500 rpm and the supernatant of each sample is transferred back to its beaker. Then 1 mL pH3 solution (prepared from 250 μL 0.3 M HCl Specified in 30 mL 18 MilliQ water) added twice to each precipitate remained in the centrifuge tubes. The precipitates mix thoroughly and centrifuged again. The supernatant is combined with the respective solution in the beaker. The solution volume in the beaker is reduced to less than 2 mL. If a white precipitate occurs during cooling of the solution or even while the sample is still on the hotplate, NH_4Cl might have formed. If NH_4Cl is present, 1.5 mL 35% HNO_3 are added and evaporated (CPA-9F).

The Be solutions are reduced to 2 mL and left to dry on a hotplate at 100 and 130°C. Once the Be solution has dried-down Be is precipitated as $\text{Be}(\text{OH})_2$ by adding drop-wise 25% NH_3 (aq) solutions until the pH of the Be solutions was brought to 9. After centrifuging for 7 minutes at 3500 - 3900 rpm the samples were decanted and the supernatant was discarded. The samples were rinsed three times with MilliQ water. The hydroxide is dissolved in as little volume of 70% HNO_3 as possible (2 drops from a 1 mL pipette are enough) and transferred to a cleaned and air-dusted quartz crucible. The solution is gradually dried down, starting at about 80°C. After the solution has been dried down: the temperature is increased from 180°C to 250°C. NO_2 is formed and is visible as brown bubbles. The whole drying and decomposition procedure on the hotplate can take 6 - 8 h. The quartz crucible with base and lid is placed into a muffle furnace and heated to 900°C at 8°C/min for 100 min and subsequently cooled down to room temperature. The crucibles are transferred to the AMS building wrapped in Al foil. Each BeO pellet was mixed using a cleaned quartz-spatula with Nb (purity of Nb: 99.99%, Alfa Aesar .325 mesh) and packed into Cu cathodes using press.

After six months of storing the Al aliquots, cosmogenic ^{26}Al was also measured in selected samples from the eluted fraction during cation exchange. The volume was reduced to about 2 mL heated on a hotplate to between 100° and 130°C. $\text{Al}(\text{OH})_3$ has been precipitated by adding 25% NH_3 (aq) PRIMAR drop-wise at pH 8. The solutions were homogenized and centrifuged for 7 minutes at 3500 - 3900 rpm. The precipitates were washed three times until they reached pH 7. $\text{Al}(\text{OH})_3$ was transferred to crucibles using

small drops of 18MilliQ water. Hydroxides were usually dry after 12hrs. After drying the crucibles were capped with their specific lids and transferred to the muffle furnace for conversion to oxides. After oxidation the sample were transferred to AMS building. During pressing 99.95%, Alfa Aesar, 100 mesh Ag (a minimum of 3.3 mg) is mixed with the Al_2O_3 and pressed into targets for AMS measurement.

C.1.3 Purification and Be extraction, Inchie Farm samples

C.1.3.1 Sample purity check

Small aliquots (~ 0.4 g) were separated from each sample and placed into 15 mL Teflon vials. Samples were dissolved in a solution of 5 mL concentrated AR grade HF (48 - 50%) and 5 - 7 drops of 1:1 H_2SO_4 , dried down on a hotplate, and then re-dissolved in 10 mL of 2% HNO_3 . Blank solutions were also prepared and measured alongside the samples. Samples that yielded Al concentrations < 150 ppm were considered to be pure. The results of the AAS measurements are shown in Table C.6

C.1.3.2 Be extraction

The Be extraction procedures described below are largely those described in Child et al. (2000), with modifications by Derek Fabel (University of Glasgow). Aliquots of ~ 15 - 20 g were separated from each sample and placed into 500 mL Teflon FEP bottles, and ~ 0.22 g of Be carrier was added to each bottle (Table C.7). Samples were dissolved in concentrated AR grade HF (~ 5 mL of HF were added for every gram of quartz in each sample bottle; ~ 100 mL of HF was added to the blank bottle). There was a strong initial reaction to the addition of HF. After this subsided the bottles were placed around the edges of a hotplate set on a low temperature ($\sim 50^\circ\text{C}$), swirled occasionally to mix HF down into the dense H_2SiF_6 forming around the quartz grains and left for a couple of days to enable all of the quartz to dissolve. Two small aliquots ($\sim 2\%$ of the solution) were taken from each dissolved sample and prepared for AAS measurement to estimate the stable ^{27}Al concentration by measuring the total Al in the sample solution (parent solution). 1 - 2 drops of 1: 1 H_2SO_4 has been added to each and dried at 90°C - 140°C on the hotplate. The remaining small dot of precipitate of Fe-Al-Be-Ti alkali salt has been dissolved in 5 mL of 5% HNO_3 . Because ^{26}Al has not been measured these aliquots have

Table C.6: Results of the AAS measurements, Inchie Farm.

Sample ID	Reported Al Conc (µg/mL)	Mass Q (g)	Mass Sol'n (g)	Dilution factor	Estimated Al Conc (ppm)	Actual Al Conc (µg/mL)	Al (ppm)
LM-01P	4.213	0.3213	4.8469	15.09	63.55	4.21	68
LM-02P	5.242	0.3507	4.8278	13.77	72.17	5.24	77
LM-03P	6.771	0.3202	4.8435	15.13	102.42	6.77	109
LM-08P	1.506	0.4637	4.8777	10.52	15.84	1.51	17
LM-01M	4.853	0.3519	4.8556	13.8	66.96	4.85	72
LM-01F	8.247	0.3544	4.8181	13.6	112.12	8.25	120
LM-02F	9.584	0.374	4.7779	12.78	122.44	9.58	132
LM-03F	7.707	0.3522	4.8217	13.69	105.5	7.71	113
LM-04F	7.141	0.3193	4.9403	15.47	110.48	7.14	118
LM-05F	8.398	0.3805	4.8257	12.68	106.51	8.4	115
LM-06F	10.878	0.3996	4.8066	12.03	130.85	10.88	142
LM-07F	6.913	0.3198	4.8894	15.29	105.7	6.91	113
LM-08F	7.631	0.3492	4.8295	13.83	105.53	7.63	113
LM-16F	9.626	0.3958	4.938	12.48	120.09	9.63	130
LM-17F	7.785	0.3655	4.9291	13.49	104.99	7.79	113
LM-0901	0.729	0.4514	5.8373	12.93	9.43	0.73	10
LM-0902	3.817	0.3945	4.8841	12.38	47.26	3.82	51
LM-0903	6.958	0.3043	5.2122	17.13	119.19	6.96	126

Blank (3% Nitric) < 0.0003
Drift correction *na*
The samples were analysed using an Atomic Absorption Spectrometer iCE 3000 series with N₂O-C₂H₂ flame parameter.

Table C.7: Sample and carrier masses, Inchie Farm.

Sample ID	Quartz (g)	Be-carrier mass (g)	Al-carrier mass (g)	Be Spike (μg)	$1\sigma\text{Be}$ Spike	Al Spike (μg)	$1\sigma\text{Al}$ Spike
LM01P	24.464	24.464	-	215.7	215.7	-	-
LM02P	19.967	19.967	-	218.1	218.1	-	-
LM03P	20.317	20.317	-	211.4	211.4	-	-
LM08P	21.521	21.521	1.0298	190.4	190.4	1026.7	20.5
LM01M	20.065	20.065	-	215.9	215.9	-	-
LM01F	21.984	21.984	-	236.1	236.1	-	-
LM02F	22.002	22.002	-	214.9	214.9	-	-
LM03F	20.546	20.546	-	225.3	225.3	-	-
LM04F	21.07	21.07	-	220.1	220.1	-	-
LM05F	22.063	22.063	-	222.2	222.2	-	-
LM06F	25.14	25.14	-	219.3	219.3	-	-
LM07F	20.589	20.589	-	220.4	220.4	-	-
LM08F	20.564	20.564	-	221.5	221.5	-	-
LM16F	20.98	20.98	-	218.2	218.2	-	-
LM17F	20.146	20.146	-	220	220	-	-
LM0901	20.499	20.499	0.8129	221	221	810.5	16.2
LM0902	22.288	22.288	-	221.8	221.8	-	-
LM0903	17.521	17.521	-	220.9	220.9	-	-

Be-carrier concentration: 980.4 ± 19.6 ppmAl-carrier concentration: 997 ± 19.9 ppm

been stored.

Once all the quartz had been dissolved, the bottles were removed from the hotplate and cooled to room temperature. Samples were transferred to 500 mL Teflon beakers. After the addition of 2 - 3 mL of 6M HCl and 1 mL of 8M HNO₃ to each beaker, the samples were dried-down on a hotplate at $\sim 130^\circ\text{C}$ - 180°C ($\sim 90^\circ\text{C}$ - 140°C during the night). After drying and cooling to room temperature, the samples were re-dissolved in ~ 2 mL of 6M HCl, and dried-down again on a hotplate at $\sim 90^\circ\text{C}$ - 140°C . The dissolution and dry-down of each sample in 6M HCl was repeated a third time, followed by a final dissolution in ~ 2 mL of 6M HCl. The final solution was typically coloured a deep yellow-green by FeCl³. By the end of the procedure some samples had produced either a fine, powdery white precipitate that does not re-dissolve (i.e., TiO₂) or a dense black substance (i.e., graphite). No Al or Be is co-precipitated with C or Ti and these precipitates were removed by centrifuging prior to anion chromatography. Anion exchange columns are used to separate remaining impurities such as Fe and Ti from the samples. In strong HCl, Fe(III) forms a range of anionic Cl⁻ complexes (FeCl₄⁻, FeCl₅²⁻ and FeCl₆³⁻), which bind tightly to the anion exchange resin. These can be seen as a brown stain in the top few mm

of the resin. Al and Be do not form strong Cl^- complexes and wash through the column as HCl is added. Ti is more problematic; Ti(IV) forms TiCl_6^{2-} , which binds, but some Ti always seems to remain cationic, to form neutral species or to revert to Ti(III), which does not form strong Cl^- complexes. Ti is seldom 100% stripped from the Al plus Be fraction. Al and Be are split and Ti is further removed using cation exchange columns. The anion chromatography procedure utilised columns filled with AG-1 X8 200-400# anion resin. Prior to loading the samples, the columns were stripped with 10 mL 1.2M HCl, and were conditioned using 10 mL 6M HCl. Al and Be were eluted from each column using 6 mL 6M HCl. After Al and Be elution, 1 mL of 0.5M H_2SO_4 was added to each sample and the solutions were dried-down on a hotplate at $\sim 70 - 90^\circ\text{C}$. None of the resulting residue had a yellow-green colour, this indicating that all Fe was removed during anion chromatography. The samples were re-dissolved using 5 - 6 drops of $\sim 2\%$ H_2O_2 and 2 mL MilliQ water containing a trace of 0.5M H_2SO_4 . The samples were dried-down again on a hotplate at $\sim 90 - 140^\circ\text{C}$. The H_2O_2 -MilliQ water addition and dry down was repeated. At the end of this procedure the samples were either a compact white cake or small syrupy droplets of involatile H_2SO_4 . The final dried cake was re-dissolved in 1 - 2 drops of MilliQ water containing a trace of $\sim 2\%$ H_2O_2 and 0.5M H_2SO_4 .

Sulphate-based cation chromatography is used to remove Ti and elute to Al and Be, separately. The cation chromatography procedure utilised columns filled with AG-50W X8 200-400# cation resin. Prior to loading the samples, the columns were stripped with 10 mL 4M HCl followed by 10 mL 1.2M HCl, and were conditioned using 10 mL 0.2M H_2SO_4 (with a trace of $\sim 2\%$ H_2O_2). The samples were loaded onto the columns. Ti formed a narrow red-brown band at the top of each column resin bed. The band of Ti was slowly moved down the column by the slow addition of 8 mL of 0.5M H_2SO_4 containing a trace of $\sim 2\%$ H_2O_2 . After the removal of Ti, Be was eluted by draining through 10 mL 1.2M HCl. Five drops of 8M HNO_3 were added to each Be solution and the samples were left to dry on a hotplate at $\sim 60^\circ\text{C}$. Al was eluted from the columns by draining through 6 mL of 4M HCl.

Once the Be solution has dried-down, the vials were cooled to room temperature and the white residue was redissolved using 2 mL 1% HNO_3 . The samples were transferred to centrifuge tubes and a further 1mL of 1% HNO_3 was added. To precipitate Be as hydroxide, the pH of the Be solutions was brought to 8 using 25% - 50% NH_4OH solutions. After centrifuging for 10 minutes at 3500 rpm the samples were decanted and the supernatant

was discarded. The samples were rinsed with 5 mL MilliQ water and 1 drop of 25% NH_4OH was added to the centrifuge tubes. The samples were dispersed by vortexing and then centrifuged again for 10 minutes at 3500 rpm. The samples were decanted and the supernatant was discarded. The samples were rinsed with MilliQ and NH_4OH three more times.

After hydroxide precipitation, the samples were dried overnight in an oven at $\sim 70^\circ\text{C}$. After drying, the centrifuge tubes were left to cool to room temperature. A set of small quartz crucibles with lids were weighed to 4 decimal places (tare weight). The resulting small pellets of Be hydroxide were transferred to the quartz crucibles (placed into a perspex holder). The crucibles were covered with their quartz lids and the perspex holder was placed into a furnace and baked at 800°C for 2 hours. After cooling to room temperature (~ 15 hours) the quartz crucibles were weighed again and the tare weights were subtracted to obtain the weight of the oxides. Each BeO pellet was mixed with Nb and packed into Cu cathodes for AMS measurement.

C.2 AMS measurements

C.2.1 ^{10}Be AMS measurements

$^{10}\text{Be}/^9\text{Be}$ ratios were measured at the SUERC 5MV NEC Pelletron AMS (Freeman et al. 2007), using NIST 30600 with a nominal value of $^{10}\text{Be}/^9\text{Be} = 3.06 \times 10^{-11}$ (Middleton et al. 1993), 14% higher than the NIST certified value ($^{10}\text{Be}/^9\text{Be} = 2.68 \times 10^{-11}$). The measurements are described in detail in Maden et al. (2007) and Schnabel et al. (2007). The $^{10}\text{Be}/^9\text{Be}$ ratios of the full chemistry procedural blanks prepared with the samples were 4.62×10^{-15} and 4.65×10^{-15} (1σ uncertainty of 1.11×10^{-15}) and 5.57×10^{-15} and 3.27×10^{-15} respectively (1σ uncertainty of 1.6×10^{-15}). This ratio was subtracted from the Be isotope ratios of the samples. Blank-corrected $^{10}\text{Be}/^9\text{Be}$ ratios of the samples ranged from 2.3×10^{-14} to 1.31×10^{-13} and 6.65×10^{-14} to 8.74×10^{-13} for Wester Cameron and Inchie Farm, respectively. Independent repeat measurements of AMS samples were combined as weighted means with the larger of the total statistical error or mean standard error. Final analytical error in concentrations (atoms g^{-1} quartz) are derived from a quadrature sum of the standard mean error in AMS ratio, 2% for AMS standard reproducibility, and 2% in Be spike assay. The results of the AMS measurements

are shown in Tables C.8 and C.9.

Table C.8: Results of the ^{10}Be AMS measurements, Wester Cameron.

Sample ID	AMS ID	Blank ID	$^{10}\text{Be}/^9\text{Be}$ ($\times 10^{-15}$)	$1\sigma^{10}\text{Be}/^9\text{Be}$
CPA-1P	b2812	CB160608 and CB200608	135.97	3.89
CPA-2P	b2807	CB160608 and CB200608	135.58	3.79
CPA-3P	b2805	CB160608 and CB200608	61.41	2.33
CPA-4P	b2802	CB160608 and CB200608	83.95	2.82
CPA-5P	b2818	CB160608 and CB200608	23.41	1.66
CPA-6P	b2817	CB160608 and CB200608	45.96	2.57
CPA-8P	b2815	CB160608 and CB200608	51.4	2.28
CPA-14P	b2814	CB160608 and CB200608	29.01	1.9
CPA-14M	b2826	CB160608 and CB200608	22.02	1.51
CPA-1F	b2808	CB160608 and CB200608	140.05	4.38
CPA-2F	b2806	CB160608 and CB200608	134.83	3.98
CPA-3F	b2803	CB160608 and CB200608	139.15	4.85
CPA-4F	b2801	CB160608 and CB200608	116.06	3.96
CPA-5F	b2800	CB160608 and CB200608	100.1	3.63
CPA-6F	b2825	CB160608 and CB200608	78.89	2.94
CPA-7F	b2824	CB160608 and CB200608	61.73	2.43
CPA-8F	b2820	CB160608 and CB200608	68.15	5.44
CPA-14F	b2819	CB160608 and CB200608	27.86	1.58

$[^{10}\text{Be}/^9\text{Be}]_{\text{CB160608}}: 4.62 \pm 0.98 \times 10^{-15}$

$[^{10}\text{Be}/^9\text{Be}]_{\text{CB200608}}: 4.65 \pm 1.24 \times 10^{-15}$

Isotope ratios were normalised to NIST 30600 using $^{10}\text{Be}/^9\text{Be} = 3.06 \times 10^{-11}$ (Middleton et al. 1993) and using a ^{10}Be half-life of 1.51×10^6 years (Yiou and Raisbeck 1972, Hofmann et al. 1987, Inn et al. 1987).

Average of two blanks used: 4.63×10^{-15} . $^{10}\text{Be}/^9\text{Be}$ ratios are presented before blank correction.

C.2.2 ^{26}Al AMS measurements

The $^{26}\text{Al}/^{27}\text{Al}$ ratios were measured with the 5MV NEC Pelletron accelerator mass spectrometer at SUERC (Freeman et al. 2004) as part of a routine Al run. The procedures for measurement are described in detail in Maden et al. (2007) and Freeman et al. (2007). The spectrometer is set for injection of Al^- , sputtered from the Al_2O_3 target, which is argon gas stripped at a terminal voltage of 4 MV. The high-energy mass spectrometer is set to analyze $^{26}\text{Al}^{3+}$ in a gas ionization detector. Typical ion currents of $^{27}\text{Al}^-$ were 400 nA. $^{27}\text{Al}^{3+}$ was collected in an offset Faraday cup after passing the high-energy magnet and digitized through a charge amplifier. The primary standard Z92-0222, kindly donated by M. Caffee (PRIME Lab, Purdue University) with a nominal $^{26}\text{Al}/^{27}\text{Al}$ ratio of 4.11×10^{-11} was used for normalization. This ratio agreed to better than 1% with the four stan-

Table C.9: Results of the ^{10}Be AMS measurements, Inchie Farm.

Sample ID	AMS ID	Blank ID	$^{10}\text{Be}/^9\text{Be}$ ($\times 10^{-15}$)	$1\sigma^{10}\text{Be}/^9\text{Be}$
LM01P	b4055	CFG1001	72.11	2.72
LM02P	b4056	CFG1001	45.93	2.7
LM03P	b4057	CFG1001	40.21	1.91
LM08P	b4058	CFG1001	26.54	3.29
LM01M	b4059	CFG1001	51.9	2.98
LM01F	b4061	CFG1001	51.78	2.98
LM02F	b4062	CFG1001	53.51	4.93
LM03F	b4063	CFG1001	40.04	2.52
LM04F	b4064	CFG1001	34.45	2.24
LM05F	b4067	CFG1001	35.98	3.19
LM06F	b4068	CFG1001	37.59	2.23
LM07F	b4069	CFG1001	26.64	2.15
LM08F	b4070	CFG1001	24.46	2.52
LM16F	b4071	CFG1001	15.35	2.85
LM17F	b4073	CFG1001	14.31	1.0
LM0901	b4075	CFG1002	35.21	1.8
LM0902	b4076	CFG1002	33.39	2.35
LM0903	b4079	CFG1002	28.37	2.23
$[^{10}\text{Be}/^9\text{Be}]_{\text{CFG1001}}: 5.57 \pm 1.49 \times 10^{-15}$				
$[^{10}\text{Be}/^9\text{Be}]_{\text{CFG1002}}: 3.27 \pm 0.94 \times 10^{-15}$				

See notes for Table C.8.

 $^{10}\text{Be}/^9\text{Be}$ ratios are presented before blank correction.

Table C.10: Results of the ^{26}Al AMS measurements, Wester Cameron.

Sample ID	AMS ID	Blank ID	$^{26}\text{Al}/^{27}\text{Al}$ ($\times 10^{-15}$)	$1\sigma^{26}\text{Al}/^{27}\text{Al}$	^{27}Al ($\times 10^9$ atoms)
CPA1P	a819	CB150908 and CB111208	130.7	8.35	8.79
CPA2P	a818	CB150908 and CB111208	110.72	5.5	8.38
CPA3P	a817	CB150908 and CB111208	132.99	9.98	3.29
CPA4P	a816	CB150908 and CB111208	82.03	4.41	6.2
CPA6P	a814	CB150908 and CB111208	132.52	7.83	2.07
CPA8P	a813	CB150908 and CB111208	79.81	4.67	4.2
CPA14P	a812	CB150908 and CB111208	30.18	4.6	5.8
CPA14M	a811	CB150908 and CB111208	27.22	2.68	2.6
CPA14F	a810	CB150908 and CB111208	26.85	2.66	5.57
$[^{26}\text{Al}/^{27}\text{Al}]_{\text{CB150908}}: 2.22 \pm 0.7 \times 10^{-15}$ $[^{26}\text{Al}/^{27}\text{Al}]_{\text{CB111208}}: 0.4 \pm 0.4 \times 10^{-15}$					

The Al fractions after cation exchange has been used and no carrier has been added.

Average of two blanks used: 1.31×10^{-15} . $^{26}\text{Al}/^{27}\text{Al}$ ratios are presented before blank correction.

dard materials of the highest $^{26}\text{Al}/^{27}\text{Al}$ ratio purchased from Kunihiro Nishiizumi (2002). The ratio of Z92-0222 also agreed to better than 2% with the two standard materials with the lowest $^{26}\text{Al}/^{27}\text{Al}$ ratio (i.e., Al01-5-2 and Al01-5-3). The $^{26}\text{Al}/^{27}\text{Al}$ ratios of the processing blanks prepared with the samples range $^{26}\text{Al}/^{27}\text{Al}$ ratios of the samples ranged from 2.5×10^{-14} to 1.31×10^{-13} . One-sigma uncertainties of the SUERC AMS measurement consist of the uncertainty of the sample measurement, the internal uncertainty of the normalization (reproducibility of the measurements of the primary standard) and the uncertainty of the blank correction. One-sigma uncertainties for the concentrations determined at SUERC include the 1σ uncertainty of the AMS measurement and the 1σ uncertainty of the determination of total Al with ICP-MS (typically between 2.0% and 2.1%, but here 3.5% and 4.5%). The 1σ uncertainties additionally includes 1.5% for the fact that a mineral aliquot was used for the determination of stable ^{27}Al instead of an aliquot from the sample that has been dissolved for ^{26}Al analysis (^{26}Al analysis was not foreseen in the beginning). Carrier solution was not used in these analyses. See Table C.10.

C.2.3 Summary of the cosmogenic ^{10}Be , ^{26}Al and ^{14}C data

The results of the cosmogenic ^{10}Be , ^{26}Al and ^{14}C analyses are summarised in Tables C.11, C.12, C.13, and C.14, below.

Table C.11: *In situ* cosmogenic ^{10}Be and ^{26}Al data for the pit samples, Wester Cameron.

Sample ID	Depth (cm)	Dry Density (g.cm^{-3})	Wet Density (g.cm^{-3})	^{10}Be (at.g^{-1})	$1\sigma^{10}\text{Be}$	^{26}Al (at.g^{-1})	$1\sigma^{26}\text{Al}$
CPA-1P	30-45	0.92	1.34	52570	1932	345000	26000
CPA-2P	45-60	1.65	1.99	52380	1896	278000	17800
CPA-3P	60-75	0.95	1.1	41420	2055	289000	24700
CPA-4P	75-90	1.71	1.96	34460	1487	199000	13600
CPA-5P	90-105	2.16	2.52	24010	2601		
CPA-6P	105-120	1.21	1.41	22710	1604	137000	10500
CPA-8P	135-150	1.74	2.03	14810	857	95400	7430
CPA-14P	225-240	1.67	1.96	8642	800	54400	9290
CPA-14M	225-240	1.67	1.96	11770	1290	51400	6220
CPA-1F	30-45	0.92	1.34	54220	2111	-	-
CPA-2F	45-60	1.65	1.99	52220	1958	-	-
CPA-3F	60-75	0.95	1.1	42170	1774	-	-
CPA-4F	75-90	1.71	1.96	34910	1465	-	-
CPA-5F	90-105	2.16	2.52	29880	1330	-	-
CPA-6F	105-120	1.21	1.41	23560	1104	-	-
CPA-7F	120-135	1.31	1.55	17880	910	-	-
CPA-8F	135-150	1.74	2.03	20060	1800	-	-
CPA-14F	225-240	1.67	1.96	9426	807	52900	6450
Site Latitude 56.00936 degrees (WGS 84)							
Site Longitude -4.4741 degrees (WGS 84)							
Site Elevation 169 m							

Table C.12: *In situ* cosmogenic ^{10}Be data for the pit samples, Inchie Farm.

Sample ID	Depth (cm)	Dry Density (g.cm^{-3})	Wet Density (g.cm^{-3})	^{10}Be (at.g^{-1})	$1\sigma^{10}\text{Be}$
LM-01P	0-15	1.35	1.85	39203	2134
LM-02P	15-30	1.55	1.86	29470	2511
LM-03P	30-45	1.72	1.91	24084	1963
LM-08P	105-120	2.12	2.36	12402	2275
LM-01M	0-15	1.35	1.85	33313	2654
LM-01F	0-15	1.35	1.85	33164	2647
LM-02F	15-30	1.55	1.86	31295	3521
LM-03F	30-45	1.72	1.91	25260	2396
LM-04F	45-60	1.23	1.35	20162	2117
LM-05F	60-75	1.41	1.6	20463	2553
LM-06F	75-90	2.01	2.29	18666	1771
LM-07F	90-105	1.81	2.05	15071	2096
LM-08F	105-120	2.12	2.36	13600	2310
LM-16F	225-240	1.21	1.32	6803	2400
LM-17F	240-255	1.77	1.96	6380	1594
Site Latitude 56.17488 degrees (WGS 84)					
Site Longitude -4.27385 degrees (WGS 84)					
Site Elevation 36 m					

Table C.13: *In situ* cosmogenic ^{14}C data for the pit samples, Wester Cameron.

Sample ID	AMS ID	Sample ID	F value	1 σ	CO ₂ (10 ⁻² mL)	Diluted CO ₂ (mL)	^{14}C (atoms.g ⁻¹)	1 σ	blank % [•]
CPA-1F	G23001	30-45	0.0256	0.0008	12.278	1.002	110027 ^a	7301	26
CPA-2F	G23000	45-60	0.0252	0.0008	13.731	1.001	110670 ^b	7495	24
CPA-3F	G29582	60-75	0.0386	0.0005	19.083	1.001	88629 ^c	14210	60
CPA-4F	G27971	75-90	0.0342	0.0005	15.083	1.002	78210 ^d	5538	61
CPA-5F	G27970	90-105	0.0344	0.0006	15.389	0.993	62646 ^e	14819	68
CPA-6F	G27969	105-120	0.032	0.0005	15.722	0.997	49820 ^f	14181	73
CPA-7F	G29573	120-135	0.0312	0.0005	16.389	0.997	45300 ^g	14168	75
CPA-8F	G22999	135-150	0.0144	0.0007	13.167	1.001	38673 ^h	6989	54
CPA-14P	G29566	225-240	0.0201	0.0004	11.861	0.999	13617 ⁱ	12184	88
Site Latitude 56.00936 degrees (WGS 84)									
Site Longitude -4.4741 degrees (WGS 84)									
Site Elevation 169 m									
a) Corrected for system blanks using the mean of bracketed extraction blank BLK14 and BLK15 value of $1.92 \pm 0.13 \cdot 10^5$ atoms									
b) Corrected for system blanks using the mean of bracketed extraction blank BLK15 and BLK16 value of $1.78 \pm 0.14 \cdot 10^5$ atoms									
c) Corrected for average system blanks of the second furnace (extraction blanks and shielded quartz) using a mean value of $6.76 \pm 0.56 \cdot 10^5$ atoms									
d) Corrected for system blanks using the mean of bracketed extraction blank BLK37 and SHQ12 shielded quartz value of $6.01 \pm 0.29 \cdot 10^5$ atoms									
e) Corrected for average system blanks of the second furnace (extraction blanks and shielded quartz) using a mean value of $6.76 \pm 0.56 \cdot 10^5$ atoms									
f) Corrected for average system blanks of the second furnace (extraction blanks and shielded quartz) using a mean value of $6.76 \pm 0.56 \cdot 10^5$ atoms									
g) Corrected for average system blanks of the second furnace (extraction blanks and shielded quartz) using a mean value of $6.76 \pm 0.56 \cdot 10^5$ atoms									
h) Corrected for system blanks using the mean of bracketed extraction blank BLK16 and BLK17 value of $2.24 \pm 0.16 \cdot 10^5$ atoms									
i) Corrected for average system blanks (extraction blanks and shielded quartz during the whole time of extraction) using a mean value of $5.13 \pm 0.49 \cdot 10^5$ atoms									
• Ratio of system blank ^{14}C to amount of ^{14}C measured in the sample									

Table C.14: *In situ* cosmogenic ^{14}C data for the pit samples, Inchie Farm.

Sample ID	AMS ID	Sample ID	F value	1σ	CO_2 (10^{-2} mL)	Diluted CO_2 (mL)	^{14}C (atoms.g $^{-1}$)	1σ	blank % \bullet
LM-01P	G29584	0-15	0.0291	0.0005	21.111	1.000	78111 ^a	7977	54
LM-01F	G29583	0-15	0.0277	0.0004	11.444	1.000	83973 ^b	7587	48
LM-02F	G29576	15-30	0.027	0.0004	11.083	0.999	63365 ^c	7771	59
LM-03F	G29575	30-45	0.0296	0.0005	12.25	0.999	70885 ^d	8232	59
LM-04F	G29574	45-60	0.0224	0.0004	10.833	0.999	36126 ^e	7985	72
LM-08F	G29572	105-120	0.0212	0.0004	11.389	0.997	34181 ^f	7828	72
LM-17F	G29571	240-255	0.0188	0.0004	11.083	0.999	6280 ^g	12120	94
Site Latitude 56.17488 degrees (WGS 84)									
Site Longitude -4.27385 degrees (WGS 84)									
Site Elevation 36 m									
a) Corrected for system blanks using the mean of bracketed extraction blank BLK39 and BLK40 value of $4.53 \pm 0.10 \cdot 10^5$ atoms									
b) Corrected for system blanks using the mean of bracketed extraction blank BLK40 and BLK41 value of $3.82 \pm 0.10 \cdot 10^5$ atoms									
c) Corrected for system blanks using the mean of bracketed system blank BLK43 and SHQ15 shielded quartz value of $4.64 \pm 0.10 \cdot 10^5$ atoms									
d) Corrected for system blanks using the mean of bracketed system blank BLK42 and SHQ15 shielded quartz value of $5.02 \pm 0.14 \cdot 10^5$ atoms									
e) Corrected for system blanks using the mean of bracketed system blank BLK42 and SHQ14 shielded quartz value of $4.69 \pm 0.13 \cdot 10^5$ atoms									
f) Corrected for system blanks using the mean of bracketed system blank BLK41 and SHQ14 shielded quartz value of $4.42 \pm 0.11 \cdot 10^5$ atoms									
g) Corrected for average system blanks (extraction blanks and shielded quartz during the whole time of extraction using a mean value of $5.13 \pm 0.49 \cdot 10^5$ atoms)									
\bullet Ratio of system blank ^{14}C to amount of ^{14}C measured in the sample									

Appendix D

R Source Code

D.1 Explanation of source code

The Monte Carlo-type analyses presented in this thesis were performed using the statistical package **R** (Ihaka and Gentleman 1996, R Development Core Team 2011). The following is an explanation of the **R** script.

D.1.1 Code dependencies

The reduced- χ^2 plots included in Chapter 5 make use of the package ‘lattice’. This is loaded using:

```
library(lattice)
```

D.1.2 Model constants

All cosmogenic nuclide production parameters are read in as constants specified by the user. Additional constants include the age of the sedimentary deposit and the rate of continuous background erosion both before and after the erosion event.

Attenuation length and material density:

```
Ln    <- 160          #neutron spallation
L1mu  <- 738.6        #slow muons
L2mu  <- 2688         #slow muons
L3mu  <- 4360         #fast muons
```

```
Rho <- 1.82 #average wet density
```

Cosmogenic nuclide specific production parameters:

```
BeP    <- 5.2          #Be-10 production rate
Be1    <- log(2)/1510000 #Be-10 decay constant
BePn   <- 0.9724       #Be-10 production fraction by neutrons
BePmu1 <- 0.0186       #Be-10 production fraction by slow muons1
BePmu2 <- 0.004        #Be-10 production fraction by slow muons2
BePmu3 <- 0.005        #Be-10 production fraction by fast muons

CP     <- 17.7         #C-14 production rate
C1     <- log(2)/5730   #C-14 decay constant
CPn    <- 0.83         #C-14 production fraction by neutrons
CPmu1  <- 0.0691       #C-14 production fraction by slow muons1
```

```
CPmu2 <- 0.0809      #C-14 production fraction by slow muons2
CPmu3 <- 0.02        #C-14 production fraction by fast muons
```

Age of sedimentary deposit and rate of background erosion:

```
TotalTime <- 10500    #age of deposit (years)
EBef <- 0.001         #background erosion rate for before erosion event (cm/yr)
EAft <- 0.001         #background erosion rate for after erosion event (cm/yr)
```

D.1.3 Input/Output routines

All data and results are read in from and written to comma separated (csv) text files. The following segment of code reads in the files holding the measured nuclide concentrations, and creates the files that will store all intermediate model results:

```
Data <- read.csv("Be-data.csv", header = TRUE)

NtotFile      <- file("BeModelled.txt", "w")
RunFile       <- file("BeRun.txt", "w")
MeasuredBeFile <- file("BeMeasured.txt", "w")
BeErrorFile   <- file("BeError.txt", "w")
hFile         <- file("Beh.txt", "w")
tFile         <- file("Bet.txt", "w")

Data <- read.csv("C-data.csv", header = TRUE)

NtotFile      <- file("CModelled.txt", "w")
RunFile       <- file("CRun.txt", "w")
MeasuredCFile <- file("CMeasured.txt", "w")
CErrorFile    <- file("CError.txt", "w")
hFile         <- file("Ch.txt", "w")
tFile         <- file("Ct.txt", "w")
```

D.1.4 Monte Carlo-type simulation

The part of the source code that performs the Monte Carlo-type simulations consists of three loops: one for the magnitude of erosion, one for the timing of erosion, and one for each of the samples in the two cosmogenic nuclide depth-profiles. This segment of the code works as follows: for a series of erosion events with magnitudes taken from 0 to 100 cm at intervals of 10 cm, and timings taken from 0 to the age of the sedimentary deposit (here 10,500 years) at intervals of 100 years, cosmogenic ^{10}Be and ^{14}C concentrations are

calculated for points at a depth equal to those where measured ^{10}Be and ^{14}C values exist. The two nuclides are treated separately, the segment of code for ^{10}Be being:

```
for (hErosion in seq(0,100,10)) {
  for (tErosion in seq(0,10500,100)) {

    for(depth in Data$Depth) {

      Pn      = (BePn * BeP) * exp((-Rho * (depth + EAft*tErosion))/Ln)
      Pmu1    = (BePmu1 * BeP) * exp((-Rho * (depth + EAft*tErosion))/L1mu)
      Pmu2    = (BePmu2 * BeP) * exp((-Rho * (depth + EAft*tErosion))/L2mu)
      Pmu3    = (BePmu3 * BeP) * exp((-Rho * (depth + EAft*tErosion))/L3mu)
      Pnb     = (BePn*BeP) * exp((-Rho * ((depth+hErosion) + EBef*(TotalTime-tErosion)))/Ln)
      Pmu1b   = (BePmu1*BeP) * exp((-Rho * ((depth+hErosion) + EBef*(TotalTime-tErosion)))/L1mu)
      Pmu2b   = (BePmu2*BeP) * exp((-Rho * ((depth+hErosion) + EBef*(TotalTime-tErosion)))/L2mu)
      Pmu3b   = (BePmu3*BeP) * exp((-Rho * ((depth+hErosion) + EBef*(TotalTime-tErosion)))/L3mu)

      N1 = ((Pnb / (Bel + (Rho*EBef/Ln))) * (1-exp(-(Bel+(Rho*EBef/Ln))*(TotalTime-tErosion))))+
            ((Pmu1b / (Bel + (Rho*EBef/L1mu))) * (1-exp(-(Bel+(Rho*EBef/L1mu))*(TotalTime-tErosion))))+
            ((Pmu2b / (Bel + (Rho*EBef/L2mu))) * (1-exp(-(Bel+(Rho*EBef/L2mu))*(TotalTime-tErosion))))+
            ((Pmu3b / (Bel + (Rho*EBef/L3mu))) * (1-exp(-(Bel+(Rho*EBef/L3mu))*(TotalTime-tErosion)))))
      N2 = ((Pn / (Bel + (Rho*EAft/Ln))) * (1-exp(-(Bel+(Rho*EAft/Ln))*tErosion)))+
            ((Pmu1 / (Bel + (Rho*EAft/L1mu))) * (1-exp(-(Bel+(Rho*EAft/L1mu))*tErosion)))+
            ((Pmu2 / (Bel + (Rho*EAft/L2mu))) * (1-exp(-(Bel+(Rho*EAft/L2mu))*tErosion)))+
            ((Pmu3 / (Bel + (Rho*EAft/L3mu))) * (1-exp(-(Bel+(Rho*EAft/L3mu))*tErosion))))

      Ntot = N2 + N1

      write.table(Ntot, file = NtotFile, append = TRUE, row.names = FALSE, col.names = FALSE)
      RunCounter <- paste(toString(hErosion),"666", toString(tErosion), sep="")
      write.table(as.numeric(RunCounter),file = RunFile,
                  append = TRUE, row.names = FALSE, col.names = FALSE)
      write.table(tErosion, file = tFile, append = TRUE, row.names = FALSE, col.names = FALSE)
      write.table(hErosion, file = hFile, append = TRUE, row.names = FALSE, col.names = FALSE)
    }

    for(BeMeasured in Data$Be10) {
      write.table(BeMeasured, file = MeasuredBeFile,
                  append = TRUE, row.names = FALSE, col.names = FALSE)
    }

    for(BeError in Data$dBe10) {
      write.table(BeError, file = BeErrorFile,
                  append = TRUE, row.names = FALSE, col.names = FALSE)
    }
  }
}
}
```

D.1.5 Goodness of fit statistic calculations

The reduced- χ^2 (χ_{red}^2) statistic is used to evaluate how good model results fit the ^{10}Be and ^{14}C data (see Chapter 5 for more details). The segment of code evaluating χ_{red}^2 is given below:

```
BeModelled <- read.csv("BeModelled.txt", header = FALSE)
BeObserved <- read.csv("BeMeasured.txt", header = FALSE)
BeError <- read.csv("BeError.txt", header = FALSE)
BehEr <- read.table("Beh.txt", header = FALSE)
BetEr <- read.table("Bet.txt", header = FALSE)
BeCounter <- read.csv("BeRun.txt", header = FALSE)

CModelled <- read.csv("CModelled.txt", header = FALSE)
CObserved <- read.csv("CMeasured.txt", header = FALSE)
CError <- read.csv("CError.txt", header = FALSE)
ChEr <- read.table("Ch.txt", header = FALSE)
CtEr <- read.table("Ct.txt", header = FALSE)
CCounter <- read.csv("CRun.txt", header = FALSE)

BeGFi = ((BeObserved - BeModelled) / BeError)^2
CGFi = ((CObserved - CModelled) / CError)^2

AllDataBe <- cbind(BeCounter, BehEr, BetEr, BeGFi, deparse.level = 0)
AllDataC <- cbind(CCounter, ChEr, CtEr, CGFi, deparse.level = 0)

BeGF <- tapply(AllDataBe[,4], AllDataBe[,1], FUN = sum)
CGF <- tapply(AllDataC[,4], AllDataC[,1], FUN = sum)

GF = (BeGF+CGF) / (16-2)

Depth <- tapply(AllDataBe[,2], AllDataBe[,1], FUN = mean)
Time <- tapply(AllDataBe[,3], AllDataBe[,1], FUN = mean)

 $\chi_{red}^2$  contour plots are created using the segment of code given below.  $\chi_{red}^2$  values for all
erosion event magnitude and timing pairs are also saved in a text file.

colour.ramp <- colorRampPalette(c("red", "white", "cyan", "blue"), space = "Lab")
contourplot(GF ~ Depth+Time, cuts=100, region = TRUE, col.regions = colour.ramp,
            main="Menteith, Rho = 1.82 g.cm-3",
            xlab="Thickness of material removed (cm)",
            ylab="Timing of event (years BP)")

SortedData <- order(GF, Depth, Time)
Results <- rbind(GF, Depth, Time) [, SortedData]
write.table(Results, file = "Results.txt", row.names = TRUE, col.names = FALSE)
```

Appendix E

Publications

This appendix contains publications to date on work contained within and/or related to the thesis. These publications are:

- (1) **Fülöp, R.-H.**, Naysmith, P., Cook, G.T., Fabel, D., Xu, S. and Bishop, P.: 2010, Update on the performance of the SUERC *in situ* cosmogenic ^{14}C extraction line, *Radiocarbon* **52**, 1288-1294.
- (2) White, D., **Fülöp, R.-H.**, Bishop, P., Mackintosh, A. and Cook, G.T.: 2011, Can *in-situ* cosmogenic ^{14}C be used to assess the influence of clast recycling on exposure dating of ice retreat in Antarctica?, *Quaternary Geochronology* **6**, 289-294.

UPDATE ON THE PERFORMANCE OF THE SUERC *IN SITU* COSMOGENIC ^{14}C EXTRACTION LINE

R H Fülöp^{1,2,3} • P Naysmith² • G T Cook² • D Fabel¹ • S Xu² • P Bishop¹

ABSTRACT. In this paper, we describe improvements to the *in situ* cosmogenic radiocarbon extraction system at SUERC made since 2004, highlighting the factors that potentially control the reduction of analytical variability. We also present new results on system blanks and of measurements of *in situ* ^{14}C in shielded quartz and a surface quartz sample used at the University of Arizona as an *in situ* ^{14}C standard (PP-4). The SUERC *in situ* ^{14}C extraction system was built in 2001 and is based on a combustion technique following the design of the extraction system at the University of Arizona. Our preliminary results suggest that the continuous running of the extraction system and the monitoring of gas collecting time and of the temperature of the cryogenic traps used in the gas cleaning steps are key to maintaining low and stable system blanks. Our latest average system blank is $2.02 \pm 0.23 \times 10^5$ ^{14}C atoms. This is consistent with those recently published by the University of Arizona and ETH *in situ* ^{14}C labs. Measurements of *in situ* ^{14}C concentrations in sample PP-4 yield an average of $3.82 \pm 0.23 \times 10^5$ atoms g^{-1} quartz, again consistent with published values.

INTRODUCTION

Although not yet routinely analyzed, *in situ* cosmogenic radiocarbon (*in situ* ^{14}C) has the potential to be a very versatile tool to geoscientists. First, it has a relatively short half-life (5730 yr), meaning that when compared to the other cosmogenic nuclides, namely, ^3He , ^{10}Be , ^{21}Ne , ^{26}Al , and ^{36}Cl , *in situ* ^{14}C is substantially more sensitive, and so, is particularly useful for dating recent (Holocene) events and identifying rapid changes in erosion rates. Furthermore, *in situ* ^{14}C is produced in quartz, a mineral that is both highly resistant to weathering and common in nature, and so it can be used alongside the routinely measured longer-lived cosmogenic ^{10}Be to resolve complex exposure histories involving burial and/or erosion occurring over the past 25 kyr.

The *in situ* ^{14}C extraction system of Scottish Universities Environmental Research Centre (SUERC) was built in 2001 and is based on the design of the extraction system at the University of Arizona (Lifton et al. 2001; Pigati 2004). The SUERC *in situ* ^{14}C system works by heating purified quartz to 1100 °C in a resistance furnace in the presence of lithium metaborate (LiBO_2) and ultra-high purity oxygen. Any released carbon is oxidized and the resulting CO_2 is cryogenically cleaned, diluted with ^{14}C -free CO_2 , and converted to graphite. The latter is pressed into targets and measured at the SUERC AMS.

Preliminary results on system blanks and CO_2 recovery obtained using the SUERC extraction system have been presented by Naysmith et al. (2004) and Naysmith (2007). In this paper, we describe improvements to the extraction system since 2004, highlighting the factors that potentially control the reduction of analytical variability. We also present new results on system blanks and of measurements of *in situ* ^{14}C in shielded quartz and a surface quartz sample previously analyzed at the University of Arizona (PP-4).

METHODS

Ultrapure quartz was prepared at the University of Glasgow following a modified version of the protocol of Kohl and Nishiizumi (1992). AMS measurements were carried out using the 5MV NEC

¹Geographical and Earth Sciences, University of Glasgow, Glasgow G12 8QQ, Scotland

²Scottish Universities Environmental Research Centre (SUERC), East Kilbride G75 0QF, Scotland.

³Corresponding author. Email: r.fulop@suerc.gla.ac.uk.

Pelletron at SUERC (Freeman et al. 2004). The measurements are described in detail by Maden et al. (2007).

¹⁴C Extraction and Graphitization Procedure

The procedure used here is largely based on that described by Naysmith et al. (2004) with the following notable exceptions: (1) the quartz tube is cleaned more rigorously and handled with utmost care; (2) the gas is collected for an additional 1 hr after the 1100 °C heating step; and (3) the temperature in all cryogenic traps is constantly monitored using a thermocouple and controlled by slowly adding liquid N₂.

The extraction procedure is started by cleaning a 65-cm-long and 41-mm-diameter quartz tube that will hold the alumina (Al₂O₃) sample boat (135 mm × 13 mm width × 17 mm depth). The quartz tube is carefully placed on a surveying tripod fitted with a quartz rod and heated up to >800 °C using a glass blower's torch for several minutes to burn off any surface contamination. After cleaning, the quartz tube is inserted into the mullite (an aluminosilicate ceramic) tube that runs through the furnace (Figure 1). In order to avoid any post-cleaning contamination, the quartz tube is carefully handled using gloves and stainless steel tongs. The Al₂O₃ boat that will hold the sample is cleaned using a jet of compressed air and placed in a separate small furnace for 8 hr at 850 °C in air. The boat is cooled and LiBO₂ is added to the Al₂O₃ boat, which is carefully placed inside the quartz tube that was cleaned earlier. The furnace and recirculating section of the extraction line are pumped until pressure drops to 10⁻⁵ mbar, then the LiBO₂ is degassed in an ultra-high-purity oxygen (UHP O₂) atmosphere at a pressure of 30–40 mbar for 2 hr at 1100 °C. The furnace is allowed to cool overnight to 120 °C before it is opened and the quartz sleeve and boat removed. Five grams of quartz, which have been washed the previous day in 50% HNO₃ solution to remove any surface contamination, are placed in the Al₂O₃ boat, which is then returned to the quartz sleeve and placed back in the furnace; when performing system blank measurements, everything is done in the same way except no quartz is added. Next, the sample undergoes a 2-stage heating process. The furnace and recirculating section are pumped until pressure drops to 10⁻⁵ mbar before heating the furnace to 500 °C in a recirculating UHP O₂ atmosphere of 30–40 mbar for 1 hr. Any CO₂ that is produced at this heating step is considered to be from atmospheric contamination and discarded (cf. Lifton et al. 2001). After the

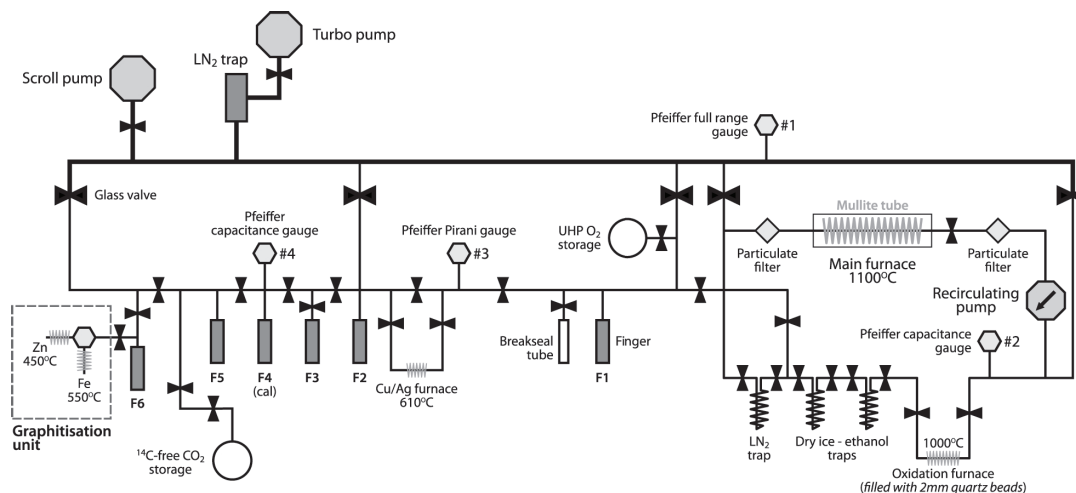


Figure 1 The SUERC vacuum system for extraction, purification, and graphitization of *in situ*-produced ¹⁴C

line is pumped down once again to 10^{-5} mbar, the furnace is reheated to 1100°C for 3 hr in a UHP O_2 atmosphere of 30–40 mbar and the resulting CO_2 —which is considered to be from *in situ* production (Lifton et al. 2001)—is cryogenically trapped using liquid N_2 for an additional 1 hr. Contaminant gases (including SO_x and NO_x species) are removed by passing the resulting CO_2 through an n-pentane/liquid N_2 trap at -130°C and reheating to 610°C in a quartz combustion tube containing Cu/Ag filter for 20 min. Next, the gas is passed through an iso-pentane/liquid N_2 trap at -150°C . The cleaned CO_2 is measured using a highly sensitive capacitance manometer and diluted to approximately 1 mL using ^{14}C -free CO_2 derived from an “infinite age” Icelandic doublespar. The CO_2 is then reduced to graphite using Fe and Zn as described by Slota et al. (1987). The graphite is removed from the vacuum extraction line and pressed into an AMS target.

RESULTS AND DISCUSSION

Results are summarized in Tables 1 and 2 and Figures 2 and 3. Prior to November 2008, all ^{14}C measurements at SUERC were done without monitoring and adjusting the temperature of the cryogenic traps—i.e. the temperature of the n-pentane/liquid N_2 and iso-pentane/liquid N_2 traps was never measured to ensure that they were at the appropriate temperatures of -130°C and -150°C , respectively. Since November 2008, this has changed and now the temperature of the cryogenic traps is monitored using a thermocouple and the slushes are kept at -130°C and -150°C , respectively, by slowly adding liquid LN_2 . In Figures 2 and 3, the switch to temperature-controlled cryogenic cleaning is indicated by vertical dashed lines. All results were calculated according to the procedures set out by Lifton (1997) and Lifton et al. (2001). Graphitization blanks were corrected for as set out by Donahue et al. (1990).

System Blanks and Shielded Quartz

In order to determine the system blanks, we followed the complete procedure described above without placing any quartz in the alumina boat. The shielded quartz was separated from a granite taken from a depth of 1.5 km from Rosemanowes Quarry, SW England (Chen et al. 1996), and so at least theoretically it should be free of any *in situ* ^{14}C .

The system blanks exhibited substantial fluctuations at the beginning of the study, suggesting that the continuous running of the extraction system was slowly cleaning contaminant carbon from the line. These fluctuations in the system blanks were also reduced with longer cleaning of the quartz sleeves and close monitoring of gas collecting time and of the temperature of the cryogenic traps used in the gas cleaning steps (Figure 2). The average of all system blanks that were measured as part of this study is $2.75 \pm 0.77 \times 10^5$ ^{14}C atoms. The average of system blanks that were measured when controlling the temperature of the cryogenic traps is lower, $2.02 \pm 0.23 \times 10^5$ ^{14}C atoms. Both values are comparable with those reported by Miller et al. (2006) and obtained at the University of Arizona using extraction procedures modified from Lifton et al. (2001)—yielding an average system blank of $2.40 \pm 0.12 \times 10^5$ ^{14}C atoms—and from Pigati (2004)—yielding an average system blank of $1.50 \pm 0.10 \times 10^5$ ^{14}C atoms (Figure 2). Our system blanks are also comparable (although slightly lower) with those recently obtained at ETH in Zurich (Hippe et al. 2009).

The shielded quartz results exhibit the same pattern as the system blanks (Figure 2). There is considerable variability in the obtained concentrations, although, similarly to the system blanks, the data suggest that the extraction system is slowly cleaning with use. The 2 data points that were obtained using temperature-controlled cryogenic traps are identical within uncertainty. However, using these 2 data points alone, it is not possible to infer whether controlling the temperature of the traps has any effect on lowering analytical variability, as suggested by the system blanks.

Table 1 Results of the system blank (top) and shielded quartz (bottom) measurements. All uncertainties are at the 1- σ level.

System blanks				
AMS ID	<i>F</i> value	CO ₂ (10 ⁻² mL)	Diluted CO ₂ (mL)	¹⁴ C (10 ⁵ atoms)
G18611	0.0399 ± 0.0004	5.748	0.996	11.51 ± 0.10
G18616	0.0183 ± 0.0003	4.056	1.015	5.39 ± 0.08
G18618	0.0063 ± 0.0002	2.668	0.994	1.83 ± 0.05
G20684	0.0029 ± 0.0002	0.868	1.012	0.84 ± 0.04
G20688	0.0026 ± 0.0002	0.824	0.990	0.74 ± 0.05
G21809	0.0070 ± 0.0003	1.779	1.002	2.04 ± 0.09
G22985	0.0037 ± 0.0004	0.954	1.001	1.08 ± 0.12
G22986	0.0062 ± 0.0005	1.475	1.001	1.79 ± 0.14
G22987	0.0056 ± 0.0004	1.497	1.001	1.62 ± 0.12
G22989	0.0114 ± 0.0005	2.061	0.998	3.28 ± 0.16
G22990	0.0070 ± 0.0004	1.518	1.000	2.03 ± 0.13
G22991	0.0063 ± 0.0005	1.302	1.000	1.82 ± 0.13
G22995	0.0060 ± 0.0005	1.215	1.000	1.74 ± 0.15
G22996	0.0094 ± 0.0006	1.562	1.002	2.74 ± 0.17
Mean value—all:				2.75 ± 0.77
Mean value—temperature control:				2.02 ± 0.23
Shielded quartz				
AMS ID	<i>F</i> value	CO ₂ (10 ⁻² mL)	Diluted CO ₂ (mL)	¹⁴ C ^a (10 ⁴ atoms g ⁻¹)
G18615	0.0399 ± 0.0003	3.991	1.006	14.20 ± 0.18
G18619	0.0063 ± 0.0002	0.954	1.001	2.97 ± 0.11
G20677	0.0017 ± 0.0001	0.694	1.009	1.01 ± 0.08
G20678	0.0020 ± 0.0002	0.716	1.006	1.17 ± 0.09
G20679	0.0061 ± 0.0002	1.302	0.995	3.52 ± 0.10
G22965	0.0074 ± 0.0005	2.256	0.999	4.31 ± 0.28
G22966	0.0065 ± 0.0005	9.284	1.002	3.76 ± 0.28
Mean value—all:				4.42 ± 1.83

^aNot corrected for system blanks.Table 2 Results of the reproducibility measurements (PP-4). All uncertainties are at the 1- σ level.

AMS ID	<i>F</i> value	CO ₂ (10 ⁻² mL)	Diluted CO ₂ (mL)	¹⁴ C (10 ⁵ atoms g ⁻¹)
G20699	0.0717 ± 0.0004	8.633	0.998	3.81 ± 0.29
G20704	0.0647 ± 0.0004	6.551	1.005	3.40 ± 0.29
G20705	0.0589 ± 0.0004	6.182	1.001	3.02 ± 0.29
G21793	0.0753 ± 0.0005	7.592	1.000	4.05 ± 0.30
G21797	0.0724 ± 0.0006	6.941	0.995	3.84 ± 0.30
G21798	0.0718 ± 0.0006	7.072	0.999	3.82 ± 0.30
G22975	0.0828 ± 0.0010	7.896	0.997	4.75 ± 0.10
G22976	0.0665 ± 0.0010	6.573	0.999	3.74 ± 0.09
G22977	0.0722 ± 0.0010	7.245	1.000	3.97 ± 0.09
Mean value:				3.82 ± 0.23

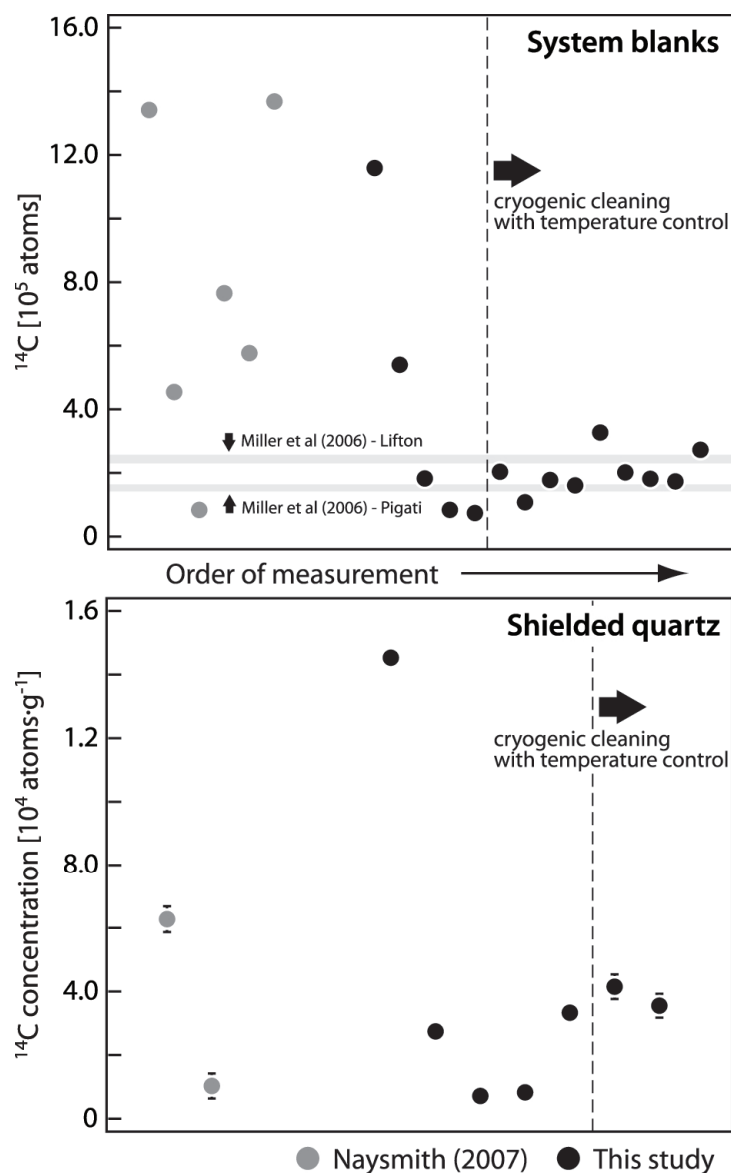


Figure 2 Results of the system blank (top) and shielded quartz (bottom) measurements. Data points plotted to the right of the dashed line were obtained by controlling the temperature of the cryogenic traps using a thermocouple and keeping the slushes at $-130\text{ }^{\circ}\text{C}$ and $-150\text{ }^{\circ}\text{C}$, respectively. The 2 gray horizontal bands on the top graph (labeled Miller et al. (2006)–Lifton and Millet et al. (2006)–Pigati, respectively) show the mean system blank values from Miller et al. (2006). The heights of the rectangles are equal to the uncertainties of the 2 mean blank values.

Reproducibility Measurements

To assess the efficiency of the system, we have also measured *in situ* ^{14}C in a Lake Bonneville shore-line surface quartz sample (PP-4), which has been used as an internal standard at the University of

Arizona (Lifton et al. 2001). Figure 3 compares our results with the latest PP-4 results from the University of Arizona *in situ* ^{14}C lab (Miller et al. 2006).

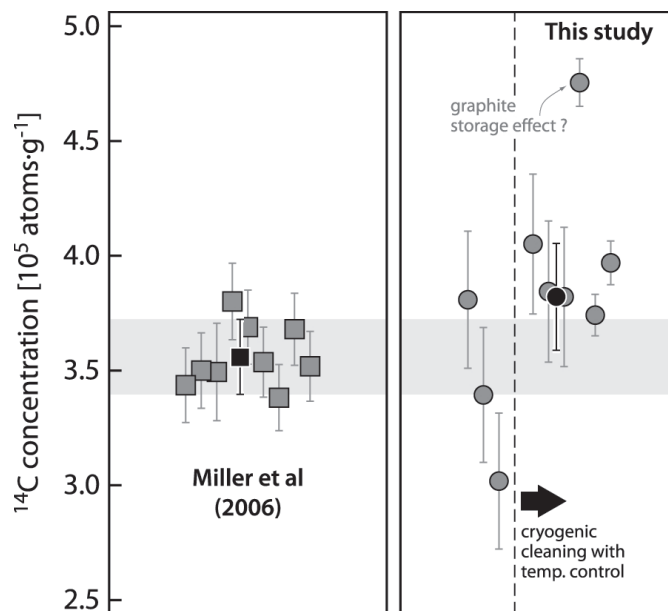


Figure 3 Results of the reproducibility measurements (PP-4). The gray symbols are the individual data points and the black symbols are the mean values obtained for each study. See text and caption of Figure 2 for more details.

Measurements of *in situ* ^{14}C concentrations in sample PP-4 yield an average of $3.82 \pm 0.23 \times 10^5$ atoms g^{-1} quartz. This value is consistent with that obtained by Miller et al (2006), namely $3.56 \pm 0.16 \times 10^5$ atoms g^{-1} . Nonetheless, our measurements show a considerably larger spread than those of Miller et al. (2006). Although we do not yet know what the cause of the variability in our PP-4 results is, we suspect 2 factors. First, some of the PP-4 measurements were carried out prior to monitoring the temperature of the cryogenic traps (Figure 3), and although we do not have an estimate of how much the temperature of the slushes may have fluctuated during these measurements, this fluctuation might have contributed to the observed variability. Second, the graphite obtained from the seventh PP-4 sample was stored for more than 4 months prior to the AMS measurement, and so there is a possibility that this sample has been contaminated. Excluding the seventh PP-4 sample and the ones that were measured prior to controlling the temperature of the cryogenic traps, yields an average that is slightly higher ($3.88 \pm 0.22 \times 10^5$ atoms g^{-1}) but still indistinguishable within uncertainty from that obtained by Miller et al. (2006). Recently, the University of Arizona ^{14}C lab stopped using sample PP-4 for repeatability measurements.

CONCLUSIONS

We have made substantial progress in developing a method for extraction and measurement of *in situ* ^{14}C at SUERC. Our preliminary results suggest that the continuous running of the extraction system and the monitoring of gas collecting time are key to maintaining low and stable system blanks. Our results also suggest that maintaining the temperature of the cryogenic traps constant could also play a role in maintaining system blanks stable. The results of our reproducibility mea-

surements are satisfactory. Our PP-4 measurements are indistinguishable within uncertainty from the latest PP-4 results published by the University of Arizona ^{14}C lab (Miller et al. 2006), but they are somewhat higher and exhibit more spread. All our future reproducibility measurements will be carried out using the new CRONUS *in situ* ^{14}C standard material.

ACKNOWLEDGMENTS

R H F is funded by a University of Glasgow Postgraduate Scholarship and a British Geological Survey—Universities Funding Initiative (BUFI) award. The authors acknowledge the help of the SUERC radiocarbon and AMS laboratories and William McCormack for his support. Nathaniel Lifton and Jeffrey Pigati are acknowledged for thorough and constructive reviews.

REFERENCES

- Chen Y, Zentilli M, Clark A, Farrar E, Grist A, Willis-Richards J. 1996. Geochronological evidence for post-Variscan cooling and uplift of the Carnmenellis granite, SW England. *Journal of the Geological Society* 153(2):191–5.
- Donahue DJ, Linick TW, Jull AJT. 1990. Isotope-ratio and background corrections for accelerator mass spectrometry radiocarbon measurements. *Radiocarbon* 32(2):135–42.
- Freeman S, Bishop P, Bryant C, Cook GT, Fallick A, Harkness D, Metcalfe S, Scott M, Scott R, Summerfield M. 2004. A new environmental sciences AMS laboratory in Scotland. *Nuclear Instruments and Methods in Physics Research B* 223–224:31–4.
- Hippe K, Kober F, Baur H, Ruff M, Wacker L, Wieler R. 2009. The current performance of the *in situ* ^{14}C extraction line at ETH. *Quaternary Geochronology* 4(6): 493–500.
- Kohl C, Nishiizumi K. 1992. Chemical isolation of quartz for measurement of *in-situ*-produced cosmogenic nuclides. *Geochimica et Cosmochimica Acta* 56(9):3583–7.
- Lifton NA. 1997. A new extraction technique and production rate estimate for *in situ* cosmogenic ^{14}C in quartz [PhD dissertation]. Tucson: University of Arizona.
- Lifton NA, Jull AJT, Quade J. 2001. A new extraction technique and production rate estimate for *in situ* cosmogenic ^{14}C in quartz. *Geochimica et Cosmochimica Acta* 65(12):1953–69.
- Maden C, Anastasi P, Dougans D, Freeman S, Kitchen R, Klody G, Schnabel C, Sundquist M, Vanner K, Xu S. 2007. SUERC AMS ion detection. *Nuclear Instruments and Methods in Physics Research B* 259(1): 131–9.
- Miller GH, Briner JP, Lifton NA, Finkel RC. 2006. Limited ice-sheet erosion and complex *in situ* cosmogenic ^{10}Be , ^{26}Al , and ^{14}C on Baffin Island, Arctic Canada. *Quaternary Geochronology* 1(1):74–85.
- Naysmith P, Cook GT, Phillips W, Lifton NA, Anderson R. 2004. Preliminary results for the extraction and measurement of cosmogenic *in situ* ^{14}C from quartz. *Radiocarbon* 46(1):201–6.
- Naysmith P. 2007. Extraction and measurement of cosmogenic *in situ* ^{14}C from quartz. Glasgow: University of Glasgow. 94 p.
- Pigati JS. 2004. Experimental developments and application of carbon-14 and *in situ* cosmogenic nuclide dating techniques [PhD dissertation]. Tucson: University of Arizona.
- Slota Jr PJ, Jull AJT, Linick TW, Toolin LJ. 1987. Preparation of small samples for ^{14}C accelerator targets by catalytic reduction of CO. *Radiocarbon* 29(2):303–6.



Research Paper

Can *in-situ* cosmogenic ^{14}C be used to assess the influence of clast recycling on exposure dating of ice retreat in Antarctica?

Duanne White^{a,*}, Réka-Hajnalka Fülöp^{b,c}, Paul Bishop^b, Andrew Mackintosh^d, Gordon Cook^c

^a Environmental Science, Macquarie University, NSW 2109, Australia

^b School of Geographical and Earth Sciences, University of Glasgow, Glasgow G12 8QQ, United Kingdom

^c Scottish Universities Environmental Research Centre, East Kilbride, G75 0QF, United Kingdom

^d Antarctic Research Centre, Victoria University of Wellington, Wellington, New Zealand

ARTICLE INFO

Article history:

Received 12 November 2010

Received in revised form

15 March 2011

Accepted 21 March 2011

Available online 29 March 2011

Keywords:

Inheritance

Multiple isotope

Glacier

Accelerator mass spectroscopy

ABSTRACT

Cosmogenic nuclide exposure dating of glacial clasts is becoming a common and robust method for reconstructing the history of glaciers and ice sheets. In Antarctica, however, many samples exhibit cosmogenic nuclide 'inheritance' as a result of sediment recycling and exposure to cosmic radiation during previous ice free periods. *In-situ* cosmogenic ^{14}C , in combination with longer lived nuclides such as ^{10}Be , can be used to detect inheritance because the relatively short half-life of ^{14}C means that *in-situ* ^{14}C acquired in exposure during previous interglacials decays away while the sample locality is covered by ice during the subsequent glacial. Measurements of *in-situ* ^{14}C in clasts from the last deglaciation of the Framnes Mountains in East Antarctica provide deglaciation ages that are concordant with existing ^{26}Al and ^{10}Be ages, suggesting that in this area, the younger population of erratics contain limited inheritance.

Crown Copyright © 2011 Published by Elsevier B.V. All rights reserved.

1. Introduction

Knowledge of how the geometry of large ice sheets (such as the East Antarctic Ice Sheet) varied during the late Quaternary is important for several reasons, including understanding past impacts on global sea level and climate (Clark et al., 2009), quantifying satellite observations of present day ice sheet changes, such as in the Gravity Recovery and Climate Experiment (GRACE, e.g. Chen et al., 2008), and testing ice sheet numerical models (Simpson et al., 2009).

Cosmogenic nuclide exposure dating of glacially deposited boulders (erratics) has become the tool of choice for dating retreat of former ice sheets (e.g. Stroeven et al., 2002; Stone et al., 2003; Gollledge et al., 2007; White et al., 2011). The age produced by this technique dates when an erratic was released from the ice and first exposed to cosmic radiation. Thus, the cosmogenic exposure age is directly related to the timing of deposition of glacial sediments by the ice sheet, giving the technique a significant advantage over traditional terrestrial dating methods. For example, organic radiocarbon can usually only provide a limiting age by dating sediments deposited above and/or below the glacial deposits. Moreover,

cosmogenic nuclide exposure dating is applicable to *any* glacial deposit or landform that has not undergone subsequent post-glacial remobilisation. This latter factor is particularly important in areas such as Antarctica where organic material is rare.

A number of second-order geological processes can cause a glacial erratic's exposure age to not correspond to the time since deglaciation. Post-depositional processes such as erosion of the boulder surface, intermittent coverage by ice or snow, and exhumation of an erratic from within sediment, such as a till, will all reduce the erratic's apparent exposure age (Gosse and Phillips, 2001; Putkonen and Swanson, 2003; Schildgen et al., 2005). In much of Antarctica, where erosion and snow accumulation rates are low, these issues can largely be addressed by careful sample selection in the field. A second issue is nuclide inheritance, when erratics are sourced from sediment or bedrock with a non-zero exposure age at the start of the most recent exposure period. For samples with such inheritance, the cosmogenic nuclide content of the boulder overestimates the true age of deglaciation. Erratics with such inheritance can sometimes be identified in the field by their weathered appearance, but they are often indistinguishable from other glacial debris.

The difficulty in identifying previously exposed erratics in the field is reflected in the results obtained from Antarctica. Erratics deposited during a single deposition event or in a single landform commonly display a bimodal cosmogenic exposure age distribution

* Corresponding author. Tel.: +61 429 868 083 (mobile); fax: +61 2 9850 8420.
E-mail addresses: wombly@hotmail.com, duanne.white@mq.edu.au (D. White).

(Brook et al., 1995; Stone et al., 2003; Mackintosh et al., 2007; Todd et al., 2010; White et al., 2011). The younger ages (e.g. Population 1 in Fig. 1) probably provide the best deglaciation timing as those erratic exposure ages generally provide consistent age–altitude (i.e. stratigraphic) trends and have concordant ages when multiple nuclides (e.g. ^{10}Be and ^{26}Al) are measured. Conversely, the older population usually has no stratigraphic age trend and often has a significant proportion of clasts with discordant multiple nuclide ages (e.g. Population 2 in Fig. 1). Nonetheless, the possibility of nuclide inheritance in the samples that provide apparently ‘correct’ exposure ages remains. The effect of clast recycling has to-date been addressed by analysing a large number of boulders from each deposit and assuming that the youngest age reflects the true age of the moraine (Stone et al., 2003). This approach is problematic for two reasons. Firstly, it assumes that none of the analysed samples has been affected by the post-depositional processes noted above that reduce exposure ages by shielding the sampled surface from cosmic radiation during part of the exposure period. Secondly, the approach of selecting the youngest erratic exposure ages as the age of deglaciation assumes that the youngest exposure age at each site is completely free of inherited nuclides.

Complex and repeated exposure is conventionally examined using multiple cosmogenic nuclides (Lal, 1991), but all of the routinely measured *in-situ* cosmogenic nuclides are either stable (e.g. ^{21}Ne) or have long half-lives $>10^5$ yrs (e.g. ^{26}Al , ^{10}Be or ^{36}Cl). The period of time (10's kyr or less) for an ice sheet to erode and redeposit older, pre-existing glacial deposits is too short for the radioactive decay necessary to ‘reset’ to zero the inherited cosmogenic nuclide concentration of these long-lived nuclides, or even to enable the application of multiple nuclide techniques using the burial dating approach. Recent technological and methodological advances in the analysis of *in-situ* ^{14}C (Lifton et al., 2001; Yokoyama et al., 2004; Naysmith et al., 2004; Pigati, 2004; Hippe et al., 2009; Fülöp et al., 2010), which has a half-life of ~ 5.7 kyr, mean that it is now theoretically feasible to detect even short periods of burial by ice (Fig. 2).

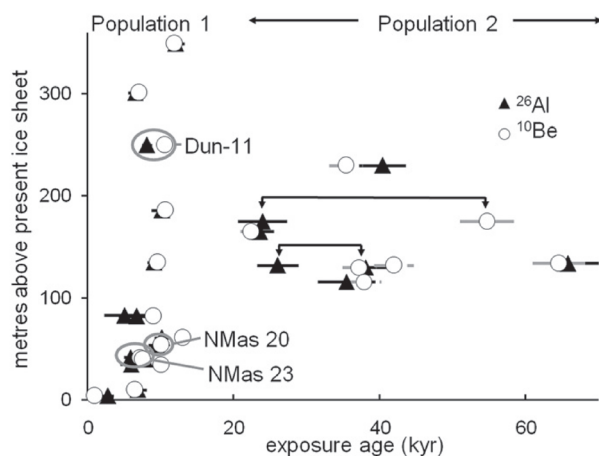


Fig. 1. ^{10}Be and ^{26}Al exposure ages from erratics in the Framnes Mountains, East Antarctica, plotted against the height of the sample above the nearest ice margin (after Mackintosh et al., 2007). The results reported here aim to test the assumption that Population 1 contains erratics that provide accurate (inheritance free) exposure (deglaciation) ages. Those in Population 2 have complex exposure histories, as indicated by the wide range in ages at any given elevation and the divergent ^{26}Al and ^{10}Be ages in a subset of these erratics (denoted by arrowed lines). The divergent ages in Population 2 can only be produced by a period of exposure to cosmic radiation followed by an extended period (>400 ka) of burial by ice (>10 m thick) or sediment (>2 m thick). Samples analysed using *in-situ* ^{14}C in this study are circled in grey.

In this study, we present results from samples from Population 1 in the Framnes Mountains, analysed for *in-situ* ^{14}C , ^{10}Be and ^{26}Al . We use these data, in combination with numerical modelling, to test the efficacy of this technique for determining inheritance in Antarctic erratics.

2. Methods

To test the multiple nuclide technique, we selected three samples (Fig. 3) from the younger population in Fig. 1 for *in-situ* ^{14}C analysis. These samples were collected during 2001/02, from two separate mountain ranges (David and Masson; Fig. 4) and are representative of the other eleven samples in this population, spanning the ^{10}Be age range of the younger population.

Nmas-23 was sampled at approximately 100 m above the modern ice sheet margin, at the same altitude as a distinct moraine. Nmas-23 has a weighted mean ^{10}Be and ^{26}Al age of 7.0 ± 0.6 ka, which is one of the youngest in the population. The presence of some till at the site indicates that this age might be affected by burial and be a few thousand years too young. Nmas-20 is much closer to the present ice edge and in a stratigraphic position below (younger than) that of Nmas-23, but has a mean ^{10}Be and ^{26}Al age of 10.0 ± 0.8 ka, which may indicate nuclide inheritance equivalent to a few thousand years of prior exposure. Dun-11 was sampled on a bedrock spur ~ 270 m above the present-day ice sheet. The mean ^{10}Be and ^{26}Al age of 9.6 ± 0.8 for Dun-11 is comparable to an age for a boulder in a similar stratigraphic position in the Central Masson Range.

Each *in-situ* ^{14}C analysis was completed on a separate, 5 g subsample of the purified, homogenised quartz used to measure ^{10}Be and ^{26}Al . *In-situ* ^{14}C analyses were carried out at the Scottish Universities Environmental Research Centre (SUERC) using an extraction system based on the design of Lifton et al. (2001). The system and extraction procedure are described in detail by Naysmith et al. (2004) and Fülöp et al. (2010).

Sample reproducibility, and the efficiency of the extraction system were tested using a Lake Bonneville shoreline surface quartz sample, which has been used as an internal standard at the University of Arizona (sample PP-4, Lifton et al., 2001). Long-term measurements of *in-situ* ^{14}C concentrations in sample PP-4 at SUERC yield an average of $3.82 \pm 0.23 \times 10^5$ atoms/g quartz. This value is consistent with that obtained at the University of Arizona by Miller et al. (2006), namely $3.56 \pm 0.16 \times 10^5$ atoms/g quartz. Samples of PP-4 measured before (G22976) and after (G22977) the Framnes Mountains samples yielded values of 3.74 ± 0.09 and 3.97 ± 0.09 atoms/g quartz respectively (Fülöp et al., 2010).

Contamination from environmental ^{14}C was assessed using both shielded quartz (before and after each batch) and system blanks (i.e. full procedural blanks, conducted after each unknown) as part of the standard quality control procedures at SUERC (Fülöp et al., 2010).

Long-term measurements for shielded quartz (which effectively should not contain any *in-situ* ^{14}C) resulted in mean values of $4.42 \pm 1.83 \times 10^4$ ^{14}C atoms/g, while those for system blanks were $2.75 \pm 0.77 \times 10^5$ ^{14}C atoms. The average of system blanks using the careful cleaning and monitoring conducted in this study was $2.02 \pm 0.23 \times 10^5$ ^{14}C (Fülöp et al., 2010). The latter value is comparable to results obtained by Miller et al. (2006; $2.40 \pm 0.12 \times 10^5$ ^{14}C atoms) and from Pigati (2004; $1.50 \pm 0.10 \times 10^5$ ^{14}C atoms). Our system blanks are also comparable with those recently obtained at ETH in Zurich (Hippe et al., 2009). All results were calculated according to the procedures set out by Lifton (1997) and Lifton et al. (2001). Graphitization blanks were corrected for as set out by Donahue et al. (1990).

The system blanks (samples G22985 to G22989 in Fülöp et al., 2010) run before and after each unknown provided ^{14}C

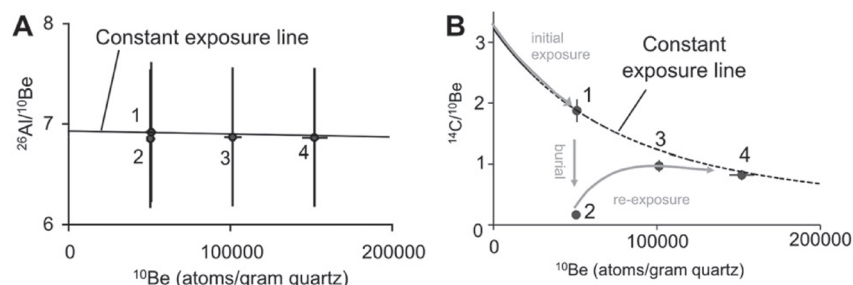


Fig. 2. Modelled cosmogenic nuclide concentrations following the sequence 1) exposure for 10 kyr 2) burial by ice for 20 kyr, 3) re-exposure for 10 kyr, 4) re-exposure for a further 10 kyr. Nuclide concentrations are modelled using production rates for an unshielded surface at sea level and high latitude. ^{10}Be , ^{26}Al and ^{14}C half lives are modelled at 1380, 700 and 5.73 kyr respectively. Short periods of burial are only observable using both ^{14}C and ^{10}Be (panel B), as indicated by the hypothetical “samples” plotting below the constant exposure line (dotted). Note that the burial signal in the ^{26}Al – ^{10}Be system (panel A) is obscured by the 10% error bars (which represent uncertainties in the production rate and measurement of nuclide concentrations). In the ^{14}C – ^{10}Be system that burial signal is preserved for up to ~20 kyr following re-exposure.

concentrations up to an order of magnitude less ^{14}C than the sample concentrations. The sample blank (i.e. the value subtracted from the measured ^{14}C concentration to obtain the ^{14}C concentration listed in the right hand column of Table 1) was the average of the system blanks measured before and after each unknown. Sample Nmas-23 was run between the blanks G22987 and G22989, Nmas-20 was blanks G22985 and G22986, Dun-11 the blanks G22986 and G22987 reported in Fülöp et al. (2010).

Accelerator Mass Spectroscopy (AMS) measurements were carried out using the 5 MV NEC Pelletron accelerator mass spectrometer at SUERC (Freeman et al., 2004; Maden et al., 2007). Uncertainties (1σ) for ^{14}C ages include 1–2% for AMS $^{14}\text{C}/^{13}\text{C}$ ratios, and 3–6% for blank correction.

We have recalculated the ^{10}Be and ^{26}Al ages and nuclide concentrations presented by Mackintosh et al. (2007) using online CRONUS calculator (V2.2; Balco et al., 2008) to reflect recent corrections to the ^{10}Be half life and improved production rate calibrations. The recalculation applied the Lal (1991)/Stone (2000) latitude and altitude scaling model, rock densities of 2.7 g/cm^3 , zero erosion and topographic and thickness shielding corrections listed in Mackintosh et al. (2007). *In-situ* ^{14}C ages were calculated using a sea level-high

latitude production rate of 15.5 at/g/yr (Miller et al., 2006), scaled using the same scaling factors as for ^{10}Be and ^{26}Al described above, and a ^{14}C half life of 5730 years.

We note that more recent, well-constrained ^{10}Be production rate calibrations from north-eastern America (Balco et al., 2009), and New Zealand (Putnam et al., 2010) suggest production rates that are lower than the Balco et al. (2008) global dataset by ~10%. Conversely, an expanded *in-situ* ^{14}C calibration sample dataset that includes further Bonneville samples and two new sites in Scotland (Dugan et al., 2008) suggests global production rates 2% higher than the Miller et al. value derived from Bonneville alone. If the newer datasets are more representative of the true production rate, then the $^{14}\text{C}/^{10}\text{Be}$ production rate ratio will be 10–15% lower than the currently accepted values from Balco et al. (2008) and Miller et al. (2006). The uncertainties quoted for ages in the text include production rate uncertainties (1σ) of 9% for ^{10}Be and ^{26}Al (Balco et al., 2008) and 2% for *in-situ* ^{14}C (Miller et al., 2006). Thus, our quoted uncertainties reflect the uncertainty in the production rate, but we acknowledge that the true values may well be at the lower end of our one-sigma confidence intervals, and discuss the potential effect of these uncertainties on our results where applicable.

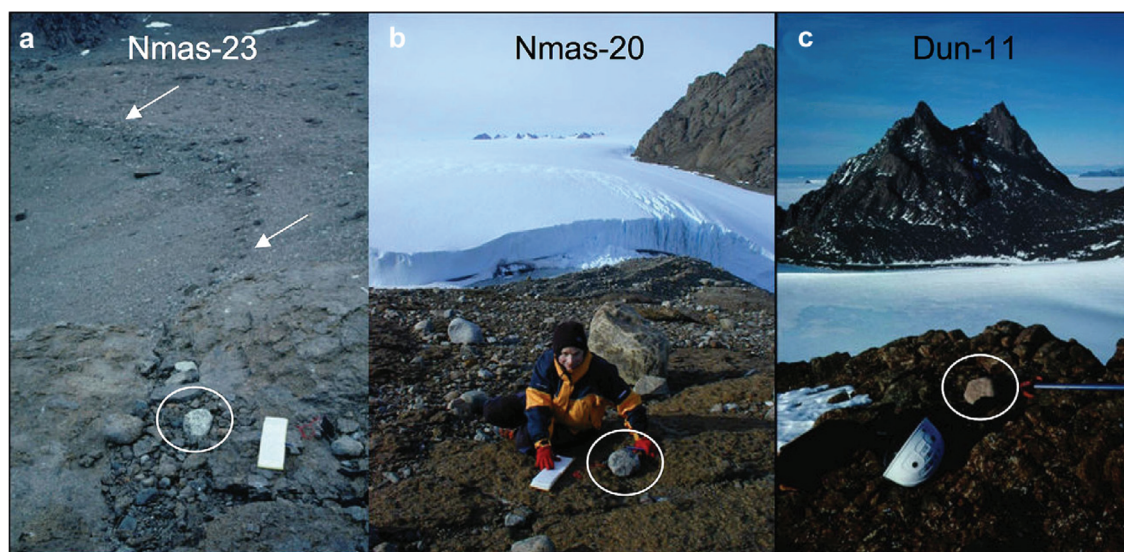


Fig. 3. Samples Nmas-23 (a), Nmas-20 (b) and Dun-11 (c). Nmas-23 is a $15 \times 15 \times 15 \text{ cm}$ pegmatitic granite gneiss clast from a thin till layer on a bedrock ridge in line with a moraine (arrows), ~100 m above the modern glacier margin. Nmas-20 is a $30 \times 30 \times 30 \text{ cm}$ pegmatitic granite gneiss clast from a bedrock spur in an ice free valley. Dun-11 is a $15 \times 15 \times 10 \text{ cm}$ metasedimentary clast sampled from a bedrock spur ~270 m from the modern glacier.

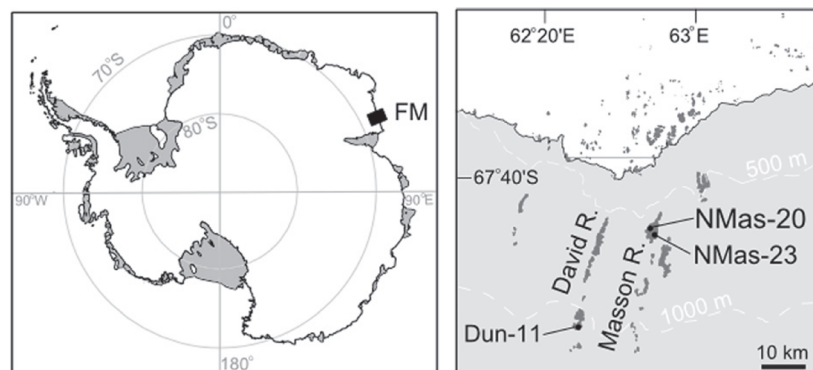


Fig. 4. Location of the Framnes Mountains, and samples analysed for *in-situ* ^{14}C in this study. The black rectangle highlights the area of the Framnes Mountains (FM), shown in detail in the right panel. Ice shelves are shown in grey on left panel. In right panel, ice free areas shown in dark grey, ocean in white and the ice sheet in light grey.

The sensitivity of the $^{10}\text{Be}/^{14}\text{C}$ ratio to a range of potential exposure histories was tested using a three stage model. In this model, the erratic is subjected to an initial exposure, a period of burial, and subsequent re-exposure (Fig. 5). We assume that the transition from exposure to burial is instantaneous, and that the erratic is buried by enough ice that production effectively ceases. The results in this study are based on the currently accepted production rates (i.e. Miller et al., 2006; Balco et al., 2008). The model simulates an exposure history experienced by an erratic which was exposed during a previous lowstand of the ice sheet, was subsequently buried by the cold-based ice that occupied this area during the last (local) glacial maximum (Mackintosh et al., 2007), and was re-exposed during ice retreat in the late Pleistocene or Holocene. The model should also represent the more complex exposure histories that an erratic in the Framnes Mountains may have experienced, provided the latest period of burial (i.e. ice advance) began earlier than ~ 20 ka BP, as most of the accumulated ^{14}C will have since decayed. All the currently available evidence indicates that LGM ice advance in the region occurred prior to this time (e.g. Domack et al., 1998; Wright et al., 2008).

3. Results

Two of the three erratics from the Framnes Mountains have *in-situ* ^{14}C ages that are concordant at the 1σ confidence level with the previously measured ^{10}Be and ^{26}Al ages (Tables 1 and 2), and all three are concordant at 2σ . As such, they are consistent with a single, continuous period of exposure since their exhumation from the ice sheet (Fig. 5). Had we chosen to use ^{10}Be production rates similar to the sea level-high latitude calibrations of Balco et al. (2009)/Putnam et al. (2010), and Dugan et al. (2008), samples Nmas-23 and Dun-11 would plot closer to the constant exposure line, while Nmas-20 would plot further into the burial field, although at the 2σ confidence level it would still be consistent with a constant exposure history.

The results from the three-step model output (Fig. 5) provide important information for the interpretation of the three Framnes Mountains samples. For the range of likely ice advance/retreat scenarios, the $^{14}\text{C}/^{10}\text{Be}$ or $^{14}\text{C}/^{26}\text{Al}$ ratio is most sensitive to the duration of the two periods of exposure, and relatively insensitive to the duration of burial, provided the period of burial was lengthy enough (10 ka is sufficient) to produce significant decay of the ^{14}C produced during the initial period of exposure. For a constant burial duration, the $^{14}\text{C}/^{10}\text{Be}$ or $^{14}\text{C}/^{26}\text{Al}$ ratio is lower for longer periods of initial exposure, and shorter periods of re-exposure. Thus, it is much easier to detect inheritance in erratics that have a substantial initial exposure, and have been re-exposed for only a short period of time. Given the uncertainties in the ^{10}Be , ^{26}Al and ^{14}C measurements and production rates, it will be impossible to positively identify a period of burial in an erratic that has been re-exposed for longer than ~ 15 ka. Similarly, detecting burial in a sample that was initially exposed for only ~ 1 ka will be impossible unless the period of re-exposure is less than ~ 2 ka.

Comparing the results from the Framnes Mountains samples with the model output, it is clear that the uncertainties in the $^{14}\text{C}/^{10}\text{Be}$ ratio reduce our ability to be certain that the erratics are free of inherited ^{10}Be . While Nmas-20 is consistent at the 2σ confidence level with a simple exposure history, it is also consistent with any complex exposure history that produced an inheritance (i.e. initial exposure) of less than ~ 4 ka ^{10}Be exposure. Dun-11 or Nmas-23 would also be consistent with a complex exposure history that produces less than ~ 1 ka of ^{10}Be inheritance. Using the alternative (i.e. Balco et al., 2009/Putnam et al., 2010 and Dugan et al., 2008) ^{10}Be production rates, permissible inheritance of Nmas-20 increases to ~ 5 ka, and Dun-11 and Nmas-23 to ~ 2 ka.

4. Discussion

The two pathways through which a subglacial erratic deposited in the Framnes Mountains could obtain exposure prior to

Table 1

In-situ ^{14}C measurement data. All uncertainties represent 1σ confidence intervals. Mackintosh et al. (2007) give further information on the sample locations. Scaling factors calculated using the Lal (1991)/Stone (2000) latitude and altitude scaling model, and topographic and atmospheric shielding corrections listed in Mackintosh et al. (2007). F = the measured fraction of the modern $^{14}\text{C}/^{12}\text{C}$ ratio, following AMS background correction. System blanks for each sample were calculated from the average of the full procedural blank conducted before and after the unknown was run, with blank uncertainties representing the average measurement uncertainty for the blanks measured before and after each unknown.

Sample	Location	Altitude m a.s.l.	Scaling Factor	Sample mass (g)	F %	Sample system blank atoms $\times 10^3$	^{14}C at/g qtz $\times 10^3$
Nmas-23	Mt Ward	642	2.025	4.9992	3.85 ± 0.08	244 ± 32	175 ± 17
Nmas-20	Mt Ward	635	2.177	5.0029	3.73 ± 0.08	143 ± 23	190 ± 19
Dun-11	Dunlop peak	1230	3.727	5.0017	7.37 ± 0.10	169 ± 36	399 ± 40

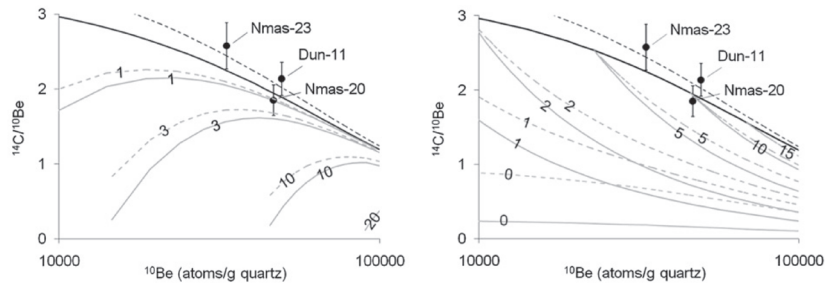


Fig. 5. ^{10}Be and ^{14}C multiple isotope plot, normalised to sea level-high latitude using the scaling factors of Lal (1991) and Stone (2000). Samples from the Framnes Mountains are shown with 1σ uncertainties, calculated to include uncertainties in both the measurement and nuclide production rate. Samples that have had a continuous, simple exposure history plot on the thick black line using presently accepted combined muon and spallation production rates of 4.6 and 15.5 at/g/yr for ^{10}Be and ^{14}C respectively (Miller et al., 2006; Balco et al., 2008), or the thin dashed line using the rates of 4.1 and 15.8 suggested by Balco et al. (2009) and Dugan et al. (2008). Light grey lines indicate isolines of equal initial exposure (left) or re-exposure (right) for the three-step complex exposure histories (initial exposure, burial, re-exposure). The duration of initial exposure (left panel), or re-exposure (i.e. the length of time since the last deglaciation, right panel), in ka, is indicated by black numbers. Solid lines represent a burial period of 20 ka, dashed lines 10 ka. In the left panel, it is clear that increasing durations of initial exposure produce lower $^{14}\text{C}/^{10}\text{Be}$ ratios, making the complex exposure history (and thus inheritance) easier to detect. Conversely, increasing durations of re-exposure increase the $^{14}\text{C}/^{10}\text{Be}$ ratio and tend to push the sample back toward the constant exposure line, to the point where for re-exposure periods of >15 ka, the complex exposure history would be undetectable given present measurement and production rate uncertainties. See Fig. 2B for an example of how one such history traces on this type of plot.

deposition on the mountains are through recycling of erratics deposited during a prior glacial lowstand and subglacial erosion of bedrock with a non-zero nuclide concentration. We consider that both these pathways are likely to produce a bimodal population erratics with either substantial (i.e. >10 ka equivalent) or very little inheritance, with limited quantities of erratics with inheritance of ~ 1 –5 ka.

Erratics deposited on the mountainside during prior glacial recessions will have received exposure during the subsequent glacial lowstands. Our understanding of the history of ice sheet advance and retreat in Antarctica during the last few glacial cycles (e.g. Pollard and Deconto, 2009; Wright et al., 2008) indicates that interglacial periods, and thus glacial lowstands, are likely to be significantly longer than 1–4 ka in duration. Thus, erratics recycled from previous glacial cycles are more likely to contain tens of thousands of years prior exposure, rather than the 1–4 ka that is permissible given the $^{14}\text{C}/^{10}\text{Be}$ ratios of the measured samples. Indeed, the older population of erratics (Population 2 in Fig. 1) contains samples with exactly this style of inheritance, and we suggest that this is the most likely mode of inheritance for Population 2. An equivalent of a few thousand years of ^{10}Be or ^{26}Al accumulation could be produced by erratics buried in moraines or other glacial sediment sequences during a more extended exposure period (e.g. 20 ka), but thick accumulations of glacial sediment are very rare in the Framnes Mountains. The small

moraine in Fig. 3 displays the only such occurrence of thick glacial sediments above the present ice sheet surface. Further, the lack of samples with ^{10}Be or ^{26}Al exposure ages between 12 and 22 ka (i.e. with an amount of inheritance equivalent to <10 ka of exposure) suggests a bimodal population of inheritance, which would not be expected if the erratics were recycled from sediment deposits such as the moraine in Fig. 3.

Glacially abraded bedrock currently exposed above the ice sheet in other areas of Antarctica have provided ages ranging from zero to many thousand years (Sugden et al., 2005), including the 2–5 ka of inheritance that is feasible in the Framnes Mountains samples. The area above the present day ice sheet is not a potential source in the Framnes Mountains, as the lithology of the measured erratics is not currently exposed anywhere within, or upglacier of the sample sites (Mackintosh et al., 2007). Erosion of bedrock currently underneath the ice sheet is feasible, but the areas of the ice sheet eroding the fastest, and therefore the source of the most subglacial erratics lie in the topographical lows least likely to have been exposed (Jamieson et al., 2010). We consider that these deeply buried, fast eroding areas are the most likely source of erratics with little to no inheritance. Conversely, the areas close to the ice surface that are most likely to have nuclide concentrations with significant inheritance are also those with the lowest erosion rates, so produce the fewest erratics.

Based on this consideration of the potential pathways for generating inheritance in subglacial erratics, we suggest that in a statistical sense, Population 1 in the Framnes Mountains (i.e. the population with inheritance less than the ~ 3 –5 ka currently detectable using the $^{14}\text{C}/^{10}\text{Be}$ ratios) will be strongly skewed toward values of zero inheritance. We interpret the two samples (Nmas-23 and Dun-11) with $^{14}\text{C}/^{10}\text{Be}$ ratios most consistent with a continuous exposure history as likely being inheritance free. While the concordant ^{10}Be and ^{14}C ages for Nmas-20 (at 2σ) suggests that it may also be inheritance free, it does have a relatively low $^{14}\text{C}/^{10}\text{Be}$ ratio, indicating that it may contain a few ka of inheritance. A few ka of inheritance for Nmas-20 would be consistent with its relatively old ^{10}Be age, despite being located close to the present ice margin, where other nearby samples have provided ^{10}Be ages ~ 3 ka younger (Mackintosh et al., 2007).

5. Conclusions

The results presented in this study indicate that measurement of *in-situ* ^{14}C in combination with longer lived isotopes such as ^{10}Be in

Table 2

Cosmogenic nuclide exposure ages. ^{10}Be and ^{26}Al data after Mackintosh et al. (2007), recalculated using new ^{10}Be half lives and production rates of the CRONUS online calculator, V2.2 using the Lal/Stone time invariant scaling model (Balco et al., 2008). ^{10}Be and ^{26}Al ages are reported with the global production rates of both Balco et al. (2008) and Putnam et al. (2010). All uncertainties represent 1σ confidence intervals. The different uncertainties for the upper and lower bounds on the *in-situ* ^{14}C ages are due to the increasing influence of radioactive decay on the *in-situ* ^{14}C concentrations with time. The ^{26}Al and ^{10}Be ages are not thus affected due to their much longer half lives.

Sample	^{14}C age (ka)	^{10}Be age (ka)		^{26}Al age (ka)	
		Balco et al., 2008	Putnam et al., 2010	Balco et al., 2008	Putnam et al., 2010
Nmas-23	9.2 \pm 1.0 –0.8	7.3 \pm 0.7	8.5 \pm 0.4	5.8 \pm 1.1	6.7 \pm 1.2
Nmas-20	9.2 \pm 1.0 –0.8	10.3 \pm 1.0	12.0 \pm 0.5	9.0 \pm 1.5	10.5 \pm 1.6
Dun-11	14.4 \pm 1.6 –1.3	10.9 \pm 1.0	12.8 \pm 0.5	8.2 \pm 0.9	9.6 \pm 0.7

glacial erratics has the potential to delineate short, but complex exposure histories in Antarctica. Further, the technique has reached a stage of development where even a few thousand years of burial is observable with this isotope pair, although the sensitivity of the isotope pair to prior burial reduces with the duration of subsequent (i.e. more recent) exposure. For samples exposed during the Holocene or latest Pleistocene, the technique can discriminate between individual samples with a continuous exposure history and those with greater than ~ 3 ka inherited ^{10}Be .

At present, the two largest uncertainties in the identification of inheritance using the $^{10}\text{Be}/^{14}\text{C}$ isotope pair are the uncertainty in the ^{14}C measurement and the uncertainty in the production rates of these two isotopes. Improvements in both these uncertainties are required to improve our ability to detect periods of inheritance of less than ~ 3 ka in an individual erratic that was last released from the ice during the early Holocene. Measuring multiple replicates of the same sample or multiple samples in a population will aid in the discrimination of significant outliers. However, until uncertainty in production rates is decreased, measuring numerous sample replicates is unlikely to improve the resolution of the technique.

Fortunately, variability in production rate uncertainties across Antarctica is likely to be relatively limited because the continent's high latitude position means that variations in the geomagnetic field have limited impact on the production rate. Thus, a single high quality production rate calibration site has the potential to provide a significant improvement in our ability to detect inheritance in Antarctic erratic and improve chronologies of glacial retreat in this important region.

Acknowledgements

R-HF is funded by a University of Glasgow Postgraduate Scholarship and a British Geological Survey – Universities Funding Initiative (BUFI) award. SUERC is supported by the Scottish Universities Consortium. *In-situ* ^{14}C samples were analysed with the assistance of an Australian Academy of Science. Samples were collected with support from the Australian Antarctic Division (AAS1332 & AAS1071) and the Australian Research Council (DP0556728). Initial sample processing was funded by AINSE (AINGRA03048). We also thank B. Wagner and two anonymous reviewers for comments on a previous version of this manuscript.

Editorial handling by: Dider Bourlès

References

- Balco, G., Stone, J., Lifton, N., Dunai, T., 2008. A simple, internally consistent, and easily accessible means of calculating surface exposure ages and erosion rates from Be-10 and Al-26 measurements. *Quaternary Geochronology* 3, 174–195.
- Balco, G., Briner, J., Finkel, R.C., Rayburn, J., Ridge, J.C., Schaefer, J.M., 2009. Regional beryllium-10 production rate calibration for late-glacial northeastern North America. *Quaternary Geochronology* 4, 93–107.
- Brook, E.J., Kurz, M.D., Ackert, R.P., Raisbeck, G., Yiou, F., 1995. Cosmogenic nuclide exposure ages and glacial history of late Quaternary Ross Sea drift in McMurdo Sound, Antarctica. *Earth and Planetary Science Letters* 131, 41–56.
- Chen, J.L., Wilson, C.R., Tapley, B., Blankenship, D., Young, D., 2008. Earth and Planetary Science Letters 266, 140–148.
- Clark, P., Dyke, A., Shakun, D., Carlson, A., Clark, J., Wohlfarth, B., Mitrovica, J., Hostetler, S., McCabe, M., 2009. The Last Glacial maximum. *Science* 325, 710–714.
- Domack, E., O'Brien, P., Harris, P., Taylor, F., Quilty, P.G., De Santis, L., Raker, B., 1998. Late Quaternary sediment facies in Prydz Bay, East Antarctica and their relationship to glacial advance onto the continental shelf. *Antarctic Science* 10 (3), 236–246. doi:10.1017/S0954102098000339.
- Donahue, D.J., Linick, T.W., Jull, A.J.T., 1990. Isotope-ratio and background corrections for accelerator mass spectrometry radiocarbon measurements. *Radiocarbon* 32 (2), 135–142.
- Dugan, B., Lifton, N., Jull, A.J., 2008. New Production Rate Estimates for In Situ Cosmogenic ^{14}C . Cronus-Earth/EU Workshop, Vancouver, July 12–13, 2008.
- Freeman, S., Bishop, P., Bryant, C., Cook, G.T., Fallick, A., Harkness, D., Metcalf, S., Scott, M., Scott, R., Summerfield, M., 2004. A new environmental sciences AMS laboratory in Scotland. *Nuclear Instruments and Methods in Physics Research B* 223, 31–34.
- Fülop, R.H., Naysmith, P., Cook, G.T., Fabel, D., Xu, S., Bishop, P., 2010. Update on the performance of the SUERC in situ cosmogenic C-14 extraction line. *Radiocarbon* 52, 1288–1294.
- Golledge, N., Fabel, D., Everest, J., Freeman, S., Binnie, S., 2007. First cosmogenic ^{10}Be age constraint of the timing of Younger Dryas glaciation and ice cap thickness, western Scottish Highlands. *Journal of Quaternary Science* 22, 785–791.
- Gosse, J.C., Phillips, F.M., 2001. Terrestrial in situ cosmogenic nuclides: theory and application. *Quaternary Science Reviews* 20, 1475–1560.
- Hippe, K., Kober, F., Baur, H., Wacker, L., Wieler, R., 2009. The current performance of the in situ ^{14}C extraction line at ETH. *Quaternary Geochronology* 4, 493–500. doi:10.1016/j.quageo.2009.06.001.
- Jamieson, S.S.R., Sugden, D.E., Hulton, N.J., 2010. The evolution of the subglacial landscape of Antarctica. *Earth and Planetary Science Letters* 293, 1–27.
- Lal, D., 1991. Cosmic ray labeling of erosion surfaces; in situ nuclide production rates and erosion models. *Earth and Planetary Science Letters* 104 (2–4), 424–439.
- Lifton, N.A., Jull, A.J.T., Quade, J., 2001. A new extraction technique and production rate estimate for in situ cosmogenic ^{14}C in quartz. *Geochimica et Cosmochimica Acta* 65 (12), 1953–1969.
- Lifton, N.A., 1997. A new extraction technique and production rate estimate for in situ cosmogenic ^{14}C in quartz. PhD dissertation, Tucson, University of Arizona.
- Mackintosh, A., White, D.A., Fink, D., Gore, D.B., Pickard, J., Fanning, P.C., 2007. Exposure ages from mountain dipsticks in Mac. Robertson Land, East Antarctica, indicate little change in ice-sheet thickness since the Last Glacial Maximum. *Geology* 35, 551–554.
- Maden, C., Anastasi, P., Dougans, D., Freeman, S., Kitchen, R., Klody, G., Schnabel, C., Sundquist, M., Vannerb, K., Xu, S., 2007. SUERC AMS ion detection. *Nuclear Instruments and Methods in Physics Research Section B* 259 (1), 131–139.
- Miller, G., Briner, J., Lifton, N., Finkel, R., 2006. Limited ice sheet erosion and complex exposure histories derived from in situ ^{10}Be , ^{26}Al and ^{14}C on Baffin Island, Canada. *Quaternary Geochronology* 1, 74–85.
- Naysmith, P., Cook, G.T., Phillips, W., Lifton, N.A., Anderson, R., 2004. Preliminary results for the extraction and measurement of cosmogenic in situ C-14 from quartz. *Radiocarbon* 46 (1), 201–206.
- Pigati, J.S., 2004. Experimental developments and application of carbon-14 and in situ cosmogenic nuclide dating techniques [PhD dissertation]. University of Arizona, Tucson.
- Pollard, D., Deconto, R., 2009. Modelling West Antarctic ice sheet growth and collapse through the past five million years. *Nature* 458, 329–332.
- Putkonen, J., Swanson, T., 2003. Accuracy of cosmogenic ages for moraines. *Quaternary Research* 59, 255–261.
- Putnam, A.E., Schaefer, J.M., Barrell, D.J.A., Vandergoes, M., Denton, G.H., Kaplan, M.R., Finkel, R.C., Schwartz, R., Goehring, B.M., Kelley, S.E., 2010. In situ cosmogenic ^{10}Be production-rate calibration from the Southern Alps, New Zealand. *Quaternary Geochronology* 5, 392–409.
- Schildgen, T., Phillips, W., Purves, R., 2005. Simulation of snow shielding corrections for cosmogenic nuclide surface exposure studies. *Geomorphology* 64, 67–85.
- Simpson, M., Milne, G., Huybrechts, P., Long, A., 2009. Calibrating a glaciological model of the Greenland ice sheet from the Last Glacial Maximum to present-day using field observations of relative sea level and ice extent. *Quaternary Science Reviews* 28, 1631–1657.
- Stone, J., 2000. Air pressure and cosmogenic isotope production. *Journal of Geophysical Research* 105, 23753–23759.
- Stone, J.O., Balco, G.A., Sugden, D.E., Caffee, M.E., Sass, L.C., Cowdery, S.G., Siddoway, C., 2003. Holocene deglaciation of Marie Byrd Land, West Antarctica. *Science* 299 (5603), 99–102.
- Stroeven, A., Fabel, D., Marshall, S., 2002. Inceptions: mechanisms, patterns and timing of ice sheet inception. *Quaternary International* 95–96, 1–5.
- Sugden, D.E., Balco, G., Cowdery, S.G., Stone, J.O., Sass III, L.C., 2005. Selective glacial erosion and weathering zones in the coastal mountains of Marie Byrd Land, Antarctica. *Geomorphology* 67 (3–4), 317–334.
- Todd, C., Stone, J., Conway, H., Hall, B., Bromley, G., 2010. Late Quaternary evolution of Reedy Glacier, Antarctica. *Quaternary Science Reviews* 29, 1328–1341.
- White, D., Fink, D., Gore, D., 2011. Cosmogenic nuclide evidence for enhanced sensitivity of an East Antarctic ice stream to change during the last deglaciation. *Geology* 39 (1), 23–26.
- Wright, A., White, D., Gore, D., Siegert, M., 2008. Antarctica at the Last Glacial Maximum, Deglaciation and the Holocene. In: Florindo, F., Siegert, M. (Eds.), *Antarctic Climate Evolution*. Elsevier, pp. 531–570.
- Yokoyama, Y., Caffee, M.E., Southon, J., Nishiizumi, K., 2004. Measurements of in situ produced ^{14}C in terrestrial rocks. *Nuclear Instruments and Methods in Physics Research Section B: Beam Interactions with Materials and Atoms* 224, 253–258.